

NASA CONTRACTOR
REPORT



NASA CR-1291

NASA CR-1291

CASE FILE
COPY

HIGH-PERFORMANCE TURBOALTERNATOR AND ASSOCIATED HARDWARE

II - DESIGN OF GAS BEARINGS

by A. Frost, J. W. Lund, and P. W. Curwen

Prepared by

UNITED AIRCRAFT CORPORATION

East Hartford, Conn.

for Lewis Research Center

HIGH-PERFORMANCE TURBOALTERNATOR AND ASSOCIATED HARDWARE

II - DESIGN OF GAS BEARINGS

By A. Frost, J. W. Lund, and P. W. Curwen

Distribution of this report is provided in the interest of information exchange. Responsibility for the contents resides in the author or organization that prepared it.

Prepared under Contract No. NAS 3-6013 by
MECHANICAL TECHNOLOGY INCORPORATED
Latham, N.Y.

under Subcontract to Pratt & Whitney Aircraft,
Division of United Aircraft Corporation, East Hartford, Conn.

for Lewis Research Center

NATIONAL AERONAUTICS AND SPACE ADMINISTRATION

ABSTRACT

The National Aeronautics and Space Administration is conducting an evaluation of candidate Brayton-cycle turbomachinery configurations. As part of this program, Pratt & Whitney Aircraft has designed a turboalternator incorporating a two-stage axial-flow turbine driving an inductor alternator supported on gas bearings. The gas bearings were designed and successfully tested in a gas bearing dynamic simulator by Mechanical Technology Incorporated. Testing of the simulator under full electrical load and under certain electrical fault conditions indicated satisfactory operation of the rotor system.

Page intentionally left blank

FOREWORD

The research described herein was conducted by Mechanical Technology Incorporated under subcontract to Pratt & Whitney Aircraft, Division of United Aircraft Corporation (NASA Contract NAS 3-6013). The project was managed by Mr. Henry B. Tryon, Space Power Systems Division, NASA-Lewis Research Center. The report was originally issued as Pratt & Whitney PWA-3070, volume 2 (Mechanical Technology Incorporated MTI-67TR29).

Page Intentionally Left Blank

TABLE OF CONTENTS

	<u>Page</u>
LIST OF TABLES-----	viii
LIST OF FIGURES-----	x
SUMMARY-----	1
I. INTRODUCTION-----	4
II. DESIGN OF TURBOALTERNATOR BEARING SYSTEM-----	8
Operating Conditions and Design Specifications-----	8
Selection of Bearing Types-----	11
Performance Characteristics of the Journal Bearings-----	12
Provisions for External Pressurization of Journal Bearings-----	23
Performance Characteristics of the Hydrodynamic Thrust Bearing-----	27
Performance Characteristics of the Hydrostatic Thrust Bearing-----	37
Rotor-Bearing System Dynamics-----	42
Bearing Cooling Design-----	48
Journal Bearing Adjustments and Assembly Details-----	54
Bearing System Fabrication Materials-----	59
Bearing Surfacing Materials-----	61
Bearing System Instrumentation-----	61
III. DESIGN OF ROTOR-BEARING SYSTEM SIMULATOR-----	69
Simulator Rotor-----	71
Simulator Bearings-----	73
Control of Bearing Loads-----	73
Simulator Casings-----	76
Simulator Turbine-----	77
Simulator Temperature Control-----	80
Simulator Instrumentation-----	80
IV. TEST EVALUATION OF THE ROTOR-BEARING SYSTEM DESIGN-----	82
Description of the Simulator Test Facility-----	82
Calibration of the Journal Bearing Flexures-----	87
Calibration of the Main Thrust Bearing Support Flexure-----	91
Test Evaluation of the Hydrodynamic Journal Bearings-----	94
Test Evaluation of the Hydrostatic Journal Lift-Off Bearings-----	98

Table of Contents (Continued)

	<u>Page</u>
Test Evaluation of the Hydrodynamic Thrust Bearing-----	100
Test Evaluation of the Main Hydrostatic Thrust Bearing-----	105
Test Evaluation of the Reverse Hydrostatic Thrust Bearing-----	107
V. ANALYTICAL INVESTIGATION OF ROTOR RESPONSE AND STABILITY TO ALTERNATOR ELECTROMAGNETIC FORCES-----	109
Discussion of the Technical Problem-----	111
Results-----	120
VI. DESIGN OF ROTOR BEARING SIMULATOR INCLUDING ALTERNATOR-----	142
Simulator Rotor-----	143
Simulator Bearings-----	148
Control of the Simulator Journal Bearing Clearance-----	148
Control of Bearing Loads-----	149
Simulator Casings and Alternator Stator-----	152
Simulator Turbine-----	154
Simulator-Alternator Temperature Control-----	158
Simulator Electrical Load Control-----	159
Simulator-Alternator Instrumentation-----	162
VII. TEST EVALUATION OF THE ROTOR-BEARING SYSTEM UNDER VARIOUS CONDITIONS OF ALTERNATOR LOAD-----	163
Description of the Simulator Test Facility-----	163
Initial Adjustment of Simulator Rotor Concentricity and Journal Bearing Clearance-----	169
Preliminary Testing-----	171
Conditions and Details of Simulator Test-----	175
Data Acquired During Test-----	179
Test Evaluation of Rotor Response and Stability-----	188
Additional Test Program-----	209
Test Evaluation of Journal Bearing Performance and Alternator Magnetic Force Gradients-----	218
Test Evaluation of Hydrodynamic Thrust Bearing Performance-----	225
VIII. CONCLUSIONS AND RECOMMENDATIONS-----	228
Specific Conclusions-----	229
General Conclusions-----	231

Table of Contents (Continued)

	<u>Page</u>
Recommendations-----	232
LIST OF REFERENCES-----	233
NOMENCLATURE-----	235
APPENDICES	
A. The Load Carrying Capacity and Dynamic Coefficients for a Partial Arc Gas Journal Bearing-----	237
B. The Numerical Solution of the Steady State Gas Film Pressures by Finite Difference Equations-----	248
C. The Numerical Calculation of the Dynamic Coefficients for the Pad Gas Journal Bearing-----	253
D. The Dynamic Coefficients and the Response of the Shoes in a Tilting Pad Journal Bearing-----	258
E. Reduction of the Magnetic Force Data from the General Electric Co.--	263
F. Analysis of Rotor Stability with Magnetic Forces-----	268
G. Method for Calculating Rotor Response and Stability-----	277
H. Solor Brayton Cycle Space Power System Environmental Specification--	286
I. Pratt and Whitney Aircraft Specification for Acceptance Testing a Turboalternator Rotor Dynamic Simulator-----	289
J. Reduction of Bearing Data Acquired During Rotor-Bearing- Alternator Testing-----	292
K. Reduction of Rotor Position Data Acquired During Rotor-Bearing- Alternator Testing-----	309

LIST OF TABLES

	<u>Page</u>
TABLE II-1 Turboalternator Journal Bearing Design Parameters-----	16
TABLE II-2 Turboalternator Journal Bearing Calculated Performance Characteristics-----	17
TABLE II-3 Turboalternator Main Hydrodynamic Thrust Bearing Design Parameters-----	29
TABLE II-4 Turboalternator Main Hydrodynamic Thrust Bearing Calculated Performance Characteristics-----	30
TABLE II-5 Hydrostatic Thrust Bearing Design Parameters and Calculated performance Characteristics-----	38
TABLE II-6 Journal Bearing Set Up Dimensions for Concentric Operation Under Design Point Conditions-----	57
TABLE II-7 Location of Bearing System Capacitance Probes-----	64
TABLE V-1 The Alternator Electromagnetic Forces-----	127
TABLE V-2 Dynamic Response of Turboalternator Rotor-Bearing System to Electromagnetic Alternator Forces-----	129
TABLE VII-1 Preliminary Test Program-----	172
TABLE VII-2 Simulator Configuration Variables-----	176
TABLE VII-3 Zero Electrical Load Test Conditions-----	176
TABLE VII-4 Balanced Electrical Load Test Conditions at 12,000 RPM and 0.8 Power Factor-----	177
TABLE VII-5 Unbalanced Electrical Load and Short Circuit Test Points-----	177
TABLE VII-6 Sequence of Testing Showing Values of Primary Variables Obtained During Tests-----	181
TABLE VII-7 Details of Data Acquired During Rotor-Bearing- Alternator-Simulator Test Program-----	182
TABLE VII-8 Calculated Dynamic Response of Simulator Rotor Bearing System to Electromagnetic Alternator Forces-----	191
TABLE VII-9 Values of Bearing Clearance, Temperature and Rotor Eccentricity Obtained During Test With Rotor Horizontal and Mechanically Unbalanced in the Plane of the Turbine Wheel (Configuration F)-----	192
TABLE VII-10 Calculated and Experimentally Determined Static Electromagnetic Force Gradient Per Alternator Pole Pair-----	221

	<u>Page</u>
TABLE J-1 Tabulation of Bearing Performance Data Acquired During Rotor-Bearing-Alternator Testing-----	297
TABLE K-1 Tabulation of Data Describing the Rotor Eccentricity During Test of the Rotor-Bearing-Alternator Simulator-----	313

LIST OF FIGURES

	Page
Fig. I - Brayton Cycle Turboalternator	3
Fig. II-1 - View of a Journal Bearing Assembly Showing the Pivot-Supports	18
Fig. II-2 - Calculated Journal Bearing Performance in a 6.0 PSIA Argon Environment. (Rotor horizontal in a 1-g gravitational field).	19
Fig. II-3 - Calculated Journal Bearing Performance in a 10.5 PSIA Argon Environment. (Rotor horizontal in a 1-g gravitational field).	20
Fig. II-4 - Calculated Journal Bearing Performance in a 12.0 PSIA Argon Environment. (Rotor horizontal in a 1-g gravitational field).	21
Fig. II-5 - Calculated Effect of Machined Clearance Ratio (C_p/R) variation on Journal Bearing Performance in a 6.0 PSIA Argon Environment. (Rotor horizontal in a 1-g gravitational field).	22
Fig. II-6 - Details of the Journal Bearing Jacking Gas System	24
Fig. II-7 - View of a Fully Instrumented Bearing Pad With Pivot-Rod, Pivot-Seat and Check Valve Parts	25
Fig. II-8 - View of the Surface of a Loaded Pad Showing the Pad to Shaft Capacitance Probe and the Jacking Gas Orifice and Recess	26
Fig. II-9 - Calculated Hydrodynamic Thrust Bearing Performance in a 12.0 PSIA Argon Environment at 6,000 RPM	31
Fig. II-10 - Calculated Hydrodynamic Thrust Bearing Performance in a 12.0 PSIA Argon Environment at 12,000 RPM. (Design Speed)	32
Fig. II-11 - Calculated Hydrodynamic Thrust Bearing Performance in a 12.0 PSIA Argon Environment at 14,400 RPM. (Over Speed)	33

	Page
Fig. II-12 - Views of Thrust Runner Showing Main and Reverse Thrust Bearing Surfaces	34
Fig. II-13 - View of Combined Hydrodynamic-Hydrostatic Main Thrust Bearing	35
Fig. II-14 - View of Combined Hydrodynamic-Hydrostatic Main Thrust-Bearing Mounted in Flexible Support	36
Fig. II-15 - Calculated Performance of the Hydrostatic Main Thrust Bearing in a 6.0 PSIA Argon Environment	39
Fig. II-16 - Calculated Performance of the Hydrostatic Reverse Thrust Bearing in a 6.0 PSIA Argon Environment	40
Fig. II-17 - View of the Hydrostatic Reverse Thrust Bearing	41
Fig. II-18 - Critical Speed Versus Journal Bearing Stiffness for Turbo-alternator Rotor Bearing System	45
Fig. II-19 - First and Second Critical Speed Mode Shapes - Turbo-alternator Rotor Using Calculated Values of Stiffnesses ..	46
Fig. II-20 - Bearing Reactions for 0.005 Oz.-In. Unbalance in the Turbine Plane - Turboalternator Rotor (No Electromagnetic Forces) - Using Calculated Values of Stiffnesses ...	47
Fig. II-21 - Liquid Cooled Thrust Bearing Operating Characteristics Versus Coolant-Flow Rate Using Calculated Values of Stiffnesses	53
Fig. II-22 - Turboalternator Journal Bearing Set-up Data for Optimum Performance at Design Point Operating Conditions	58
Fig. II-23 - Position and Identity of Capacitance Probes in Number 1 Journal Bearing	65
Fig. II-24 - Position and Identity of Capacitance Probes in Number 2 Journal Bearing	66
Fig. II-25 - View Showing a Typical Range of Capacitance Probe Configurations for Bearing System Performance Measurement	67
Fig. II-26 - View Showing the Location of Journal Bearing Pad Thermocouples	68

	Page
Fig. III-1 - Turboalternator Rotor-Bearing Simulator	70
Fig. III-2 - View of Rotor for Initial Rotor-Bearing Simulator	72
Fig. III-3 - Partial Assembly of the Rotor-Bearing Simulator in a Horizontal Position (Initial Configuration)	74
Fig. III-4 - Partial Assembly of the Rotor-Bearing Simulator in a Vertical Position (Initial Configuration)	75
Fig. III-5 - View of Impulse Turbine Wheel and Tie Bolt for Rotor- Bearing Simulator (Initial Configuration)	79
Fig. IV-1 - View of Rotor-Bearing Simulator Mounted Vertically on the Test Stand	84
Fig. IV-2 - View of Simulator Control Panel and Partial Set-Up of Bearing System Instrumentation Read-Out Equipment	85
Fig. IV-3 - Schematic Diagram of the Simulator Test Set-Up for Test-Evaluation of the Rotor-Bearing System	86
Fig. IV-4 - Measured Load Versus Deflection Plots For the Upper and Lower Pivot-Support Flexures for the Turboalternator Journal Bearings	90
Fig. IV-5 - Measured Load Versus Deflection Characteristic for the Main Thrust Bearing Whipple-Plate Support Flexure	93
Fig. IV-6 - Comparison of Measured and Calculated Performance of the No. 1 Journal Bearing During Hydrodynamic Operation in Air	97
Fig. IV-7 - Measured Performance of the No. 1 and No. 2 Hydrostatic Journal Bearings at 8.8 and 14.7 PSIA Ambient Pressure	99
Fig. IV-8 - Measured Load Versus Film Thickness for the Hydrodynamic Thrust Bearing at 12,000 RPM	103
Fig. IV-9 - Measured Load Versus Film Thickness of the Hydrodynamic Thrust Bearing at 12,000 and 9,000 RPM	104

	Page
Fig. IV-10 - Measured Load Versus Film Thickness Data for the Main Hydrostatic Thrust Bearing	106
Fig. IV-11 - Measured Load Versus Film Thickness Data for the Reverse Hydrostatic Thrust Bearing	108
Fig. V-1 - Calculated Film-Thickness Parameter versus Dimensionless Pad Load	131
Fig. V-2 - Calculated Bearing Load and Film-Thickness Data versus Bearing Eccentricity Ratio	132
Fig. V-3 - Calculated Dimensionless Pad Radial Stiffness versus Frequency Ratio	133
Fig. V-4 - Calculated Dimensionless Pad Tangential Stiffness versus Frequency Ratio	134
Fig. V-5 - Calculated Dimensionless Pad Cross-Coupling Stiffness versus Frequency Ratio	135
Fig. V-6 - Calculated Dimensionless Pad Cross-Coupling Stiffness versus Frequency Ratio	136
Fig. V-7 - Calculated Dimensionless Pad Radial Damping versus Frequency Ratio	137
Fig. V-8 - Calculated Dimensionless Pad Tangential Damping versus Frequency Ratio	138
Fig. V-9 - Calculated Dimensionless Pad Cross-Coupling Damping versus Frequency Ratio	139
Fig. V-10 - Calculated Dimensionless Pad Cross-Coupling Damping versus Frequency Ratio	140
Fig. V-11 - Calculated Stability Map for the Turboalternator Rotor-Bearing System	141
Fig. VI-1 - Turboalternator Rotor-Bearing-Alternator Simulator	145.

	Page
Fig. VI-2 - View of Simulator Rotor Prior to Final Machining_____	146
Fig. VI-3 - View of the Simulator Rotor_____	146
Fig. VI-4 - View of the Component Parts of the Simulator Rotor_____	147
Fig. VI-5 - View of the Simulator Rotor Assembly_____	147
Fig. VI-6 - View of Complete Simulator Installed in a Hori- zontal Position on the Test Stand_____	150
Fig. VI-7 - View of Complete Simulator Installed in a Ver- tical Position on the Test Stand_____	151
Fig. VI-8a - Front View of Alternator Stator_____	153
Fig. VI-8b - Rear View of Alternator Stator_____	153
Fig. VI-9 - View of Simulator Turbine Wheel and one of Two Nozzles_____	156
Fig. VI-10 - View of Simulator Turbine Wheel and Casing_____	157
Fig. VI-11 - View of the Load Bank Used to Dissipate the Power Generated During Test of the Rotor-Bearing- Alternator Simulator_____	161
Fig. VII-1 - View Showing the Left-Hand Side of the Simulator Control Panel and Instrument Read-out Equipment_____	166
Fig. VII-2 - View Showing the Right-Hand Side of the Simulator Control Panel and Instrument Read-out Equipment_____	166
Fig. VII-3 - View Showing the Simulator Control Panel and Instrument Read-out Equipment During Test_____	167
Fig. VII-4 - Schematic Diagram of the Simulator Test Set- up for Test Evaluation of the Rotor-Bearing- Alternator Simulator_____	168

	Page
Fig. VII-5 - Oscilloscope Photographs of the Turbine End Journal Bearing Performance at 12,000 RPM, 10.5 PSIA Ambient Pressure (Air) and a 12 KW, 0.8 PF Electrical Load (Rotor Horizontal and Eccentric. Test Point No. F 18) -----	197
Fig. VII-6 - Oscilloscope Photographs of the Turbine End Journal Bearing Performance at 12,000 RPM, 10.5 PSIA Ambient Pressure (Air) and zero Alternator Excitation. (Rotor Horizontal and Eccentric. Test Point No. F 15). -----	198
Fig. VII-7 - Oscilloscope Photographs of the Thrust End Journal Bearing Performance at 12,000 RPM, 10.5 PSIA Ambient Pressure (Air) and a 12 KW 0.8 PF Electrical Load. (Rotor Horizontal and Eccentric. Test Point No. F 18). -----	199
Fig. VII-8 - Oscilloscope Photographs of the Thrust End Journal Bearing Performance at 12,000 RPM, 10.5 PSIA Ambient Pressure (Air) and zero alternator Excitation. (Rotor Horizontal and Eccentric. Test Point No. F 15). -----	200
Fig. VII-9 - Oscilloscope Photographs of the Turbine End Journal Bearing Performance at 12,000 RPM and 7.2 PSIA Ambient Pressure (Air). (Rotor Vertical and Eccentric by 0.002-0.003 inches. Test Points No's. D22 and D23) ---	204
Fig. VII-10 - Oscilloscope Photographs of the Turbine End Journal Bearing Performance at 12,000 RPM and 7.2 PSIA Ambient Pressure (Air). (Rotor Vertical and Eccentric by 0.002-0.003 inches. Test Point No's. D32 and D36). ---	205
Fig. VII-11 - Oscilloscope Photographs of the Turbine End Journal Bearing Performance at 12,000 RPM and 7.2 PSIA Ambient Pressure (Air). (Rotor Horizontal and Eccentric by 0.003-0.004 inches. Test Point No's. F10 and F11). ---	206
Fig. VII-12 - Oscilloscope Photographs of the Turbine End Journal Bearing Performance at 12,000 RPM and 7.2 PSIA Ambient Pressure (Air). (Rotor Horizontal and Eccentric by 0.003-0.004 inches. Test Point No. F34). -----	207
Fig. VII-13 - Oscilloscope Photographs of the Turbine End Journal Bearing Performance at 12,000 RPM and 7.2 PSIA Ambient Pressure (Air). (Rotor Horizontal and Eccentric by 0.003-0.004 inches. Test Point No. F29). -----	208

Fig. VII-14 - Oscilloscope Photographs of the Turbine End Journal Bearing Performance During Tests to Determine the Maximum Permissible Bearing Clearance. Speed 12,000 RPM, 10.5 PSIA Ambient Pressure (Air). Rotor Horizontal, Eccentric and Mechanically Unbalanced. (Configuration F, Test Points 14 and 15).	215
Fig. VII-15 - Oscilloscope Photographs of the Turbine End Journal Bearing Performance During Tests to Determine the Maximum Permissible Bearing Clearance. Speed 12,000 RPM, 10.5 PSIA Ambient Pressure (Air), Rotor Vertical, Concentric and Balanced. (Configuration A, Test Point 23).	216
Fig. VII-16 - Oscilloscope Photographs of Journal Orbits Showing the Residual Unbalance, Out-of-roundness and Effect of Excitation Over the Speed Range 5,000-14,400 RPM. Rotor Vertical and Concentric. Bearing Ambient Pressure 14.7 PSIA (Air).	217
Fig. VII-17 - Calculated and Experimental Performance of the Journal Bearing Adjacent to the Thrust Bearing at High Preloads (Rotor Vertical).	222
Fig. VII-18 - Calculated and Experimental Performance of the Journal Bearing Adjacent to the Thrust Bearing at Low Preloads (Rotor Vertical).	223
Fig. VII-19 - Calculated and Experimental Performance of the Journal Bearing Adjacent to the Thrust Bearing at Low Preloads (Rotor Horizontal).	224
Fig. VII-20 - Oscilloscope Photographs of the Hydrodynamic Thrust Bearing Performance Over a Range of Electrical Load Conditions. Rotor Vertical, Concentric and Mechanically Balanced. Speed 12,000 RPM, 14.7 PSIA Ambient Pressure (Air).	227
Fig. K-1 Terminology and Sign Convention Used in the Tabulation of Data Describing the Rotor Eccentricity During Test of the Rotor-Bearing-Alternator Simulator.....	312

SUMMARY

A gas-bearing rotor support system has been designed, fabricated, and tested by Mechanical Technology Incorporated for the NASA Brayton-cycle axial-flow turboalternator developed by Pratt & Whitney Aircraft under prime contract from the NASA-Lewis Research Center. (A cross-section view of the turboalternator is shown in Figure 1.) The gas-bearing system was experimentally evaluated in a full-scale rotor-bearing system test rig which

1. exactly simulated the design of the turboalternator bearings,
2. very closely simulated the mechanical configuration and physical parameters of the turboalternator rotor (the actual turboalternator turbine was not, however, used), and
3. permitted testing of the rotor-bearing system under operating conditions, including generation of rated electrical power, similar to those which would exist in the turboalternator (turbine inlet temperature, however, was not simulated).

In addition to the experimental evaluation, analyses were performed and computer programs written which permit quantitative determination of rotor-bearing system response and stability under conditions of electrical power generation wherein the rotor is subjected to dynamic electromagnetic forces. These forces exist when the rotor is mechanically eccentric in the alternator air gap.

The bearing system performed satisfactorily throughout the test program and successfully passed the required P & WA acceptance tests. Operation of the bearings was not impaired (i.e., there was no rupture of the gas film) by an extensive turbine labyrinth rub which occurred when testing under extreme conditions of rotor eccentricity. At these extreme eccentricities, approximately 4 mils at the alternator pole planes, the bearings could safely carry the combined loads due to alternator electromagnetic forces and rotor weight. Finally, satisfactory operation was demonstrated over a very wide range of journal bearing clearances (up to essentially zero preload) without any evidence of rotor whirl.

Instability of one pad was observed at the zero preload condition, but even in this case there was no rupture of the bearing gas film. In actual operation, the bearing preloads will range between 0.3 and 0.6 and the pad instability mode will never be encountered.

Development of a reliable turboalternator gas-bearing system has been achieved for the conditions imposed by the design specifications, as well as for additional conditions imposed during simulator testing. The system has been proven to be sufficiently rugged and tolerant of variations from design point to give confidence that turboalternator performance will be fully satisfactory under static environmental conditions. It remains, however, to demonstrate the overall reliability of this system under actual thermal conditions of turboalternator operation, as well as under the short and long term environmental conditions which will exist during a space-system mission.

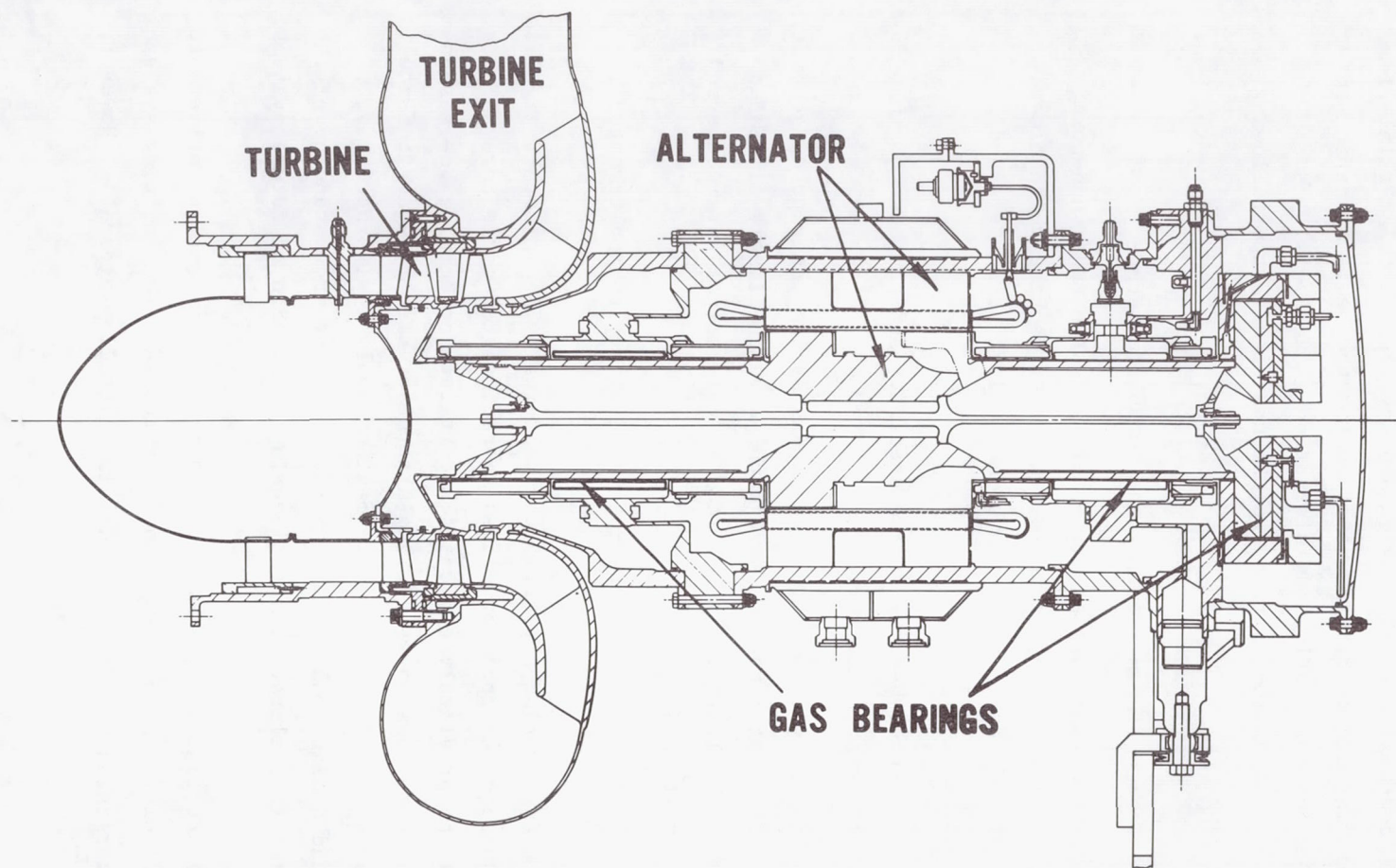


Fig. 1 Brayton Cycle Turboalternator

I. INTRODUCTION

Mechanical Technology Incorporated (MTI), under subcontract to Pratt & Whitney Aircraft (P&WA), has cooperated in the design and development of an axial-flow turboalternator employing gas-lubricated bearings for the Lewis Research Center of the National Space and Aeronautics Administration (NASA-Lewis). More specifically, MTI's participation in this program has been in the following areas:

1. design of a gas-bearing system for the turboalternator;
2. test evaluation of the complete gas-bearing system under non-power generating conditions, in a rotor-bearing test machine which closely simulated most of the turboalternator mechanical parameters and operating conditions;
3. analysis of the rotor-bearing system stability and response to the alternator electromagnetic forces;
4. test evaluation of the complete gas-bearing system under power generating conditions, in a rotor-bearing test machine which closely simulated most of the turboalternator mechanical and electrical parameters and operating conditions;
5. manufacture of the bearing parts for the delivery turboalternators.

The development of a gas-bearing-supported turboalternator is a further significant advance in the technology required for closed-system Brayton-cycle power plants. The advance removes the previously expressed uncertainty concerning the response and stability of the rotor-bearing system to alternator electromagnetic forces. The program has also resulted in the development of analytical procedures, computer programs and design tools which contribute to the understanding of the problems and which will facilitate the engineering and design of future systems.

The most noteworthy attribute of gas lubrication for the present turboalternator application is simplicity. In a conventional gas turbine, the rotating system is supported on oil-lubricated bearings (fluid film or rolling element). However,

for closed-system operation where the same gas is continuously circulated, means must be provided to ensure that the oil cannot contaminate the gas stream. Leakage of oil into this stream would ultimately degrade power plant performance to an unacceptable level due to fouling of critical heat exchanger parts and build-up of decomposition products.

To prevent contamination rotating seal systems must be used to isolate the oil from the cycle gas. Auxiliary equipment in the form of oil pumps, scavenging pumps, oil-gas separators, reservoirs, and possibly coolers and adsorbers, is also required. To obtain long-term non-degrading performance from an oil-lubricated, closed-cycle power plant may be a problem, particularly if the plant must be capable of repeated start-ups and shutdowns.

In a gas-bearing machine, the rotating system is supported on a film of gas. Recent developments of motor-driven gas-bearing compressors and circulators, which have jointly accumulated over 67,000 hours of field operation, have created an understandable impetus to apply gas-bearings to closed-system gas turbine machinery [1]*. By utilizing cycle gas for the bearing system lubricant, the contamination problem and auxiliary equipment requirements for the closed Brayton cycle, as mentioned above, can be eliminated. The potential ability of a well-designed gas-lubricated turbomachine to operate reliably for long periods of time with repeated start-ups and shutdowns should therefore be quite high.

As in all new technologies, problem areas do exist in the design and application of gas bearings. The complete lack of boundary lubrication in the event of an accidental high-speed bearing rub is probably the most critical problem area in the practical application of gas-bearing turbomachinery. Such rubs may occur due to passage of dirt through the bearings, vibration and shock loads, or improper operation of the machine. The solution to this boundary lubrication problem is to obtain bearing surfacing materials which are capable of surviving many dry rubs with negligible wear or performance degradation. A second inherent problem area which is common to self-acting bearings, the type of bearings used in the turbo-

* Numbers in brackets refer to similarly numbered references listed on page 345.

alternator, is that of low load capacity. The load capacity in a self-acting bearing is, for all practical purposes, limited to several pounds per square inch of projected bearing area. Finally, gas bearings have very low damping capability, and hence are prone to rotor dynamic and rotor-bearing stability problems. The limitations of low load capacity, absence of boundary lubrication, and low damping, imposes several new and stringent requirements on rotor dynamics design. Close attention to these requirements at all times, and particularly during the early conceptual and design phases, is vital to the successful development of gas-lubricated turbomachinery.

The requirements for the turboalternator bearing system (described in Section II of this report) necessitated a number of advancements in the technology of gas-bearing design and application. To obtain maximum assurance of a successful development, the following engineering philosophy was used throughout the program.

1. Make maximum use of existing gas-bearing design technology and operational experience with respect to (a) selection of types of bearings to be used and (b) selection of basic design criteria for these bearing types.
2. Conduct component and subsystem test programs in critical areas where existing technology and/or operational experience was either non-existent or inadequate to permit quantitative evaluation of design concepts. Two such test programs were conducted. The first was the evaluation of a complete rotor-bearing system under actual operating conditions but without alternator electromagnetic forces. The second was evaluation of the complete rotor-bearing system under actual operating conditions including alternator electromagnetic forces. The latter program utilized the prototype turboalternator rotor and stator developed by the General Electric Company [2]. Full electrical power was generated during the course of the tests.
3. Maintain very close liaison with P&WA during the design phase to ensure that all aerodynamic, thermodynamic, and mechanical interactions and interfaces were properly identified and evaluated. In particular, the areas of aerodynamic thrust and radial loads, rotor design, heat transfer design, casing design, instrumentation provisions, balancing techniques, and assembly procedures, were integrated very closely with the P&WA design effort.

One set of bearing components was used during the test phases of the two programs—a total of approximately 100 hours of operation being accumulated. The basic bearing system consists of pivoted-pad self-acting journal bearings (with provisions for external pressurization of the bearings during start-up and shutdown), a spiral-grooved self-acting unidirectional thrust bearing for normal operation, and a bi-directional externally-pressurized thrust bearing for use during start-up and shutdown. The design permitted the use of a single thrust runner for both the self-acting and pressurized thrust bearings.

The design of the bearing system was based upon design criteria which, on the basis of past experience, gave maximum assurance of successful development. This design is described in Section II of the report. The system, which was tested in a rotor-bearing simulator, successfully passed the P&WA acceptance test as described in Section IV.

Having demonstrated the suitability of the rotor-bearing system in the simulator, it was then required to ascertain the effect of alternator electromagnetic forces on the rotor bearing system. This was accomplished in two phases. A theoretical analysis was performed, as described in Section V of this report, to assess the effects of alternator electromagnetic forces on rotor-bearing system response and stability. The rotor-bearing system was then retested using a modified simulator which incorporated the actual turboalternator rotor and stator. During the course of these tests the alternator developed the full power requirement of 12 KW and was also subjected to all of the specified short circuit and unbalanced electrical load conditions. Section VII presents the actual test and performance data for the bearing system when subjected to alternator electromagnetic forces.

The analytical and test phases of this program also included the effect of increasing the journal bearing clearance to achieve a reduction in the bearing friction loss.

The test program was successfully completed for all of the operating conditions specified. The dynamic performance of the rotor-bearing system, when subjected to alternator electromagnetic forces, was as predicted by analysis. The static electromagnetic forces, however, were found to be considerably less than those originally calculated by the alternator manufacturer. A detailed listing of conclusions and recommendations is given in Section VIII.

II. DESIGN OF THE TURBOALTERNATOR BEARING SYSTEM

As mentioned in the preceeding section of this report, the bearing system designed for the turboalternator was built and tested in a rotor-bearing simulator. The tests were conducted in two separate phases, the first of which involved evaluation of the rotor-bearing system in a simulator under all of the conditions of turboalternator operation except the generation of electrical power and temperature distribution. The second phase, which required considerable modifications to the simulator, involved test evaluation of the rotor-bearing system while generating electrical power and, also, while subject to various electrical unbalanced load and short circuit conditions. This second phase, like the first, did not include turboalternator temperature distributions.

The design of the bearing system was based, whenever possible, upon tried and proven state-of-the-art design criteria, so as to give maximum assurance of successful operation at the onset of the program. During the course of the second test phase, which used the same bearing parts as the first phase, certain of these design criteria were refined to more closely tailor the bearing design to the needs of a dynamic space-power system. These extensions were in the direction of minimizing the machinery parasitic losses while maintaining the dynamic integrity of the rotor bearing system.

The following design information concerning the bearing system relates to the original design which was shown by test to be suitable for operation in the turboalternator under the conditions specified.

Operating Conditions and Design Specifications

At the commencement of the program the basic operating conditions and design specifications were defined as follows:

"Hydrodynamic journal and thrust gas bearings are required for the turboalternator package. These bearings shall have as design objectives a life of 10,000 hours under the environmental conditions specified in NASA Specification P0055-1 and

multiple restart capability for ground test and prelaunch checkout. The gas bearings shall be designed to use design point compressor discharge argon gas at approximately 800°R, and a pressure of 13.8 psia with some degree of performance margin. Also, in the event that no major performance penalty or mechanical compromise is incurred, the gas journal and thrust bearings shall be designed to permit their operation with argon supplied at 6.1 psia and 800°R. The design shall provide for operation of the unit both in the horizontal and vertical positions with the alternator facing either up or down. The use of an auxiliary high pressure argon source may be considered for multiple hydrostatic lift-off, start, and shutdown."

During the first several months of the turboalternator development program, numerous aerodynamic, rotor-dynamic, bearing sizing, and heat-transfer design studies were made. During this period, frequent design review meetings, jointly attended by P&WA and MTI, were held to evaluate the studies and to be certain that all interactions between the various engineering disciplines were being properly accounted for and properly weighed with respect to obtaining the best overall integrated design of the turboalternator. The selection of rotor speed, and to a considerable extent rotor mass, was dictated by the design of the alternator which, being a 4 pole machine, must be operated at a speed of 12,000 rpm to generate the 400 cycle power required by the turboalternator specifications. As a result of this approach, the following set of more specific bearing system operating conditions were quickly evolved as being reasonable from rotor-bearing, aerodynamic and alternator system standpoints.

Design Speed	-	12,000 RPM
Overspeed	-	14,400 RPM
Rotor mass	-	54.5 lb
Bearing lubricant (system fluid)	-	Argon
Bearing ambient pressure (minimum)	-	6 PSIA
Bearing ambient pressure (design point)	-	10.5 PSIA (Bearing No. 1)* 12.0 PSIA (Bearing No. 2)*

Maximum operating thrust load	-	85 lb. main (rearward) thrust
Range of maximum thrust load at start-up	-	100 lb. reverse thrust ** 250 lb. rearward thrust **

* The journal bearing adjacent to the turbine wheel and the thrust runner are described as the No. 1 and No. 2 bearings respectively.

** The terminology used to describe each of the thrust bearings is derived from consideration of the direction of the thrust force. Consequently, a rearward thrust load is a force directed from the turbine towards the alternator. This is the direction of the thrust force under normal conditions of operation with the turboalternator horizontal or, alternatively, vertical with the turbine end uppermost. Similarly, a reverse thrust load would be a force directed from the alternator towards the turbine.

The distribution of rotor mass results in a static force on the No. 1 bearing of 27.8 pounds and 26.7 pounds on the No. 2 bearing when the rotor is horizontal in a 1-g gravitational field. However, all design calculations have been made on the basis of a 35 pound static load on each journal bearing. This was done to provide a margin for electromagnetic force reactions due to possible eccentricity between the magnetic and geometric centers of the alternator rotor and stator. Such eccentricity could result from manufacturing tolerances, bearing setup tolerances, and/or magnetic field dissymmetry.

The difference between the design values of ambient pressure for bearings No. 1 and No. 2 reflects the pressure distribution throughout the turboalternator which is necessary to obtain the required thrust balance and also, the required flow of coolant gas.

The previously referenced NASA environmental specification P0055-1 is enclosed as Appendix H of this report.

Selection of Bearing Types

During the early stages of the design phase, careful consideration was given to the type of journal and thrust bearings that should be used in the turboalternator. The bearing types selected for the initial bearing system design were:

1. flexibly-supported, pivoted-pad, self-acting journal bearings with provisions for hydrostatic lift off during start-up and shutdown;
2. flexibly-supported, helical-grooved (Whipple plate) self-acting thrust bearing; and
3. inherently-compensated, annular, externally-pressurized thrust bearings to support the thrust loads at start-up and shutdown.

No change in bearing types were made during the course of the development of the bearing system.

The basic reasons for selection of these bearing types were as follows:

1. Pivoted-pad journal bearings could readily be designed to be stable over the operating range of the machine. The freedom of angular motion of the pivoted-pads also provides good alignment capability. In addition, this freedom of motion, and the interruptions between pads, have proved to be effective safeguards against damage from foreign particles in the gas stream. Finally, and perhaps most importantly, this type of journal bearing had been successfully used in several previous gas-bearing turbomachinery developments. To ensure the attainment of the required multiple restart capability, provisions for hydrostatic lift-off during start-up and shutdown were incorporated into the design of the hydrodynamic journal bearings.
2. The load capacity of properly designed helical-grooved thrust bearings is relatively insensitive to the compressibility number ($\Lambda = \frac{6\mu\omega R^2}{P_s h^2}$) of the application. This is in sharp contrast to other types of self-acting thrust bearings (e.g., pivoted-pad, tapered land, step type, and

others) whose load capacity rapidly approaches an asymptotic value as the compressibility number is increased. The helical-grooved thrust bearing is, however, quite sensitive to the degree of parallelism between the thrust runner and the thrust stator. Accordingly, the thrust stator should be flexibly mounted to permit it to "track" misalignment and wobble of the thrust runner. Once again, this type of bearing had been successfully applied in previous turbomachinery developments.

3. The present application may be subject to high axial loads during start-up and shutdown, making it mandatory to externally pressurize the thrust bearing during these intervals. With proper design, the inherently-compensated externally-pressurized thrust bearing has a much higher threshold of onset of pneumatic hammer than other externally-pressurized bearing types, such as orifice compensated and pocketed bearings.

In the following paragraphs, the individual components of the bearing system are reviewed in more detail. Attention is focused on calculated performance data and on practical considerations of the design. Sound theoretical analyses are essential in gas-bearing development, and were used to establish the steady-state and dynamic characteristics of the bearing system. These procedures, however, have been covered extensively in prior research and in general purpose design papers and reports, and hence will not be repeated here. (References 3 through 15 list some of the standard texts and recent publications in these areas.)

Performance Characteristics of the Journal Bearings

As noted previously, the journal bearings selected for the turboalternator are of the pivoted-pad type. Detailed analyses of this type of bearing are available based on numerical integration of the compressible Reynolds equation. The resulting normalized pad data is assembled as a function of pivot position, pad eccentricity ratio, and compressibility number ($\Lambda = \frac{6\mu\omega}{P_a} \left(\frac{R}{C} \right)^2$). The static

and dynamic characteristics of the bearings are then obtained by vectorial summation of the characteristics of the individual pads. By storing this

bearing data in computer memory, high-speed digital computer programs can be utilized for making screening and final design calculations for any specified combination of operating conditions and bearing geometry.

The turboalternator journal bearings, which are entitled Bearing No. 1 for the bearing adjacent to the turbine, and Bearing No. 2 for the bearing adjacent to the thrust runner, have been designed to operate satisfactorily under the following conditions:

1. at any orientation of the turboalternator in a zero to 0.18-g gravitational field;
2. at any angle between zero and 90 degrees shaft angle (where zero would correspond to a vertically oriented shaft with the turbine end up and 90 degrees would be horizontal) in a 1.0-g gravitational field. (At all angles other than zero the circumferential orientation must allow the journal bearing load vector to pass between the pivots of the lower journal bearing pads*);
3. at any ambient pressure above 6.0 psia; and
4. to withstand, while in any of the above orientations, an unbalance of 0.005 ounce-inches in the plane of the turbine wheel.

The pivots for each of the journal bearing pads are mounted on individual support flexures. These flexures serve several purposes:

1. They inherently improve the ability of the bearings to accommodate thermal expansion changes which would tend to change the bearing clearance.
2. They reduce bearing preload changes due to centrifugal growth of the journals.
3. They reduce the rigid-body critical speeds of the system.

* The terms "lower" or "loaded" pads in the context of this report refer to the two pads in each journal bearing which contain provisions for hydrostatic lift-off.

Two of the pivot-support flexures in each journal bearing are relatively stiff flexures so as to limit radial displacement of the rotor, relative to the concentric position of the various shaft labyrinth seals, when the turboalternator is operated in a horizontal position in a 1-g gravitational field. These stiff flexures are referred to as the lower (or loaded) flexures for each journal bearing. The remaining two flexures in each bearing, referred to as the upper (or unloaded) flexures, are considerably less stiff than the lower flexures. These softer flexures provide most of the accommodation to changes in the thermal expansion and centrifugal growth of the journals. A photograph of a journal bearing showing the flexures is given in Figure II-1. This particular photograph also shows the bearing support which was designed for use in the rotor-bearing simulator.

A summary of the design parameters and calculated design-point performance characteristics for the two journal bearings is given in Tables II-1 and II-2. Presentation of the calculated journal bearing performance over the turboalternator operating speed range is given in Figures II-2 thru II-4. These figures show plots of the performance characteristics listed below as a function of rotor speed when the turboalternator is operating horizontally in a 1-g gravitational field.

1. bearing film thickness at the pivot location of the loaded pads,
2. bearing friction loss,
3. bearing radial stiffness,
4. ratio of pad resonant frequency to rotor synchronous frequency in the roll direction for the upper and lower pads (or equivalently, the unloaded and loaded pads), and
5. ratio of pad resonant frequency to rotor synchronous frequency in the pitch direction for the upper (unloaded) and lower (loaded) pads.

The data in Figures II-2 thru II-5 includes the effects of pivot support deflection and journal centrifugal growth. The temperatures of the bearings were held constant at design-point conditions for all the calculations.

During the period when the turboalternator design was being established, a bearing clearance ratio (C_B/R) of 0.5×10^{-3} was used, in conjunction with nominal values of pad clearance ratio (C_P/R) and preload (m) of 1.0×10^{-3} and 0.5 respectively, to size the journal bearings. While fabricating the journal bearings intended for use in both the rotor-bearing simulator and the turboalternator, some difficulty was experienced in machining the pad radius within the originally established tolerance of ± 0.1 mils. Calculations were, therefore, made to ascertain the effect on bearing performance of increased pad radius tolerance. The basis of these calculations was the retention of the previously established bearing clearance ratio (C_B/R) of 0.5×10^{-3} . The values of preload corresponding to the range of C_P/R under consideration were determined from the following geometrical relationship.

$$m = 1 - \frac{C_B/R}{C_P/R}$$

where m = Preload ratio

R = Journal radius at design speed

C_P = Difference between the machined radii of the pads and the journal at design speed

C_B = Difference between the dimension from the bearing geometric center to the pad surface (at the pivot point) and the journal radius at design speed.

The results of these calculations, which are shown in Figure II-5, show that for constant bearing clearance (C_B/R) the bearing performance is virtually unaffected by the machined clearance ratio C_P/R . It was, therefore, concluded that an increase in pad radius tolerance to ± 1.0 mils could be introduced. The values of tolerance selected result in a nominal C_P/R of 1.28×10^{-3} , with a minimum C_P/R of 1.0×10^{-3} when the pad radius is at the lower limit of the tolerance, and a maximum C_P/R of 1.6×10^{-3} when the pad radius is at the upper limit of the tolerance. The design calculations presented are, therefore, based on the nominal C_P/R of 1.28×10^{-3} and the associated value of preload (m) of 0.612.

TABLE II-1

TURBOALTERNATOR JOURNAL BEARING DESIGN PARAMETERS

Configuration	Pivoted-pad (with hydrostatic lift-off)
Journal Diameters, Inches	3.500
Bearing Length-to-Diameter Ratio (L/D)	1.0
Number of Pads per Bearing	4
Pad Orientation (Referenced to horizontal orientation of the rotor)	Rotor weight between pivots
Arc Length (β) of Pad, Degrees	80.0
Pivot Location (θ/β) from Leading Edge	0.65
Pad Clearance Ratio (C_p / R)	1.28×10^{-3}
Bearing Preload Ratio (m)	0.612
Individual Pad Mass, Ounces	9.7 (with capacitance probe)
Pivot Ball Diameter, Inches	0.625
Pivot Socket Diameter, Inches	0.812
Measured Pivot Support Radial Stiffness, Lb/In	34,800 (upper Pads) 84,000 (lower pads)
Shaft Material	AMS 6294 (AISI 4620)
Shaft Material Coefficient of Expansion, Inch/Inch/ $^{\circ}$ F	6.65×10^{-6} at 300° F
Pad Material	M-1 Tool steel
Pivot Material	M-1 Tool steel
Pivot Material Coefficient of Expansion, Inch/Inch/ $^{\circ}$ F	6.65×10^{-6} at 300° F
Journal and Pad Surfacing Material	Chrome Oxide
Bearing Support Housing Material	AMS 5646
Bearing Support Housing Material Coefficient of Expansion, Inch/Inch/ $^{\circ}$ F	9.3×10^{-6} at 212° F

TABLE II-2

TURBOALTERNATOR JOURNAL BEARING CALCULATED PERFORMANCE CHARACTERISTICS

All data given below is based upon the following operating conditions.

Rotor Speed	12,000 RPM
Lubricant gas	Argon
Bearing Temperature	300°F

a. Horizontal operation in a 1.0 g gravitational field.

Bearing Load, Pounds	35		
Bearing Ambient Pressure, PSIA	6.0	10.5	12.0
Operating Clearance at Pivot, Mils (loaded pads)	0.51	0.60	0.62
Friction Loss Per Journal, Watts	91.6	89.5	90.2
Radial Gas Film Stiffness, Lb./In.	1.14×10^5	1.4×10^5	1.45×10^5

b. Space operation in a zero-g gravitational field. Bearing load due to 0.005 ounce-inch unbalance in the plane of the turbine wheel.

Bearing Ambient Pressure, PSIA	10.5	12.0
Operating Clearance at Pivot, Mils (All pads)	0.87	0.87
Friction Loss per Journal, Watts	83.9	84.5
Radial Gas Film Stiffness, Lb./In.	1.14×10^5	1.239×10^5

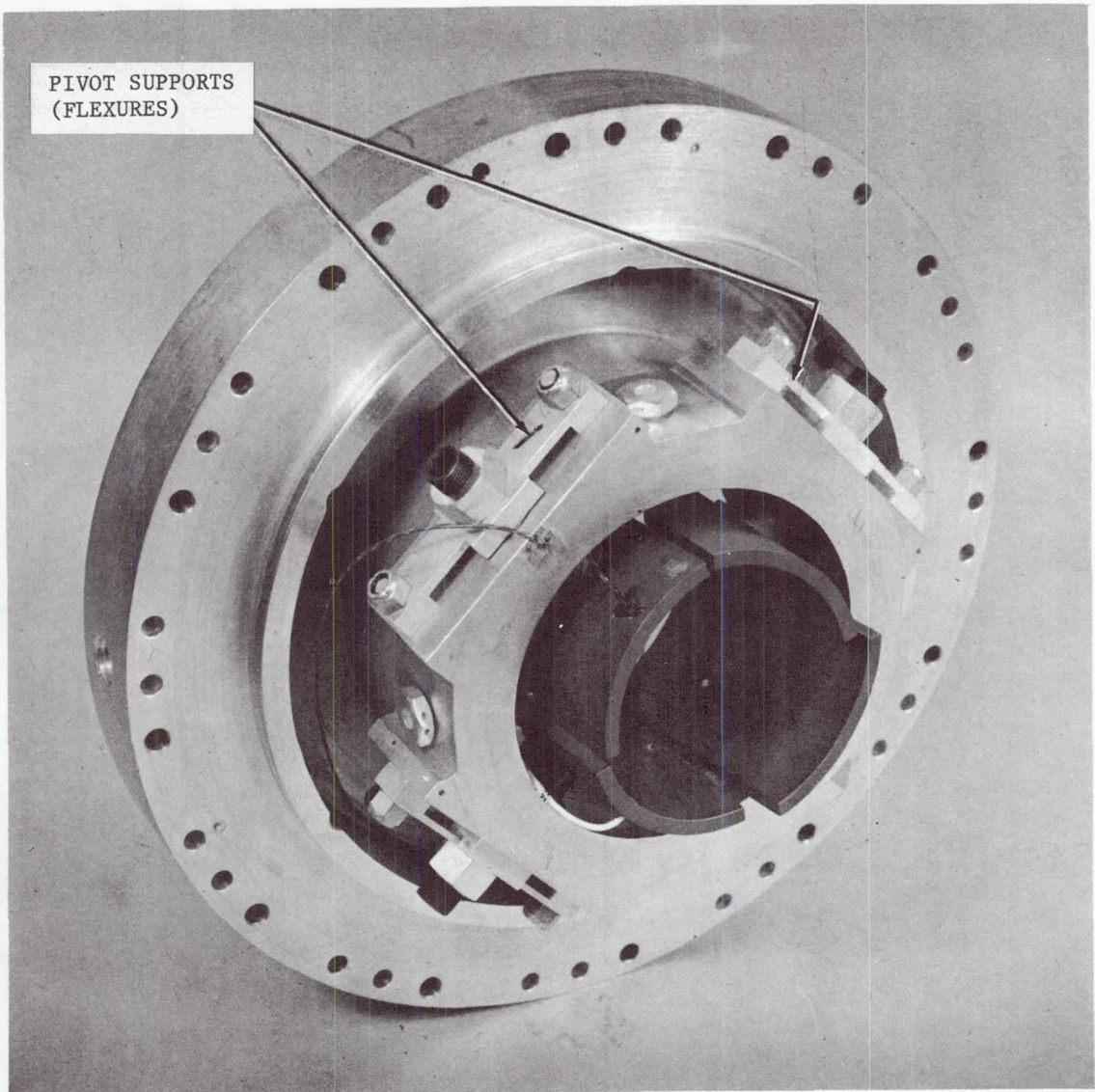
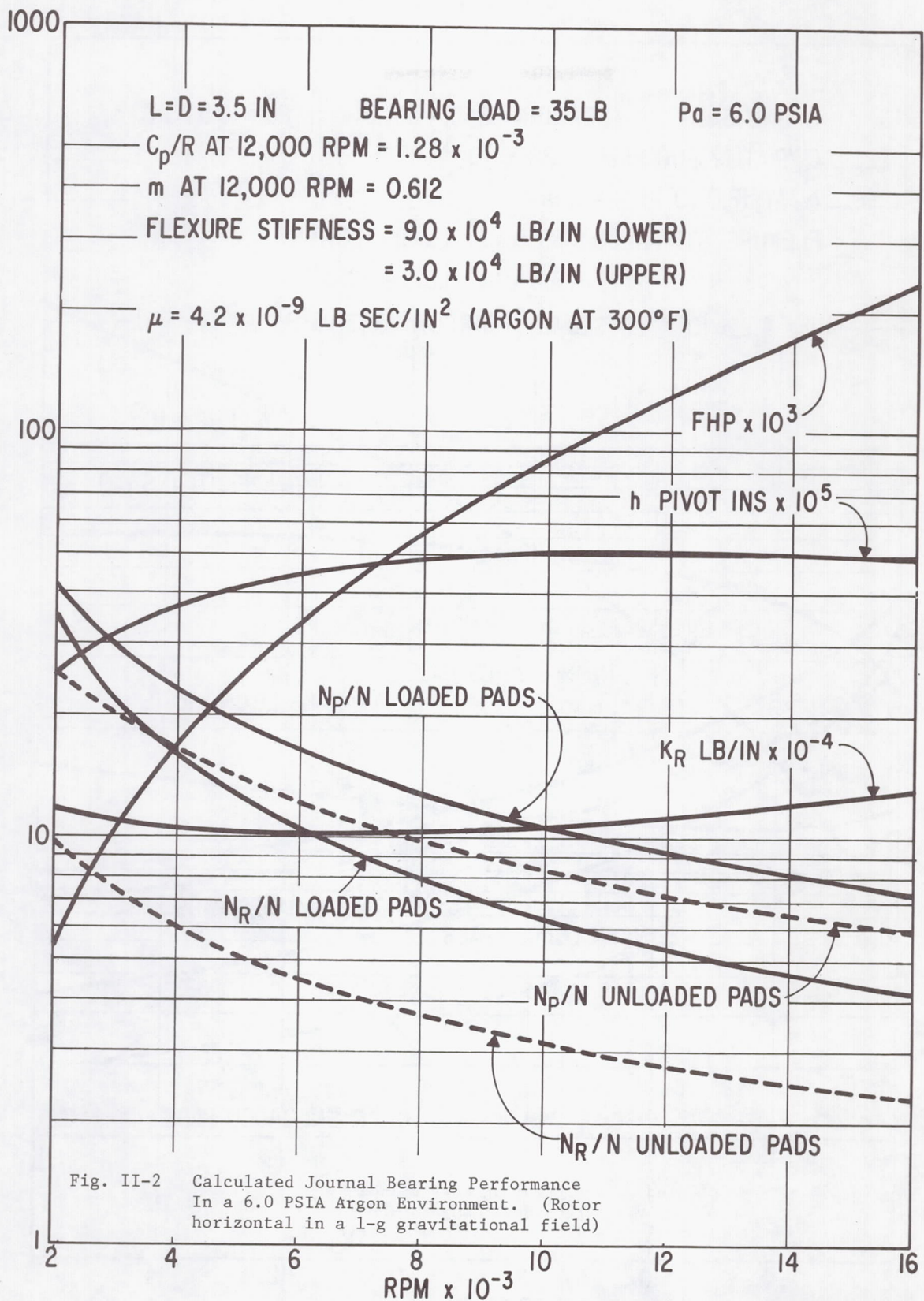
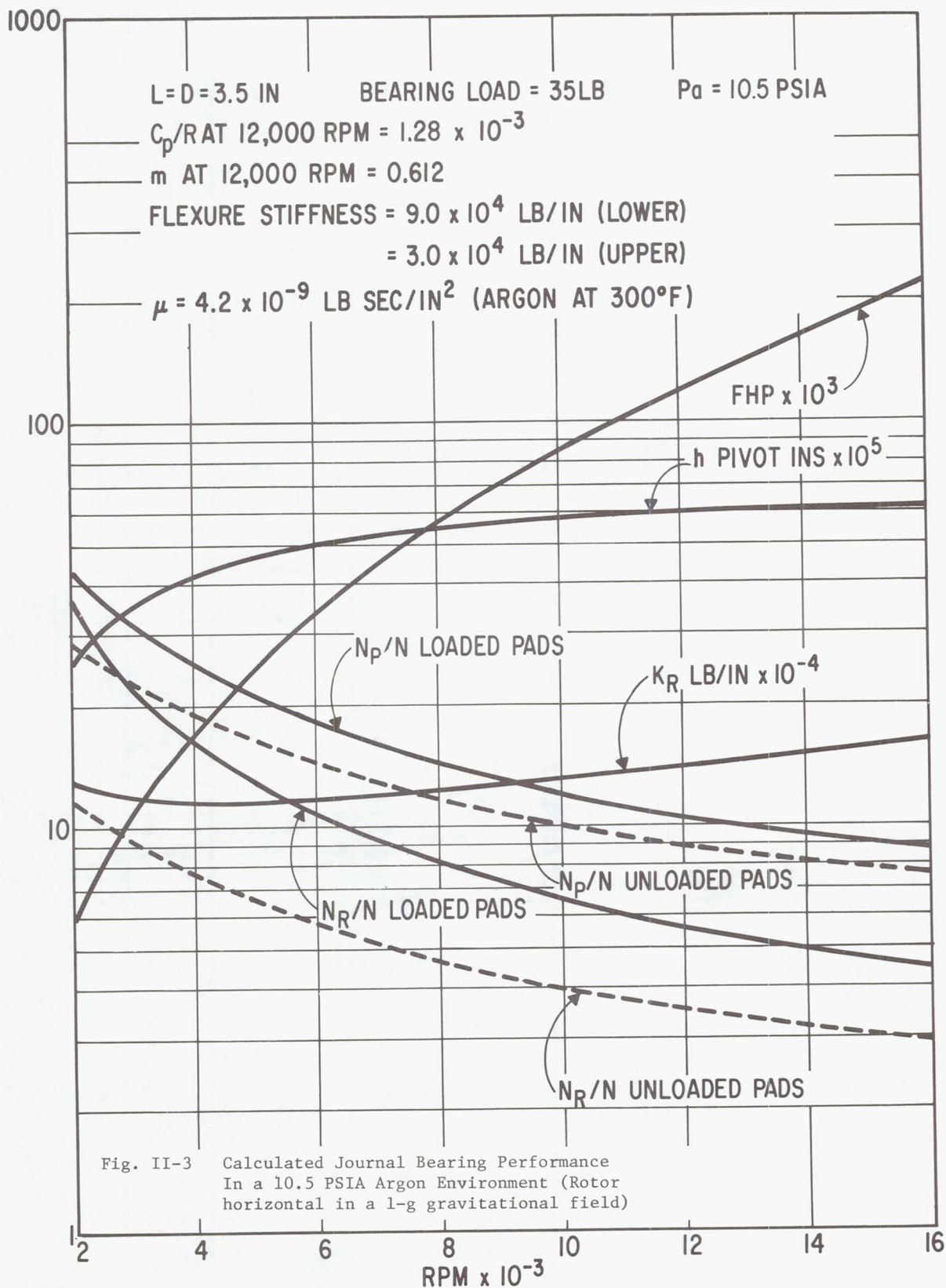
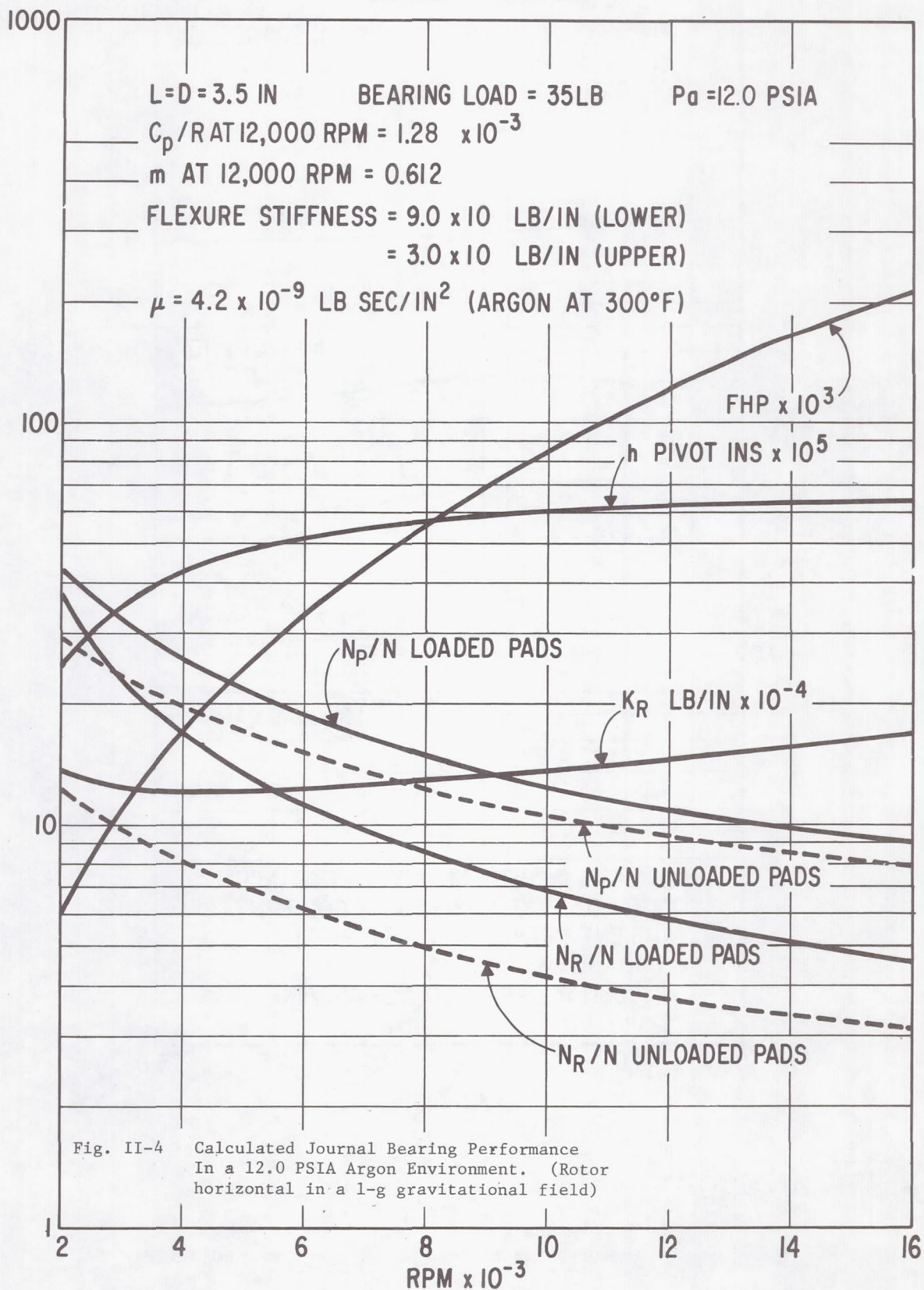


Fig. II-1 View of a Journal Bearing Assembly
Showing the Pivot Supports







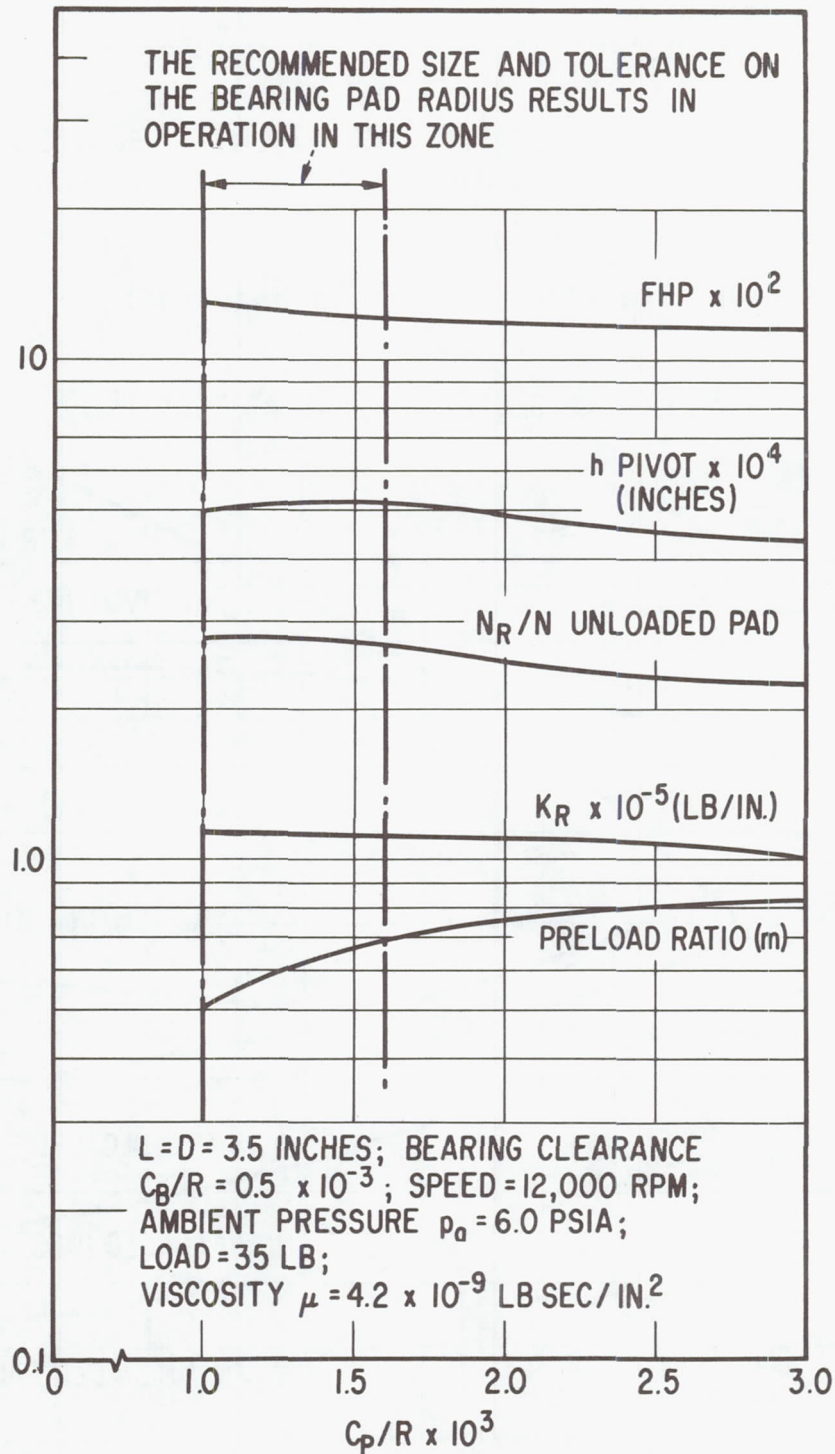


Fig. II-5 Calculated Effect of Machined Clearance Ratio (C_p/R) Variation on Journal Bearing Performance in a 6.0 PSIA Argon Environment (Rotor horizontal in a 1-g gravitational field)

Provisions for External Pressurization of Journal Bearings

The average loading on the journal bearings at start-up is approximately 2.35 PSI in a 1-g gravitational field when the shaft is horizontally oriented. Although recent tests have shown that chrome oxide bearing coatings can survive many hydrodynamic starts and stops at bearing loads up to 4 PSI, hydrostatic bearings have nonetheless been built into the hydrodynamic journal bearings. This feature greatly reduces the start-up friction torque and, consequently, allows the rotor to rapidly accelerate to design speed.

Hydrostatic lift-off is accomplished by feeding pressurized gas through a 0.013 inch diameter orifice in each of the two lower pads of the journal bearings. A recess in the surface of the pads, 0.0002 inches deep with an area of 0.75 square inches, distributes the hydrostatic gas within the bearing. Gas is fed to the pad orifice through drillings in the body of the pivot rod. These drillings are positioned in such a manner that the pivot contact area is not interrupted. This ensures that pivot fretting problems will not be introduced by the lift-off system. In order to preclude the possibility of leakage of the gas film through the orifice causing deterioration of the hydrodynamic bearing performance under normal conditions of operation, the orifices have been equipped with check valves. These valves consist of an "O" ring seal which is lifted off the valve seat by the hydrostatic pressure when the lift-off system is in operation. The elasticity of the "O" ring maintains the required seal during hydrodynamic operation of the bearings. Design of the supply-gas feed line and check valve is shown in Figure II-6. Figure II-7 is a photograph of an instrumented bearing pad, pivot-rod and check valve parts. Figure II-8 shows the recess and orifice in the surface of a bearing pad.

The hydrostatic lift-off bearings have been designed to provide approximately 0.4 Mils film thickness at the pivot point for a supply pressure of 100 PSIA. The total flow rate of argon through two hydrostatic journals will be about 2.6×10^{-4} pounds per second. To prevent the rotor from contacting the unloaded pads, which are not provided with hydrostatic lift-off capabilities, jacking gas should not be supplied to the journal bearings when the rotor is operating in a vertical position or a zero-g gravitational field.

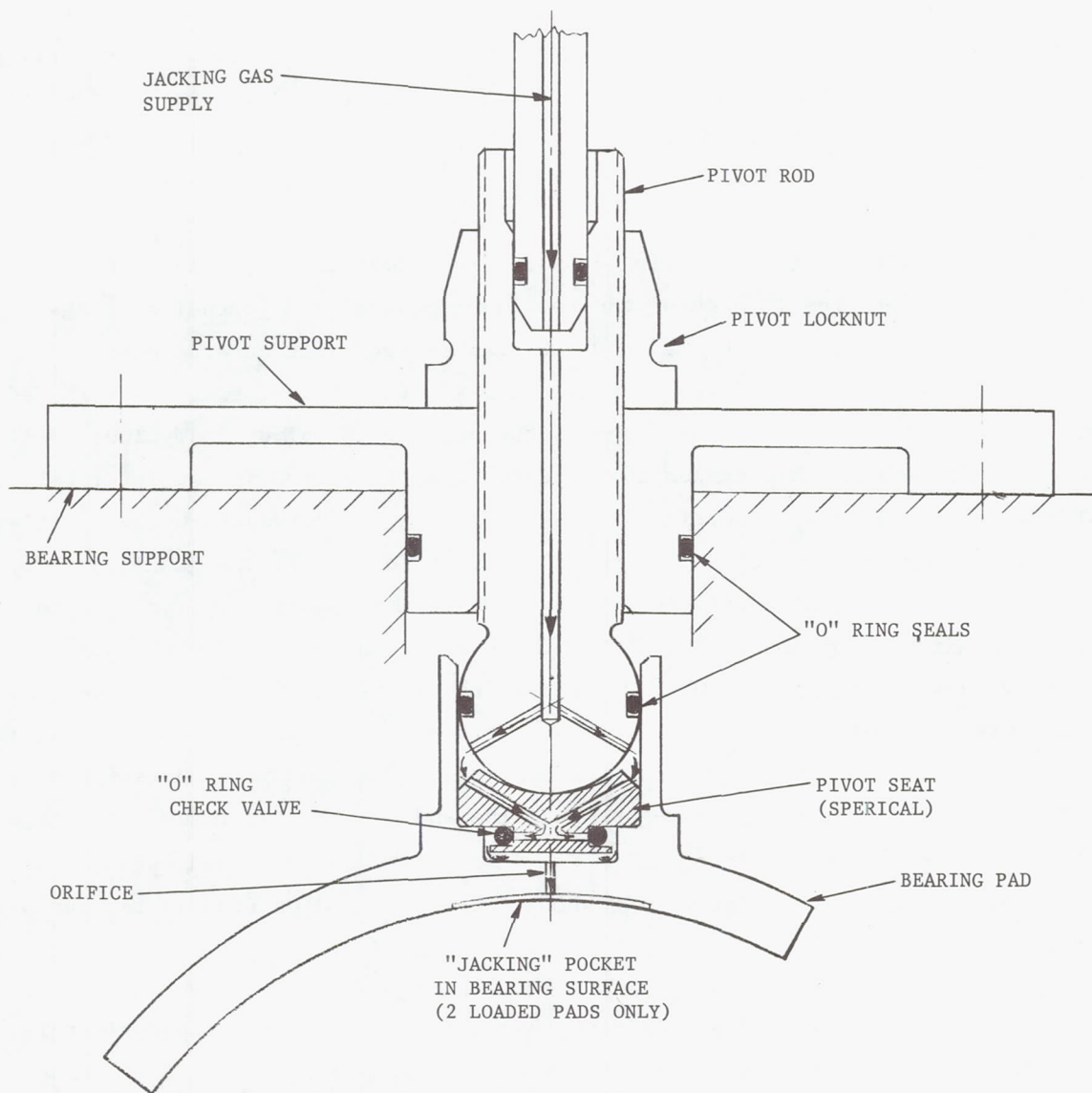


Fig. II-6 Details of the Journal Bearing Jacking Gas System

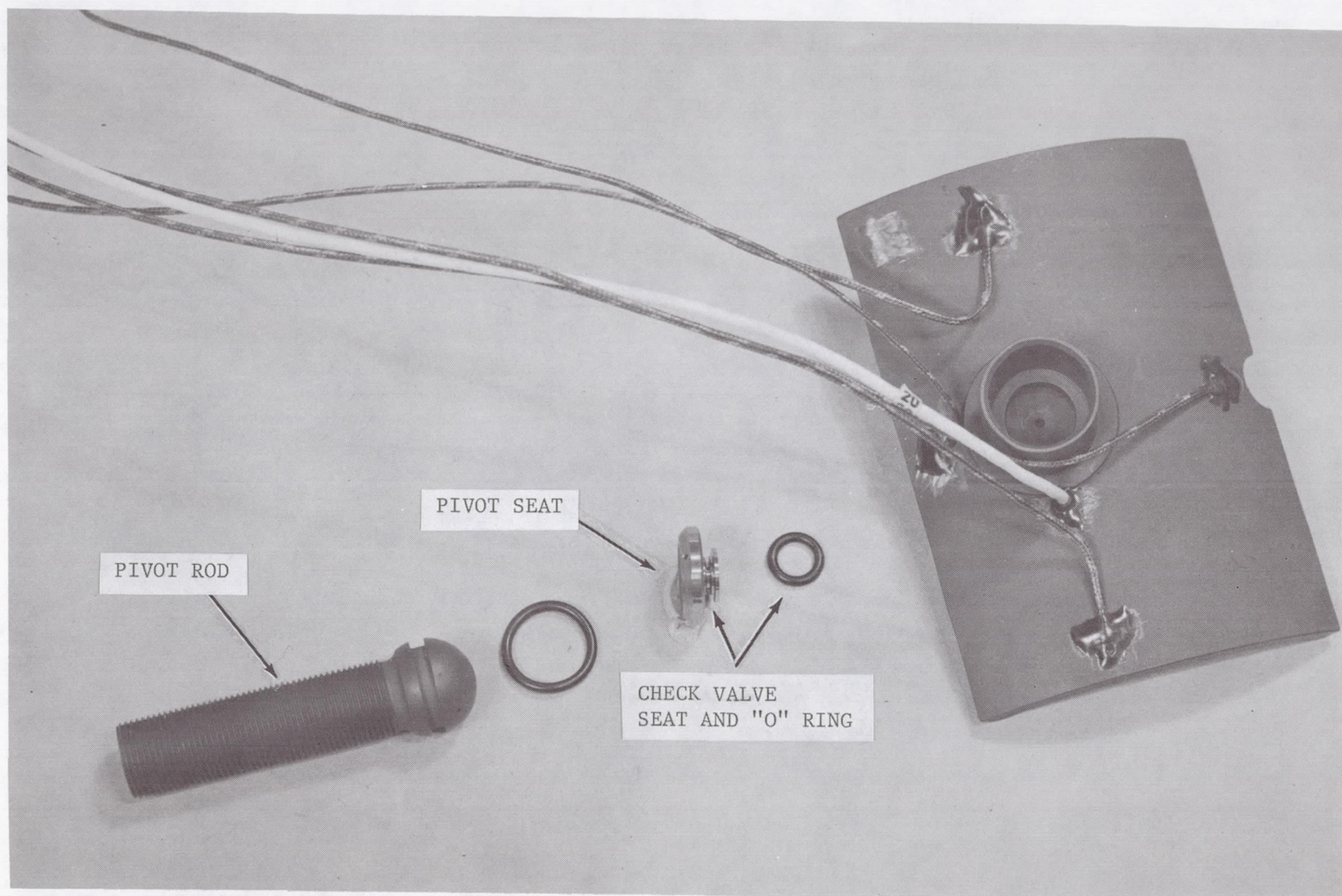


Fig. II-7 View of a Fully Instrumented Bearing Pad With Pivot Rod, Pivot Seat and Check Valve Parts

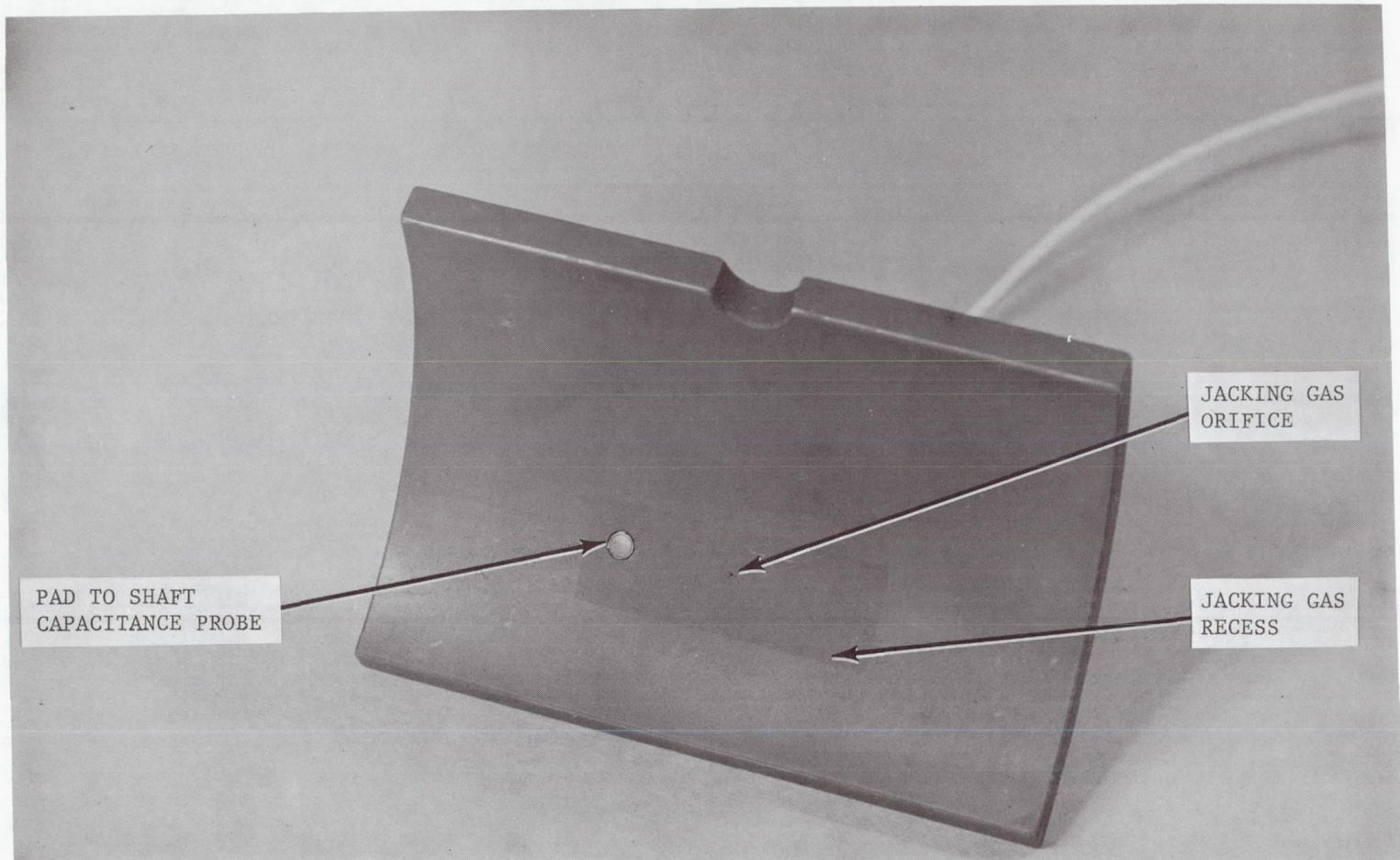


Fig. II-8 View of the Surface of a loaded Pad Showing the Pad to Shaft Capacitance Probe and the Jacking Gas Orifice and Recess

Performance Characteristics of the Hydrodynamic Thrust Bearing

The design of the turboalternator is such that the thrust load, at design conditions, is in the rearward direction, i.e., directed from the turbine towards the alternator.

The thrust bearing has been designed to operate satisfactorily under the following conditions:

1. in any orientation of the turboalternator,
2. at any ambient pressure above 6 psia, and
3. with small misalignments which may occur during operation.

As previously noted, a helical-grooved (Whipple plate) hydrodynamic bearing with a flexibly-mounted stator was selected. This bearing was designed using analytical and computational procedures that were previously developed and programmed by MTI. These take full account of gas compressibility effects, as well as of the important geometrical factors (radius ratio, seal-to-groove ratio, groove width and depth ratios, and helix angle).

To achieve compact, low power-loss design, this bearing is built around the hydrostatic bearing which is used for start-up and shut down. In this design the radius of the row of hydrostatic orifices has been conservatively assumed to be the inner radius of the hydrodynamic bearing.

The 12,000 rpm design load for the hydrodynamic bearing is 85 pounds which is achieved at a film thickness of 1.1 Mils. Changes in orientation, however, can reduce this load to 30 pounds, at which time the film thickness will approach 1.8 Mils.

The flexible mount for the thrust stator has been designed such that the stator will accurately track dynamic misalignment of the thrust runner in the critical, high-load regions of operation. Such misalignment may result from manufacturing tolerances and from conical shaft motions during operation with mechanical

unbalance. The flexure mount also allows some degree of self-alignment of the stator to the average plane of the thrust runner.

The thrust bearing is maintained at near isothermal temperature, using liquid as the coolant. The calculated performance of the hydrodynamic thrust bearing at 6,000, 12,000 and 14,000 rpm is shown on Figures II-9, II-10 and II-11 respectively. Summaries of the design parameters and calculated design-point performance characteristics are given in Tables II-3 and II-4.

Figure II-12 shows the main and reverse thrust faces of the thrust runner and Figures II-13 and II-14 show the grooved surface of the hydrodynamic thrust bearing and the bearing support flexure respectively.

TABLE II-3

MAIN HYDRODYNAMIC THRUST BEARING DESIGN PARAMETERS

Configuration	Helical grooved, inward pumping
Thrust Runner Diameter, Inches	7.00
Helical-Grooved Bearing O.D., Inches	7.00
Helical-Grooved Bearing I.D., Inches	2.80
Groove Depth, Inches	0.0022
Number of Grooves	12
Stator Support Stiffness in Axial Direction, Lb./In.	38,600
Stator Support Stiffness in Tilt Direction, In.-Lb./rad.	99,000
Stator Temperature, °F	216
Runner Temperature, °F	220
Runner Material	AMS 6415 (AISI 4340)
Stator Material	AMS 4027 (aluminum 6061-T6)
Stator and Runner Surfacing Material	Chrome Oxide

TABLE II-4

TURBOALTERNATOR MAIN HYDRODYNAMIC THRUST BEARING CALCULATEDPERFORMANCE CHARACTERISTICS

All data given below is based upon the following bearing operating conditions:

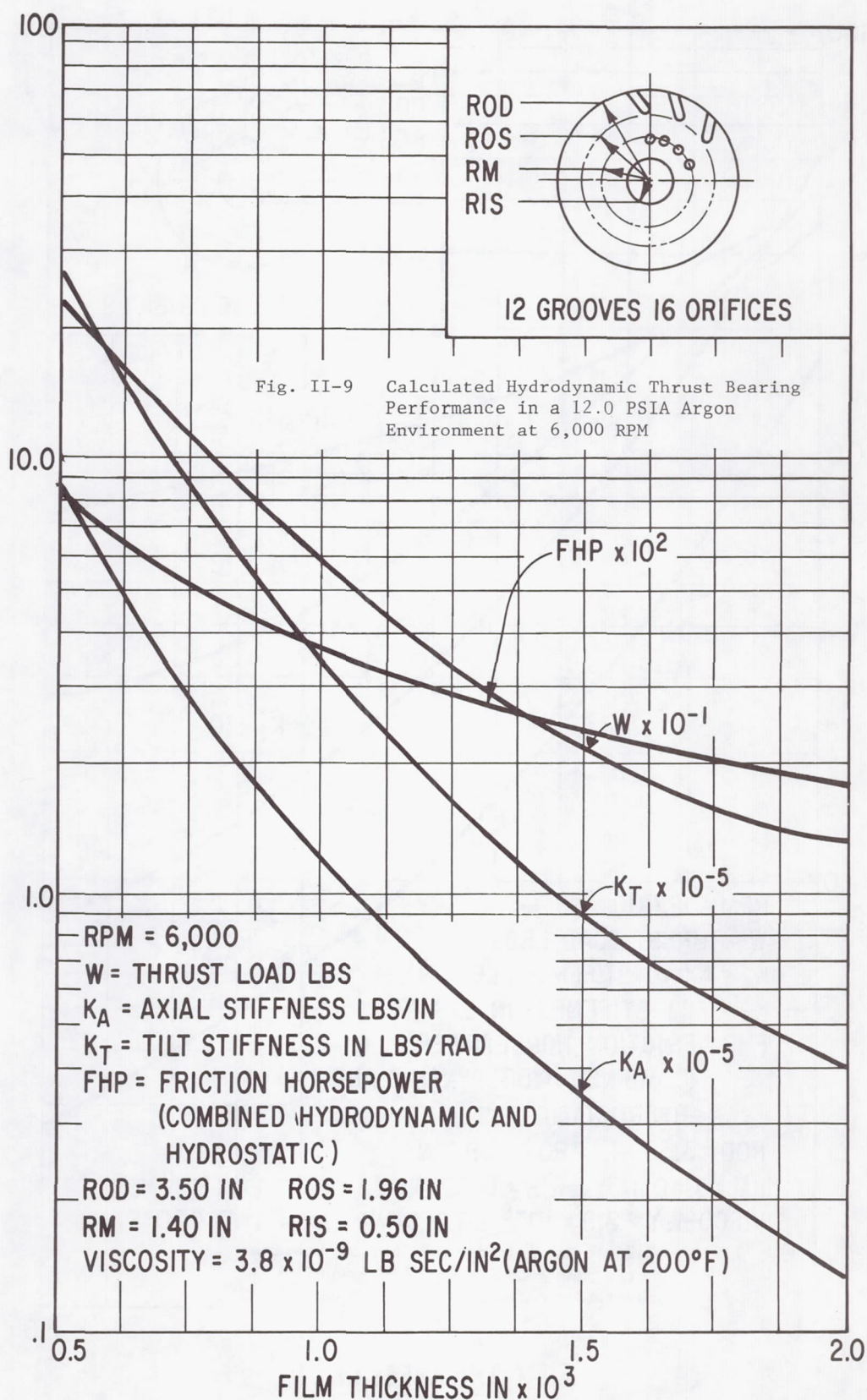
Rotor Speed	12,000 RPM
Lubricant Gas	Argon
Bearing Temperature	200°F
Ambient Pressure	12.0 PSIA

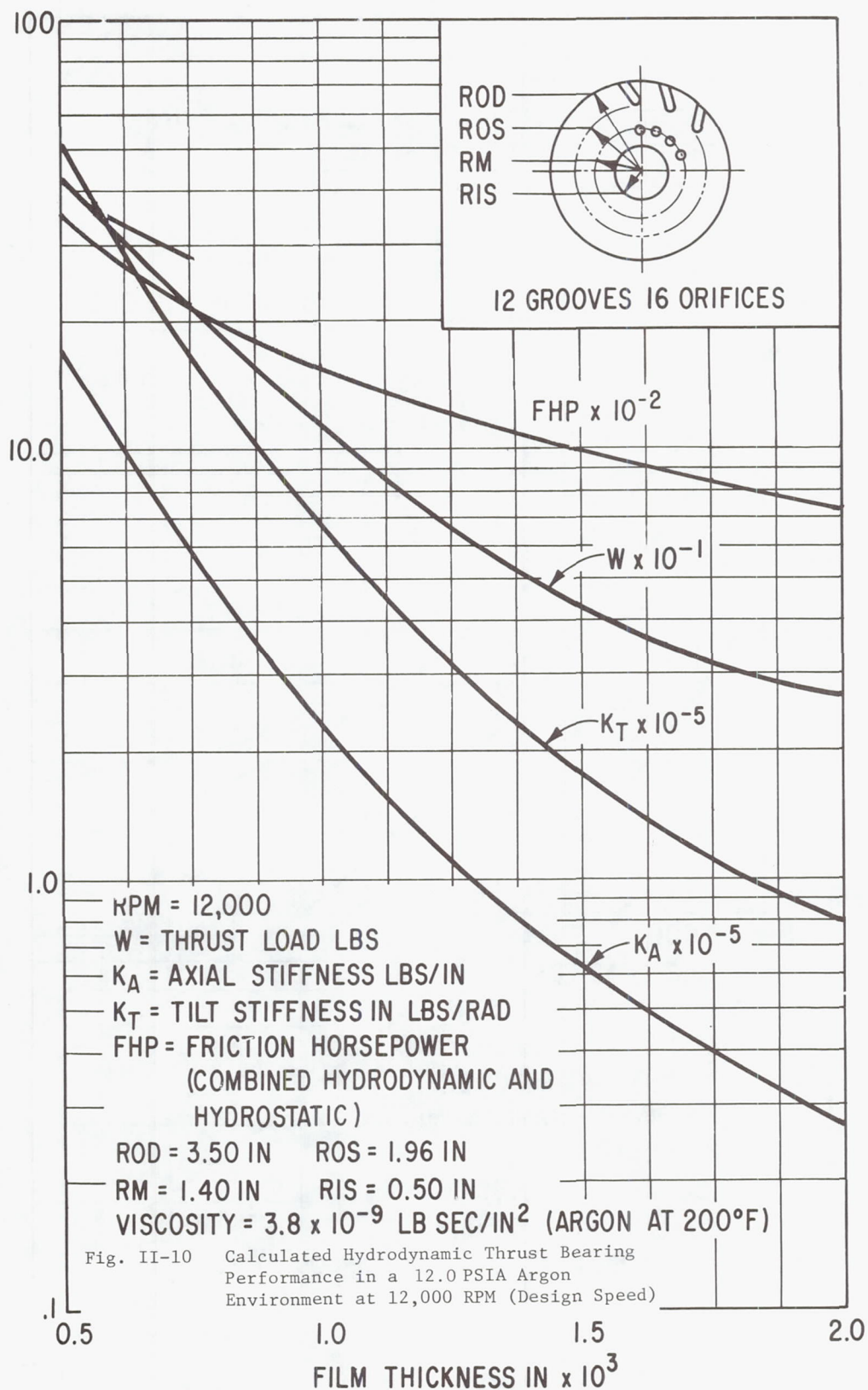
a) Vertical Operation in a 1-g gravitational field (turbine end up)

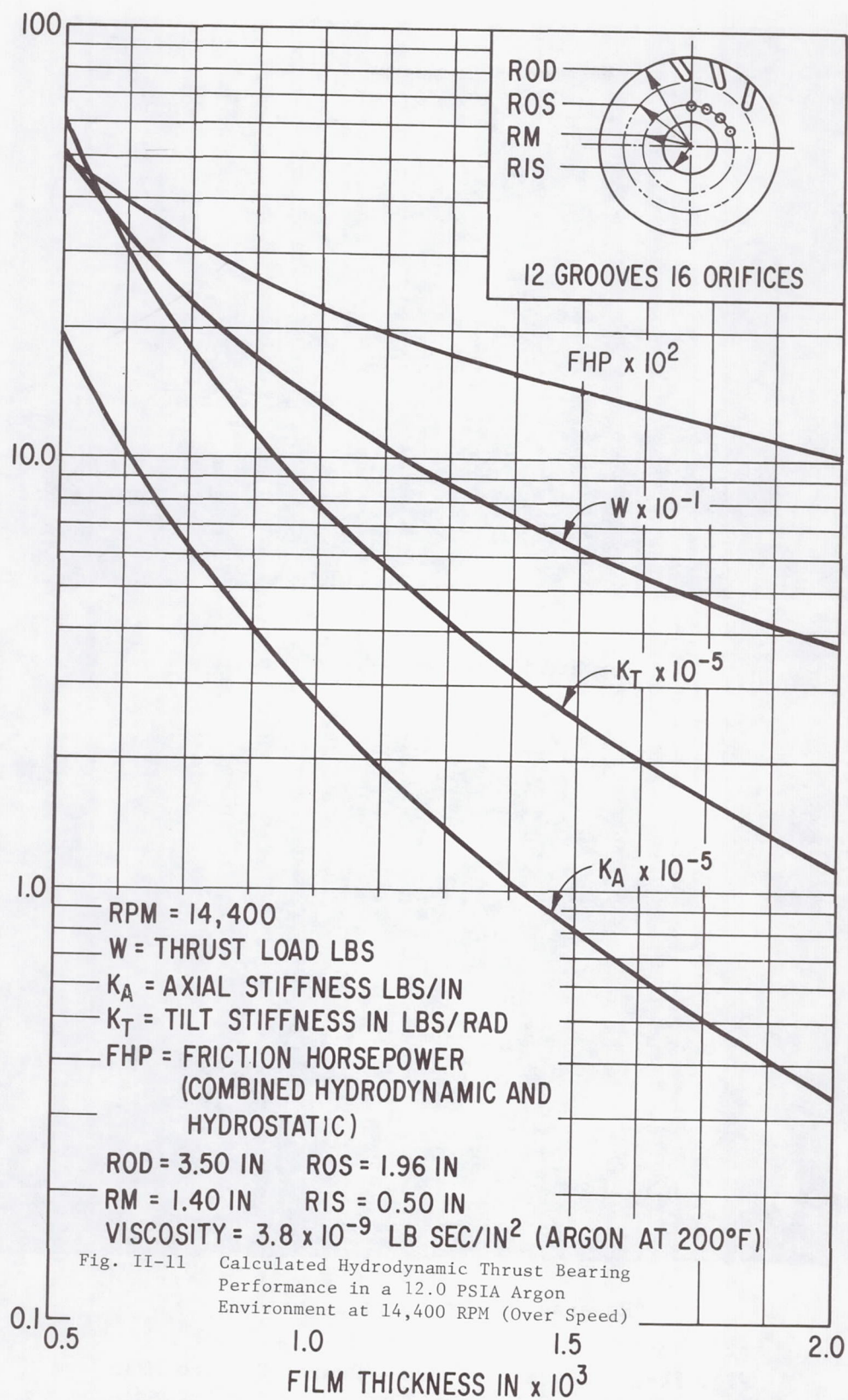
Bearing Load, Pounds	85.0
Friction Loss, Watts (Combined hydrodynamic and hydrostatic main thrust bearing)	104.0
Operating Bearing Clearance, Mils	1.12
Axial Gas Film Stiffness, Lb/In.	1.55×10^5

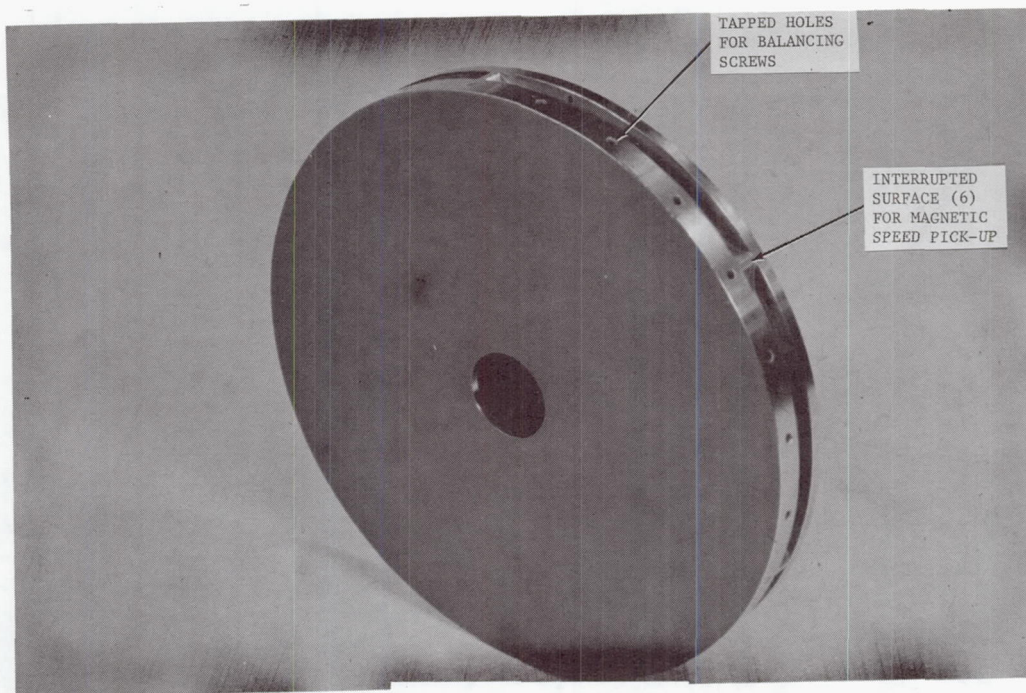
b) Space Operation in a zero-g gravitational field

Bearing Load, Pounds	30
Friction Loss, Watts (Combined hydrodynamic and hydrostatic main thrust bearing)	59.0
Operating Bearing Clearance, Mils	1.8
Axial Gas Film Stiffness, Lb/In.	0.35×10^5

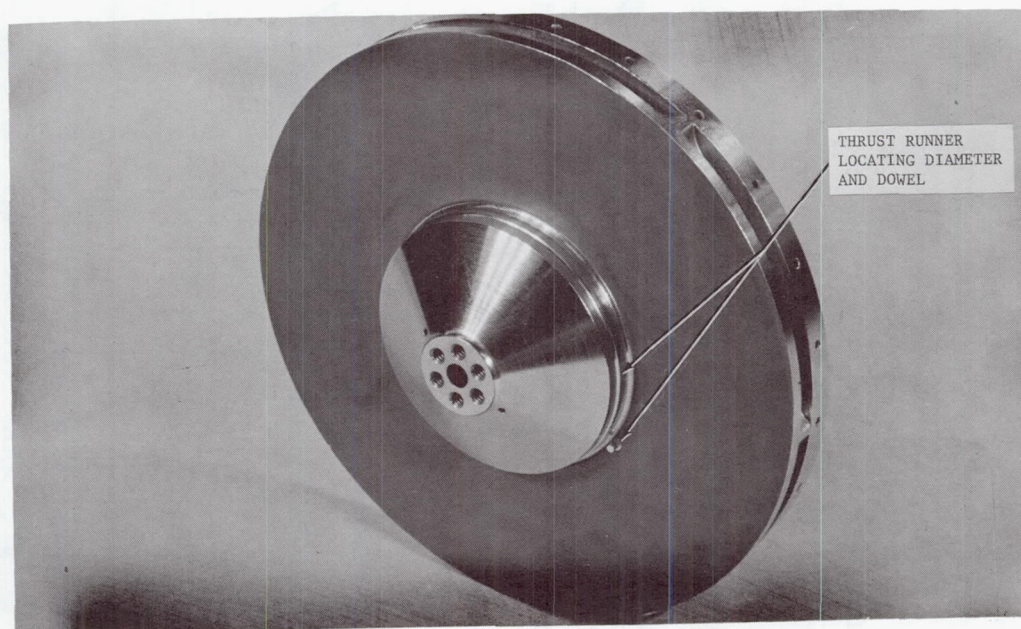








Forward Main-Bearing Surface



Reverse Thrust-Bearing Surface

Fig. II-12 Views of Thrust Runner Showing Main and Reverse Thrust Bearing Surfaces

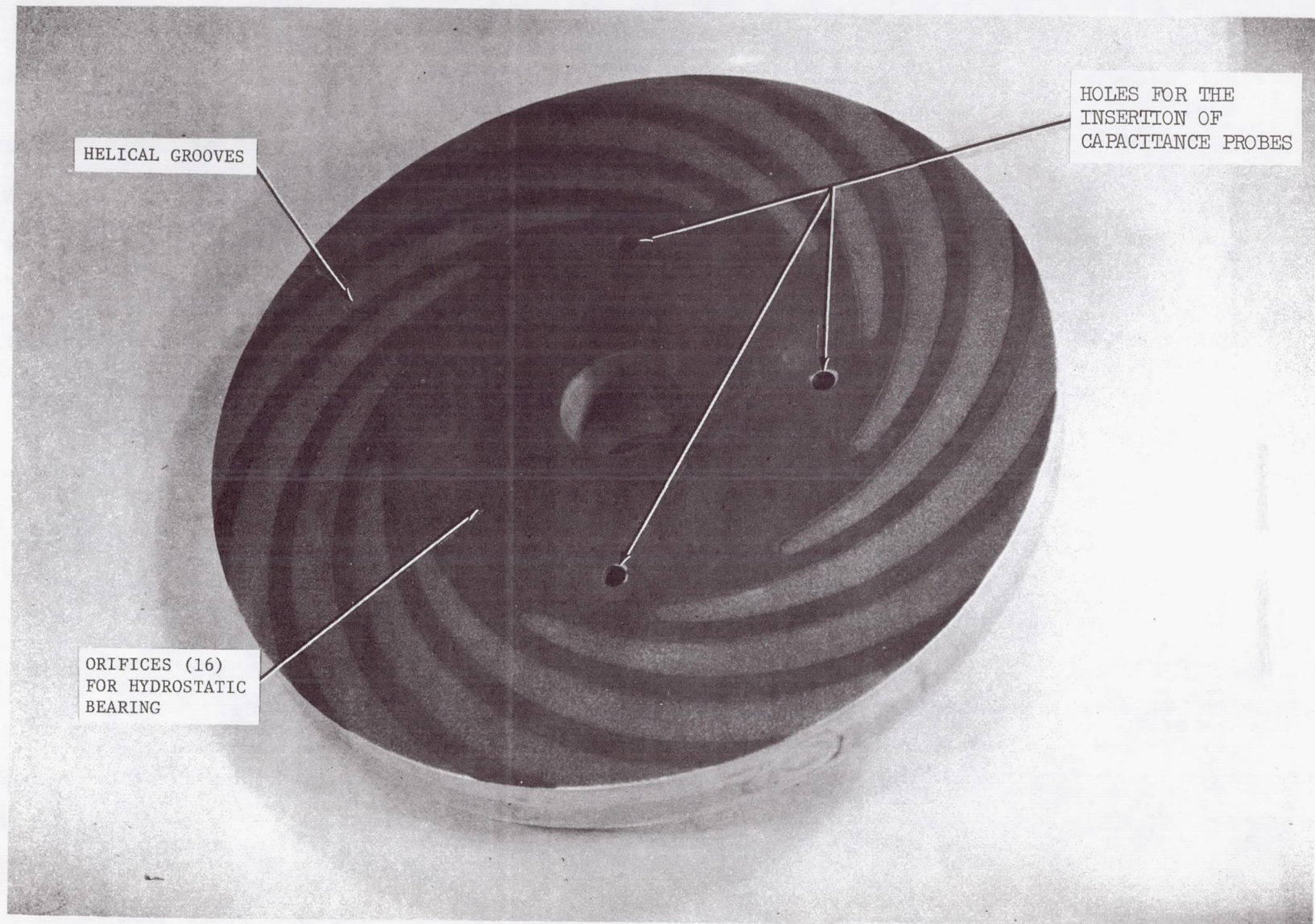


Fig. II-13 View of Combined Hydrodynamic-Hydrostatic
Main Thrust Bearing

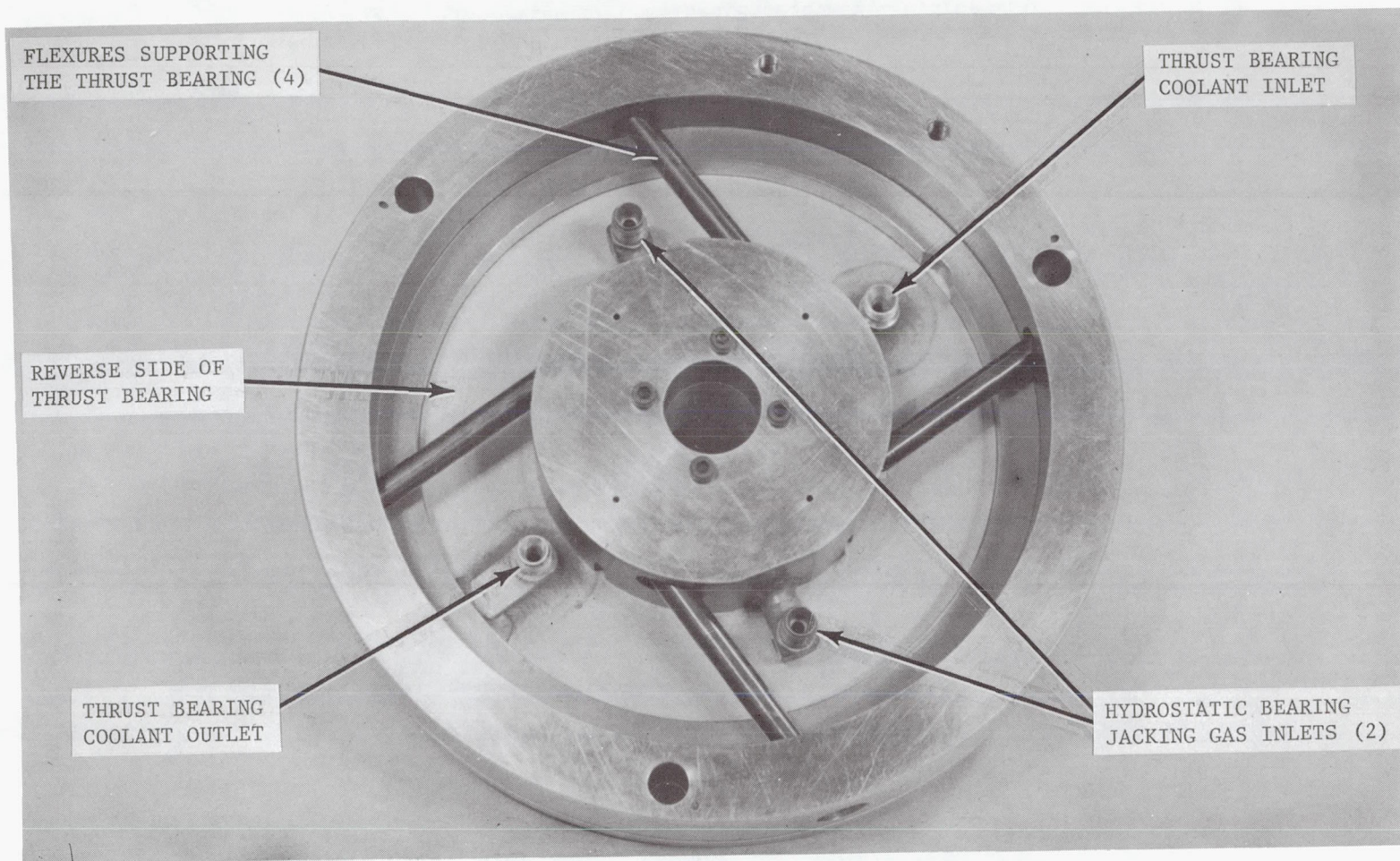


Fig. II-14 View of Combined Hydrodynamic-Hydrostatic
Main Thrust Bearing Mounted in Flexible
Support

Performance Characteristics of the Hydrostatic Thrust Bearings

The method by which the turboalternator is started and stopped may impose large thrust loads at low rotor speeds. Since a hydrodynamic thrust bearing cannot carry large thrust loads at low speeds, two hydrostatic thrust bearings have been provided, one on each side of the thrust runner.

The conditions under which these bearings have been designed to operate are as follows:

	<u>Reverse Thrust</u>	<u>Main Thrust</u>
Load (lb.)	100	250
Supply pressure (psia)	100	100
Ambient pressure (psia)	6	6

Both bearings are of the inherently compensated type in order to minimize the possibility of pneumatic hammer at ambient pressures below 6 psia (this being a possible condition at start-up).

The bearings were designed using existing computer programs which are basically a development of the "line feed" method, but which take account of the discreteness of the individual feeder holes and the circumferential flow between holes. In computing the orifice pressure drops, both the losses in the feeder holes and in the annular "curtain" areas around the rims of the holes are taken into account. Since in this case an inherently compensated design was selected for improved stability, the feeder hole diameters are large enough that the dominant restriction occurs in the annular "curtain" areas instead of inside the feeder holes.

The calculated performance of the main and reverse thrust hydrostatic bearings is shown on Figures II-15 and II-16 respectively. A summary of the design parameters and calculated design-point performance characteristics are given in Table II-5. Figure II-17 is a photograph of the reverse hydrostatic thrust bearing. The orifices in the main hydrostatic thrust bearing can be seen in Figure II-13.

TABLE II-5

HYDROSTATIC THRUST BEARING DESIGN PARAMETERS AND CALCULATEDPERFORMANCE CHARACTERISTICSMain Hydrostatic Bearing

Bearing OD, Inches	3.92
Bearing ID, Inches	1.00
Number of Orifices	16
Diameter of Orifices, Inches	0.028
Hydrostatic Gas Supply Pressure at Start-Up, PSIA	100.0
Hydrostatic Gas Supply Temperature at Start-Up ° F	100
Ambient Pressure, PSIA	6.0
Bearing Load at Start-Up, Pounds	250
Bearing Film Thickness at Start-Up, Mils	1.4
Argon Gas Flow at Start-Up Pounds/Sec.	0.0058
Stator Material	AMS-4027 (aluminum 6061-T6)
Stator Surfacing Material	Chrome Oxide

Reverse Hydrostatic Bearing

Bearing OD, Inches	4.92
Bearing ID, Inches	3.58
Number of Orifices	16
Diameter of Orifices, Inches	0.028
Hydrostatic Gas Supply Pressure at Start-Up, PSIA	100.0
Hydrostatic Gas Supply Temperature at Start-Up °F	100
Ambient Pressure, PSIA	6.0
Bearing Load at Start-Up, Pounds	100
Bearing Film Thickness at Start-Up, Mils	1.5
Argon Gas Flow at Start-Up, Pounds/Sec.	0.0063
Stator Material	AMS-5646E (AISI 347)
Stator Surfacing Material	Chrome Oxide

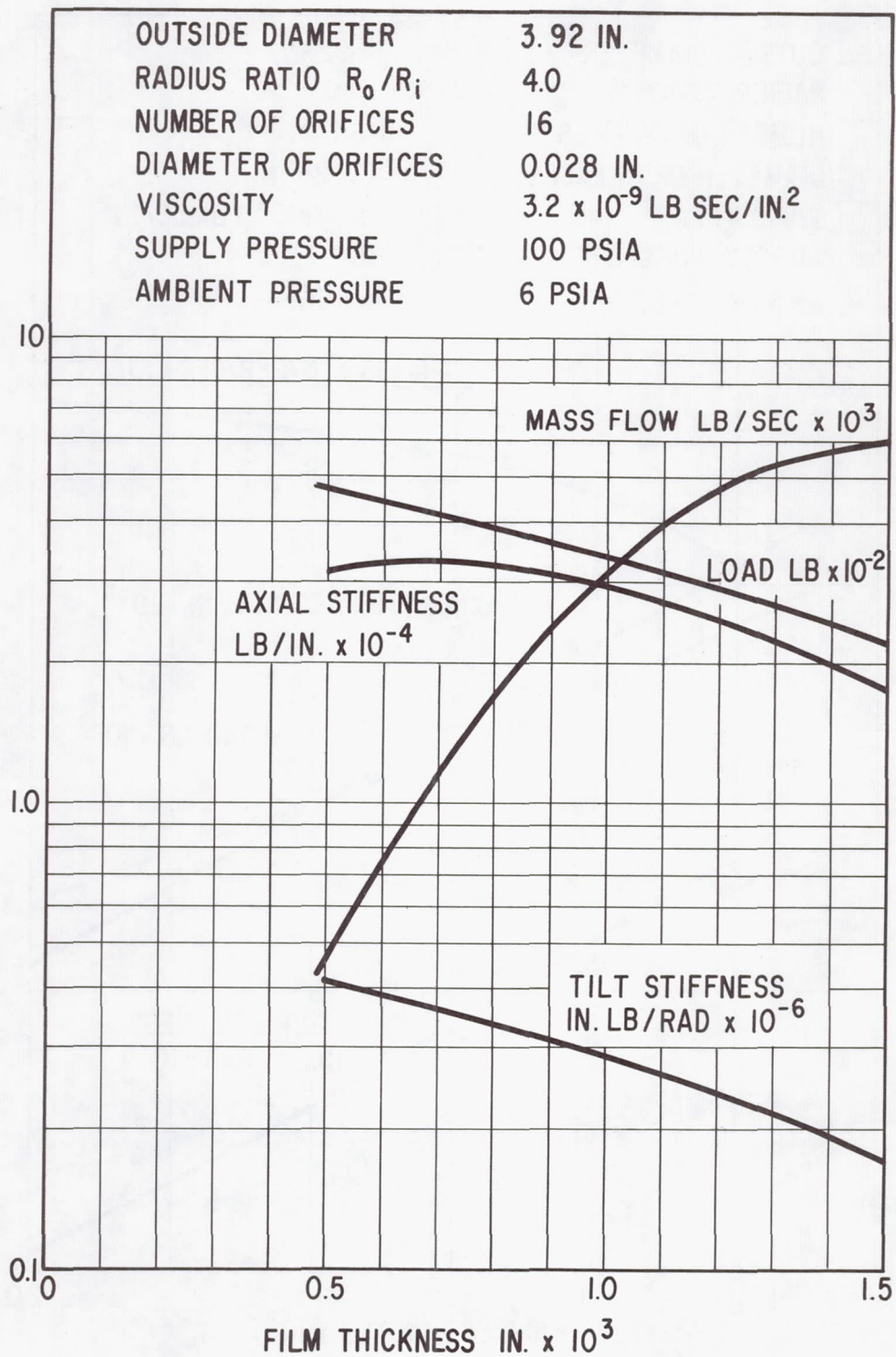


Fig. II-15 Calculated Performance of the Hydrostatic Main Thrust Bearing in a 6.0 PSIA Argon Environment

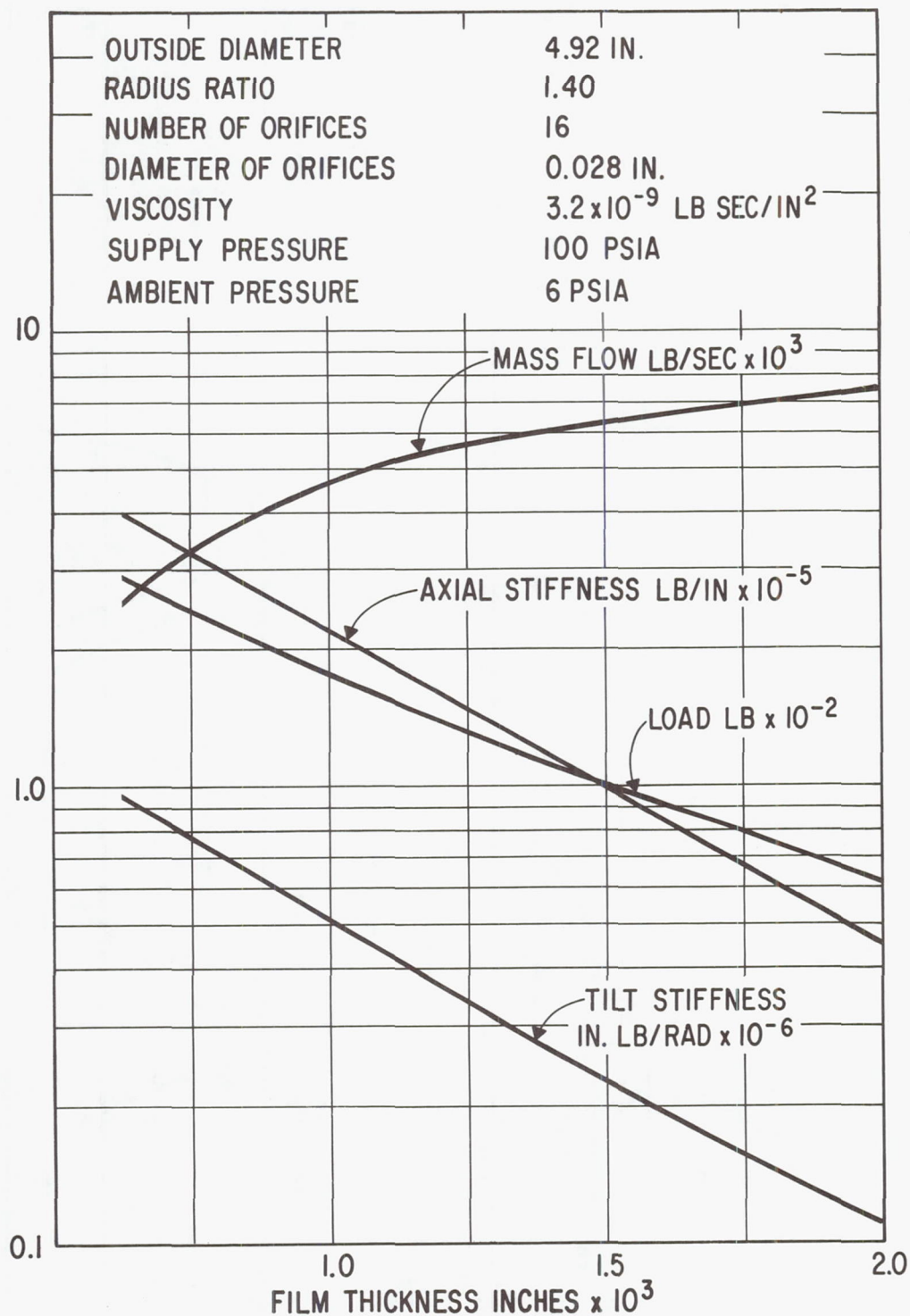


Fig. II-16 Calculated Performance of the Hydrostatic Reverse Thrust Bearing in a 6.0 PSIA Argon Environment

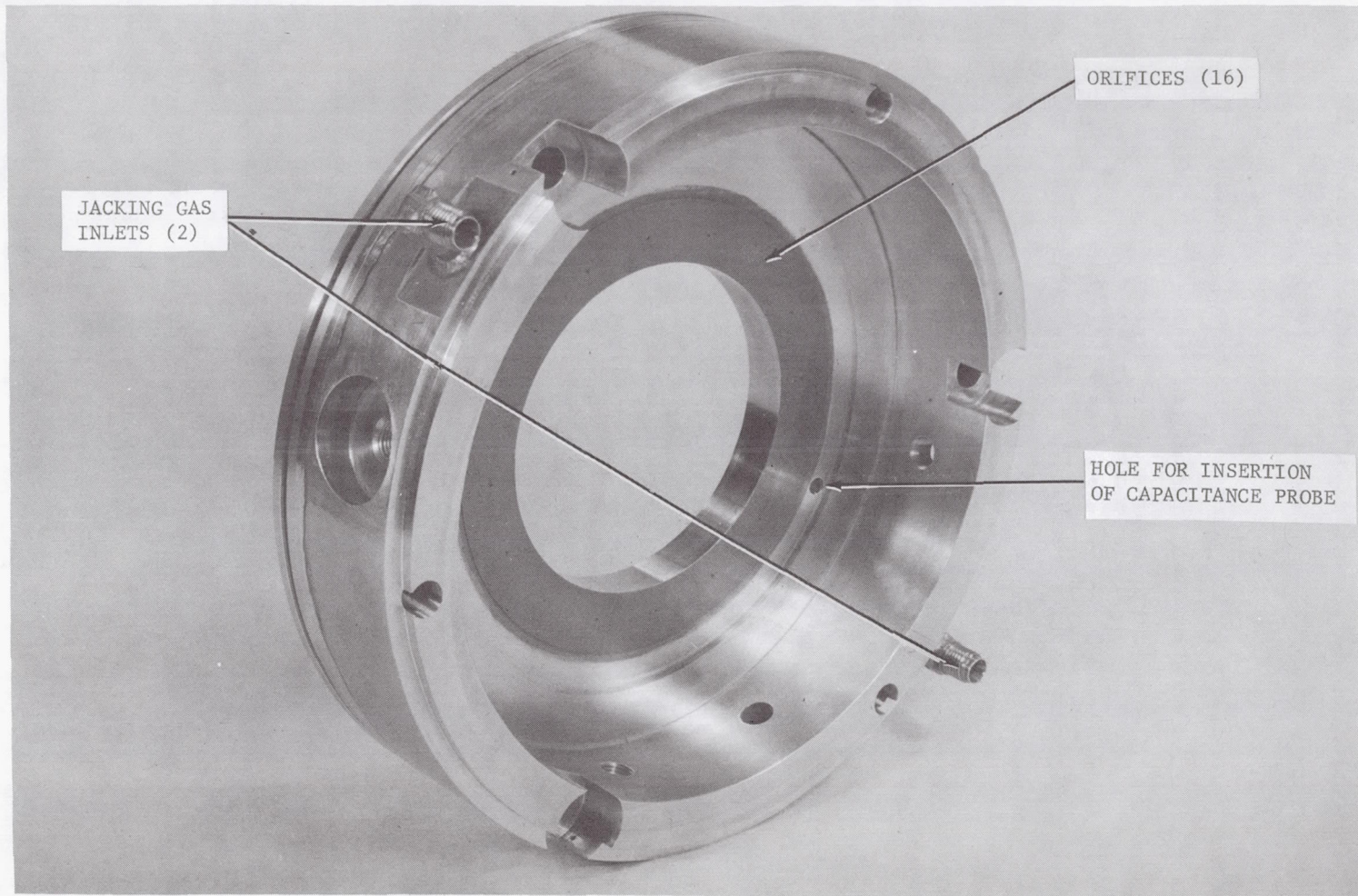


Fig. II-17 View of the Hydrostatic Reverse Thrust Bearing

Rotor-Bearing System Dynamics

It is particularly important in the design of gas-bearing machinery to be sure that the rotor-bearing system will not develop excessive amplitudes of either stable or unstable vibration over the desired range of operating speeds. The simplest and most common form of vibration is synchronous rotor whirl resulting from excitation of transverse resonant frequencies of the rotor in its rigid or flexible beam modes. The excitation most commonly derives from mechanical unbalance of the rotor, although other forms of excitation are possible. The speeds at which transverse resonant beam modes of rotor whirl can occur are called the transverse critical speeds of the rotor.

Because of the limited amount of damping in a gas bearing, it is difficult to design a gas-bearing machine for safe operation through a "bent shaft" critical speed unless some auxiliary means of damping is provided. The design philosophy used on all previous gas-lubricated machinery developments required that the "bent shaft" critical should be well above the maximum operating speed.

The alternator was expected, however, to exert electromagnetic forces of a significant magnitude on the rotor at a fundamental frequency of two-per-rev. To ensure that the two-per-rev did not excite the rotor in the "bent shaft" mode of vibration, the design philosophy was extended. The resulting criterion of turboalternator design was that the "bent shaft" critical should be in excess of twice the overspeed condition.

A critical speed analysis for the turboalternator was carried out using a Holzer-type calculation programmed for digital computer solution. The calculation provides both the critical speeds and the associated rotor displacement mode shapes, and includes the effects of rotor mass, rotor stiffness, bearing mass, bearing stiffness, bearing support stiffness, and rotor gyroscopic effects.

The critical speeds for the final design of the rotor-bearing system are plotted in Figure II-18 as a function of journal bearing stiffness. Superimposed on this plot are the calculated journal bearing stiffnesses at 12.0 psia and 6.0 psia

ambient pressure as a function of speed (obtained from Figures II-2 and II-4). The intersections of the critical speed curves and the journal bearing stiffness curves identify the speeds at which rotor resonances could be expected to occur in the presence of sufficient rotor unbalance. The two lowest critical speeds are essentially rigid-body resonances of the rotor due to the stiffnesses of the gas film and the pivot-support flexures. It is seen from Figure II-18 that the two rigid-body resonances should occur in the 7,000 to 9,000 RPM range, which is sufficiently low to be of little concern to turboalternator operation. The third critical speed, which is slightly above 32,000 RPM, is the first free-free "bent shaft" critical of the rotor and is virtually unaffected by bearing stiffness. No influence of this critical speed would be expected at the 12,000 and 14,400 RPM design and overspeed conditions. Balancing of the rotor should prove, therefore, to be well within the state-of-the-art of present balancing techniques.

The value of pedestal stiffness used in the calculation of rotor critical speeds presented in Figure II-18 was determined from the measured values of upper and lower pivot support stiffness and calculated values of pivot/seal contact zone stiffness.

The rigid-body critical speed mode shapes for the rotor are plotted in Figure II-19. It is seen that for pure modal excitation, the No. 1 journal would experience the largest resonant amplitudes at the lowest rigid-body critical, while the No.2 journal would experience the largest resonant amplitudes at the second rigid-body critical. The nodal point for the lowest rigid-body critical is located in the plane of the alternator, while the nodal point for the second critical speed is located outboard of the turbine wheel.

The calculated steady-state plus dynamic bearing loads for a horizontal rotor orientation in a 1-g field and 0.005 ounce-inches of unbalance in the turbine plane (the rotor being otherwise perfectly balanced and not subjected to electromagnetic forces) are plotted in Figure II-20 as a function of speed. The value of 0.005 ounce-inches of unbalance was assumed to occur over a period of 10,000 hours due to unsymmetrical mass shift (creep) in the turbine. It is seen from Figure II-20 that the unbalance causes both journals to resonate simultaneously between 9,000 and 10,000 RPM. There is no distinction between the first and second rigid-body criticals because of the closeness of these two criticals.

It should be pointed out that the bearing damping values used in the calculation of the dynamic bearing loads of Figure II-20 are, rigorously speaking, valid only at 12,000 rpm. Also, the values of flexure stiffness used in the calculations were design values and did not include pivot zone contact stiffnesses. Hence, the absolute values of bearing force are approximate and the speeds at which the critical speeds are seen to occur in Figure II-20 are somewhat higher than those shown in Figure II-18. At the speed of 12,000 rpm it is seen that the 0.005 ounce-inches of unbalance adds approximately 2.80 pounds of rotating load to the steady-state loading of the No. 1 journal bearing, and approximately 0.85 pounds of rotating load to the No. 2 journal bearing.

In lieu of using the rigorous analytical approach described in Section V of this report, it has been common practice to analyze, for design purposes, each of the pivoted pads as a completely uncoupled linear vibration system. The resonant frequency of each possible mode of pad vibration is calculated based on a simple one-degree-of-freedom model. A more-or-less intuitive design criterion has been to design the pads such that the resonant frequency of each vibration mode is at least 30 percent higher than the maximum operating speed of the machine. This implies that the pads should be able to track motions of the rotor with little phase lag. Hence, the dynamics of the pads should have little effect on rotor dynamics.

The pad frequencies which were computed are the roll and pitch resonant frequencies of the pad against the gas-film stiffness, and the radial resonant frequency of the pad, pivot-screw, and flexure assembly against the gas-film and flexure stiffnesses. Figures II-2 through II-4 show calculated ratios of roll and pitch resonant frequencies to rotor speed for both the loaded and unloaded pads (assuming horizontal rotor orientation in a 1-g gravitational field). It is seen that the pitch resonant frequencies of the No. 1 and No. 2 bearing pads are always greater than 6 times rotor speed for ambient pressures down to 6.0 psia. Similarly, the roll resonant frequencies of the No. 1 and No. 2 pads are always greater than twice rotor speed at ambient pressures down to 6.0 psia.

The calculated radial resonant frequencies of the No. 1 and No. 2 bearing pads were found to be well above rotor speed throughout the 14,400 rpm speed range. The response of the rotor-bearing system including the effect of electromagnetic forces is described in Section V of this report.

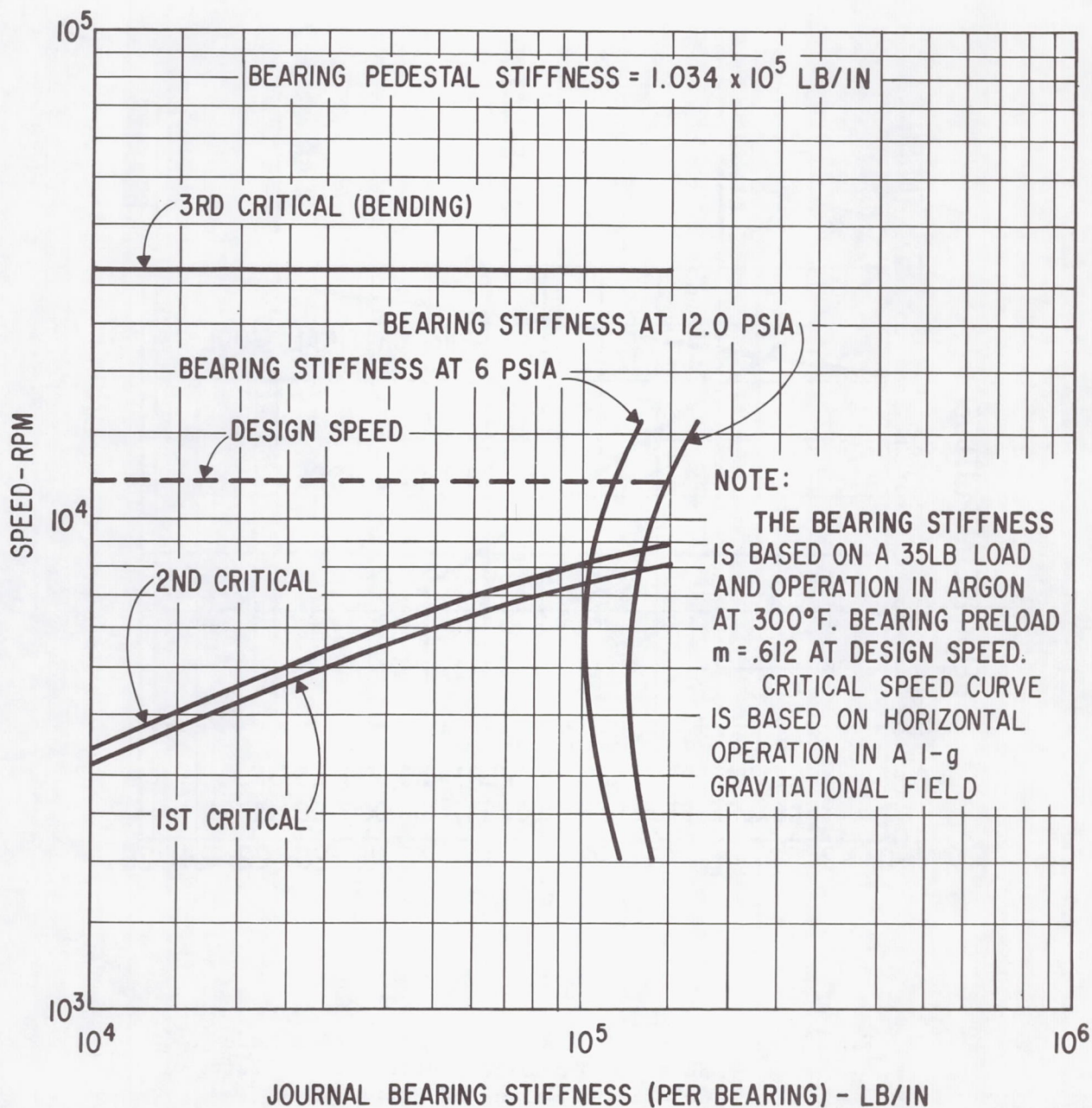


Fig. II-18 Critical Speed Versus Journal Bearing Stiffness for Turboalternator Rotor Bearing System

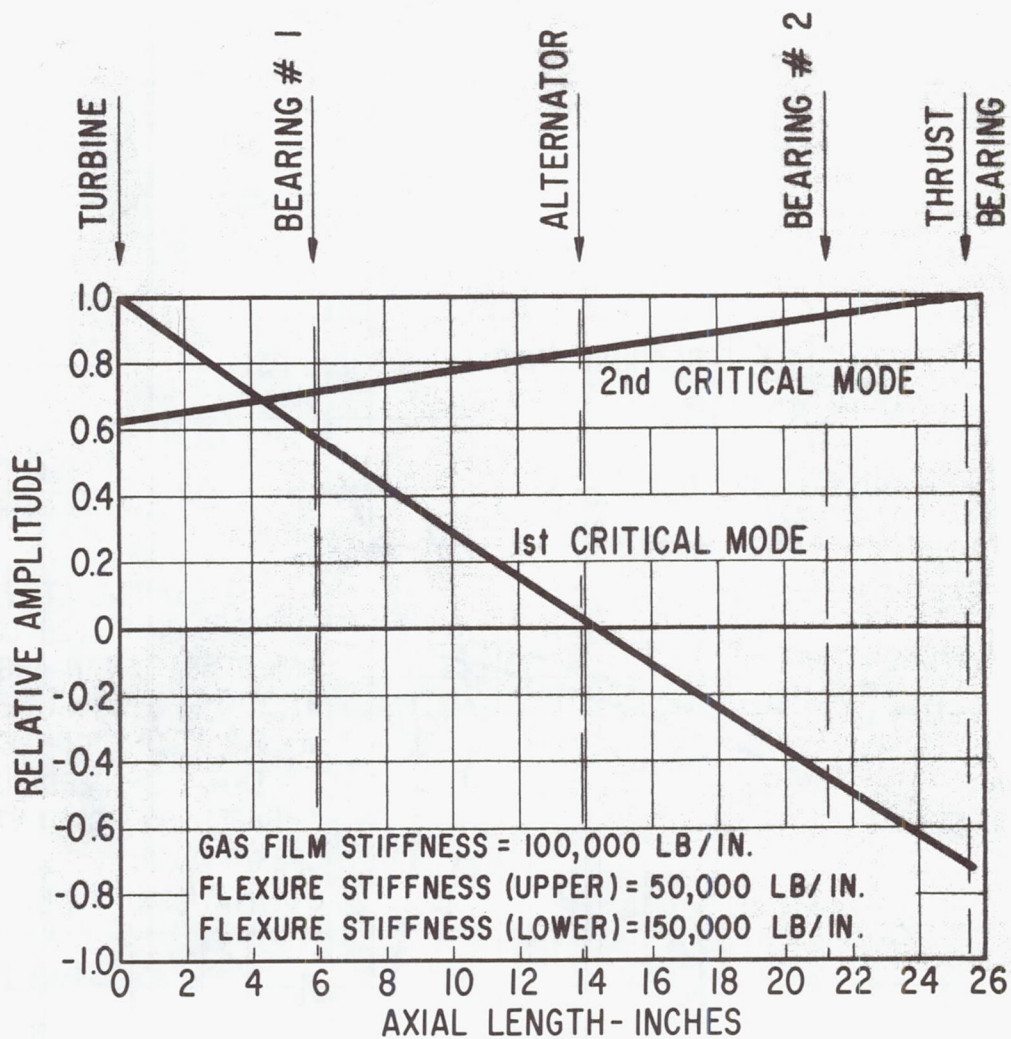


Fig. II-19 First and Second Critical Speed Mode Shapes - Turboalternator Rotor - Using Calculated Values of Stiffnesses

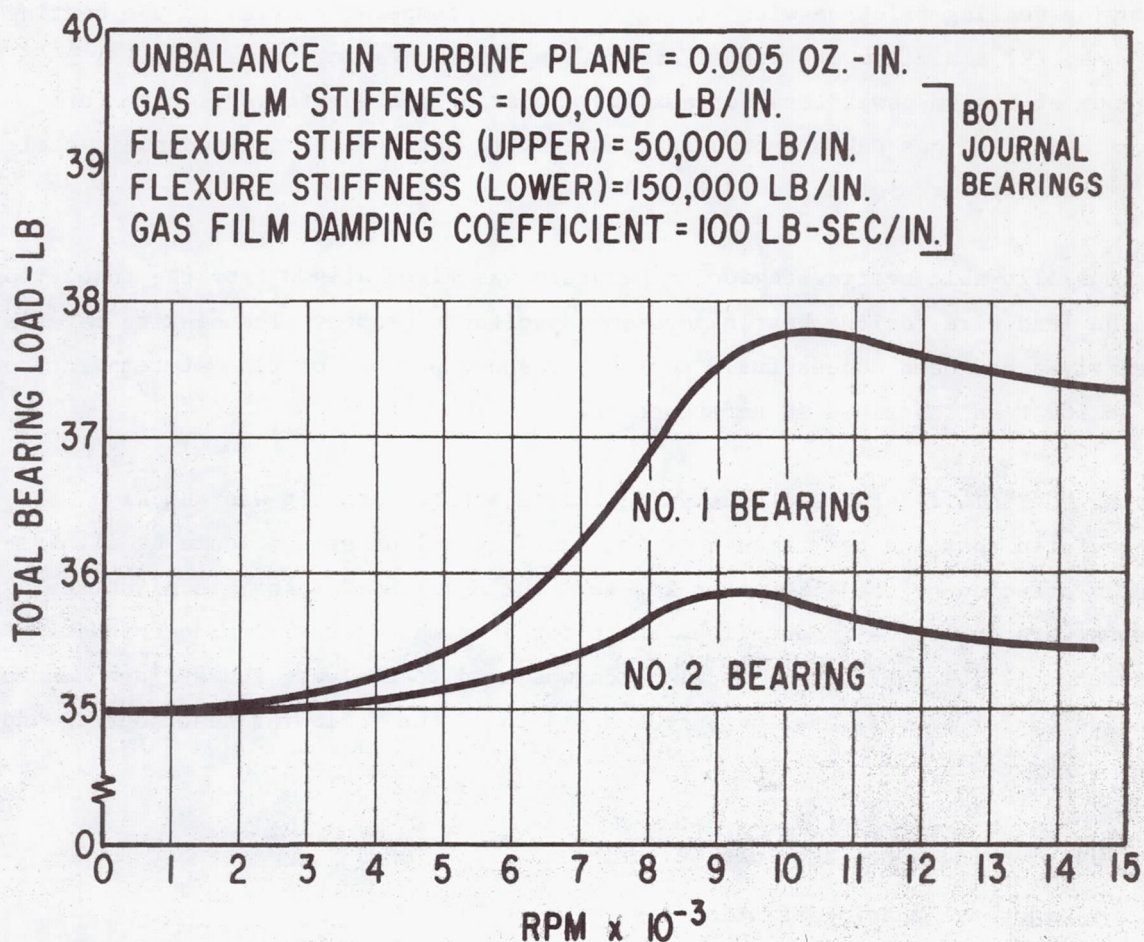


Fig. II-20 Bearing Reactions for 0.005 Oz. In. Unbalance in the Turbine Plane - Turboalternator Rotor (No Electromagnetic Forces) - Using Calculated Values of Stiffnesses

Bearing Cooling Design

The design of a satisfactory cooling mechanism for the turboalternator bearing system was a task which, in particular, illustrates the importance of careful consideration of all the various interrelated aspects of turbomachinery design. The problem was defined as one of maintaining safe gas-bearing clearances while removing bearing friction with (1) an acceptable temperature rise in the bearing regions, (2) a minimum of thermal distortion of the bearing parts, and (3) a minimum of system power loss for auxiliary bearing coolant flows (in the form of either bleed gas taken from a low temperature part of the thermodynamic cycle or externally circulated liquid flow.)

Maximum allowable bearing region temperature was fixed at 400 F by the insulation of the lead wire for the bearing system capacitance probes. The bearing materials themselves had been successfully tested for short periods of time at temperatures up to 500 F as described in Reference [22].

During the initial stages of designing the turboalternator, it was quickly appreciated that the performance of the bearing cooling system would be significantly affected by the alternator losses. The magnitude and origin of these losses were evaluated in detail by the alternator manufacturer as described in Reference [23]. The thermal model which was used to evaluate the various concepts considered for bearing cooling purposes included the following heat sources and heat sinks:

- 1) turbine wheel and turbine casings,
- 2) journal bearing friction loss (two bearings),
- 3) thrust bearing friction loss (two bearings),
- 4) alternator stator electrical losses,
- 5) alternator rotor electrical and windage losses, and
- 6) alternator coolant system

After evaluation of the various concepts under consideration, a basically conductive mechanism was chosen for transferring the journal bearing losses to a liquid-cooled heat sink. This method was selected because it incurred a minimum loss, from overall system standpoint, and because a supply of coolant fluid was readily available from the alternator cooling system. For this same reason, a conductive mechanism was also selected for cooling the thrust bearing.

The design of the cooling mechanism, which is the same for each of the two journal bearings, consists of an electrodeposition of copper (1/8 inch radial thickness) in the bore of each journal. This plating extends approximately 1-1/2 inches beyond each end of the actual journal bearing region. Heat generated in the bearing film is conducted radially through the steel journal and into the copper plating. The heat is then conducted axially along the copper away from the bearing and then conducted radially back through the steel journal and across a close clearance gap to stationary, liquid-cooled, heat sinks which are located at each end of both bearings. These heat sinks are maintained at approximately 200 F by a flow of the same type of coolant fluid that is used for cooling the alternator. In addition to removing the friction loss heat from the journal bearings, the two heat sinks which are located adjacent to the alternator remove, by conduction across a small axial clearance, a significant proportion of the pole face electrical and windage losses.

Preliminary calculations performed by MTI indicated that peak bearing pad temperatures would be about 270 F and peak journal temperatures, occurring at the mid-plane of the bearing, about 268 F. The temperature gradient from the mid-plane to the ends of the bearings would be about 4 F. More refined calculations made by P&WA, using a computer code, confirmed these calculations to be as follows:

	<u>Peak Pad</u> <u>Temperature</u> °F	<u>Peak Journal</u> <u>Temperature</u> °F	<u>Journal Temp.</u> <u>Gradient</u> °F
No. 1 Bearing	292	288	6
No. 2 Bearing	299	296	6

The thermally-induced distortion of the bearings which results from the axial temperature gradients appears in the form of crowning and amounts to approximately 75 microinches. This should not cause any appreciable loss in bearing load-carrying capacity.

While the heat sinks are equipped with separate coolant inlets and outlets these sinks are constructed as an integral part of the member which is used to support each bearing assembly. It follows that the temperature of this support member is largely determined by the temperature of the coolant which, at design point, is 200 F. The selection of the material from which the bearing support was fabricated was based on a number of considerations. Primarily, the material should be nonmagnetic to prevent the establishment of a magnetic flux path through the bearing system to the rotor rather than through the pole faces. An alternate flux path of this type would be expected to detract from the alternator performance. Secondly, the material should exhibit good corrosion resistance to the coolant with which the material would be in contact. Finally, the coefficient of expansion of the selected material should permit the retention of essentially constant bearing clearance for all conditions of operation. To meet this latter requirement, it was necessary to use a material with an expansion coefficient sufficiently in excess of that possessed by the journal to offset the design-point temperature difference of approximately 80 F that existed between the journal and the support. The material selected to meet all of these requirements was an austenitic stainless steel, AMS 5646 (type 347).

An essential requirement of the bearing system design is the retention, within acceptable limits, of journal bearing clearance during the thermal transients involved in start-up and shut-down of the turboalternator. These limits are intended to preclude contact between the journal and pads- in the case of minimum bearing clearance, and pad flutter- in the case of increased bearing clearance. To ensure that the clearance limits were not exceeded, several calculations were made of the thermal response of the system to a step change of zero to 12,000 RPM. The first calculation assumed that the bearing heat exchangers were not supplied with coolant. The results showed that the response of the bearing support lagged that of the journal by a considerable amount, and neglecting the effect of the flexible pivot supports, the minimum clearance criteria may well be exceeded. The second calculation allowed for the introduction of liquid coolant at design-point temperature, and flow rate to the bearing heat exchangers at the time the turboalternator was started. The results of this calculation showed that the transient bearing clearances would be within acceptable limits. The response of the bearing support was still,

however, rather slow. To improve this response, and thereby improve both the flexibility of operation and allow for bearing clearance adjustments to be made during operation, the design of the bearing support was modified. This modification introduced passages (on either side of the pivot and within the body of the bearing support) through which liquid coolant could be passed independent of the coolant flow to the bearing heat exchangers. Calculations based on this, the final design, showed that the response of the bearing support would be improved by a factor of between 2 and 3 when coolant at design point-temperature was passed through these passages at the time the turboalternator was started. The position and extent of the bearing heat exchangers may be seen in Figure 1.

The steady-state and transient thermal analyses and the detail design of the journal bearing cooling system was performed by Pratt and Whitney Aircraft. Initial verification of the techniques required to electroplate the bore of the journals with an extremely heavy deposition of copper was likewise performed by Pratt and Whitney Aircraft.

When designing the main thrust-bearing, calculations indicated that gas cooling would result in unacceptable temperature gradients and, hence, thermal distortion of the thrust-plate. The use of liquid cooling alleviated these problems and the decision was made, therefore, to use a liquid-cooled hydrodynamic thrust-bearing for the turboalternator. The design of the thrust plate utilizes a welded aluminum construction containing internal annular passages through which the coolant can be passed.

Figure II-21 shows the effect of coolant flow rate on pressure drop, coolant temperature rise, and average temperature difference between the coolant and the aluminum thrust plate. The curves are based on a friction loss of 0.13 HP which is the combined hydrostatic-hydrodynamic bearing loss at 12,000 rpm for an 85 pound thrust load (i.e., for a film thickness of 1.1 mils). Under zero-g operating conditions when the thrust load will reduce to about 30 pounds and the combined bearing loss to 0.075 HP, the temperature differences shown on Figure II-21 would be reduced in direct proportion to the reduction in friction loss.

For the purposes of design, the coolant fluid was assumed to be G.E. Versilube F-50. With a nominal flow of 150 pounds per hour, it is seen from Figure II-21 that the aluminum thrust plate will run about 13.5 F above the average coolant temperature. The coolant temperature rise and pressure drop will be about 6.0 F and 1.0 psi respectively. As a result of the aluminum construction material and the small temperature rise of the coolant fluid, thermal distortion of the bearing surface due to radial and circumferential temperature gradients should be negligible. Dishing of the bearing surface due to the axial heat transfer temperature gradient should be less than 90 micro-inches. This is a quite acceptable condition.

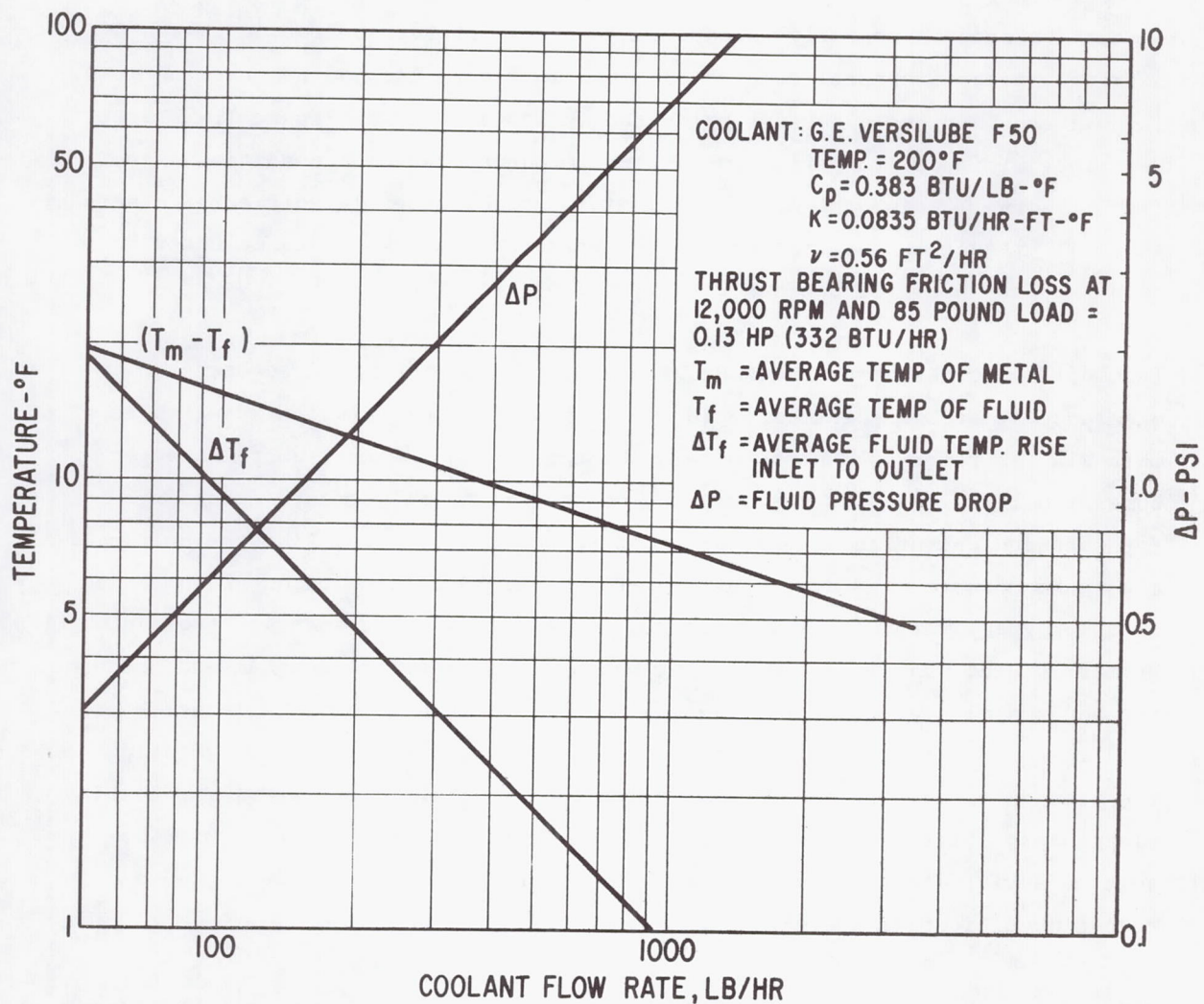


Fig. II-21 Liquid Cooled Thrust Bearing Operating Characteristics Versus Coolant Flow Rate

Journal Bearing Adjustment and Assembly Details

During assembly of the turboalternator, it will be necessary to adjust the bearings at zero speed and room temperature to dimensions which will give the correct clearance at design operating conditions. The specific value of clearance to be used on assembly is dependent on the intended operating values of bearing ambient pressure, temperature, gas lubricant and journal bearing load. The values of set-up clearance presented in Table II-6 and Figure II-22 are, therefore, intended to permit optimum performance under the conditions specified. However, using the average value of bearing assembly diametral clearance will result in satisfactory turboalternator bearing clearance under both 1-g and zero-g conditions of operation.

In addition to the adjustments necessary to achieve the required bearing clearance at design-point conditions, the bearings must also be adjusted to maintain the rotor concentric within the turbine labyrinths, heat-exchanger bores and the alternator stator. The concentricity adjustments necessary for intended operation in a zero-g gravitational field are, like the bearing clearance adjustments, different from those required for horizontal operation in a 1-g gravitational field. The reasons for this difference are twofold. Primarily, the upper and lower pivot support stiffness are unequal and, secondly, the horizontal operation in a 1-g gravitational field involves a larger bearing load which results in an increase in bearing eccentricity. However, using the average value of the dimension between the geometric center of the bearing clearance profile and the geometric center of the turboalternator will result in satisfactory turboalternator rotor concentricity under both 1-g and zero-g conditions of operation.

When making the bearing adjustments for concentric operation in both a zero-g gravitational field and horizontal operation in a 1-g gravitational field at the design point conditions given in Table II-6, the following steps should be taken:

- 1) The turboalternator should be in the vertical position (preferably turbine end down) with the thrust runner and the turbine wheel accessible.
- 2) The reverse thrust bearing jacking gas should be turned on, and the ground-to-shaft and pad to shaft probes connected. The probe signals should be displayed on CRO's at a sensitivity of 50 MV/CM.
- 3) The bearing clearance profile displayed on the CRO's (a square for a 4 pad bearing) as observed by the ground-to-shaft probes, should be established. This can be accomplished by moving the rotor shaft within the limits allowed by the bearing clearance.
- 4) The position of all 4 pads should be adjusted until the geometric center of the clearance profile is positioned relative to the geometric center of the turboalternator by the distance given in Table II-6.
- 5) Ensure that the amount of bearing clearance is in accordance with the values given in Table II-6. A check of these values is advisable after the pivot locknuts have been tightened.

The dimensions given in Table II-6 and Figure II-22 for bearing diametral clearance and rotor positioning assume that NO LOAD is imposed on the bearing pads during bearing adjustment, hence the recommended vertical orientation of the rotor during this operation. In the event that an assembly technique is required which will permit adjustment of the pads when the turboalternator is in a horizontal position with the rotor weight being supported by the pads, the given bearing and concentricity adjustment dimensions must be revised. This revision must account for the initial deflection of the loaded-pad pivot supports due to the load imposed by the rotor.

The journal bearing assembly dimensions given in Table II-6 and Figure II-22 for operation in a zero-g gravitational field will allow satisfactory, but not optimum, operation in the horizontal position in a 1-g gravitational field. The rotor during horizontal operation will be approximately 0.5 mils eccentric to the alternator geometric center and the diametral bearing clearance will be approximately 0.2 mils less than optimum. Conversely, adjustments made for horizontal operation in a 1-g gravitational field will allow satisfactory, but not

optimum, bearing performance in a zero-g gravitational field.

It should be noted that the turboalternator bearing system may be operated satisfactorily under conditions which result in increased diametral bearing clearances and considerable eccentricity between rotor and stator. The extent of these deviations as experienced during the rotor-bearing-alternator simulator test program are discussed in Section VII of this report.

From the foregoing comments, it will be apparent that the clearance profile, as described by the ground-to-shaft probes with the turboalternator at 70⁰F and zero speed, will change as the turboalternator attains design-point operating conditions, or alternatively, is subjected to off design-point conditions. For this reason, it is advisable to monitor bearing performance using the film thickness dimensions obtained from the pad-to-shaft capacitance probes rather than the performance as indicated by the ground-to-shaft capacitance probes.

TABLE II-6
JOURNAL BEARING SET UP DIMENSIONS FOR CONCENTRIC
OPERATION UNDER DESIGN POINT CONDITIONS

Design-point conditions for horizontal or vertical operation in either 1-g or zero-g gravitational fields are as follows:

Speed (RPM)	12,000 RPM	
Gas	Argon	
<u>Temperatures</u>	<u>#1 Bearing</u>	<u>#2 Bearing</u>
Bearing Journals ($^{\circ}$ F)	288	296
Bearing Pads ($^{\circ}$ F)	292	299
Bearing Supports ($^{\circ}$ F)	200	200
Ambient Pressures (PSIA)	10.5	12.0

For horizontal operation in a 1-g gravitational field, the assembly dimensions at 70 F are as follows (see also Figure II-22):

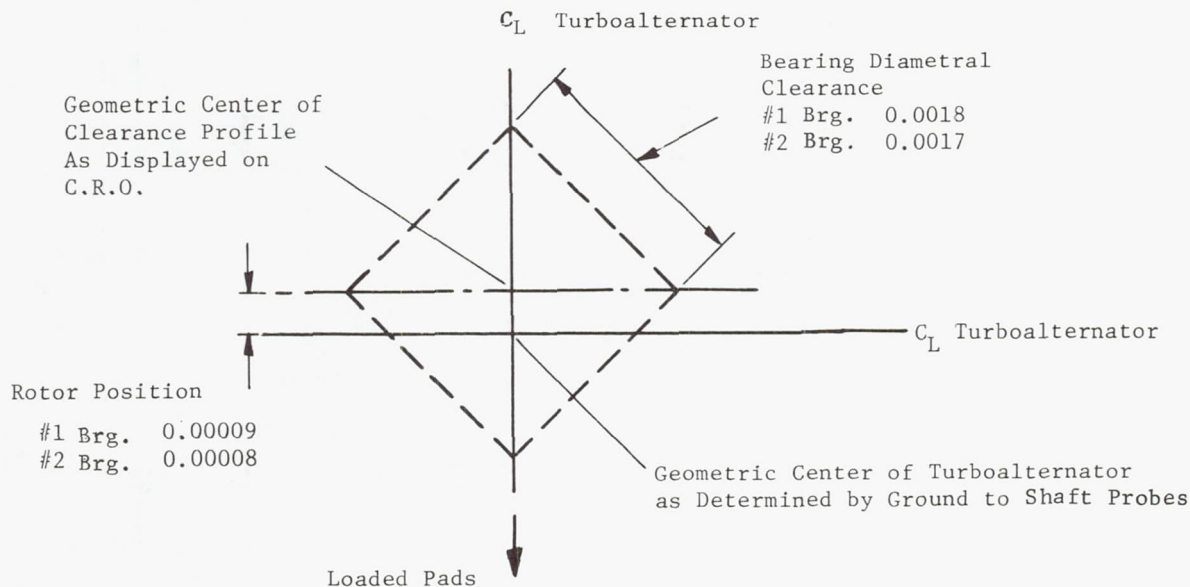
	<u>#1 Bearing</u>	<u>#2 Bearing</u>
Bearing Assembly Diametral Clearance (Mils)	1.8	1.7
Geometric Center of the Bearing Clearance Profile Relative to the Geometric Center of the Turboalternator (Mils)	0.09 (High)*	0.08 (High)*

For operation in a zero-g gravitational field, the assembly dimensions at 70 F are as follows (see also Figure II-22):

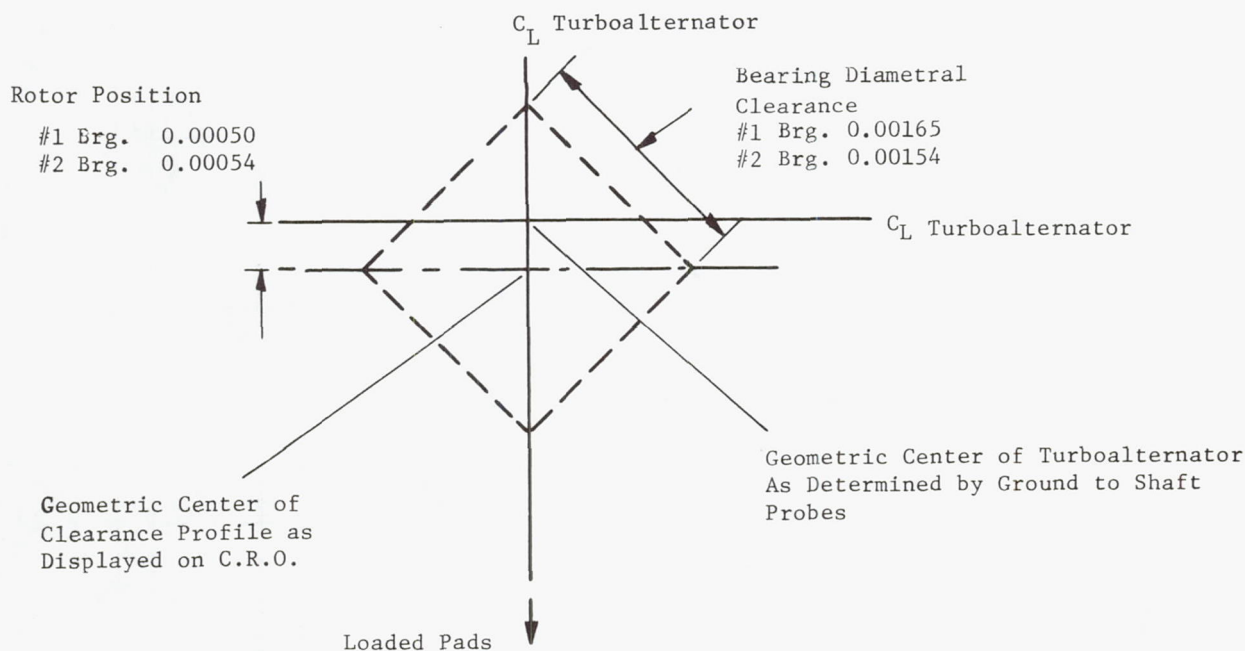
	<u>#1 Bearing</u>	<u>#2 Bearing</u>
Bearing Assembly Diametral Clearance (Mils)	1.65	1.54
Geometric Center of the Bearing Clearance Profile Relative to the Geometric Center of the Turboalternator (Mils)	0.50 (Low)*	0.54 (Low)*

Design performance values associated with the above setup clearances are given in Table II-2.

*The terms high and low denote the direction toward the upper and lower pads respectively.



a) Set Up Dimensions for Horizontal Operation in a 1-g Acceleration Field



b) Set Up Dimensions for Operation in a 0-g Acceleration Field

Fig. II-22 Turboalternator Journal Bearing Set-Up Data for Optimum Performance at Design Point Operating Conditions

Bearing System Fabrication Materials

The materials selected for the basic bearing parts are listed below.

Rotor Journals	AMS 6294 C (AISI 4620)
Pivoted Pads	M-1 Tool Steel
Pivots	M-1 Tool Steel
Pivot Supports	AMS 6370D (AISI 4130)
Thrust Bearing Housing	AMS 5646E (AISI 347)
Thrust Plate	AMS 4027C (6061 Aluminum)
Thrust-Runner	AMS 6415F (AISI 4340)

The basis for selection of the above materials is as follows:

1. Rotor Journals

The journals are an integral part of the alternator rotor. Hence, alternator considerations, such as magnetic properties and fabrication techniques, dictated the choice of AMS 6294C journal material.

2. Pivoted-Pads

The use of M-1 tool steel hardened to RC 58 has proved successful in previous designs employing pivoted-pad journal bearings.

3. Pivots

Previous experience has demonstrated the suitability of using M-1 tool steel against M-1 tool steel for pivot configuration operating at temperatures up to 500 F and with stress levels in the contact-zone of approximately 100,000 lb/in.². The use of an electrofilm coating on one or both of the components has proved helpful in inhibiting corrosion of the pivot contact zone.

4. Pivot Support Flexures

AMS 6370D (AISI 4130) steel hardened to R_c 32-36 and shot peened in the region of maximum stress was selected for the flexure material because of its high fatigue strength and good stability. Silver plating is used for protection against corrosion.

5. Thrust Bearing Housing

AMS 5646E (AISI 347) stainless steel was selected so that corrosion of the internal gas passages to the hydrostatic bearing would not be a problem. The thermal expansion coefficient of this material also matches that of the journal bearing support to which it is attached.

6. Thrust Plate

The material properties required for this item are those of low density for dynamic tracking reasons, high thermal conductivity for heat-transfer reasons, and high dimensional stability for bearing performance reasons. These requirements were satisfied by the use of AMS 4027C (6061 Aluminum).

7. Thrust Runner

For rotor dynamic reasons, it was necessary to use a reasonably heavy thrust runner. AMS 6415F (AISI 4340) alloy steel is a good stable material which satisfies all bearing requirements and which can be readily interfaced with the rotor design. The magnetic properties of this material facilitate the use of electromagnetic pick-ups for the measurement of rotor speed. Corrosion protection is effected by means of nickel plating.

A number of O-rings are used in the bearing system assembly. The first of these, as shown in Fig. II-6, is used as a check valve in the gas supply for the journal bearing hydrostatic lift-off system. This valve prevents back-flow, and hence loss of load capacity, when the bearings are running hydrodynamically. The second O-ring seals the pad pivot cavity to prevent by-pass leakage of the supply gas during hydrostatic lift-off operation. During hydrodynamic operation, there is no pressure differential across this seal. The third O-ring effects a seal between the bearing support and each pivot-support. This seal ensures that the small gas cooling flow, which circulates through the turboalternator, passes between the journals and the heat-exchangers.

Each of these O-rings is manufactured from a fluoro-elastomer (Viton) which is suitable for long-term operation at temperatures up to 450 F and hence should be satisfactory for the pad temperatures of approximately 300 F expected in this application.

Bearing Surfacing Materials

Gas-lubricated bearings have no boundary lubrication safeguards. It is, therefore, extremely important that the bearing surfaces be of highly compatible materials, so that incidental high-speed contacts due to shock, vibration, passage of dirt through the bearing, or improper use of the machine will not result in serious damage to the rotor-bearing system. Also, where it is intended to omit the use of hydrostatic jacking of the journal bearings (which is necessary with the present design for operation in a zero-g gravitational field), the bearing surfaces must be capable of surviving sliding contact over an appreciable number of starts and stops without damage or significant wear.

It was known that the compatibility of the bearing substrate materials, as defined in the preceding subsection, would not be acceptable for the sliding and high-speed contact conditions of operation. The mating surfaces in each of the journal and thrust bearings were therefore coated with a flame-sprayed deposition of chrome oxide, a material which in previous tests (see Reference[22]) was found to be suitable for the service conditions involved.

Bearing System Instrumentation

Successful and rapid development of advanced high-speed gas-bearing turbomachinery requires that the static and dynamic behavior of the rotor-bearing system be monitored with precision during the test and evaluation phases. In particular, the rotor-bearing system instrumentation must

1. provide data for quantitative evaluation of overall performance,
2. provide data for detailed evaluation of component performance and for refinement of component design, and
3. indicate whether or not the equipment is in a safe mode of operation.

To measure static and dynamic bearing film thicknesses in the prototype turbo-alternator, displacement measuring instrumentation was selected based on

measuring electrical capacitance between the tip of a capacitance probe and the moving surface of the journal and thrust bearings. Specifically, a capacitance system based on the Wayne-Kerr Model DM 100 Distance Meter was selected for the following reasons:

1. calibration of the combined transducer and readout system is extremely stable with time and temperature;
2. the calibration factor is essentially constant over a wide range of probe clearance gap (i.e., output is linear over a wide displacement range) and hence, recalibration is not required each time the transducer probes are reset;
3. the calibration factor is essentially constant over a wide range of temperature (i.e., from 75 to 700 F) — only slight changes in calibration occur up to 1200 F;
4. high sensitivities are possible, ranging from 0.2 volts per mil to 0.1 volts per mil for the capacitance probes selected for the turbo-alternator;
5. frequency response, though not outstanding, was adequate for the application — being flat to approximately 6,000 hertz;
6. the capacitance probe is unaffected by magnetic fields; and
7. the capacitance probes could be made very small, light and rugged.

In order to adequately measure bearing system performance, a total of 21 capacitance probes were incorporated into the bearing system design to measure (1) thrust bearing film thickness, (2) orbital motion of the two journals, and (3) actual film thickness between the eight pivoted-pads and the journals at a point close to the pivot location. In addition, several probes were incorporated to measure dynamic motions of several of the pads and of the main thrust stator relative to the "fixed" bearing housings.

Locations of the various capacitance probes are listed in Table II-7. Figures II-23 and II-24 show location of the probes in the No. 1 and No. 2 journal bearings in more detail. Figure II-25 is a photograph showing a typical

range of capacitance probes used in a turbomachinery application. Views of the probe locations in the thrust bearings and the installed probes in the pivoted-pads can be seen in the photographs of Figures II-7, II-8, II-13 and II-17.

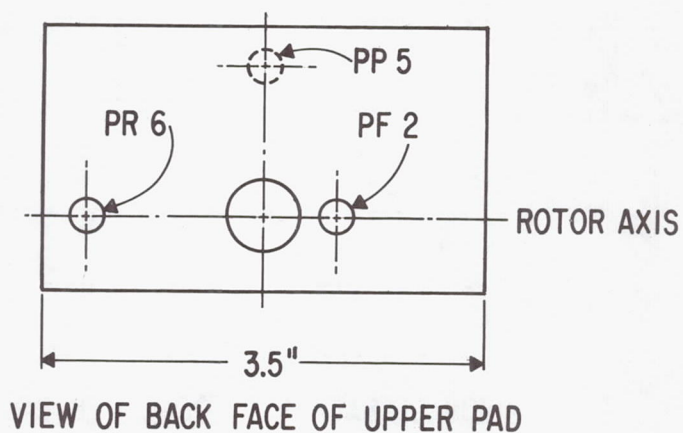
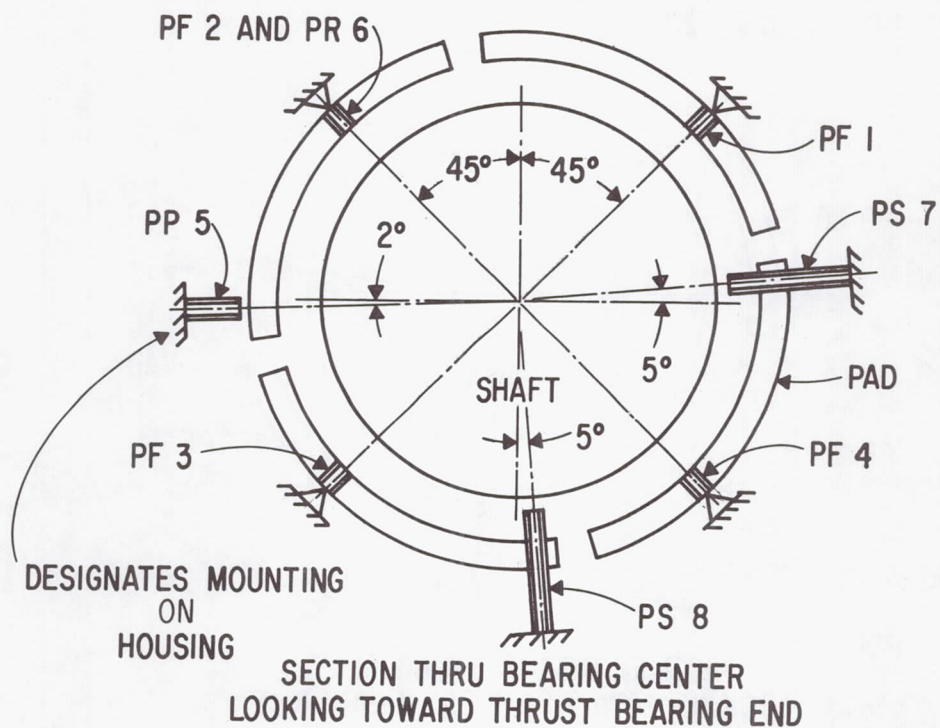
In addition to the capacitance probe instrumentation, a total of 33 chromel-alumel thermocouples were incorporated to measure temperatures of the bearing housings, thrust plates, and pivoted-pads. Figure II-26 shows typical thermocouple location positions on the pivoted-pads and Figure II-7 shows a bearing pad with the thermocouples installed.

TABLE II-7

LOCATION OF BEARING SYSTEM CAPACITANCE PROBES

<u>No. 1 Journal Bearing</u>			
<u>Location</u>	<u>Measurement</u>	<u>No. of Probes</u>	<u>Probe Designation</u>
Pivoted-pads (Pad-to-shaft)	Film thickness between each pad and No. 1 journal	4 at 90°	PF 1, PF 2, PF 3, PF 4
Pad Flutter (Pad-to-shaft)	Dynamic movement between pad and journal in the roll direction (unloaded pad)	1	PR 6
Pad Flutter (Ground-to-back of pad)	Pad flutter in the pitch direction (Unloaded pad)	1	PP 5
No. 1 Bearing Support (Ground-to-shaft)	Dynamic Motion of No. 1 journal	2 at 90°	PS 7, PS 8
<u>Thrust Bearing and No. 2 Journal Bearing</u>			
Main Thrust Bearing Housing (Ground-to-main thrust stator)*	Dynamic movement of main thrust stator	1	PT 33
Main Thrust Bearing Stator (Main stator-to-runner)	Main thrust bearing film thickness	3	PT 30, PT 31 PT 32
Reverse Thrust Bearing Stator (Ground-to-runner)	Reverse thrust bearing film thickness	1	PT 29
No. 2 Bearing Support (Ground-to-shaft)	Dynamic Motion of No. 2 journal	2 at 90°	PS 27, PS 28
Pivoted-pads (Pad-to-shaft)	Film thickness between each pad and No. 2 journal	4 at 90°	PF 21, PF 22 PF 23, PF 24
Pad Flutter (Ground-to-back of pad)	Pad flutter in pitch direction (unloaded pad)	1	PP 25
Pad Flutter (Ground-to-back of pad)	Pad flutter in roll direction (unloaded pad)	1	PR 26

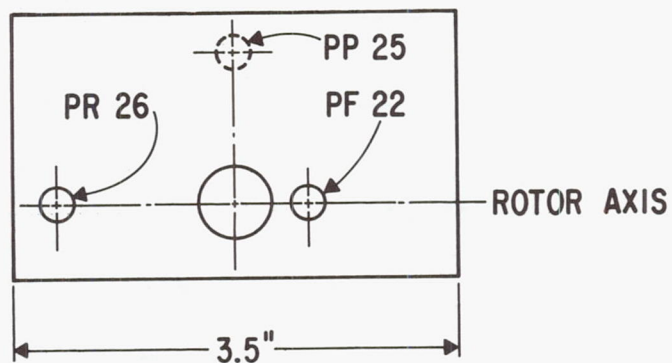
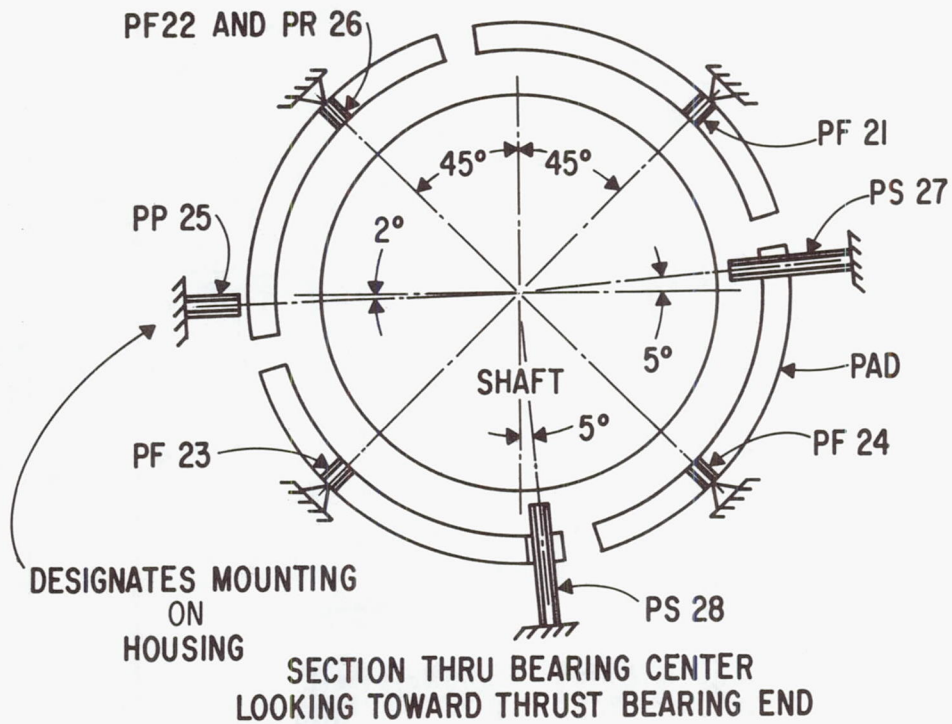
* the work "Ground" refers to any static structure to which a probe is rigidly attached.



PF - PAD PIVOT - FILM THICKNESS
PS - HOUSING - TO - SHAFT PROBES

PP - PAD PITCH PROBE
PR - PAD ROLL PROBE

Fig. II-23 Position and Identity of Capacitance Probes in Number 1 Journal Bearing



VIEW OF BACK FACE OF UPPER PAD

PF - PAD PIVOT-FILM THICKNESS
PS - HOUSING - TO - SHAFT PROBES

PP - PAD PITCH PROBE
PR - PAD ROLL PROBE

Fig. II-24 Position and Identity of Capacitance Probes in Number 2 Journal Bearing

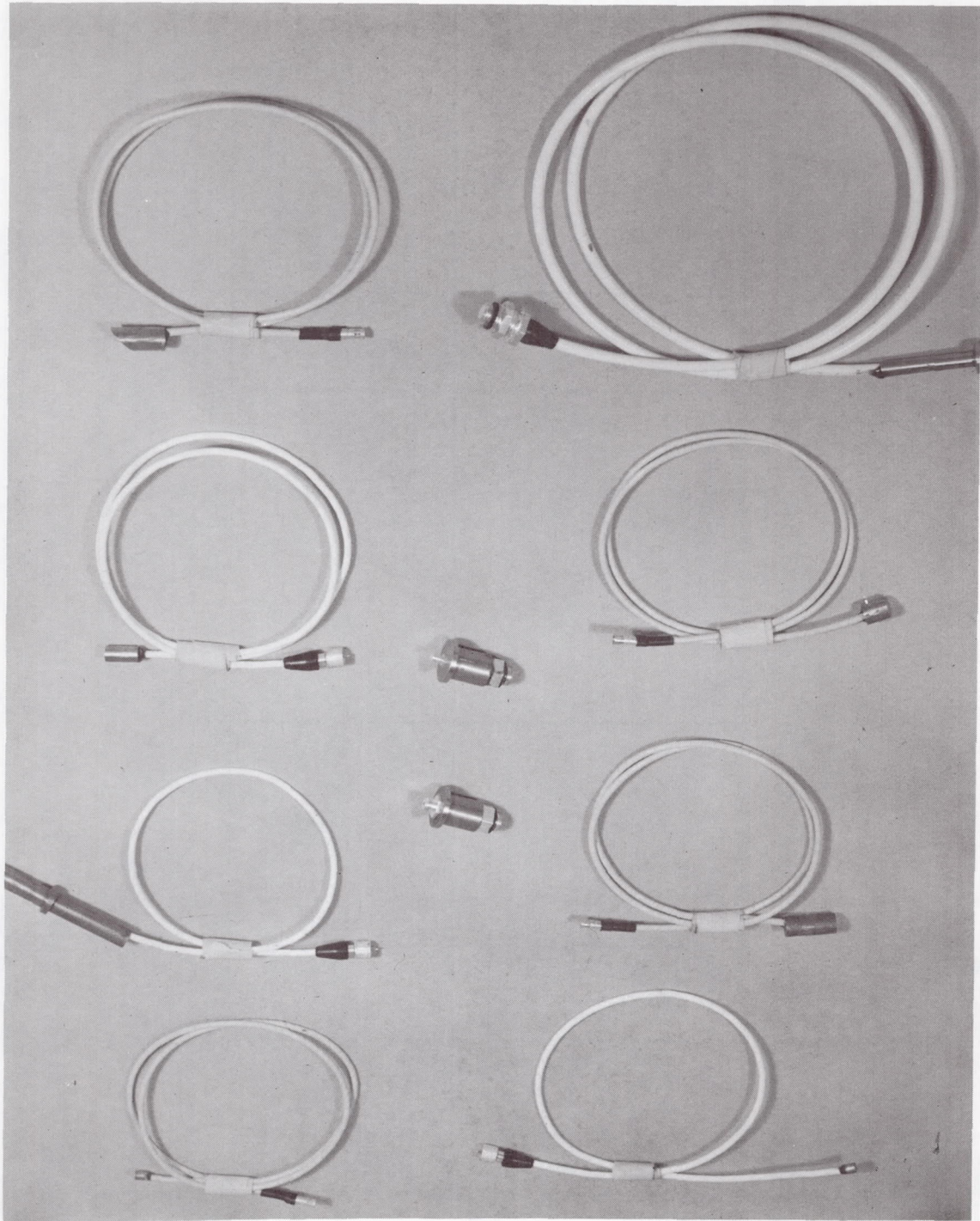
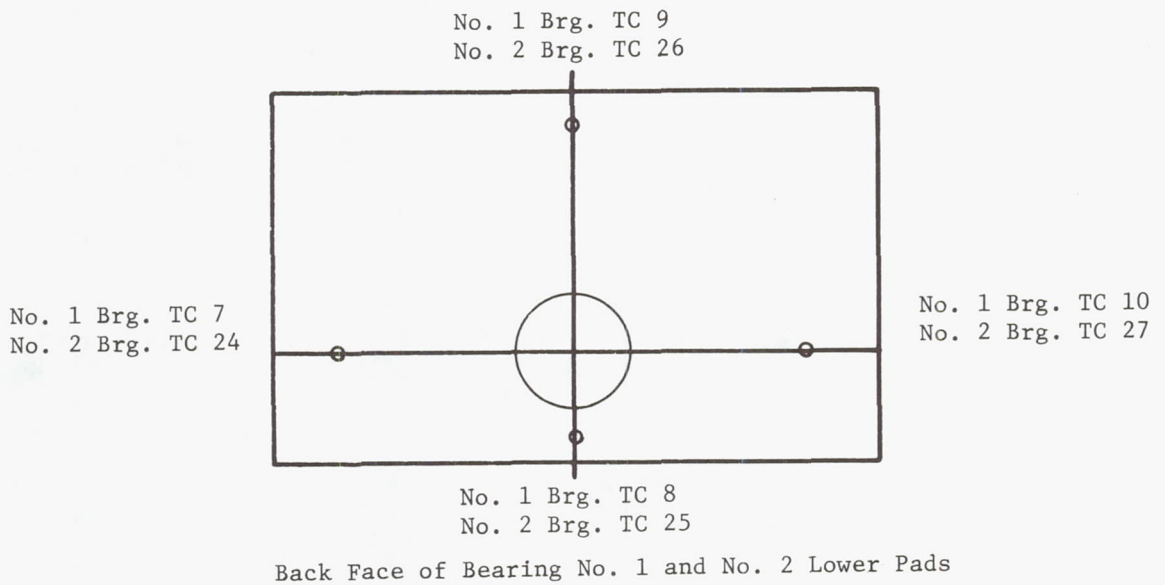
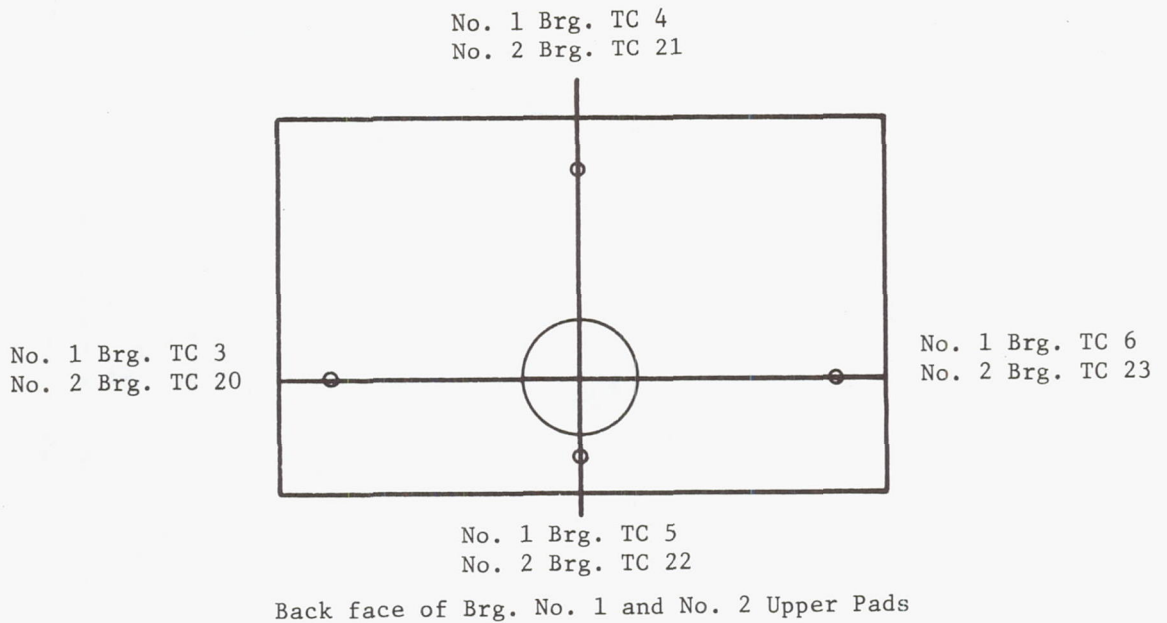


Fig. II-25 View Showing a Typical Range of Capacitance Probe Configurations for Bearing System Performance Measurement



Thermocouples spot welded to back surface of pads where shown o

Fig. II-26 View Showing the Location of Journal Bearing Pad Thermocouples

III. DESIGN OF ROTOR-BEARING SYSTEM SIMULATOR

In any major development program where relatively new techniques are being extended to the limits of known experience, and where the cost and complexity of the prototype machinery demands the utmost assurance of sound design, it becomes exceedingly important to be able to isolate, evaluate and remedy possible problem areas by means of component or subsystem test programs. With respect to the NASA axial flow turboalternator, it was "required" (by contract) that the design of the gas-lubricated rotor-bearing system, as described in Section II of this report, be experimentally evaluated and optimized in a specially-constructed rotor-bearing system simulator. This would permit development and acceptance testing of the rotor-bearing system independent of, and yet parallel to, the turboalternator aerodynamic and electrical components.

After a preliminary design of the rotor-bearing system simulator was approved by NASA, the final design was begun in December 1964. The design was carried out such that the simulator could readily be used to:

1. define rotor balancing requirements and procedures;
2. evaluate bearing system performance under both balanced and unbalanced rotor conditions;
3. evaluate bearing system performance at design-point and off design conditions (such as at maximum overspeed, at reduced ambient pressure, and at higher-than-expected thrust loads); and
4. identify unknown problem areas.

The initial simulator design, however, did not include the alternator stator or rotor. The machine, therefore, could not be used in the initial configuration to generate electrical power. A cross-section view of the rotor-bearing system simulator is shown in Figure III-1. Significant features of the simulator are described in the following subsections.

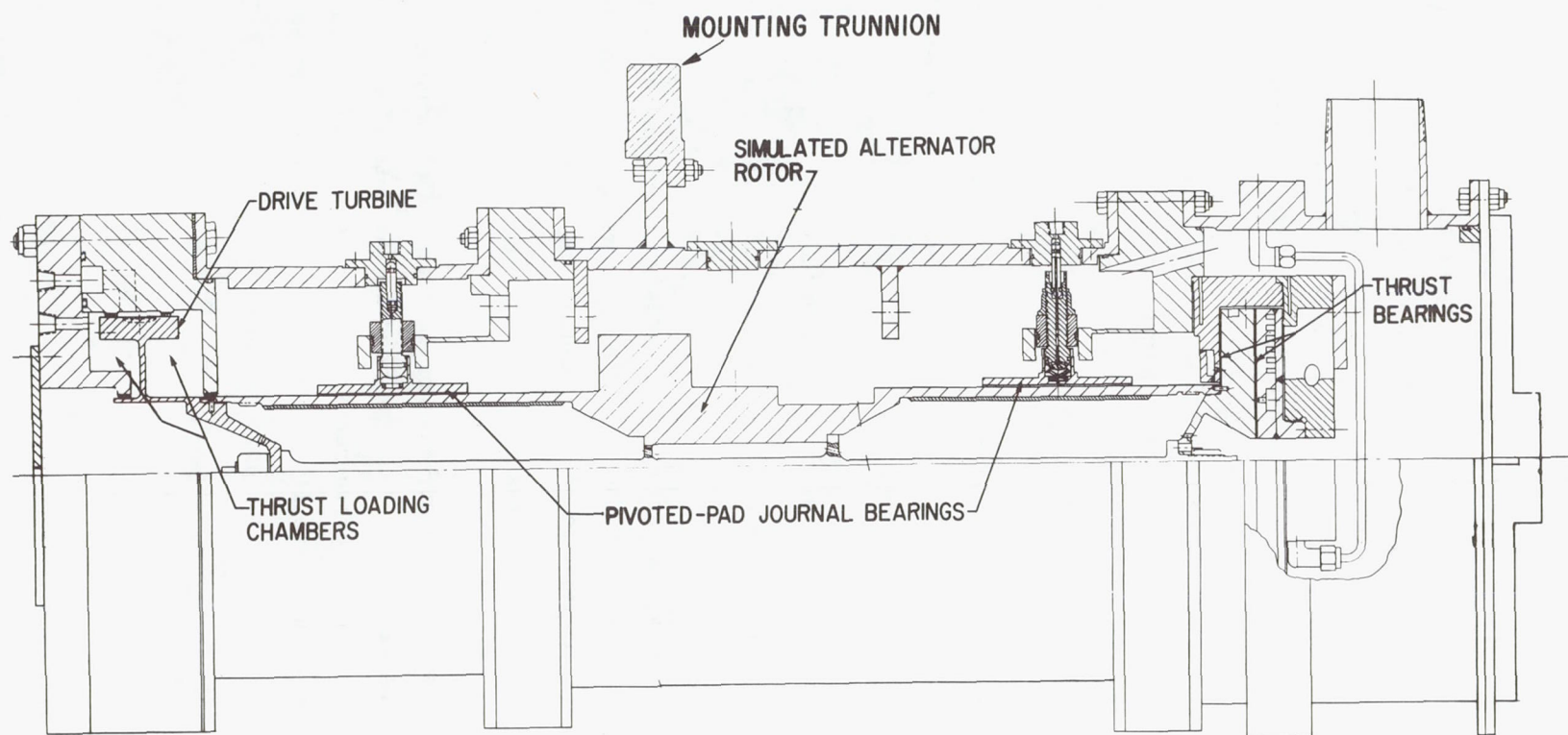


Fig. III-1 Turboalternator Rotor-Bearing Simulator

Simulator Rotor

A photograph of the simulator rotor less turbine wheel and thrust runner is shown in Figure III-2. The rotor possesses the same principal dimensions, total mass, mass distribution, and stiffness characteristics as is inherent in the turboalternator rotor. The total calculated weight and polar and transverse (about the c.g.) mass moments of inertia of the complete rotor assembly, including turbine wheel and thrust runner, were 56.5 pounds, 0.627 in.-lb.-sec.², and 9.656 in.-lb.-sec.² respectively. The calculated location of the c.g. for the complete assembly was 11.72 inches from the reverse thrust face of the thrust runner.

Copper plating, 1/8 inches thick, was deposited on the I.D. of each of the rotor journals. These thermal shunts which transfer bearing friction losses to the bearing-mounted heat exchangers, are identical in design to those which are used in the turboalternator. They were included in the simulator rotor to enable a demonstration of the mechanical integrity of the copper plating under strains resulting from centrifugal growth. Additionally, any effects of such growth on rotor balance needed to be evaluated.

The material from which the turboalternator rotor was manufactured is AMS 6294C. The simulator rotor was manufactured from the same material, but did not include the pole face laminations, amortisseur bars, or the pole face windage baffles. This allowed the manufacture of the simulator rotor without the engineering, design and manufacturing associated with the turboalternator rotor. Selection of the simulator rotor material was based on the following requirements:

1. good stability to meet dimensional and tolerance requirements, and
2. the duplication of the bond between the copper plate and the journal material.

The journal bearing portions of the simulator rotor were, like the turboalternator rotor, coated with flame-sprayed chrome oxide. The basis of selection for the chrome oxide surfacing material is described in Section II of this report.

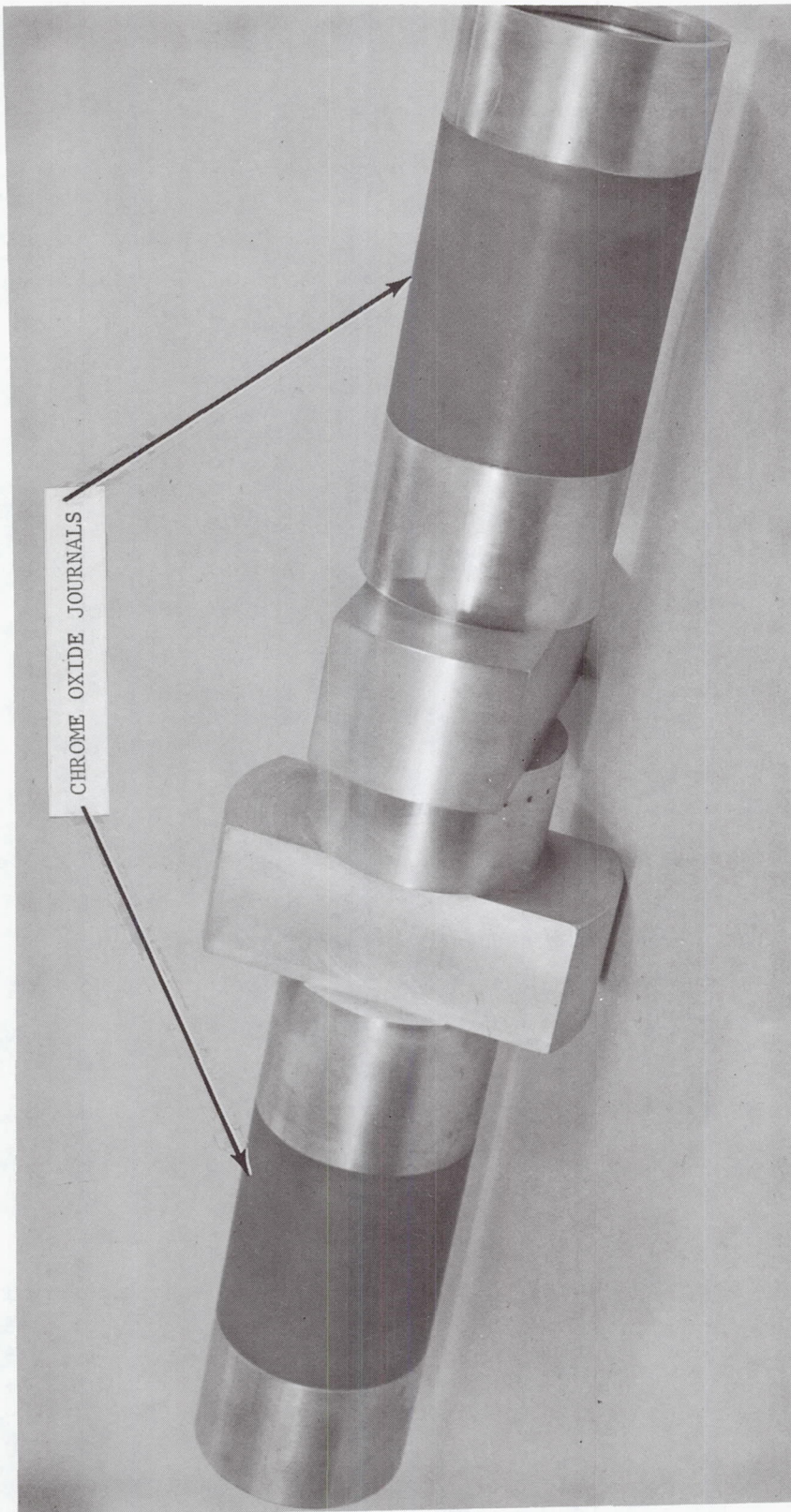


Fig. III-2 View of Rotor for Initial Rotor-Bearing Simulator

Simulator Bearings

The simulator was designed to use precisely the same bearing system as designed for the turboalternator. Photographs of the journal bearing assembly and component parts are shown in Figures II-1, II-7 and II-8, and of the thrust bearing parts in Figures II-12, II-13, and II-14. For both journal bearings, the bearing components include the pivoted pads, pivots, pivot support flexures, pivot "O" ring seals and the bearing system instrumentation transducers (capacitance probes and thermocouples). These components formed two complete journal bearing assemblies that have the same interfaces for both the simulator and the turboalternator. In the thrust bearing region, the bearing components included the thrust runner, the reverse thrust bearing housing, the main thrust bearing, the main thrust bearing support, and the bearing system instrumentation transducers (capacitance probes and thermocouples). Again the interface for the thrust bearing components was identical in both the simulator and the turboalternator.

Control of Bearing Loads

Variation in journal bearing loads, from zero-to-full rotor weight reaction, was made possible by rotation of the complete simulator on its mounting trunnions from a vertical to a horizontal rotor orientation. Figures III-3 and III-4 are photographs of the partial simulator assembly in a horizontal and vertical orientation respectively.

For control of thrust load, at any orientation of the rotor, the simulator casings fore and aft of the turbine wheel were extended radially inward and labyrinth seals provided between these extensions and the rotor (see Figure III-1). This permitted the turbine wheel to be used as a double-acting piston. Variable magnitude and direction of thrust load was obtained by control of the pressure in the cavities on each side of the turbine wheel. These cavities were connected by suitable pressure control valves to a gas supply manifold as shown in Figure IV-3. Leakage across the labyrinths passed into the main simulator casing from where it was vented to atmosphere (via a vacuum pump when the simulator was being operated at sub-atmospheric ambient pressures).

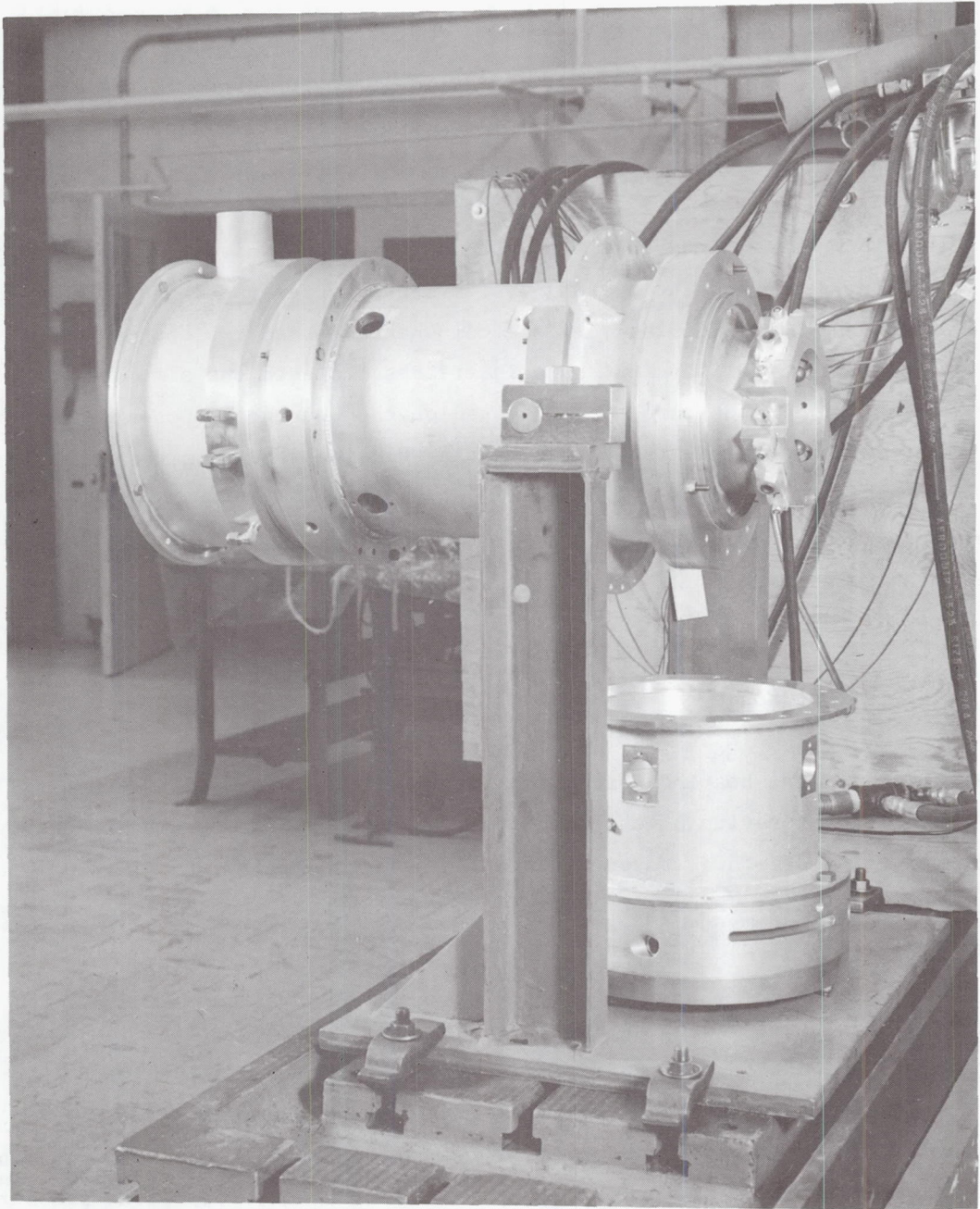


Fig. III-3 Partial Assembly of the Rotor-Bearing Simulator in a Horizontal Position (Initial Configuration)

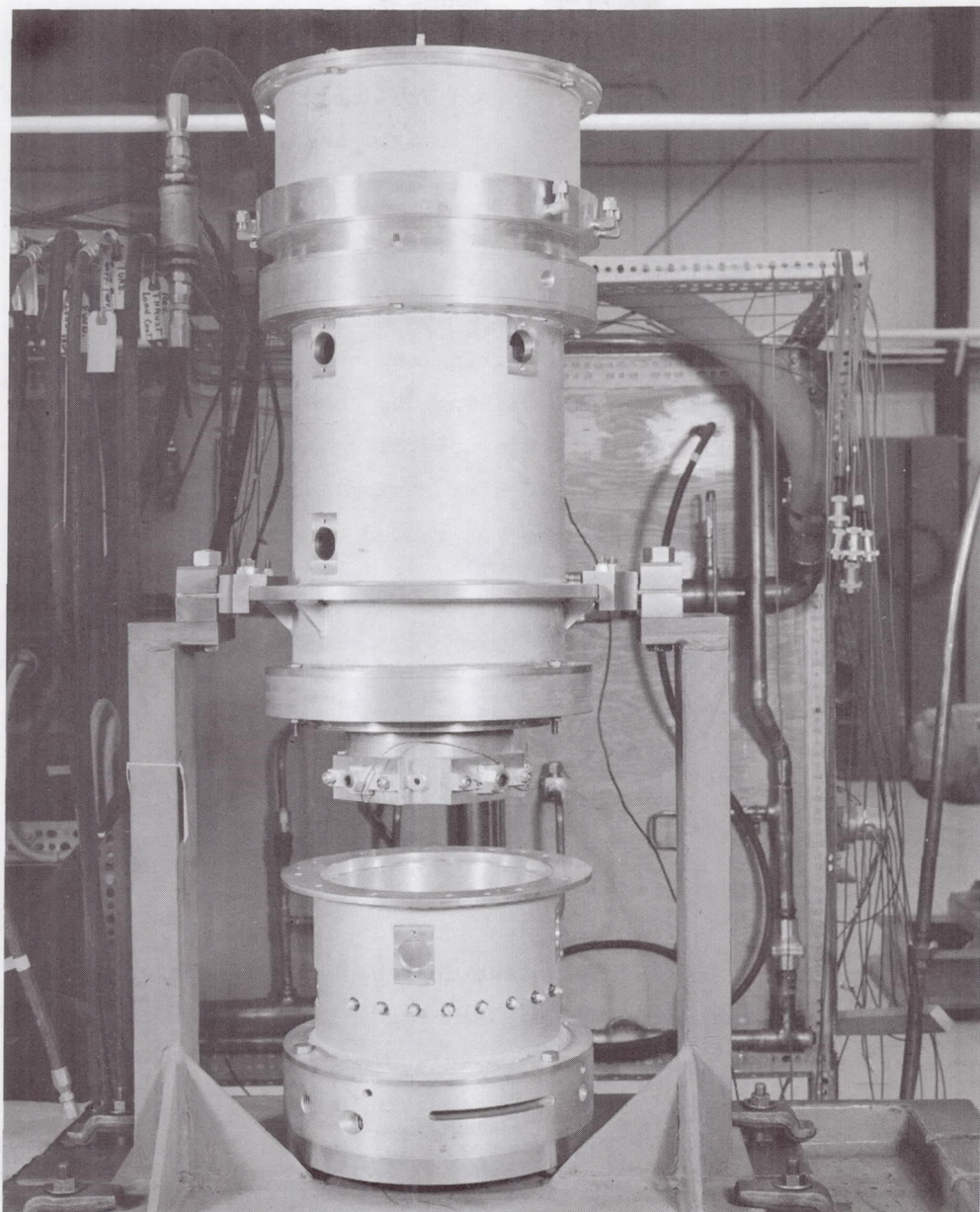


Fig. III-4 Partial Assembly of the Rotor-Bearing Simulator in a Vertical Position (Initial Configuration)

Simulator Casings

The primary functions of the simulator casings were to provide an enclosure and support structure for the bearing system and turbine drive. Since the ambient conditions for simulator operation involved sub-atmospheric pressures in the bearing areas, considerably elevated pressures in the turbine supply system, and intermediate pressures in the chambers used for the control of thrust bearing loads, the casings were designed with suitable labyrinth seals to separate the high and low pressure regions within the enclosure.

The casing which enclosed the thrust bearing region was provided with a connection to a vacuum pump by means of suitable piping and control valves. This permitted the control of ambient pressure in the simulator and exhausted the various bearing system gas flows and thrust loading system labyrinth leakage flow to atmosphere. The turbine discharge gas was vented to atmosphere through slots cut into the turbine wheel casing.

With the exception of the casing which simulated the alternator stator casing, the casings were designed to roughly approximate the mass and stiffness characteristics of the turboalternator casings. Mounting of the simulator was accomplished in approximately the same plane as the turboalternator mounting. This was done so that any potential structural resonance problems could be identified during the test program.

An item of considerable importance in the design of the simulator casings was the accommodation and accessibility of leak-tight instrumentation and supply connections to the bearings. The design as shown in Figure III-1 utilized permanently-installed pass-throughs in the casing at No. 1 bearing and in the end closure in the thrust bearing area. This permitted the easy coupling of all connections on the inboard side prior to completing the enclosure. Figure III-4 shows the No. 1 bearing region instrument connections for the partially assembled simulator.

Simulator Turbine

In selecting the type of drive for the rotor-bearing dynamic simulator, a number of requirements were taken into consideration. These are as follows:

1. The speed range requirement was zero to 14,400 rpm with variable speed control.
2. The maximum power requirement would be approximately 1.5 HP at 12,000 rpm. This power requirement was based on bearing friction and rotor windage losses at the minimum anticipated bearing clearances and maximum ambient pressures and temperatures.
3. The selected drive should not interact with rotor-bearing dynamic performance or introduce characteristics which would prove difficult to correctly interpret.
4. The selected drive should not introduce indeterminant axial forces which would interfere with the thrust loading system.
5. Speed control should be sufficiently precise to permit in-place balancing of the rotor.

To meet these requirements an impulse turbine was selected. The design of this turbine, however, was strongly influenced by the primary requirement for correctly simulating the size, inertia, and elastic characteristics of the turboalternator rotor. The resulting turbine wheel, although not possessing optimum specific diameter or specific speed for the available shop air line pressures, was capable of producing sufficient power for the range of speeds under consideration. During operation of the turbine under the above conditions, the efficiency was very low (approximately 25 percent). The duration of testing, however, was relatively short and the low efficiency value was of no concern.

The nominal dimensions of the turbine are as follows:

wheel diameter	-	7.30 inches
number of buckets	-	40
number of nozzles	-	3
diameter of nozzles	-	0.168 inches
radius of buckets	-	0.375 inches

The turbine buckets were formed on the outside diameter of the wheel by end milling, using a 0.75 inch diameter cutter. The three convergent-divergent nozzles were manufactured as separate components that were then inserted into the simulator casing. The flow to the nozzles was supplied via drillings from an annulus located within the simulator casing.

Exhaust from the turbine was conducted to atmosphere by three radial slots cut into the simulator casing, each being 0.375 inches wide and extending over a 48 degree circumferential arc.

Figure III-5 is a photograph of the initial simulator turbine wheel and the tie bolt used to attach the turbine wheel and thrust runner to the rotor shaft.

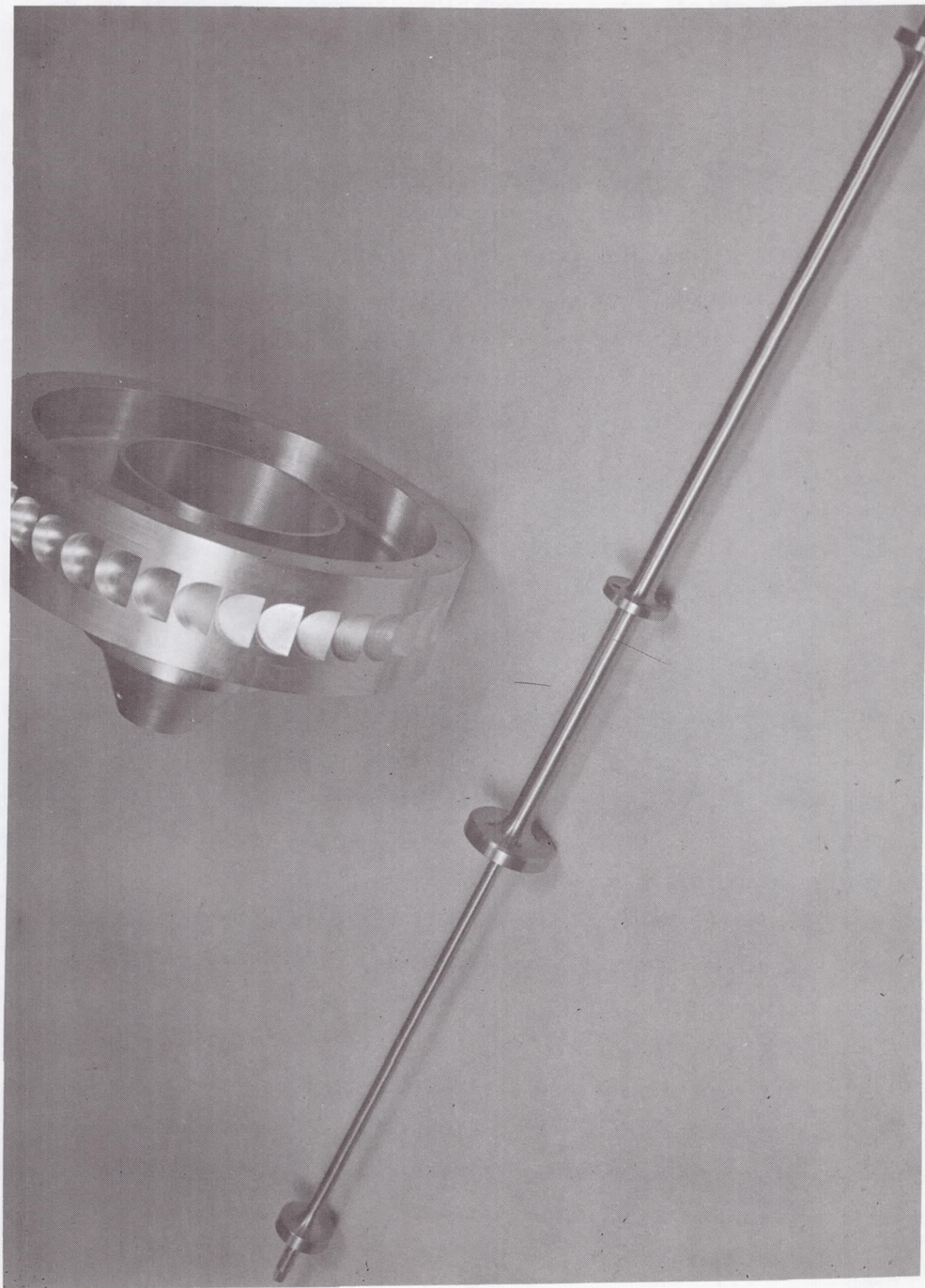


Fig. III-5 View of Impulse Turbine Wheel and Tie Bolt for Rotor-Bearing Simulator (Initial Configuration)

Simulator Temperature Control

The temperature levels and gradients within the simulator, when operating over the range of conditions specified, are considerably different from those found in the turboalternator. This is largely due to the use of a low temperature impulse turbine and the omission of the alternator, with its attendant losses, in the simulator design. The remaining sources of heat generation in the simulator are, therefore, bearing friction and rotor windage losses. Based on previous experience with machines of comparable size, performance and thermal boundary conditions, it was judged that, unlike the turboalternator, heat exchangers would not be required in the regions of the simulator journal bearings, the copper shunts in the bore of each journal being considered capable of maintaining acceptable temperature gradients in these bearings. The thrust bearing design included a heat exchanger as an integral part of the bearing construction. The temperature of the thrust bearing was controlled by the passage of a small flow of coolant, the inlet temperature of which was controlled by an externally-located electrical heater. The temperature of the gas supplied to both hydrostatic thrust bearings was also controlled by means of externally-located electrical heaters.

Simulator Instrumentation

As mentioned in Section II of this report, successful and timely development of a prototype gas-bearing machine requires extensive rotor-bearing system instrumentation for quantitative measurement of performance and for minimum risk operation. Accordingly, the simulator rotor-bearing system was equipped with exactly the same capacitance probe and thermocouple transducers as recommended for the prototype turboalternator design.

In addition to the bearing system instrumentation, numerous additional thermocouples were installed to monitor simulator casing temperatures, as well as temperatures of the various coolant fluids. A Model 3040 Electro Products Laboratories magnetic speed pickup was used to measure rotor speed. The

pickup sensed six notches cut in the OD of the thrust runner. Finally, the simulator was equipped with numerous pressure taps for measurement of turbine, thrust loading, and bearing ambient pressures. A description of the simulator instrumentation readout equipment, and the simulator control system is given in Section IV of this report. A schematic of the control system is shown in Figure IV-3.

IV. TEST EVALUATION OF THE ROTOR-BEARING SYSTEM DESIGN

Assembly of the bearing system and the simulator described in Sections II and III of this report commenced on October 21, 1965. Component calibration and assembly (such as journal and thrust bearing support flexures) had progressed sufficiently by November 24, 1965, to permit in-place balancing of the rotor system. Following balancing, assembly of the machine and installation of instrumentation was completed; and check runs were conducted prior to commencing with the bearing system acceptance test in accordance with P&WA Specification 6359-A (this specification is enclosed in Appendix I of this report). The acceptance test was successfully completed on January 2 and 3, 1966.

The following subsections describe the simulator test facility in which the bearing system evaluation tests were performed and the specific test results pertaining to performance of the bearing system.

Description of the Simulator Test Facility

The simulator test facility consisted of the following items:

1. the rotor-bearing system simulator (described in Section III),
2. the simulator control panel, and
3. instrumentation read-out equipment.

Figure IV-1 is a photograph of the rotor-bearing system simulator mounted on a test bench behind the control panel. In this photograph the simulator is vertical with the turbine-end up.

Figure IV-2 is a photograph of the simulator control panel and a partial set-up of the instrumentation read-out equipment. A Hewlett Packard 521A electronic counter, seen mounted above the left-hand end of the control panel, was used to continuously monitor rotor speed. A 24-point temperature recorder, located on the right-hand table, was used to monitor bearing system temperatures. Microdyne

consoles (located at the immediate right and left of the control panel), together with Wayne-Kerr DM-100 distance meters and Tektronic 502-A oscilloscopes, were used to monitor bearing system capacitance probe signals.

Figure IV-3 is a schematic diagram of the simulator control system. All controls, except for heater exit temperatures and air-manifold supply pressure, were manually operated. It is seen from Figure IV-3 that individual control valves were supplied for:

1. fine and coarse control of turbine nozzle pressure (V-4 and V-5),
2. control of main thrust loading pressure (V-6),
3. control of reverse thrust loading pressure (V-7),
4. control of main hydrostatic thrust bearing supply pressure (V-10),
5. control of reverse hydrostatic thrust bearing supply pressure (V-9),
6. control of water coolant supply pressure to the main thrust bearing stator (V-12),
7. control of jacking gas to the journal bearings (V-8), and
8. control of simulator bearing region ambient pressure (V-14, V-15 and V-16).

All pertinent pressures and flows for the above listed control functions were measured via Bourdon tube pressure gages and Rotometer flowmeters mounted on the control panel, as seen in Figure IV-2.

Shop air at 120 psig supply pressure was used to drive the simulator turbine over the required speed range.

Control of gas temperature as supplied to the hydrostatic thrust bearing was achieved by regulating heaters H-2 and H-3. Control of thrust bearing temperature was obtained by regulating flow and inlet temperature of the thrust bearing coolant water.

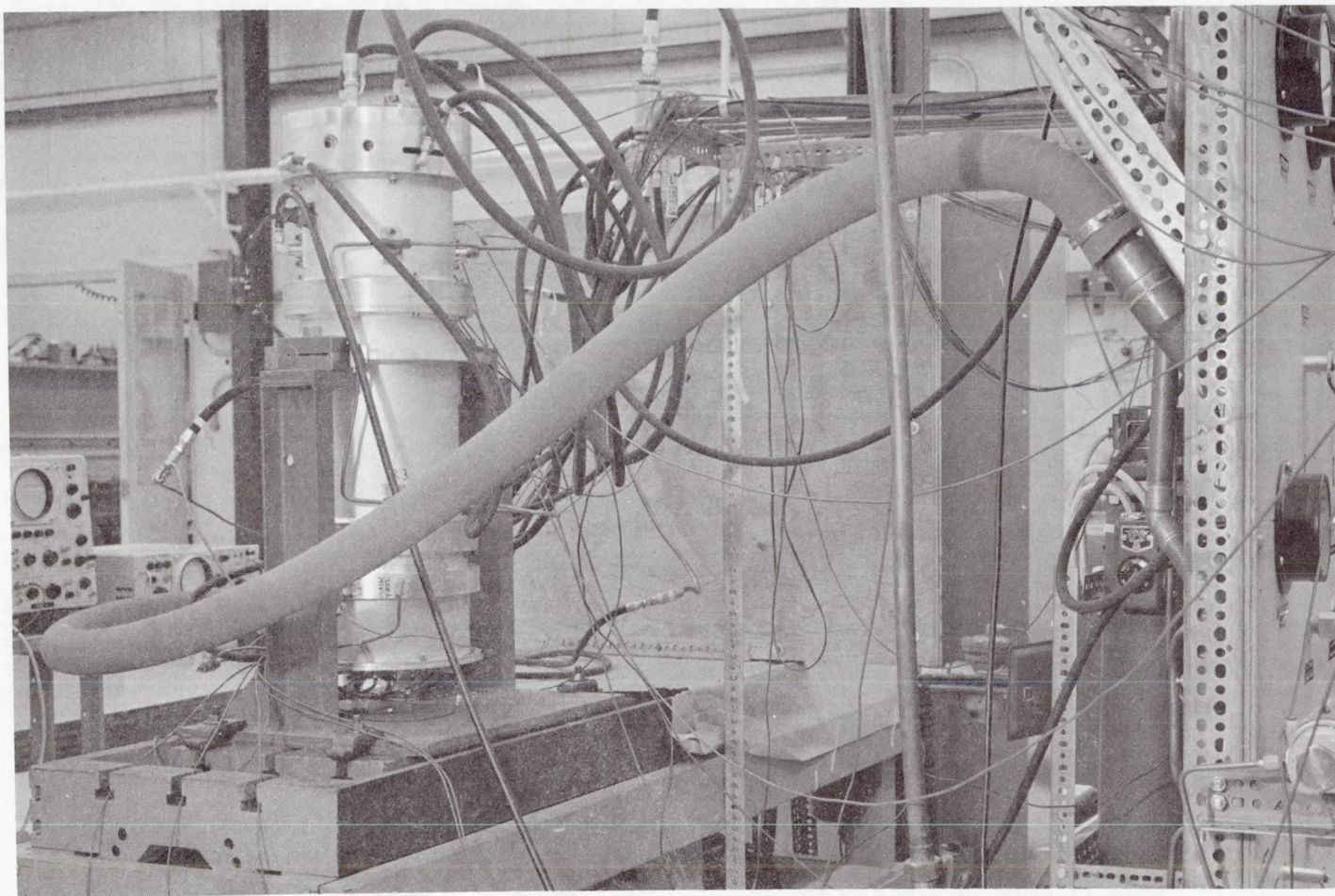


Fig. IV-1 View of Rotor-Bearing Simulator Mounted Vertically on the Test Stand

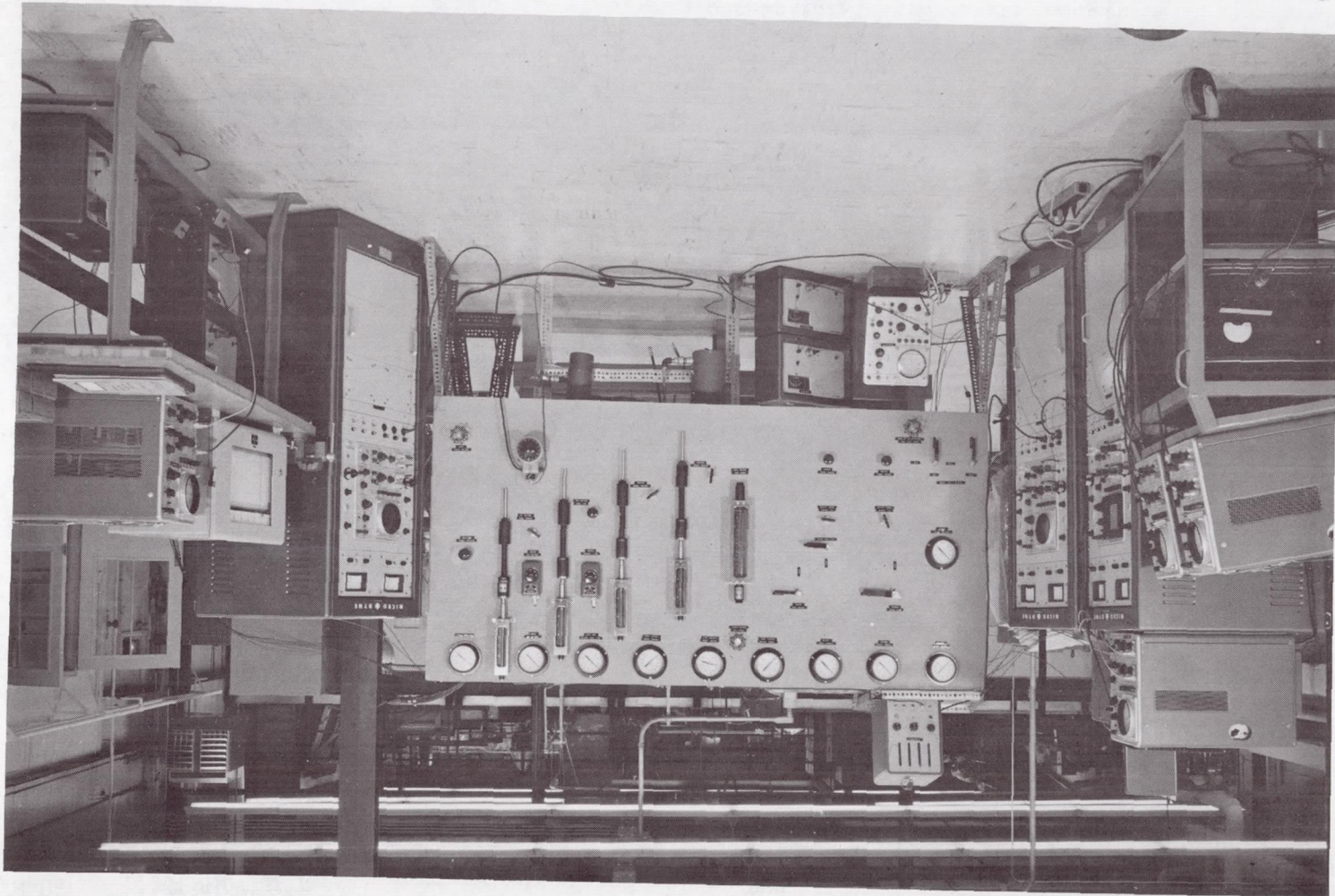
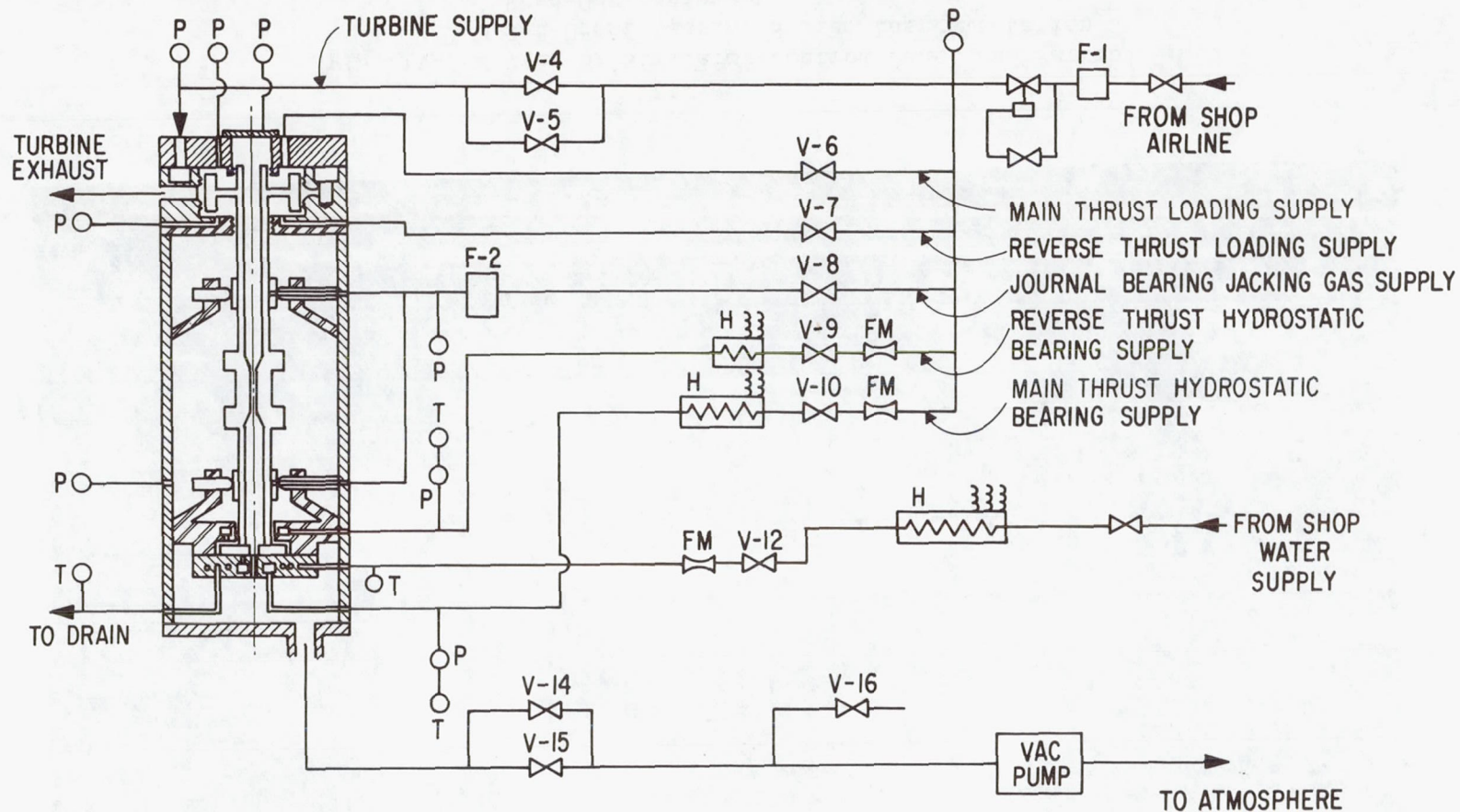


Fig. IV-2 View of Simulator Control Panel and Partial Set-Up of Bearing System Instrumentation Read-Out Equipment



LEGEND FOR FIGURE IV-3




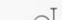
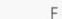
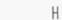
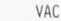
-  VALVE-HAND OPERATED-LOCATED ON CONTROL PANEL
-  VALVE-PNEUMATICALLY OPERATED-REMOTELY LOCATED
-  P - PRESSURE GAUGE - LOCATED ON CONTROL PANEL
-  T - THERMOCOUPLE - READ OUT ON TEMPERATURE RECORDER
-  F - FILTER - LOCATED IN SUPPLY PIPE LINES
-  H - ELECTRIC HEATER - LOCATED IN SUPPLY LINES
-  VAC - VACUUM PUMP

Fig. IV-3 Schematic Diagram of the Simulator Test Set-Up for Test Evaluation of the Rotor-Bearing System

Calibration of Journal Bearing Flexures

Prior to assembly of the simulator journal bearing parts, load versus deflection characteristics were experimentally obtained for each of the journal bearing pivot-support flexures. Load versus deflection plots for the upper and lower pivot-support flexures are shown in Figure IV-4.

It is seen from Figure IV-4 that the load-deflection characteristic for the four lower pivot-support flexures is quite linear up to 70 pounds and that the average stiffness over the linear range is 84,000 lb./in. The four upper flexures are linear up to the maximum applied load of 103 pounds and have an average stiffness of 34,800 lb./in.

The design stiffness values for the pivot-support flexures were 150,000 and 50,000 pounds per inch for the lower and upper flexures respectively. The measured stiffness values noted above are appreciably less than the design values. The discrepancy between design and measured values of flexure stiffness is believed to be due to "non-ideal" boundary conditions which exist at the ends of the flexure sections. For the purposes of design, a zero-slope boundary condition was assumed at the ends of the two beam sections of which each flexure is comprised (see Figure II-1). In actual fact, this assumption is probably somewhat in error due to (1) some deflection of the thicker central portion of the flexure (which carries the pivot screw), and (2) some deflection within the clamping zone at the two ends of the flexure.

The effects of lower-than-anticipated stiffness values for the flexures are as follows:

1. a small reduction in rigid-body critical speeds of the rotor-bearing system,
2. an increase in the radial shift of journal position when rotor orientation is changed from vertical to horizontal in a 1-g acceleration field,

3. a reduction in maximum bending stress,
4. an improved ability of the bearings to accommodate differential thermal expansions and journal centrifugal growth which would otherwise tend to change bearing clearance; and
5. an increase in sensitivity of the bearing system to radial electromagnetic alternator forces arising from eccentricity of the alternator rotor to the alternator stator.

The calculated radial shift in journal position resulting from a change in rotor orientation (item 2 above) is as follows:

<u>Flexure Stiffness</u> <u>lb./in.</u>		<u>Component of Journal</u> <u>Shift due to Flexure</u> <u>Stiffness- mils</u>
50,000	design values	0.14
150,000		
34,800	measured values	0.24
84,000		

By proper set-up of the bearing during assembly, the maximum eccentricity of the journals (relative to the centerline of the bearings and labyrinth seals), resulting from the component of journal shift due to flexure stiffness, can be held to one-half of the shift value. Hence, the maximum eccentricity of the journals, based on measured flexure stiffnesses, can be theoretically held to 0.12 mils. This amounts to 6 percent of the total allowable eccentricity (total allowable journal eccentricity being 2.0 mils as determined from alternator electromagnetic force considerations). Since total journal eccentricity under normal turboalternator operating conditions should not exceed 0.6 mils, and an assembly eccentricity tolerance of 1.0 mil is entirely reasonable, the lower-than-design flexure stiffness values present no problem with respect to meeting the desired total eccentricity criterion.

With respect to the increased sensitivity of the bearings to alternator electromagnetic forces (item 5 listed above), the question is one of overall change in

total bearing stiffness. Calculated total bearing stiffness values, based on turboalternator operation in argon at 6.0 psia and 12,000 rpm, are as follows:

Flexure Stiffness lb./in.	Total Bearing Stiffness lb./in.
50,000 150,000 design values	72,600
34,800 84,000 measured values	57,800

The negative static force gradient (stiffness) per pole pair due to the alternator electromagnetic forces was predicted to be about 5,600 pounds per inch (test data presented in Section VII of this report show the measured gradient values to be somewhat less). The net restorative (positive) static stiffness value for one bearing and one alternator pole-pair would thus be as follows:

	Net Static Stiffness lb./in.
Based on design values of flexure stiffness	67,000
Based on measured values of flexure stiffness	52,200

Thus the lower-than-design flexure stiffnesses result in a 22 percent reduction in net static stiffness per bearing and pole-pair combination. It was not felt that this change would jeopardize safe operation of the rotor-bearing system. This feeling was subsequently confirmed by the theoretical rotor-bearing system dynamic study (Section V of this report) in which the lower values of flexure stiffness were used. Further confirmation of very satisfactory operation with the softer flexures was obtained from rotor-bearing system test data taken under alternator power generating conditions (see Section VII of this report).

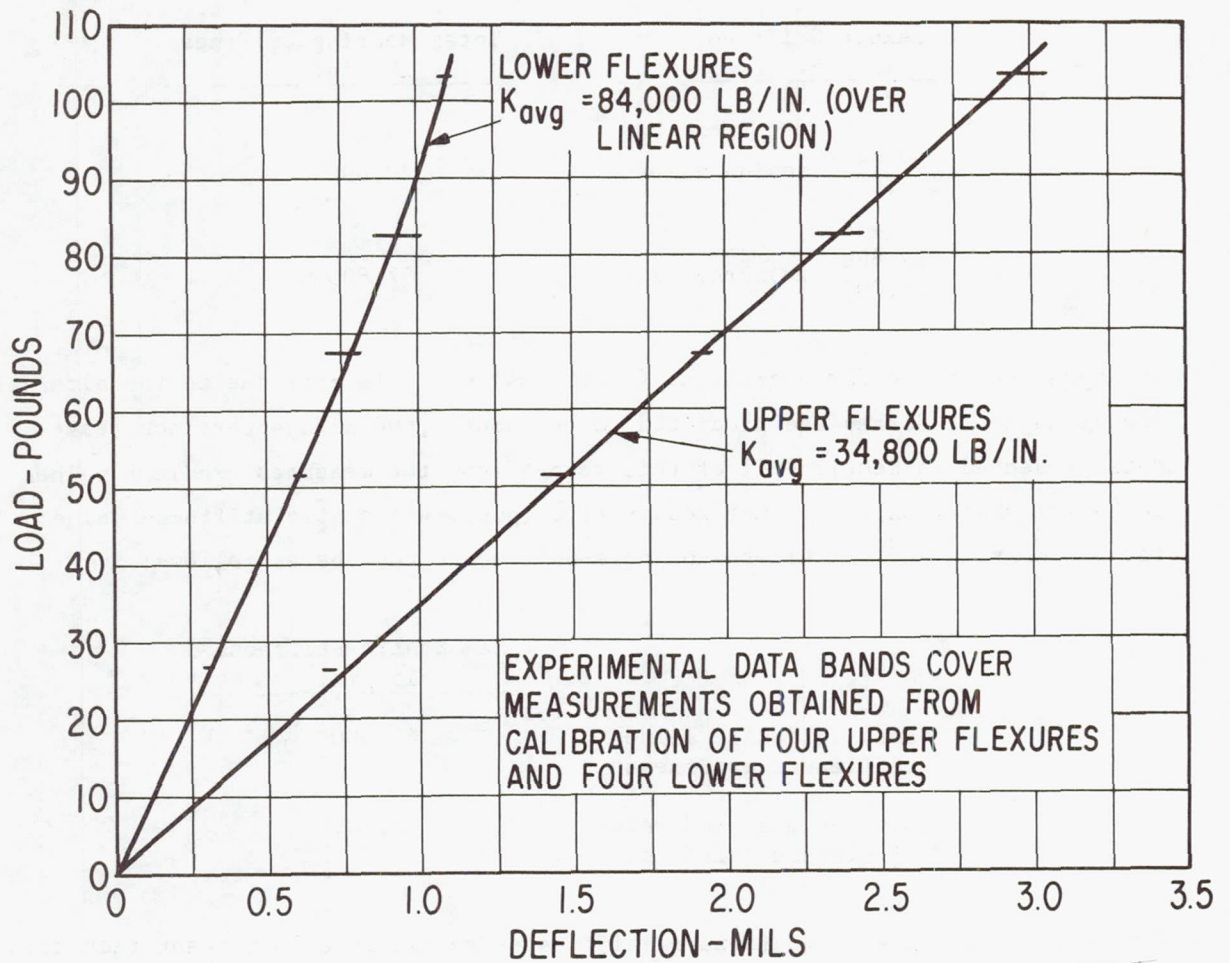


Fig. IV-4 Measured Load Versus Deflection Plots for the Upper and Lower Pivot-Support Flexures for the Turboalternator Journal Bearings

Calibration of Main Thrust Bearing Support Flexure

Prior to assembly of the simulator thrust bearing parts, an axial load versus deflection characteristic was experimentally obtained for the main thrust bearing support flexure. This is the flexure which supports the spiral-grooved thrust plate. The load versus deflection plot is shown in Figure IV-5.

It is seen from Figure IV-5 that the load-deflection characteristic for the thrust-plate support flexure is linear up to the maximum applied load of 200 pounds. The measured axial stiffness of the flexure is 33,100 pounds per inch as compared to the theoretical design stiffness of 38,600 pounds per inch. The probable reasons for the lower measured stiffness value are the same as previously mentioned for the journal bearing pivot-support flexures — namely, non-attainment in practice of the ideal boundary conditions which were assumed for the ends of the four flexure spokes (these spokes are pictured in Figure II-14).

Although no attempt was made to calibrate the support flexure in the tilt direction, the actual tilt stiffness should be lower than the design value of 99,000 in. lbs. per radian for the same reasons given for the axial stiffness results.

The dynamic response characteristics of the main thrust bearing assembly were reviewed based on the somewhat lower value of measured axial stiffness. It was observed that the resonant frequencies of the assembly would change, at most (i.e., neglecting gas-film stiffness effects), in proportion to the square root of stiffness. Hence, the maximum possible reduction of the axial resonant frequency would be 7.4 percent — that is, from 16,400 cpm to 15,200 cpm when gas-film stiffness was neglected. Under a 30 pound thrust load, the axial resonant frequency would be approximately 24,400 cpm.

Assuming the same percentage reduction in tilt stiffness as was measured for axial stiffness, the tilt resonant frequency would be reduced from 18,250 cpm to 16,900 cpm under no-load conditions. At a 30 pound thrust load condition, the resonant frequency would be 28,300 cpm.

In addition to the acceptable resonant frequency situation, the effect of lower axial and tilt stiffnesses of the support flexure was checked with respect to ability of the spiral-grooved thrust plate to track dynamic motions (in the axial and tilt directions) of the rotating thrust runner. It was found that the reduced stiffness values would not significantly alter the tracking capability.

Based on the results of the dynamic review summarized above, and recognizing that the reduced stiffness values would have beneficial effects of

1. reducing maximum flexure stresses, and
2. improving ability of the thrust plate to align to the average plane of the thrust runner,

the design of the flexure support, as calibrated, was judged satisfactory for initiation of simulator testing. Subsequent test results fully confirmed that the flexure design was satisfactory for the turboalternator application.

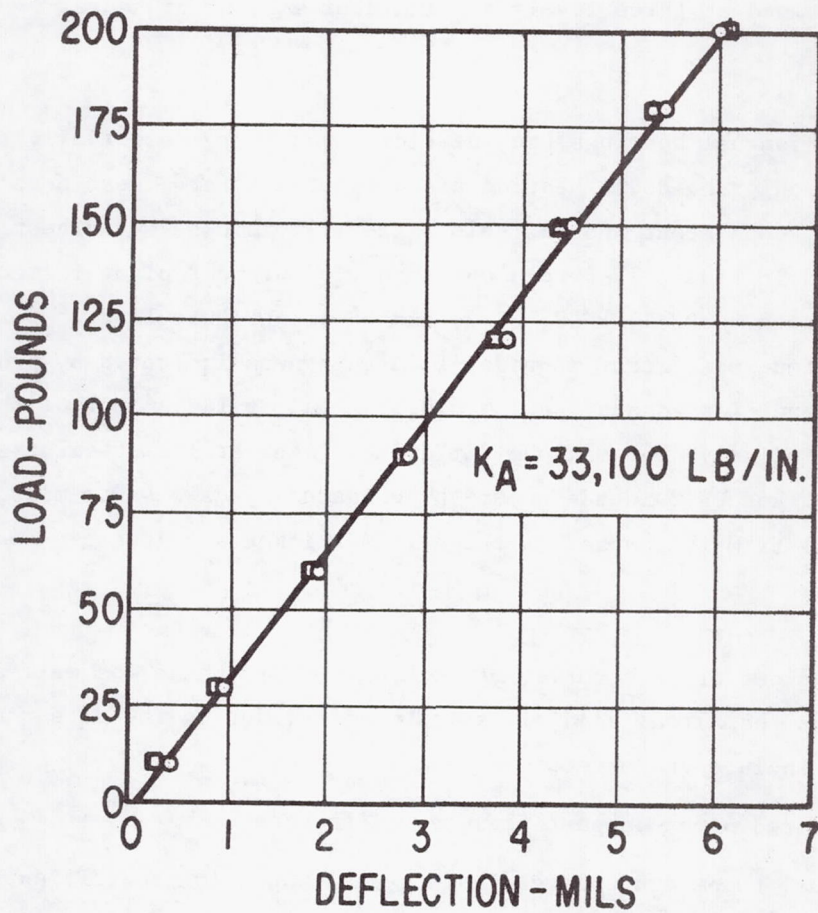


Fig. IV-5 Measured Load Versus Deflection Characteristic for the Forward Thrust Bearing Whipple-Plate Support Flexure

Test Evaluation of the Hydrodynamic Journal Bearings

A comparison of measured and calculated performance for the No. 1 journal bearing during self-acting operation in air is shown in Figure IV-6. Calculated and test data were obtained at three levels of simulator ambient pressure — 14.7, 8.8, and 6.7 psia.

Since the two journal bearings are identical, and carry essentially the same loads, test data for only the No. 1 bearing are presented here. These data were judged to be the most consistent and reliable. The film thickness and bearing eccentricity values plotted in Figure IV-6 were obtained via the four pivot-film capacitance probes designated as PF-1, PF-2, PF-3, and PF-4 in Figure II-23. During the data runs, the maximum difference in pivot-film thickness indicated by probes PF-3 and PF-4 in the lower (or loaded) pads was 0.07 mils, or 14 percent of the nominal film thickness. Similarly, the maximum difference in pivot-film thickness indicated by probes PF-1 and PF-2 in the upper (or unloaded) pads was 0.5 mils, or 30 percent of the nominal film thickness. Average film-thickness values are shown on Figure IV-6.

The calculated performance curves of Figure IV-6 are based, as well as could be determined, on the actual conditions that existed during the data runs. The calculations include the effects of

1. measured pivot-support flexure stiffnesses,
2. actual temperature levels and thermal expansion coefficients for the various bearing parts, and
3. measured zero-speed set-up clearance of the bearing.

It is seen from Figure IV-6 that there is quite good agreement (within 10 percent) between the calculated and measured film thickness and eccentricity ratio values at ambient pressures of 6.7 and 8.8 psia.

At the 14.7 psia ambient pressure condition, the measured film thickness values are considerably smaller than the calculated values. At design speed, the measured films range from 14 to 24 percent smaller than calculated; while at 4,000 rpm, the discrepancy has increased to about 40 percent. Data taken in January of 1967 shows somewhat greater film thickness than the original data taken in December of 1965 under the same operating conditions and using the same bearing parts. While the later data may be somewhat more accurate as a result of more careful calibration of the complete capacitance probe readout system, there is no question that the measured film thicknesses are significantly lower than predicted.

There is no obvious explanation for the discrepancy between calculated and measured bearing performance, particularly at the 14.7 psia ambient pressure condition. The theoretical procedures are known to be reasonably accurate, as is evidenced by the fairly good agreement obtained at 6.7 and 8.8 psia ambient pressure. It can only be concluded that there was some experimental parameter which was not accurately controlled, measured, or taken into account.

In spite of the discrepancy between the calculated and measured bearing performance, the measured performance is entirely adequate for the turboalternator application. For operation in argon, the film thicknesses will be greater than in air for any given ambient pressure condition. For vertical orientation of the rotor, the pivot-film thickness for all pads will be greater than 0.8 mils.

Oscilloscope photographs of the journal bearing film thickness traces and journal motions are presented and discussed in Section VII of this report, in connection with test evaluation of the bearings under various conditions of alternator load. These photographs, as well as additional plots of calculated and measured performance, were obtained using the same bearing parts as were used for the first series of simulator tests without alternator load. In particular, Figures VII-9, 11, 17, 18 and 19 show film thickness traces, journal motions, and comparison of measured and calculated performance under no-load alternator conditions. Figures VII-16a and 16c document the state-of-balance (in terms of unbalance orbit size) achievable with the rotor-bearing system. These data are all typical of the journal bearing performance obtained during the first simulator test program, and, in the interest of brevity, will not be further presented or discussed in this section.

In summary, performance of the journal bearings was excellent throughout the first simulator test program (as well as throughout the subsequent test program with alternator load). No sign of bearing or rotor-bearing instability was detected at any time. Likewise, no bearing failures or rubs were experienced.

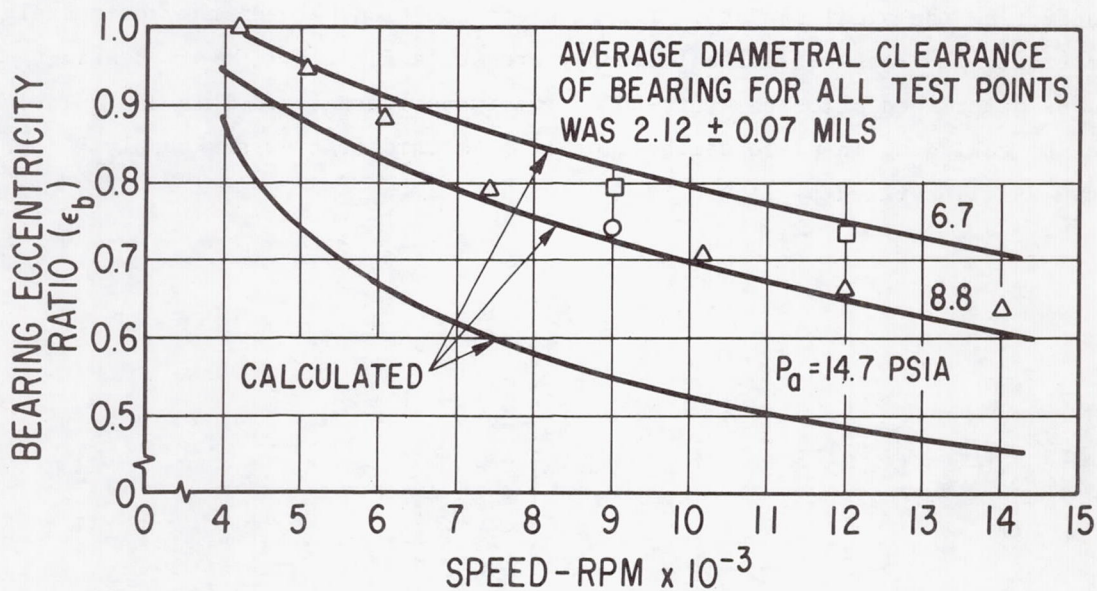
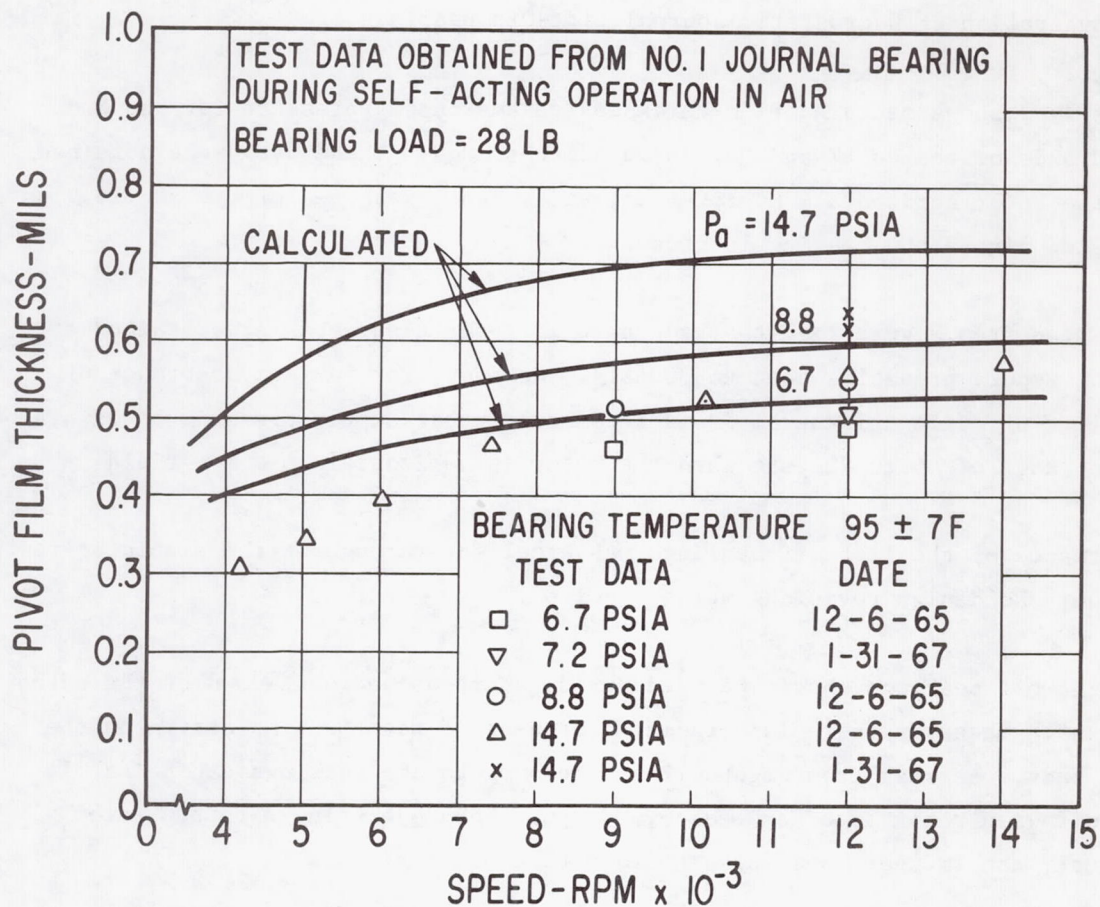


Fig. IV-6 Comparison of Measured and Calculated Performance of the No. 1 Journal Bearing During Hydrodynamic Operation in Air

Test Evaluation of Hydrostatic Journal Lift-Off Bearings

Figure IV-7 shows measured film thickness versus supply pressure for the two loaded pads of the No. 1 and No. 2 journal bearings. These data were obtained with the rotor horizontal, no rotation, at ambient pressures of 8.8 and 14.7 psia, and using air as the bearing lubricant.

It is seen from Figure IV-7 that adequate lift-off clearances are obtained at bearing supply pressures down to 30 psig. However, for maximum assurance of safe lift-off film thickness, it is recommended that supply pressure be maintained in the range of 40 to 70 psig when the rotor is horizontal in a 1-g field.

Performance of the lift-off bearings was excellent throughout the simulator test program. No design revisions were required.

The lift-off bearings should be used during start-up and shut-down of the turbo-alternator whenever there is a radial component of rotor weight acting on the lower pads. As seen from Figure IV-6, pressure to the bearings can be safely shut off when rotor speed exceeds 8,000 rpm. When operating with the rotor vertical, the lift-off bearings should not be pressurized.

When operating the simulator at an intermediate position between the horizontal and vertical, the range of suitable supply pressures for the lift-off bearings should be determined prior to start-up of the turboalternator. This can quickly be done by making an in-place calibration of film thickness versus supply pressure as illustrated by Figure IV-7.

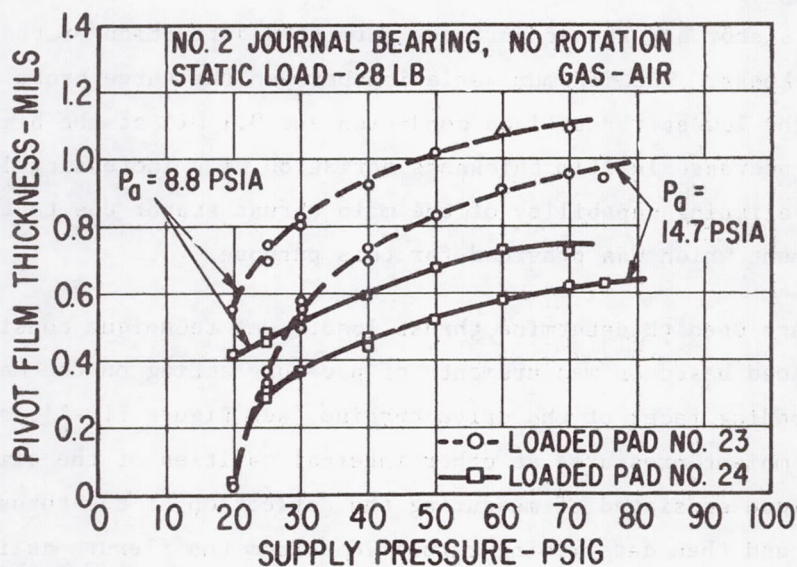
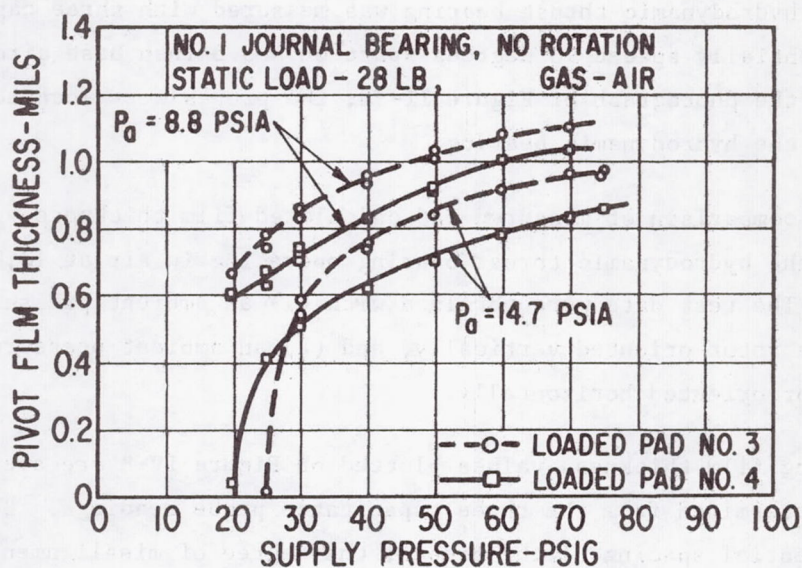


Fig. IV-7 Measured Performance of the No. 1 and No. 2 Hydrostatic Journal Bearings at 8.8 and 14.7 PSIA Ambient Pressure

Test Evaluation of the Hydrodynamic Thrust Bearing

The same hydrodynamic thrust bearing was used throughout the simulator test program — no modifications to its design were required. During all tests, film thickness of the hydrodynamic thrust bearing was measured with three capacitance probes circumferentially spaced 90 degrees apart on a 3.3 inch base circle. As can be seen from the photograph of Figure II-13, the probes were located in the "seal" region of the hydrodynamic bearing.

Figure IV-8 is a comparison of measured and calculated film thickness versus thrust load for the hydrodynamic thrust bearing operating in air at 12,000 rpm (design speed). The test data were obtained with (1) an ambient pressure of 14.7 psia and the rotor oriented vertically, and (2) an ambient pressure of 8.8 psia and the rotor oriented horizontally.

The thrust bearing film thickness values plotted on Figure IV-8 are average values of the film as determined from the three capacitance probe readings. Because of the circumferential spacing of the probes, the degree of misalignment between the thrust bearing stator and runner could be measured. Knowing the relative positions of the stator and runner surfaces permitted definition of the average bearing film thickness. The maximum variation between the three probe readings was 0.2 mils at the lowest thrust load condition and 0.1 mil at the highest load condition. This decrease in film thickness variation with increasing load demonstrates the self-aligning capability of the main thrust stator due to the flexure mounting arrangement which was provided for this purpose.

Two techniques were used to determine thrust load. One technique consisted of calculating the load based on measurements of pressure acting on the main and reverse thrust-loading faces of the drive turbine (see Figure III-1), as well as measurements of ambient pressures at other internal cavities of the simulator. The second technique consisted of measuring the deflection of the thrust-stator support flexure, and then determining thrust load from the flexure calibration curve of Figure IV-5. The data for both techniques of load determination are plotted on Figure IV-8. At loads greater than 80 pounds, the agreement between the two load measuring techniques is very good. At the lowest load condition (approximately 22 pounds) there was a 50 percent discrepancy between the two load values. Since both measurement techniques involved various experimental uncertainties, it was not possible to determine which technique was giving the more accurate value.

It is seen from Figure IV-8 that the measured load capacity of the hydrodynamic thrust bearing is less than the calculated value at film thicknesses less than 0.83 mils. At film thicknesses greater than 0.83 mils, the load capacity exceeds the calculated value. At the maximum design load of 85 pounds, a very satisfactory film thickness of 1.0 mil was obtained, this being slightly in excess of the calculated 0.92 mil film thickness. These data indicate that the thrust bearing performance in argon should be very close to, or may slightly exceed, the predicted design-point performance summarized in Table II-4.

It is also seen from Figure IV-8 that while the measured load capacity exceeds calculated load capacity for films greater than 0.83 mils, there is considerable discrepancy in the experimental data for the two ambient pressure conditions. In theory, there should be very little difference in the load versus film thickness curve for a variation of 8.8 to 14.7 psia. If anything, the load capacity should be slightly less at 8.8 psia. The test data, however, shows considerable variation in load capacity at film thicknesses greater than 1.1 mils, with a greater capacity at the lower ambient pressure.

There is no logical explanation for the effect of ambient pressure as indicated by the test data. However, at the same time that ambient pressure was changed, so also was rotor orientation. It is believed that this change in orientation may have effected the accuracy of the load data via some unrecognized mechanism. No attempt was made to track down the source of error, since the error was significant only at conditions of large film thickness, and at these conditions the measured load capacity was always considerably greater than the predicted.

The fact that the measured load capacity of the thrust bearing is less than predicted at small values of film thickness is typical of all spiral-grooved bearings thus far tested. The predicted load curve assumes that the thrust plates are perfectly flat and aligned. In actual fact, there is always some degree of non-flatness and misalignment. At small film thicknesses, these practical effects result in a significant deviation from the idealized flat and parallel condition, and a significant loss in load capacity occurs. Nonetheless, operation of the thrust bearing down to film thicknesses of 0.7 mils is considered to be reasonable for a bearing of this size (assuming, of course, that the bearing has been

properly installed and set-up). It is clear from Figure IV-8, that the bearing is capable of carrying a significant amount of overload at 0.7 mils clearance.

Figure IV-9 shows the effect of speed on hydrodynamic load capacity for constant ambient pressure of 8.8 psia. This data exhibits the expected trend for the effect of speed change, and also indicates that the thrust bearing can safely carry design thrust at speeds down to 9,000 rpm.

Oscilloscope photographs of the thrust bearing film thickness probe signals during hydrodynamic operation in 14.7 psia ambient air are shown in Figure VII-20a. These are typical of thrust bearing performance during the first simulator test. It is seen that total indicated runout of the thrust runner was less than 0.1 mil.

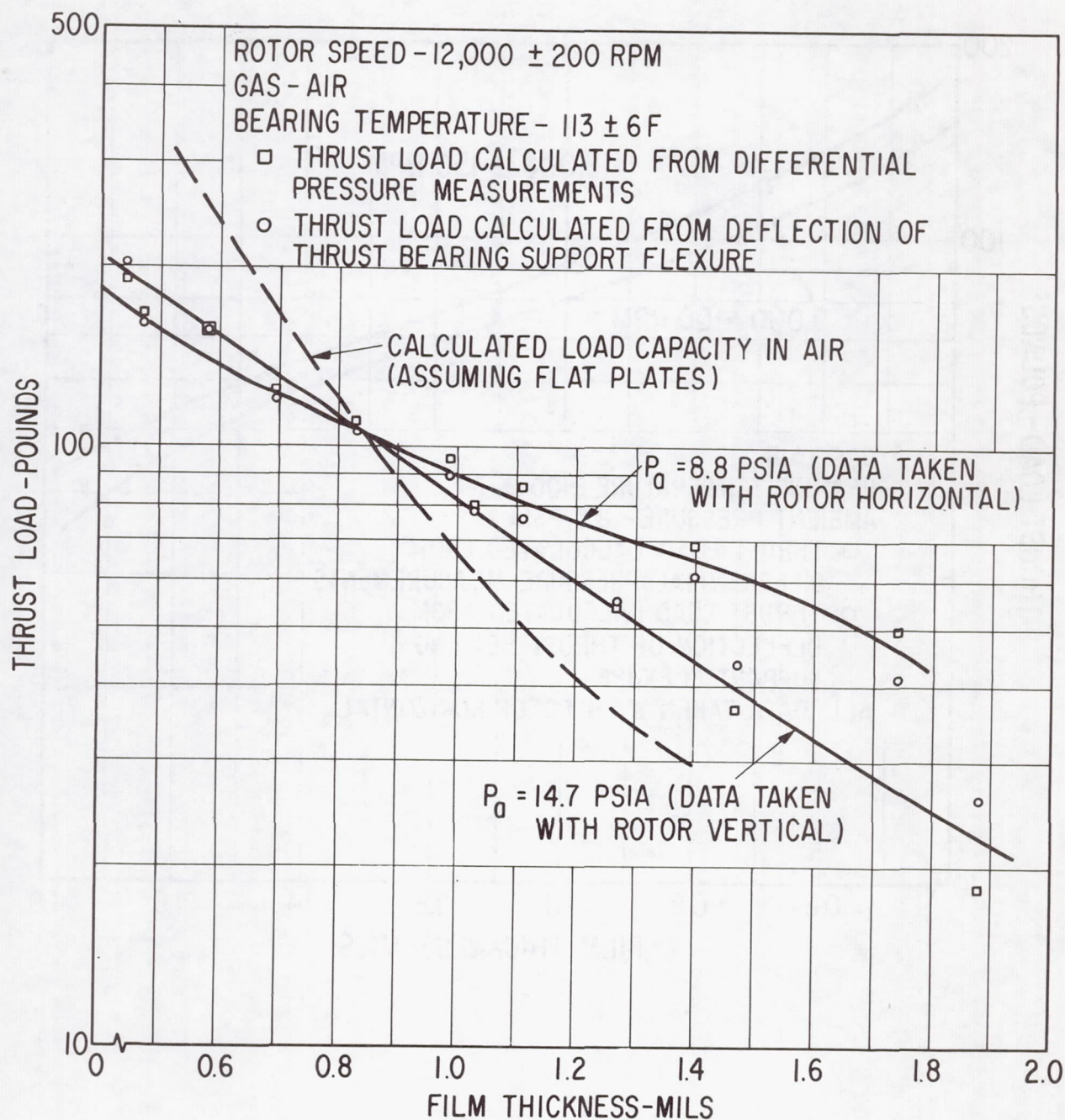


Fig. IV-8 Measured Load Versus Film Thickness for the Hydrodynamic Thrust Bearing at 12,000 RPM

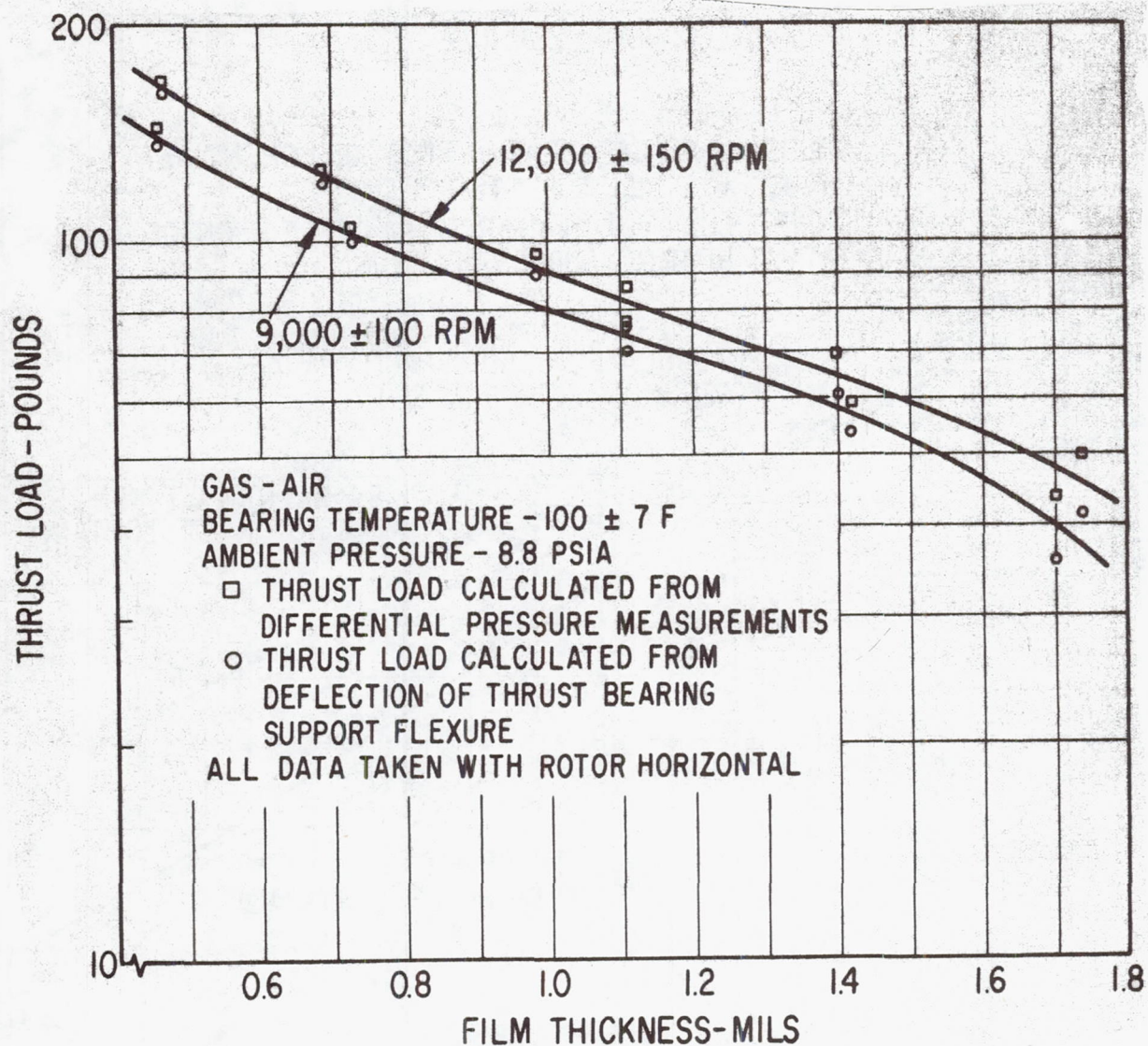


Fig. IV-9 Measured Load Versus Film Thickness of the Hydrodynamic Thrust Bearing at 12,000 and 9,000 RPM

Test Evaluation of the Main Hydrostatic Thrust Bearing

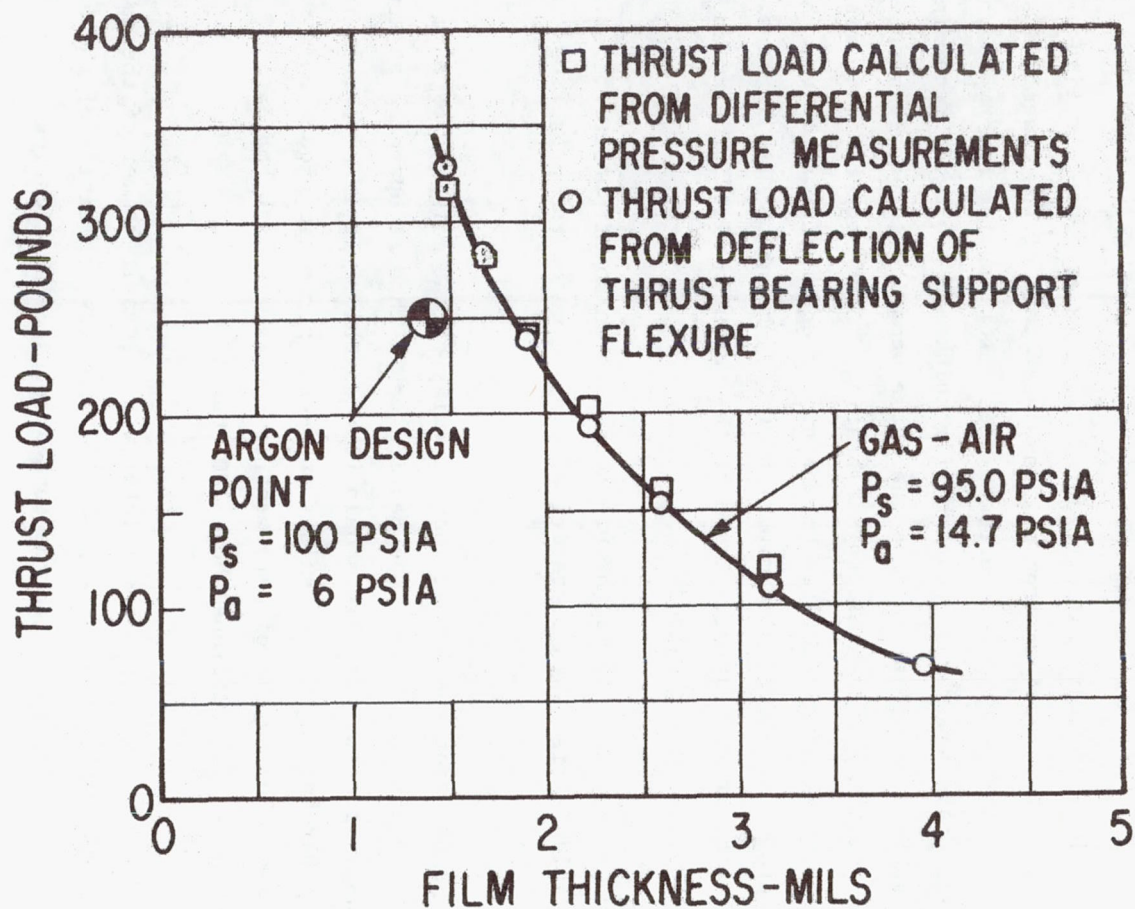
Test data for the main hydrostatic thrust bearing is presented in Figure IV-10. The plotted curve was obtained from an "in-place" test of the assembled simulator. Thrust load was measured by the two techniques described for the hydrodynamic thrust bearing. Average thrust bearing film thickness was again determined via film thickness readings obtained from the three capacitance probes mounted in the "seal" region of the hydrodynamic thrust bearing. Since the hydrodynamic and main hydrostatic thrust bearings utilize common stator and runner surfaces, the three capacitance probes permitted determination of the amount of misalignment in the main hydrostatic thrust bearing. Based on the measured misalignment, an average film thickness value was obtained.

Also plotted on Figure IV-10 is the predicted design-point condition for the main hydrostatic bearing when operating with argon under the prescribed conditions of pressure.

Figure IV-10 shows that the actual load capacity of the main hydrostatic slightly exceeds the predicted capacity. The bearing could thus be operated at lower values of supply pressure if this should be desirable. It is also seen from Figure IV-10 that good agreement exists between the two techniques used for measuring thrust load. The degree of agreement is consistent with the data of Figures IV-8 and IV-9 at load conditions above 100 pounds.

At no time during testing of the simulator was pneumatic hammer of the main hydrostatic thrust bearing observed. In all respects, operation of the bearing was judged to be satisfactory for the turboalternator application.

Fig. IV-10 Measured Load Versus Film Thickness Data
for the Main Hydrostatic Thrust Bearing



Test Evaluation of the Reverse Hydrostatic Thrust Bearing

Figure IV-11 shows load versus film thickness test data for the reverse hydrostatic thrust bearing. The data was obtained from an "in-place" test of the assembled simulator. In this case, thrust loads could only be determined by the differential pressure measurement technique as described for the hydrodynamic thrust bearing. Since the reverse thrust bearing is rigidly mounted, the flexure load-deflection calibration technique was not applicable. Film thickness was measured with the single capacitance probe which was located in the bearing.

Also plotted on Figure IV-11 is the predicted design-point condition for the reverse hydrostatic bearing when operating with argon under the prescribed pressure conditions. It is seen that the measured film thickness under the air test conditions is 33 percent below the argon design-point film thickness at the 100 pound load condition.

Using the measured test data in air as a reference point, the performance of the bearing was analytically extrapolated to the argon design-point condition. The resulting calculated film thickness for a 100 pound load was 1.2 mils — still 20 percent below the predicted design value. A concerted effort to track down the reason for this discrepancy was not attempted since, from a practical standpoint, 1.2 mils of clearance at the 100 pound design load condition was more than adequate for safe operation of the bearing. In addition, the bearing was safely operated at clearances down to 0.7 mils, which means that it had considerable overload margin. It is suspected that part of the discrepancy between measured and predicted load capacity may have been due to bearing misalignment.

At no time during the simulator test program was pneumatic hammer of the reverse hydrostatic bearing observed. Performance of the bearing was judged to be adequate for the turboalternator application.

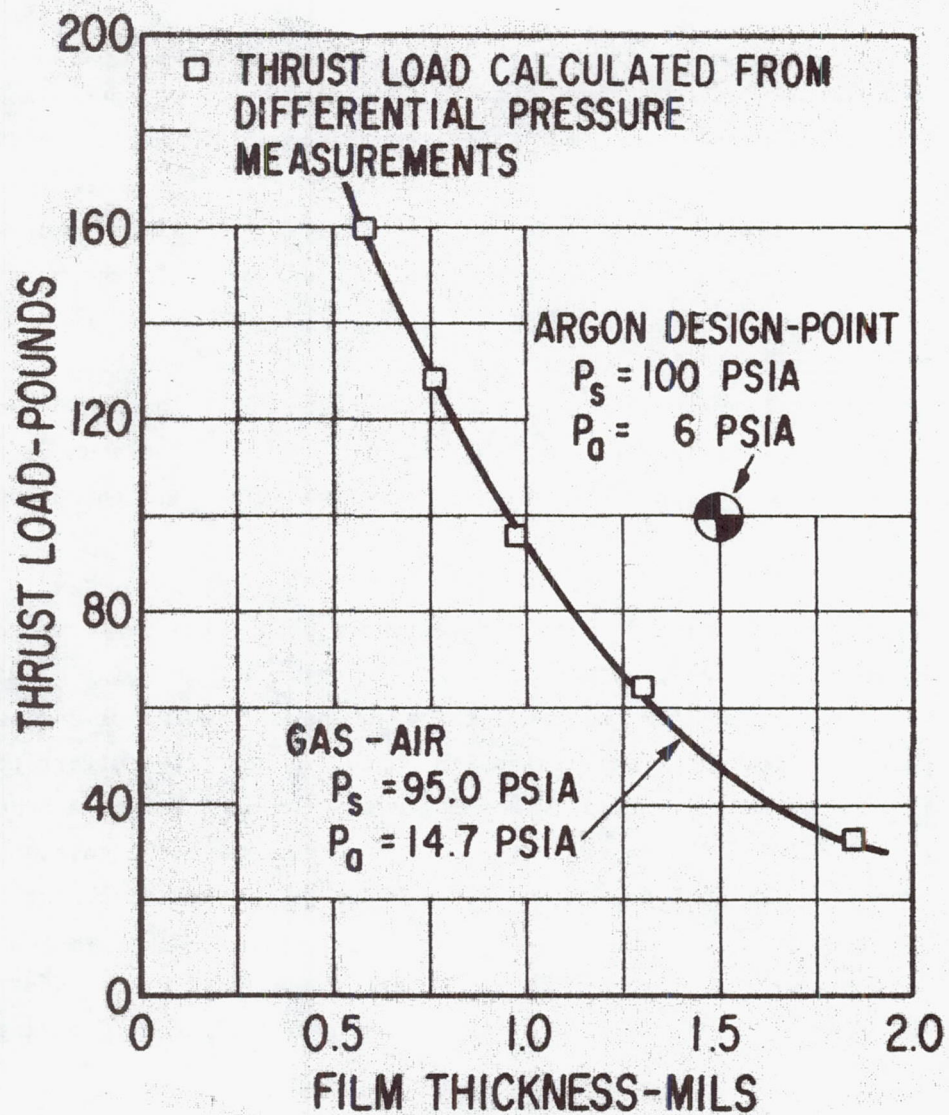


Fig. IV-11 Measured Load Versus Film Thickness Data for the Reverse Hydrostatic Thrust Bearing

V. ANALYTICAL INVESTIGATION OF ROTOR RESPONSE AND STABILITY TO ALTERNATOR ELECTROMAGNETIC FORCES

The practical application of gas bearings to high-speed rotating machinery is a sufficiently recent event that many important technical problem areas are far from fully explored. Whereas gas bearings offer many advantages in particular applications, and even must be considered essential to certain types of machinery, their use requires special attention in areas which many times would not be considered with conventionally lubricated bearings. One such example is the application of gas bearings to electrical machinery.

Conventional electrical machinery runs in ball bearings or oil-lubricated journal bearings. These bearings are normally dimensioned and designed in the same way as in any other piece of rotating machinery and without paying any special attention to the magnetic forces present in the machine. This is possible because these bearings are not overly sensitive to changes in load or to dynamic excitations. With gas bearings, however, it is not possible to ignore the magnetic forces. The load-carrying capacity of gas bearings is considerably smaller than that of oil bearings, and it is necessary to know the bearing reactions accurately when designing the bearings. Furthermore, gas bearings have less stiffness than oil bearings and, of even greater significance, they have less damping—especially with high frequency excitation. It is, therefore, to be expected that electrical machinery with gas bearings will exhibit higher amplitudes and a more pronounced frequency response than similar conventional machinery. Actual experience shows this to be the case, and in several machines the encountered vibration amplitudes were sufficiently large to require modifications or redesigns of the unit. Although this experience was limited to machines with electric motors, it is natural to expect alternators to behave in a similar fashion. For this reason an analytical investigation of the NASA turboalternator was undertaken to check its vibrational response and stability, and on the basis of the results, determine if the design was adequate or would require modification.

To perform such an investigation, it is first necessary to know what the alternator magnetic forces are. Although it is possible, as shown later, to estimate the fundamental part of the magnetic forces from a rather simple analysis, an

extensive study is required to obtain all the force components. Such a study has been performed by the General Electric Company as a part of the same overall investigation, and the calculations in the present report are based on the force values supplied by G.E. The forces are calculated for six different operating conditions of the alternator of which three cases are for balanced load conditions and the other three cases are for short circuit conditions. Only in the latter cases are there force components with frequencies higher than the fundamental frequency.

The magnetic forces cause the rotor to vibrate and they also affect the stability of the rotor. Since the forces may contain a number of frequencies, there always exists the possibility of exciting one or more of the resonances of either the rotor or the shoes in the pivoted-pad bearings. Depending on the magnitude of the forces and the available damping in the system, the corresponding amplitudes could become prohibitively large, especially at higher frequencies where the bearings lose most of their damping capacity. Furthermore, since the magnetic forces depend directly on the eccentricity between the axes of the alternator stator and the rotor, any rotor vibration will produce forces, thereby making it possible to transfer energy from the alternator field into vibrations of the rotor which may create a situation of self-excited instability.

It is the purpose of this discussion to present the methods developed to calculate the amplitude response and to check stability of the turboalternator, and to give the results of computations performed for the machine operating at 12,000 rpm in a vertical position for six alternator load conditions.

Based on the developed analyses, three computer programs were written to perform the calculations. These programs are sufficiently general that a wide range of operating conditions of the turboalternator could be investigated. However, for the particular specified operating conditions, the results did not show any response amplitudes of significance nor was any danger of instability indicated. Thus, it was concluded that for the specified conditions, the magnetic forces have no adverse effect on the performance of the machine.

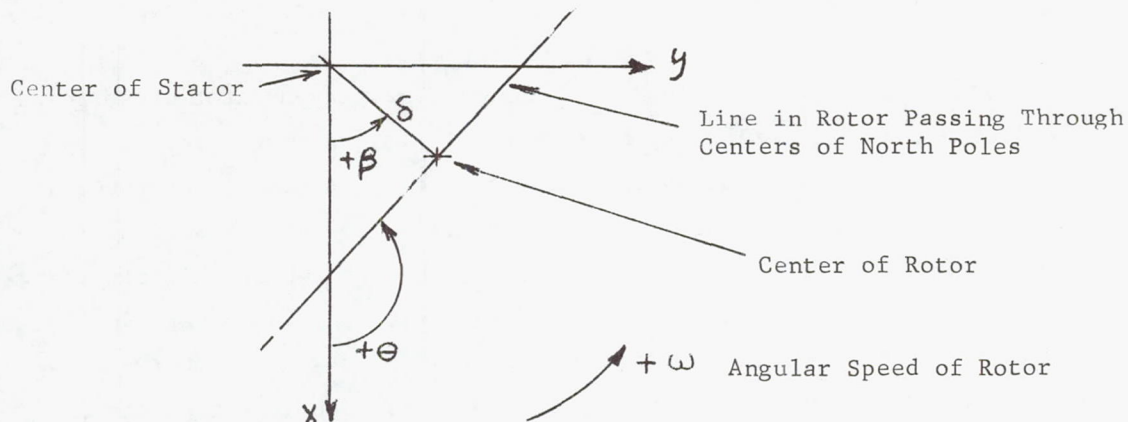
Discussion of the Technical Problem

The turboalternator consists of a four-pole homopolar-type generator whose poles are integral with the shaft. The shaft is supported in two four-shoe pivoted-pad gas journal bearings, and the wheel of the two-stage turbine is overhung at one end of the shaft. At the other end of the shaft is the thrust bearing runner, also overhung. The generator poles are arranged such that two of the poles (say the two northpoles) are in one plane, 180 degrees apart, and the other two poles, southpoles are in a different plane, displaced 90 degrees from the northpoles. When the rotor is eccentric with respect to the magnetic axis of the alternator stator, forces will be set up in each pole plane because of the magnetic unbalance. Since the allowable eccentricity is small in comparison with the generator air gap, the forces can be taken to be directly proportional to the displacement of the rotor center. One force consists of a steady magnetic pull, acting as a negative spring force in the direction of rotor displacement. In addition there are a number of force components which also are directly proportional to rotor eccentricity and vary harmonically with time. When the alternator load is balanced and there are no short circuits, the predominant force frequency by far is twice the angular speed of the rotor. Other frequencies also present are caused by stator slotting, amortisseur slots, and harmonics in the MMF; but, except for certain short circuit conditions, these force components are so small they can be ignored. On this basis, it is possible to arrive at an expression for the magnetic forces by means of a very simple analysis which, though approximate, gives a good estimate of the forces [16].

Assume the MMF to be constant, i.e., ignore any harmonics in the MMF and ignore the armature reactance. Then the flux density B in the alternator air gap is

$$B = \frac{\mu MMF}{h}$$

where μ is the permeability of air and h is the air gap. Introduce a cartesian coordinate system with origin in the center of the alternator stator, the x-axis vertical downwards and the y-axis horizontal.



The rotor is eccentric by the amount δ and the angle between the x-axis and the direction of eccentricity is β . The angular speed is ω . If the mean airgap is C , the airgap thickness can be written as

$$h = C - \delta \cos(\theta - \beta)$$

where θ is the angle from the stator x axis to a radial line in the rotor passing through the centers of the north poles.

Since $\delta \ll C$, the flux density becomes

$$B = \frac{\mu \cdot \text{MMF}}{C \left[1 - \frac{\delta}{C} \cos(\theta - \beta) \right]} \approx B_0 \left[1 + \frac{\delta}{C} \cos(\theta - \beta) \right] \quad (1)$$

where

$$B_0 = \frac{\mu \cdot \text{MMF}}{C}$$

B_0 is the flux density when the rotor is concentric with the stator. To find the magnetic forces caused by one pole, it is necessary to integrate B^2 over the pole area. The force has two components, F_x and F_y .

$$F_{x,\text{pole}} = \frac{1}{72} \int_A B^2 \cos\theta \, dA$$

$$F_{y,\text{pole}} = \frac{1}{72} \int_A B^2 \sin\theta \, dA$$

where the numerical factor is a conversion factor to get the force in pounds when the area A is in square inches and B is in kilolines per square inch. The pole has a radius R , a length L and extends over an angle α . Assume that at time equal zero

the north poles are on the x-axis such that the center of one pole will be at $\theta = \omega t$ and the center of the other pole at $\theta = \omega t + \pi$. The total magnetic force is the sum of the two pole forces and becomes

$$F_x = \frac{RLB_0^2}{72} \left\{ \int_{\omega t - \frac{\pi}{2}}^{\omega t + \frac{\pi}{2}} [1 + 2\frac{\delta}{C} \cos(\theta - \beta)] \cos \theta d\theta + \int_{\omega t + \pi - \frac{\pi}{2}}^{\omega t + \pi + \frac{\pi}{2}} [1 + 2\frac{\delta}{C} \cos(\theta - \beta)] \cos \theta d\theta \right\}$$

or

$$F_y = \frac{RLB_0^2}{72} \left\{ \int_{\omega t - \frac{\pi}{2}}^{\omega t + \frac{\pi}{2}} [1 + 2\frac{\delta}{C} \cos(\theta - \beta)] \sin \theta d\theta + \int_{\omega t + \pi - \frac{\pi}{2}}^{\omega t + \pi + \frac{\pi}{2}} [1 + 2\frac{\delta}{C} \cos(\theta - \beta)] \sin \theta d\theta \right\}$$

$$F_x = \frac{RLB_0^2}{72} \cdot 2\frac{\delta}{C} \int_{\omega t - \frac{\pi}{2}}^{\omega t + \frac{\pi}{2}} 2 \cos(\theta - \beta) \cos \theta d\theta = \frac{RLB_0^2}{36} \cdot \frac{\delta}{C} \int_{\omega t - \frac{\pi}{2}}^{\omega t + \frac{\pi}{2}} [\cos \beta (1 + \cos 2\theta) + \sin \beta \sin 2\theta] d\theta$$

$$F_y = \frac{RLB_0^2}{72} \cdot 2\frac{\delta}{C} \int_{\omega t - \frac{\pi}{2}}^{\omega t + \frac{\pi}{2}} 2 \cos(\theta - \beta) \sin \theta d\theta = \frac{RLB_0^2}{36} \cdot \frac{\delta}{C} \int_{\omega t - \frac{\pi}{2}}^{\omega t + \frac{\pi}{2}} [\cos \beta \sin 2\theta + \sin \beta (1 - \cos 2\theta)] d\theta$$

From the figure above it is seen that:

$$x = \delta \cos \beta \quad y = \delta \sin \beta$$

Hence, in the plane of the northpoles,

$$F_x = \frac{\alpha RLB_0^2}{36 \cdot C} \left[\left(1 + \frac{\sin \alpha}{\alpha} \cos(2\omega t)\right) x + \frac{\sin \alpha}{\alpha} \sin(2\omega t) \cdot y \right]$$

$$F_y = \frac{\alpha RLB_0^2}{36 \cdot C} \left[\frac{\sin \alpha}{\alpha} \sin(2\omega t) \cdot x + \left(1 - \frac{\sin \alpha}{\alpha} \cos(2\omega t)\right) \cdot y \right]$$

or

$$F_x = [Q_0 + Q_1 \cos(2\omega t)] x + Q_1 \sin(2\omega t) y \quad (2)$$

$$F_y = Q_1 \sin(2\omega t) x + [Q_0 - Q_1 \cos(2\omega t)] y \quad (3)$$

where

$$Q_0 = \frac{\alpha RLB_0^2}{36 \cdot C} \quad \frac{\text{lbs}}{\text{inch}} \quad (4)$$

$$Q_1 = \frac{\sin \alpha RLB_0^2}{36 \cdot C} \quad \frac{\text{lbs}}{\text{inch}} \quad (5)$$

The southpoles are lagging the northpoles by 90 degrees. Hence, the magnetic forces in the plane of the southpoles become:

$$F_x = [Q_0 - Q_1 \cos(2\omega t)]x - Q_1 \sin(2\omega t) \cdot y \quad (6)$$

$$F_y = -Q_1 \sin(2\omega t) \cdot x + [Q_0 + Q_1 \cos(2\omega t)] \cdot y \quad (7)$$

Thus, if the rotor displacements are the same in the two pole planes, the net force on the rotor is independent of time, but there will be a time varying moment.

The poles have the following dimensions:

length: $L = 1.96$ inch
 radius: $R = 2.6$ inch
 arc: $\alpha = 63^\circ = 1.1$ radian
 radial airgap: $C = 0.040$ inch

Assuming a flux density of 45 kilolines per sq. inch at rated power, the force gradients become:

$$Q_0 = \frac{1.1 \cdot 2.6 \cdot 1.96 \cdot (45)^2}{36 \cdot 0.040} = 7,870 \frac{\text{lbs}}{\text{inch}}$$

$$Q_1 = \frac{\sin(63^\circ) \cdot 2.6 \cdot 1.96 \cdot (45)^2}{36 \cdot 0.040} = 6,370 \frac{\text{lbs}}{\text{inch}}$$

which is close to the more accurate values of $Q_0 = 5,630$ and $Q_1 = 6,870$ calculated by the General Electric Co. from their more comprehensive analysis for the condition of the alternator operating with balanced load, 0.8 PF, 15 KVA and no saturation effects.

For other operating conditions of the alternator, especially under short circuit conditions, the forces may be different such that there appear terms involving the cosines and sines of not only $2\omega t$, but also of $4\omega t$, $6\omega t$, and so on, in the

force equations. As shown in Appendix E, the general expressions for the forces are of the form:

$$F_x = -x \sum_{n=0}^N [Q_{xn} \cos(2n\omega t) - q_{xn} \sin(2n\omega t)] + y \sum_{n=0}^N [q_{yn} \cos(2n\omega t) + Q_{yn} \sin(2n\omega t)] \quad (8)$$

$$F_y = -x \sum_{n=0}^N [q_{xn} \cos(2n\omega t) + Q_{xn} \sin(2n\omega t)] - y \sum_{n=0}^N [Q_{yn} \cos(2n\omega t) - q_{yn} \sin(2n\omega t)] \quad (9)$$

It is seen that the equations derived above from the simple analysis conform to this form by setting $N=1$, $Q_{x0}=Q_{y0}=-Q_0$, $Q_{x1}=-Q_{y1}=Q_1$ and $q_{x1}=q_{y1}=0$. It is found that for the three balanced load conditions analyzed by G.E., this simpler form of the equations apply. Only for the three short circuit conditions is it necessary to use the more general form.

Let the rotor center be eccentric with respect to the center of the alternator stator and have the static coordinates (x_0, y_0) where x_0 and y_0 are specified values. If the rotor amplitudes x and y are measured from this steady-state point, the magnetic forces can be written as

$$F_{x, \text{total}} = F_{x0} + F_x \quad (10)$$

$$F_{y, \text{total}} = F_{y0} + F_y \quad (11)$$

where F_x and F_y are given by Eqs. (8) and (9) above, and

$$\begin{aligned} F_{x0} &= -x_0 \sum_{n=0}^N [Q_{xn} \cos(2n\omega t) - q_{xn} \sin(2n\omega t)] + y_0 \sum_{n=0}^N [q_{yn} \cos(2n\omega t) + Q_{yn} \sin(2n\omega t)] \\ &= \sum_{n=0}^N [A_n \cos(2n\omega t) + B_n \sin(2n\omega t)] \end{aligned} \quad (12)$$

$$\begin{aligned} F_{y0} &= -x_0 \sum_{n=0}^N [q_{xn} \cos(2n\omega t) + Q_{xn} \sin(2n\omega t)] - y_0 \sum_{n=0}^N [Q_{yn} \cos(2n\omega t) - q_{yn} \sin(2n\omega t)] \\ &= \sum_{n=0}^N [-B_n \cos(2n\omega t) + A_n \sin(2n\omega t)] \end{aligned} \quad (13)$$

where

$$A_n = -Q_{xn} x_0 + q_{yn} y_0 \quad (14)$$

$$B_n = q_{xn} x_0 + Q_{yn} y_0 \quad (15)$$

Thus, the magnetic forces are composed of two parts: one part, namely F_{x0} and F_{y0} , which is independent of the amplitudes; and one part, namely F_x and F_y , which is directly proportional to the amplitudes x and y . F_{x0} and F_{y0} can be considered to be external to the rotor and taken as active forces; whereas, F_x and F_y are passive forces. The active forces will make the rotor whirl, while the passive forces are an integral part of the rotor-bearing-alternator dynamic system.

By adding the passive magnetic forces to the rotor-bearing system, the possibility arises that the system may become unstable. To explain this phenomena, assume that the rotor equilibrium is disturbed, and the rotor center is set in harmonic motion described by:

$$x = x_c \cos(\nu t) - x_s \sin(\nu t) \quad (16)$$

$$y = y_c \cos(\nu t) - y_s \sin(\nu t) \quad (17)$$

where ν is the frequency of the motion. The power E imparted to the rotor by the magnetic forces is

$$E = \frac{1}{T} \int_0^T \left[F_x \frac{dx}{dt} + F_y \frac{dy}{dt} \right] dt \quad \frac{\text{lb-inch}}{\text{sec}}$$

where T is the time of one cycle. Substituting for F_x and F_y from Eqs. (8) and (9), and for x and y from Eqs. (16) and (17), the integral becomes

$$\begin{aligned} E = \frac{\nu}{2T} \int_0^T & \left\{ [(x_c^2 - x_s^2) \sin(2\nu t) + 2x_c x_s \cos(2\nu t)] \sum_{n=0}^N (Q_{xn} \cos(2n\omega t) - q_{xn} \sin(2n\omega t)) \right. \\ & - [(x_c y_c - x_s y_s) \sin(2\nu t) + (x_c y_s + x_s y_c) \cos(2\nu t) - x_c y_s + x_s y_c] \sum_{n=0}^N (q_{yn} \cos(2n\omega t) + Q_{yn} \sin(2n\omega t)) \\ & + [(x_c y_c - x_s y_s) \sin(2\nu t) + (x_c y_s + x_s y_c) \cos(2\nu t) + x_c y_s - x_s y_c] \sum_{n=0}^N (q_{xn} \cos(2n\omega t) + Q_{xn} \sin(2n\omega t)) \\ & \left. + [(y_c^2 - y_s^2) \sin(2\nu t) + 2y_c y_s \cos(2\nu t)] \sum_{n=0}^N (Q_{yn} \cos(2n\omega t) - q_{yn} \sin(2n\omega t)) \right\} dt \end{aligned}$$

Introduce the trigonometric identities:

$$\cos(2n\omega t) \cos(2\nu t) = \frac{1}{2} [\cos 2(n\omega + \nu)t + \cos 2(n\omega - \nu)t]$$

$$\sin(2n\omega t) \sin(2\nu t) = \frac{1}{2} [\cos 2(n\omega - \nu)t - \cos 2(n\omega + \nu)t]$$

$$\cos(2n\omega t) \sin(2\nu t) = \frac{1}{2} [\sin 2(n\omega + \nu)t - \sin 2(n\omega - \nu)t]$$

$$\sin(2n\omega t) \cos(2\nu t) = \frac{1}{2} [\sin 2(n\omega + \nu)t + \sin 2(n\omega - \nu)t]$$

The integral $\frac{1}{T} \int_0^T \sin 2(n\omega \pm \nu)t \, dt$ is always zero, and the integral $\frac{1}{T} \int_0^T \cos 2(n\omega \pm \nu)t \, dt$ is, in general, zero except for $(n\omega \pm \nu) = 0$ in which case the integral is equal to one. Thus, setting $\nu = n\omega$ the power is found to be:

$$E = \frac{1}{4} n\omega \left[(x_s^2 - x_c^2) \dot{q}_{xn} + 2x_c x_s \dot{Q}_{xn} + (y_s^2 - y_c^2) \dot{q}_{yn} + 2y_c y_s \dot{Q}_{yn} \right. \\ \left. + (x_c y_c - x_s y_s)(Q_{xn} - Q_{yn}) + (x_c y_s + x_s y_c)(\dot{q}_{xn} - \dot{q}_{yn}) \right] \quad (18)$$

Hence, for proper values of x_c , x_s , y_c and y_s the power input to the rotor from the magnetic forces may become positive. Thereby, net energy will be transferred from the magnetic field to a whirling motion of the rotor, and if the rotor damping is insufficient to dissipate this energy, the rotor will be unstable. It should be noted that the frequency of the instability motion is one half of the frequency of the magnetic forces. Hence, when the predominant magnetic force frequency is twice the speed of the rotor, the whirl frequency will equal the rotor speed. It is to be expected, therefore, that the rotor's tendency to instability will be most pronounced in the neighborhood of the critical speeds of the rotor. This is found to be the case. A more detailed discussion and analysis is given in Appendix F.

Whereas the passive magnetic forces only disturb the static rotor equilibrium when the rotor is unstable, any built-in eccentricity between the stator and the rotor produces active forces which cause the rotor to whirl. To calculate the corresponding amplitude response of the rotor, the frequency components of the active forces are applied to the rotor one at a time, and the total amplitude is then determined by superposition of the results from the individual calculations. Since the magnetic force gradients are much smaller than the rotor-bearing stiffness (the latter is of the order 10^5 whereas the magnetic force gradients are maximum of the order 6×10^3), only those components of the passive forces which have a frequency of twice the applied frequency enter into the calculations. The details are given in Appendix G.

The principal reason for calculating the amplitude response is to determine if the rotor amplitude becomes too large for an acceptable performance of the machine. Since the applied magnetic forces are rather small, not

exceeding 14 pounds for the specified built-in eccentricity of 0.002 inches, it is to be expected that the rotor amplitudes will be small in general. However, the forces may contain several frequency components. There is, therefore, always a possibility that if one or more of these frequencies are sufficiently close to a resonance of either the rotor or the shoes in the pivoted-pad journal bearings, large amplitude vibrations may be excited. This is especially true at the high frequencies where the bearings lose most of their damping capacity. Thus, it is necessary as a part of this investigation to calculate the stiffness and the damping of the gas film in the pivoted-pad journal bearings. The methods for doing this are developed in Appendices A to D.

The basic analysis is given in Appendix A where the equation governing the pressure distribution in the gas film of a single pad (Reynolds equation) is set up in a form suitable for numerical evaluation. By performing a small perturbation on the displacements and velocities of the journal center, additional equations are derived from which the corresponding changes in the gas film pressure can be found. The stiffness and damping coefficients for the pad can then be obtained by integration of the differential pressures. The numerical procedures employed in solving the equations are described in Appendix B and Appendix C. It is found that the pad film coefficients are functions of the pad geometry (arc length, length-to-diameter ratio and pivot position), the static eccentricity of the journal center with respect to the center of the pad arc, the compressibility number Λ ($\Lambda = \frac{6\mu\omega}{p_a} \left(\frac{R}{C}\right)^2$ where μ is the gas viscosity, p_a is the ambient pressure, ω is the angular speed of the rotor, R is the pad radius and C is the radial clearance), and finally, the ratio $\frac{\nu}{\omega}$ between the frequency ν of the rotor motion and the angular speed ω of the rotor. Hence, for a pad with specified geometry and load, and where the gas has a known viscosity and ambient pressure, the gas film stiffness and damping are functions of the rotor speed and the frequency of the dynamic motion. For a fixed speed they depend only on the frequency as shown in Figures V-3 to V-10.

Once the dynamic coefficients have been obtained for each of the individual pads, they can be combined to determine the dynamic coefficients representing the complete pivoted-pad bearing. In combining the pad coefficients, it is necessary to include the dynamic motion of the shoes on their pivots and flexures.

The method is described in detail in Appendix D. Here, it is also shown how the motion of the pads can be found.

With the spring and damping coefficients for the complete pivoted-pad bearing known, the dynamic model of the rotor-bearing-alternator system can be set up and it can be tested for stability as described in Appendix G. Similarly, the amplitude response of the rotor, caused by the magnetic forces and the mechanical unbalance present in the rotor, can be calculated as discussed in detail in Appendix G.

The methods used for testing the stability of the rotor and for calculating the response of the rotor are approximate, at least in theory. By adding the harmonically-varying passive magnetic forces to the rotor-bearing system, it no longer is a single frequency-response system, which means that the system will not vibrate with just one frequency. Any vibration will contain a series of frequencies (actually, infinite many). However, when the gradients of the magnetic forces are considerably smaller than the rotor-bearing stiffness, the amplitude of the fundamental harmonic dominates the vibration completely and all other frequency components can be ignored. With the ratio between the magnetic force gradients and the bearing stiffness being of the order 0.1 as for the present machine, the error involved is less than one percent.

RESULTS

Calculations were performed for the rotor operating vertically at 12,000 rpm. The rotor has a mechanical unbalance of 0.005 oz-inch in the turbine wheel, and its response and stability were investigated for six operating conditions of the alternator. The bearing data are

diameter: $D = 3.5$ inch

length: $L = 3.5$ inch

radial clearance of pad: $C = 0.00175$ inch

preload: $m = 0.5$

number of pads: 4

pad arc: 80 degrees

pivot position: 65 per cent from leading edge

mass of one pad: $m_p = 0.568$ lb.

pad mass moment of inertia for pitch axis: $I_p = 0.00102$ lbs-in-sec²

pad mass moment of inertia for roll axis: $I_\gamma = 0.00150$ lbs-in-sec²

pad mass moment of inertia for yaw axis: $I_\xi = 0.00252$ lbs-in-sec²

upper pivot flexure stiffness: $K_p = 30,000$ lbs/in

lower pivot flexure stiffness: $K_p = 90,000$ lbs/in

gas viscosity: $\mu = 4.2 \cdot 10^{-9} \frac{\text{lbs-sec}}{\text{in}^2}$ (Argon at 300°F)

ambient pressure: $P_a = 12.5$ psia for thrust bearing end

$P_a = 10.5$ psia for turbine end bearing

The bearing compressibility number Λ is defined as

$$\Lambda = \frac{6\mu\omega}{P_a} \left(\frac{R}{C} \right)^2$$

where R is the journal radius and ω is the angular speed of the rotor, i.e., $\omega = 1257$ radians/sec. The remaining symbols are defined above. Introducing the numerical values, Λ becomes

for bearing at thrust bearing end $\Lambda = 2.5$

for bearing at turbine end $\Lambda = 3.0$

With these values of Λ and the given pad dimensions (length-to-diameter ratio: $L/D = 1$, 80 degree arc length and 0.65 pivot position), the pad load W_p can be calculated from the computer program based on the analysis in Appendices A and B. The results are plotted in Fig. V-1 where the ordinate gives the pad load in dimensionless form as $W_p/P_a LD$ (W_p is in lbs.) and the abscissa is $\epsilon_p \cos \phi_p$ where ϵ_p is the eccentricity ratio for the pad and ϕ_p is the attitude angle. The gas film thickness over the pivot is

$$h_{pivot} = C(1 - \epsilon_p \cos \phi_p) \quad (19)$$

Thus, Fig. V-1 gives the load on the pad as a function of radial journal displacement. Only the results for $\Lambda = 3$ are shown since the data for $\Lambda = 2.5$ are almost the same.

The pivoted-pad bearing has four shoes located 45 degrees from the vertical. Knowing the load characteristics of each pad, the total bearing load can be determined. Let the journal downward displacement from the bearing center be e_B and let the corresponding eccentricity between the journal center and a pad center be e_p . Then from geometrical considerations,

$$e_p \cos \phi_p = C - C' \mp e_B \cos(45^\circ) \quad (20)$$

(- for top pads, + for bottom pads)

where C' is the pivot film thickness when the journal is concentric in the bearing. Define

$$\text{bearing eccentricity ratio: } \epsilon_B = e_B/C' \quad (21)$$

$$\text{pad eccentricity ratio: } \epsilon_p = e_p/C \quad (22)$$

$$\text{preload: } m = 1 - C'/C \quad (23)$$

whereby Eq. (20) can be written as

$$\epsilon_p \cos \phi_p = m \mp \frac{1-m}{\sqrt{2}} \epsilon_B \quad (24)$$

(- for top pads, + for bottom pads)

With $m = 0.5$,

$$\epsilon_p \cos \psi_p = 0.5 + \frac{\epsilon_B}{2\sqrt{2}} \quad (25)$$

the total bearing load W_B , lbs. becomes

$$W_B = 2 \cos(45^\circ) \left[(W_p)_{\text{Bott. pad}} - (W_p)_{\text{Top pad}} \right] \quad (26)$$

On this basis Fig.V-2 can be plotted. Select a value of ϵ_B , find $\epsilon_p \cos \psi_p$ for the top and bottom pads from Eq. (25), enter Fig.V-1 to find $W_p / P_a LD$ for both pads, multiply by $p_a LD$ from the data given above, and obtain the corresponding total load from Eq. (26). Repeat this for several values of ϵ_B whereby the two load curves, one for the turbine end bearing and one for the thrust bearing end bearing, are obtained as shown in Fig. V-2. Also shown on Fig. V-2 is the gas film thickness at the pivot for the bottom pads as obtained by combining Eqs. (19) and (25):

$$(h_{\text{pivot}})_{\text{bott. pads}} = 0.00175 \left[1 - 0.5 - \frac{\epsilon_B}{2\sqrt{2}} \right] = 0.000875 \left[1 - 0.707 \epsilon_B \right]$$

In addition, Fig.V-2 gives $\epsilon_p \cos \psi_p$ for the top and bottom pads as a function of ϵ_B from Eq. (25).

Fig. V-2 is used to determine the operating point for the pads. With a known bearing load, Fig.V-2 can be entered to read off the corresponding bearing eccentricity ratio ϵ_B and the pivot film thickness can be checked to see that it is not too small. For the determined value of ϵ_B , $(\epsilon_p \cos \psi_p)$ for the bottom and top pads can be taken directly from Fig.V-2 after which Fig. V-1 can be entered to calculate the load on each of the pads. Knowing $(\epsilon_p \cos \psi_p)$ and W_p for a pad, Figs.V-3 to V-10 can be entered to determine the 8 dynamic film coefficients as a function of the vibratory frequency.

There are 8 dynamic coefficients for each pad: four spring coefficients,

$K_{\xi\xi}$, $K_{\xi\eta}$, $K_{\eta\xi}$, $K_{\eta\eta}$ (lbs/inch); and four damping coefficients, $B_{\xi\xi}$, $B_{\xi\eta}$, $B_{\eta\xi}$, and $B_{\eta\eta}$ (lbs-sec/inch). For a given rotor speed and given dimensions of the bearing, they are only functions of the bearing load (or, equivalently, $\xi_r \cos \phi_p$) and the vibratory frequency ν . They are calculated as explained in Appendices A and C, and are plotted in dimensionless form in Fig.V-3 to V-10 where the ordinate gives either $CK_{\xi\xi}/W_p$ (and similarly for the other three spring coefficients) or $C\omega B_{\xi\xi}/W_p$ (and the three analogous coefficients). Here, C is the radialpad clearance ($C=0.00175$ inch), ω is the angular speed ($\omega = 1257$ radians/sec) and W_p is the pad load in lbs. The abscissa gives the ratio ν/ω between the vibratory frequency ν , radians/sec, and the angular speed ω . For stability calculations and mechanical unbalance response calculations, $\nu/\omega = 1$. For magnetic force response calculations, however, ν/ω equals 2,4,6---, depending on the number of frequencies contained in the magnetic forces for the specific alternator operating condition under consideration.

Apart from the general stiffening of the gas film as the frequency is increased, the most noteworthy feature of the curves is the rapid loss of damping at high frequencies. Thus, at a frequency of 10 times the rotor speed, only approximately 0.1 percent of the total damping is left in the pad film. This, however, does not necessarily imply a similar loss of damping for the pivoted-pad bearing as a whole, since the combined bearing damping also includes the phase shift between pad motion and journal motion. On the other hand, it is obvious that the loss of pad film damping is going to decrease the overall damping to some degree and, in any case, the damping available to control the pad inertia is small at high frequencies.

Once the 8 coefficients have been obtained for each of the individual pads, they can be combined to obtain the spring and damping coefficients for the complete pivoted-pad bearing as described in Appendix D. This is not done as a separate calculation but internally within the computer programs for calculating stability and response. In other words, these computer programs accept the data for the individual pads as input and perform the combination internally. The programs also accept as input the dynamic coefficients for roll and yaw of the pads (see Appendices A and D) in order to obtain the complete pad motion. It is not part of this investigation to calculate these coefficients from the exact theory

given in Appendix A. Instead they have been obtained by employing scalefactors, derived from data available for incompressible pad films.

$$\frac{G_{\xi\xi}}{L^2 K_{\xi\xi}} = 0.047$$

$$\frac{\omega D_{\xi\xi}}{L^2 \omega B_{\xi\xi}} = 0.036$$

$$\frac{G_{\xi\eta}}{L^2 K_{\xi\eta}} = 0.038$$

$$\frac{\omega D_{\xi\eta}}{L^2 \omega B_{\xi\eta}} = 0.051$$

$$\frac{G_{\eta\xi}}{L^2 K_{\eta\xi}} = 0.058$$

$$\frac{\omega D_{\eta\xi}}{L^2 \omega B_{\eta\xi}} = 0.050$$

$$\frac{G_{\eta\eta}}{L^2 K_{\eta\eta}} = 0.053$$

$$\frac{\omega D_{\eta\eta}}{L^2 \omega B_{\eta\eta}} = 0.051$$

From these relationships, the 8 roll and yaw coefficients, $G_{\xi\xi}$, $D_{\xi\xi}$, etc. can be computed from the already obtained values of $K_{\xi\xi}$, $B_{\xi\xi}$, etc.

The rotor is represented by stations at which the rotor mass is lumped. The length between the stations, and the mass and stiffness distribution of the rotor are given by the following table:

Station No.	Mass, lbs.	Length Between Stations, Inch	Cross-Sect. Mom. of Inertia, Inch ⁴
1	6.839	1.93	1.545
2	3.391	3.94	3.062
3	3.713	4.61	3.062
4	10.058	1.25	3.72
5	0.	2.18	3.72
6	7.91	1.99	3.72
7	0.	1.34	3.72
8	9.577	4.08	3.062
9	3.559	4.23	3.062
10	9.92	----	-----

The turbine wheel is at Station 1, the thrust runner is at Station 10 and the two journal bearings are located at Stations 3 and 9, respectively. The alternator pole planes are at Stations 5 and 7.

The magnetic force data computed by the General Electric Company for six alternator operating conditions have been reduced to a form more suited to response and stability calculations than the form in which the data was reported by General Electric. The procedure for reducing the data is described in Appendix E, and the results are given in Table V-1. The reduction consists mainly in an elimination of the power angle and the position angle β , giving the direction of rotor displacement. The General Electric data was obtained from a number of Fourier series and the results from each series have not been combined. Thus, there are instances where quite large force components exist in General Electric's equations, but which cancel out when they are combined such that the final result is a remainder of a subtraction involving large numbers. This obviously affects the accuracy. Case 4 in Table V-1 offers an example. Thus, for $n = 1$, the force A_n is 0.03 lbs which is obtained from: $277.60 - 277.57 = 0.03$ lbs. This remainder is probably smaller than the error involved in calculating the individual components. It is also seen that B_n for $n=0$ in Cases 1, 2, 3 and 6 is not quite zero which it obviously should be. While this is of no physical importance, it does give an indication of the accuracy of the numbers.

The results of the rotor response calculations are summarized in Table V-2. There are six operating conditions of the alternator and a seventh condition, where saturation effects in the alternator have been ignored, is also included (Case 1). Furthermore, a mechanical unbalance of 0.005 oz.-in. in the turbine wheel can be present. Several cases were investigated: First, the rotor may have a uniform eccentricity of 0.002 inch (i.e., the same eccentricity in each pole plane) in which case the time varying magnetic forces in general exert a moment on the rotor. This case is calculated both without and with mechanical unbalance for all the operating conditions of the alternator. Secondly, the case where the rotor is tilted and only eccentric in one pole plane was calculated. The effect of the magnetic forces is then predominantly to exert a force on the rotor.

Thirdly, the rotor is tilted such that it is eccentric in each pole plane but in opposite directions. Again, the effect is predominantly to exert a force on the rotor. Finally, the case of a mechanical unbalance alone has been studied. It is found that the rotor and bearing shoes have very small vibration amplitudes under all conditions. The rotor amplitudes never exceed 56 microinches and the largest pad motion is a pitch amplitude of 98 microinches per inch. In almost all instances the amplitudes are less than 50 microinches. These amplitudes are so small that it will be extremely difficult to observe them in the actual machine where just the run-out of the shaft is of the same magnitude. It can, therefore, be concluded that for an operating speed of 12,000 rpm the magnetic forces have no important influence on the rotor response.

Turning next to the effect of the magnetic forces on the stability of the rotor, the results are shown in Fig.V-11. There, the abscissa gives the rotor speed in rpm, and the ordinate gives the stiffness of the magnetic forces in lbs/inch. In the case of balanced load and no short circuit conditions, (i.e. Cases 1, 2, 3 and 6 in Table V-1) this stiffness can be taken from Table V-1 as the value of $\sqrt{Q_{xn}^2 + q_{xn}^2}$ for $n = 1$ (i.e., corresponding to the $2\omega t$ -component of the magnetic forces). For the three short circuit cases (Cases 4, 5 and 7 in Table V-1), the corresponding magnetic stiffness is determined as discussed in Appendix F. In total, the magnetic stiffness for the 7 operating conditions of the alternator are

Case	Magnetic Stiffness for Stability Investigation, lbs/in
1	6,864
2	4,414
3	3,970
4	17
5	2,310
6	3,080
7	2,050

It is seen, that the rotor operates far below the threshold of instability in all cases. Thus, there is no danger of encountering rotor instability due to the magnetic forces.

TABLE V-1
THE ELECTROMAGNETIC ALTERNATOR FORCES

for 0.002 inch eccentric

Case ^{*)}	n	A _n , lbs	B _n , lbs	Q _{xn} , lbs/in	q _{xn} , lbs/in	Q _{yn} , lbs/in	q _{yn} , lbs/in	$\sqrt{Q_{xn}^2 + q_{xn}^2}$, lbs/in
1	0	11.25	-0.09	-5,625	-46	-5,625	-46	5,625
	1	12.81	-4.94	-6,403	-2,471	6,403	2,471	6,864
2	0	11.44	-0.09	-5,720	-44	-5,720	-44	5,721
	1	7.96	-3.82	-3,980	-1,909	3,980	1,909	4,414
3	0	10.01	-0.05	-5,004	-26	-5,004	-26	5,004
	1	7.38	-2.94	-3,689	-1,468	3,689	1,468	3,970
4	0	13.11	0.00	-6,555	0	-6,535	0	6,555
	1	0.03	0.00	-15	0	-5	0	15
	2	0.02	0.00	-10	0	0	0	10
	3	-0.02	0.00	10	0	0	0	10
	5	0.04	0.00	-20	0	0	0	20
	6	0.04	0.00	-20	0	0	0	20
	9	-0.16	0.00	80	0	0	0	80
	12	0.04	0.00	-20	0	0	0	20
	13	0.04	0.00	-20	0	0	0	20
	15	-0.02	0.00	10	0	0	0	10
	24	0.16	0.00	-80	0	-80	0	80
	25	-0.06	0.00	30	0	-30	0	30
	49	0.04	0.00	-20	0	20	0	20
5	0	33.34	0.41	-16,670	203	-12,730	-1,700	16,670
	1	3.05	1.08	-1,523	540	167	64	1,615
	2	5.30	-6.87	-2,648	-3,436	-2,488	4,738	4,338
	3	0.72	5.55	-359	2,775	-707	-2,137	2,798
6	0	7.64	-0.02	-3,819	-10	-3,819	-10	3,819
	1	6.16	-0.10	-3,080	-50	3,080	50	3,080
7	0	7.86	0.03	-3,930	17	-3,930	17	3,930
	1	3.47	0.96	-1,733	479	1,925	-81	1,798
	2	-3.35	0.08	1,672	39	653	-686	1,673
	3	-1.57	-2.69	787	-1,347	-560	958	1,560
	4	-0.09	0.04	47	22	47	22	51

*) For case numbers, see note to Table V-2

TABLE V-1 (continued)

The electromagnetic alternator forces are given by the following equations:

$$F_x = \sum_{n=0}^N \left\{ A_n \cos(2n\omega t) + B_n \sin(2n\omega t) - x \left[Q_{xn} \cos(2n\omega t) - q_{xn} \sin(2n\omega t) \right] \right. \\ \left. + y \left[q_{yn} \cos(2n\omega t) + Q_{yn} \sin(2n\omega t) \right] \right\}$$

$$F_y = \sum_{n=0}^N \left\{ -B_n \cos(2n\omega t) + A_n \sin(2n\omega t) - x \left[q_{xn} \cos(2n\omega t) + Q_{xn} \sin(2n\omega t) \right] \right. \\ \left. - y \left[Q_{yn} \cos(2n\omega t) - q_{yn} \sin(2n\omega t) \right] \right\}$$

where x and y are the amplitudes of the rotor in inches, ω is the angular speed at the rotor in radians/sec and t is time in seconds.

TABLE V-2
DYNAMIC RESPONSE OF TURBOALTERNATOR ROTOR-BEARING SYSTEM
TO ELECTROMAGNETIC ALTERNATOR FORCES

Condition	Case	Min. Film Thickness for Static Load (Microinch)	Amplitude of Rotor in Journal Bearings (Microinch)		Pitch Amplitude of Journal Bearing Shoes (Microinch/Inch)			
			Thrust Brg. End	Turbine End	Thrust Bearing End		Turbine End	
					Top Shoe	Bottom Shoe	Top Shoe	Bottom Shoe
Rotor eccentric by 0.002 inch in both pole planes; no mechanical unbalance	1	775	5.1	6.2	4.2	8.8	5.4	11.1
	2	770	3.3	3.9	2.3	5.7	3.0	7.1
	3	782	3.0	3.6	2.4	5.1	3.1	6.4
	4	755	0.3	0.3	0.3	0.3	0.4	0.5
	5	595	2.5	2.3	5.1	3.5	4.0	2.7
	6	805	2.3	2.8	3.0	3.5	3.7	4.4
	7	802	1.8	1.8	2.5	3.1	2.9	2.8
Rotor eccentric by 0.002 inch in both pole planes; 0.005 oz.in. mechanical unbalance in turbine	1	775	7.6	38.3	7.4	12.0	44.7	53.4
	2	770	5.8	36.3	5.5	8.9	43.7	51.1
	3	782	5.3	35.8	5.3	8.1	43.3	50.1
	4	755	3.2	34.2	3.9	4.4	43.7	52.0
	5	595	11.6	42.7	16.3	15.0	53.6	64.2
	6	805	4.2	35.1	5.3	6.1	42.9	48.0
	7	802	3.6	34.2	4.8	5.6	46.6	52.2
Rotor eccentric by 0.002 inch in pole plane closest to turbine, no mechanical unbalance	1	775	11.0	23.4	9.0	18.7	20.5	42.1
	2	770	7.0	14.9	4.9	12.1	11.3	27.1
	3	782	6.3	13.5	5.1	10.9	11.6	24.4
	4	755	0.6	1.1	0.7	0.8	1.6	1.8
	5	595	6.0	7.5	8.6	14.3	9.4	13.7
	6	805	4.9	10.5	6.3	7.3	14.2	16.7
	7	802	4.0	6.7	6.1	5.2	10.9	8.9
0.005 oz.in mech- anical unbalance in turbine; no magnetic forces			1.5	30.9	1.8	2.2	39.3	46.8
Rotor eccentric by +0.002 inch in one pole plane, -0.002 inch in other plane; no mechanical unbalance			17.2	25.9	12.2	29.8	29.1	47.1
Same as preceeding case but with 0.005 oz.-in mechanical unbalance in turbine			19.7	56.5	15.4	33.0	53.7	97.7

TABLE V-2 (Continued)

Note: The results are for the rotor operating in a vertical position at 12,000 rpm. Response amplitude values in the above table are single amplitude values measured from the static eccentricity position of the rotor resulting from the d-c component, A_o , of the electromagnetic forces.

Code:

- Case 1: 15 KVA, 0.8 power factor lagging, balanced load, unsaturated
- Case 2: 15 KVA, 0.8 power factor lagging, balanced load, saturated
- Case 3: 11.25 KVA, 0.8 power factor lagging, balanced load
- Case 4: 3-phase balanced, short circuit condition
- Case 5: Single-phase fault, rated power
- Case 6: No-load condition, operating at 120V L-N balanced 3 ϕ , no armature current
- Case 7: 3.33 KVA, 1.0 power factor, with the load connected from one phase to neutral.

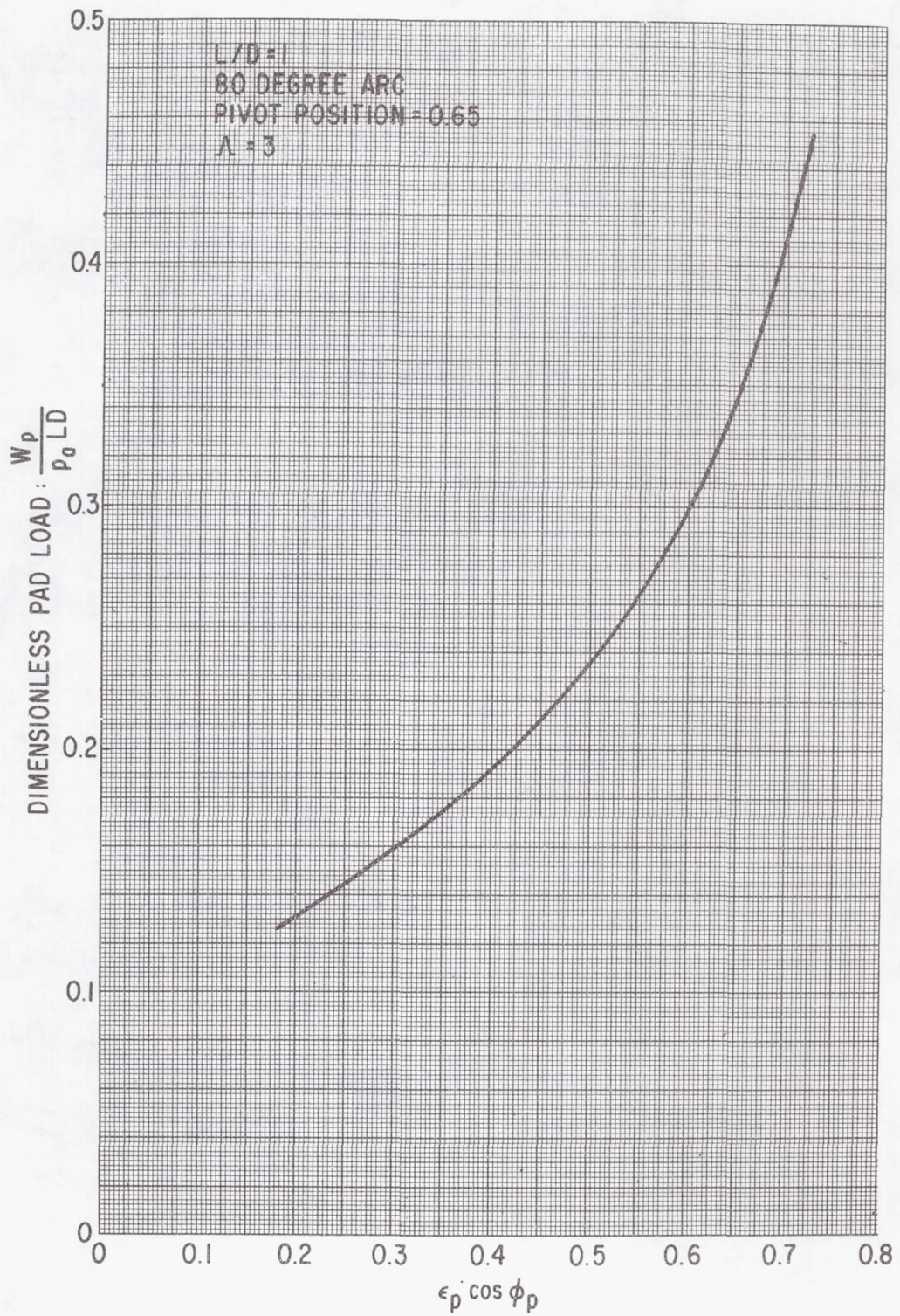


Fig. V-1 Calculated Film-Thickness Parameter versus Dimensionless Pad Load

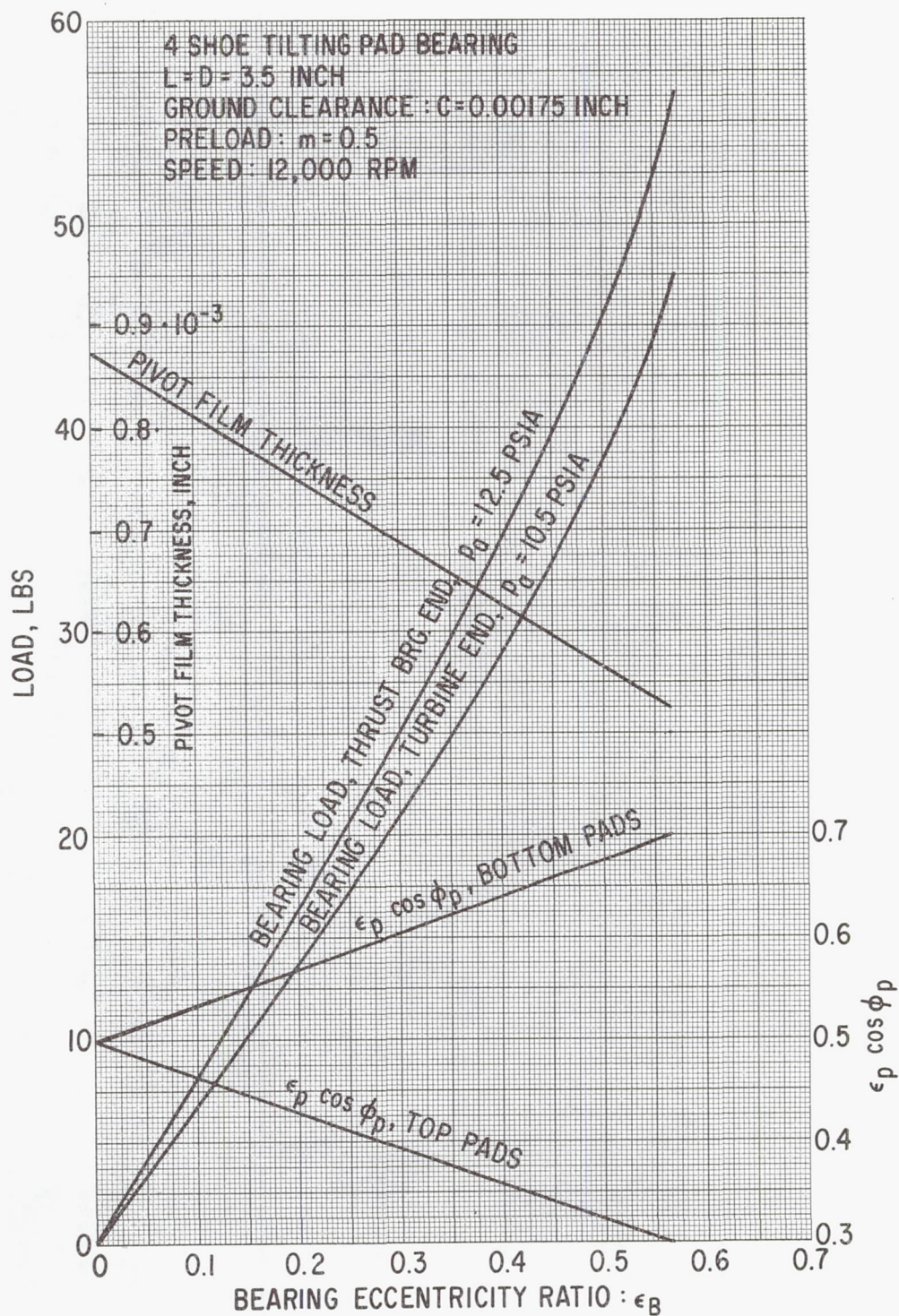


Fig. V-2 Calculated Bearing Load and Film Thickness Data versus Bearing Eccentricity Ratio

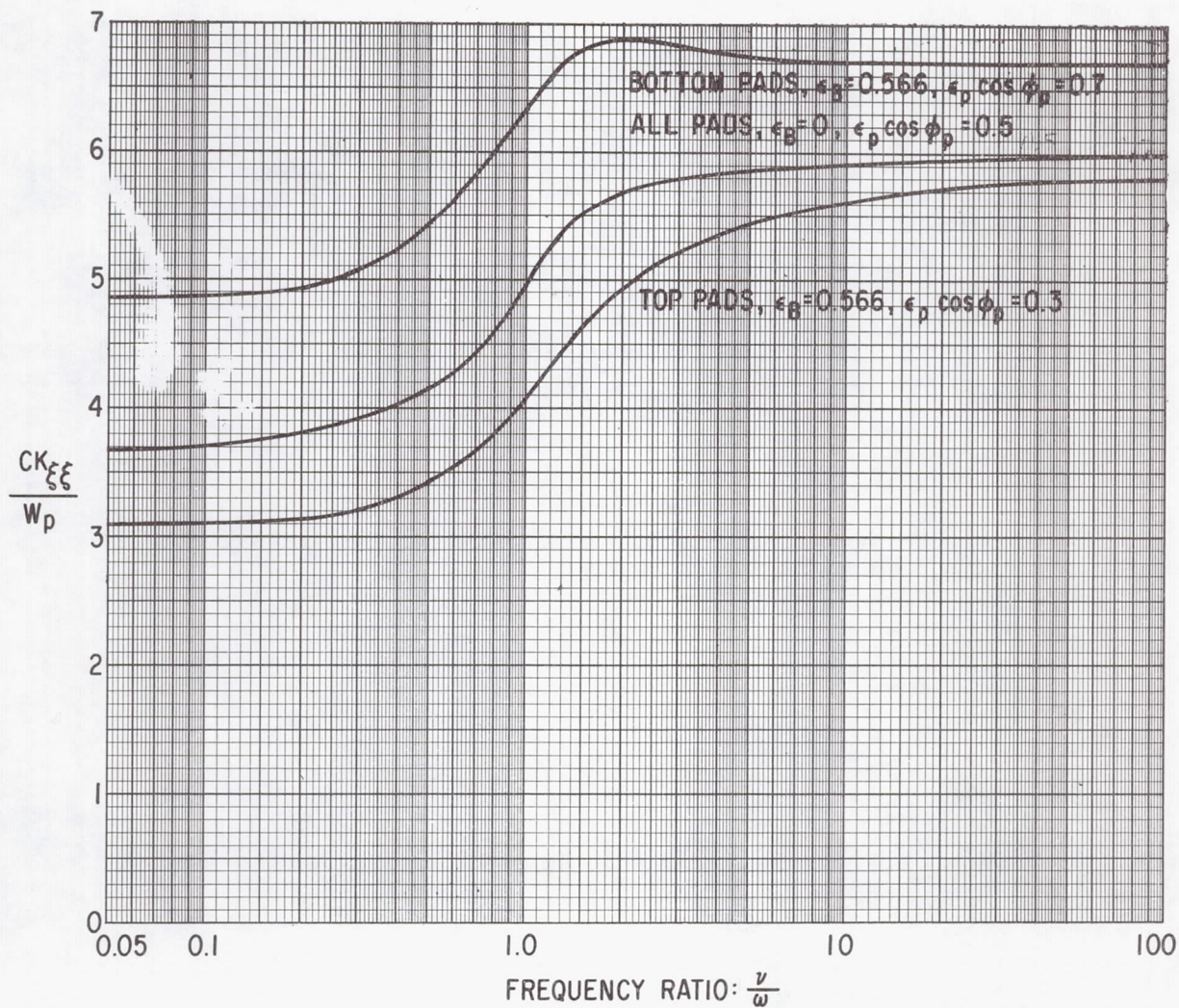


Fig. V-3 Calculated Dimensionless Pad Radial Stiffness versus Frequency Ratio

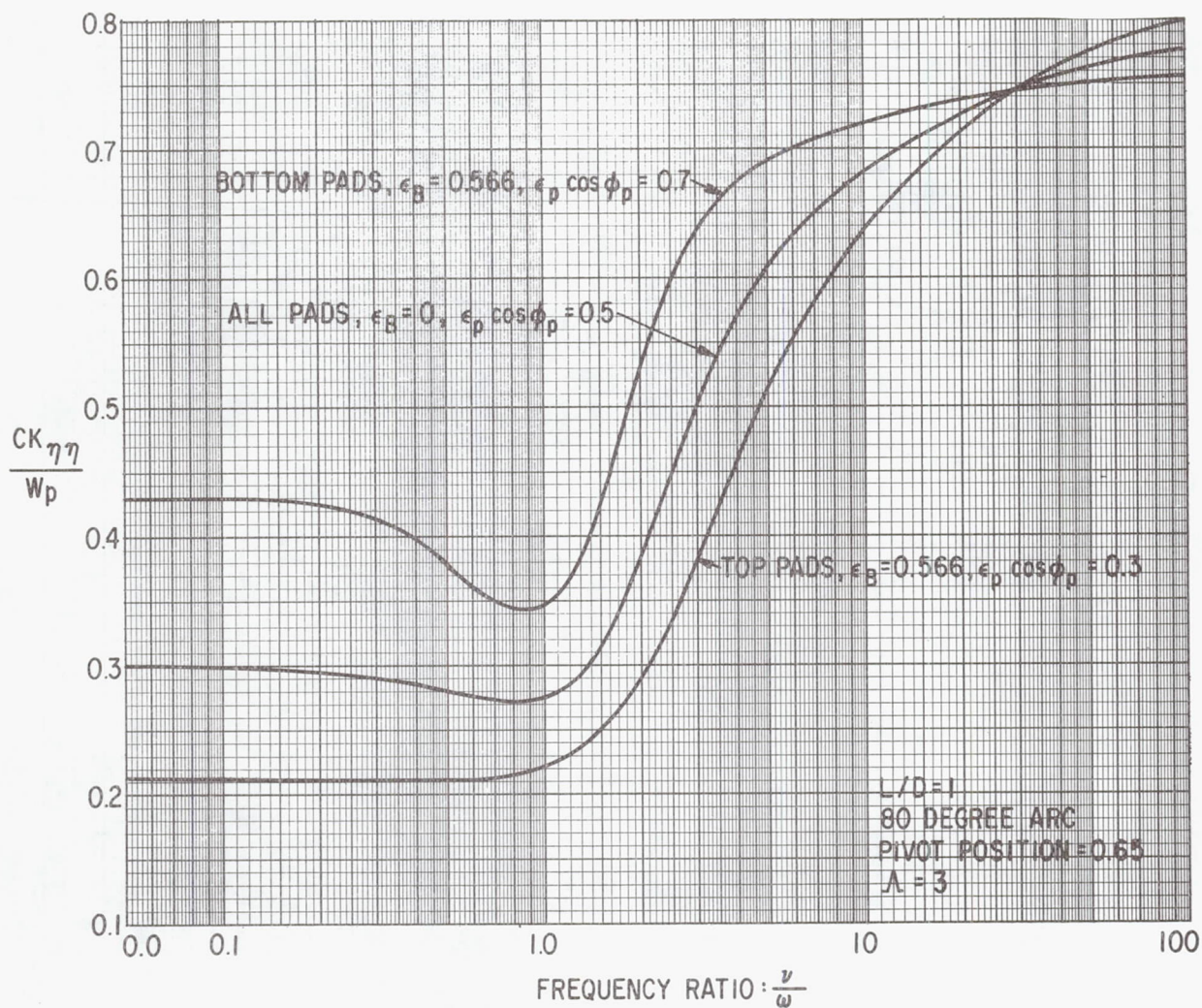


Fig. V-4 Calculated Dimensionless Pad Tangential Stiffness versus Frequency Ratio

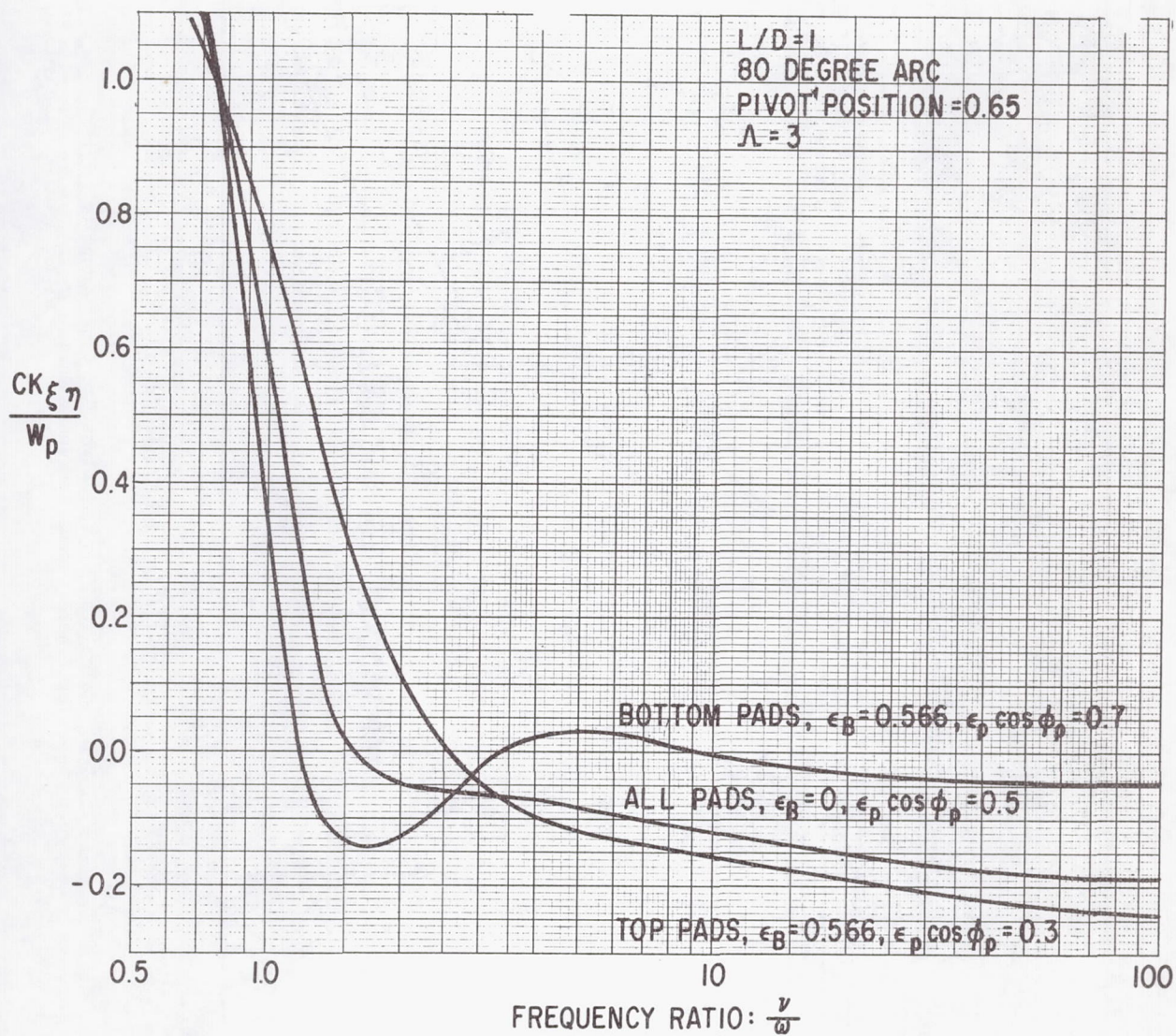


Fig. V-5 Calculated Dimensionless Pad Cross-Coupling Stiffness versus Frequency Ratio

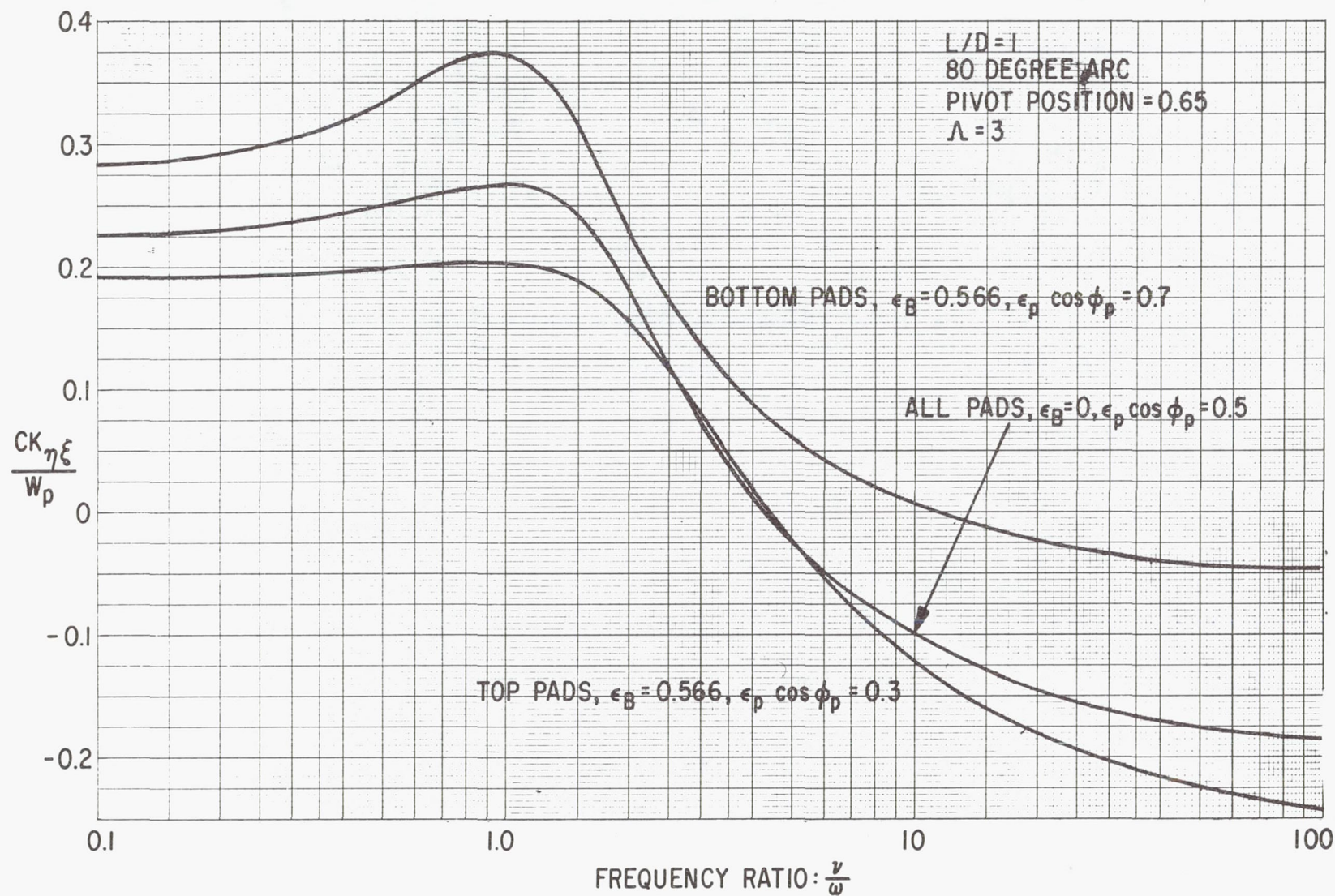


Fig. V-6 Calculated Dimensionless Pad Cross-Coupling Stiffness versus Frequency Ratio

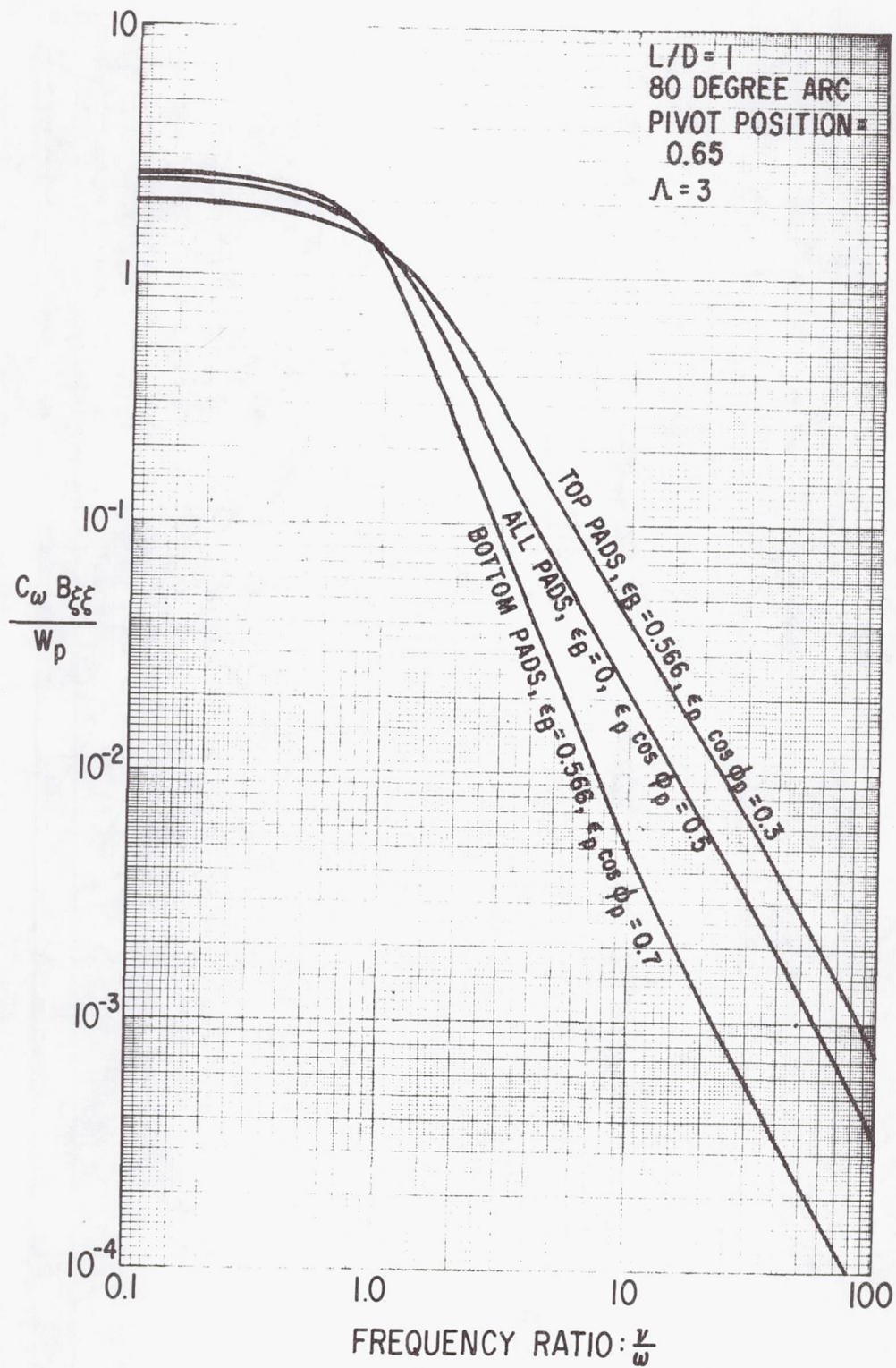


Fig. V-7 Calculated Dimensionless Pad Radial Damping versus Frequency Ratio

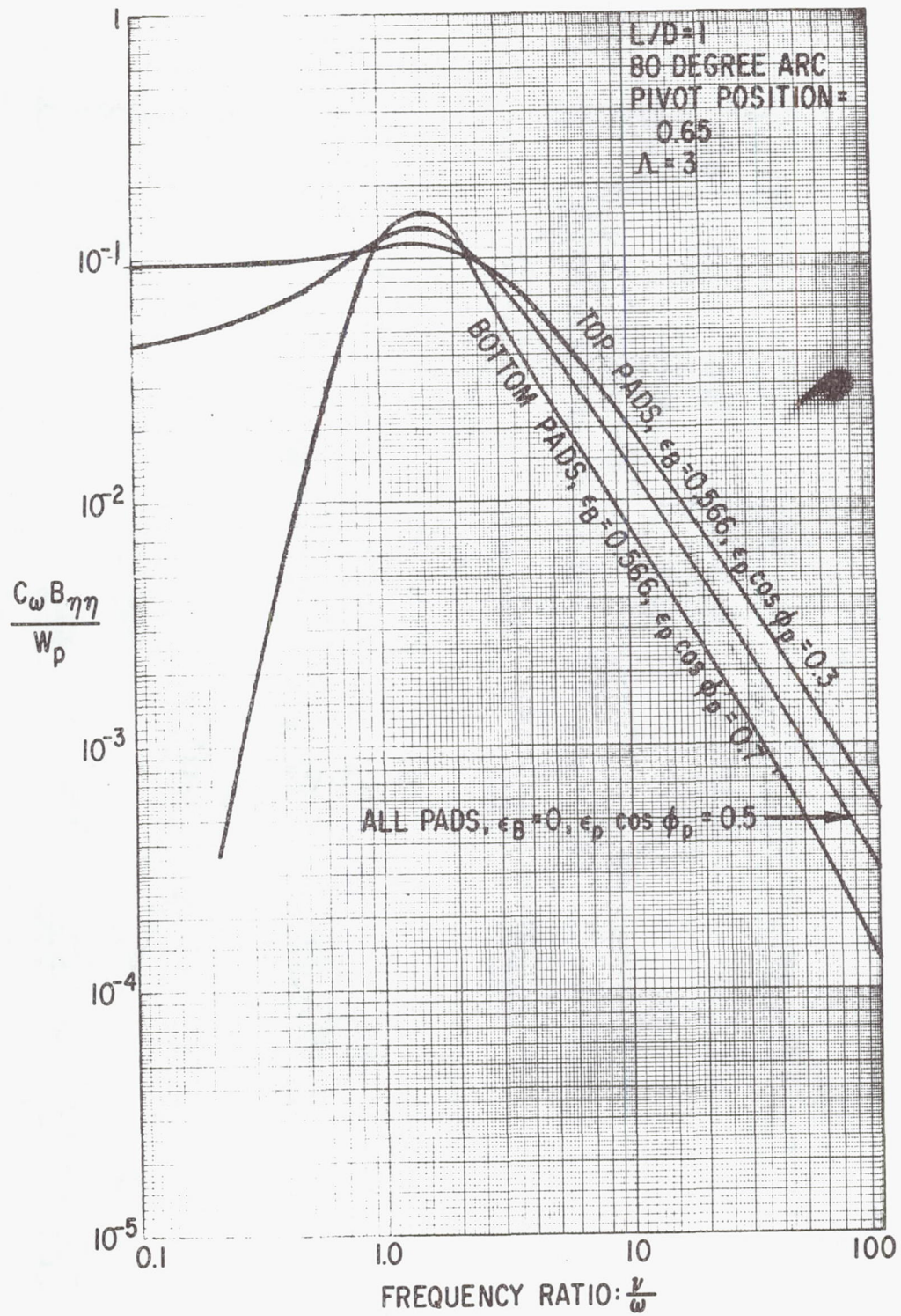


Fig. V-8 Calculated Dimensionless Pad Tangential Damping versus Frequency Ratio

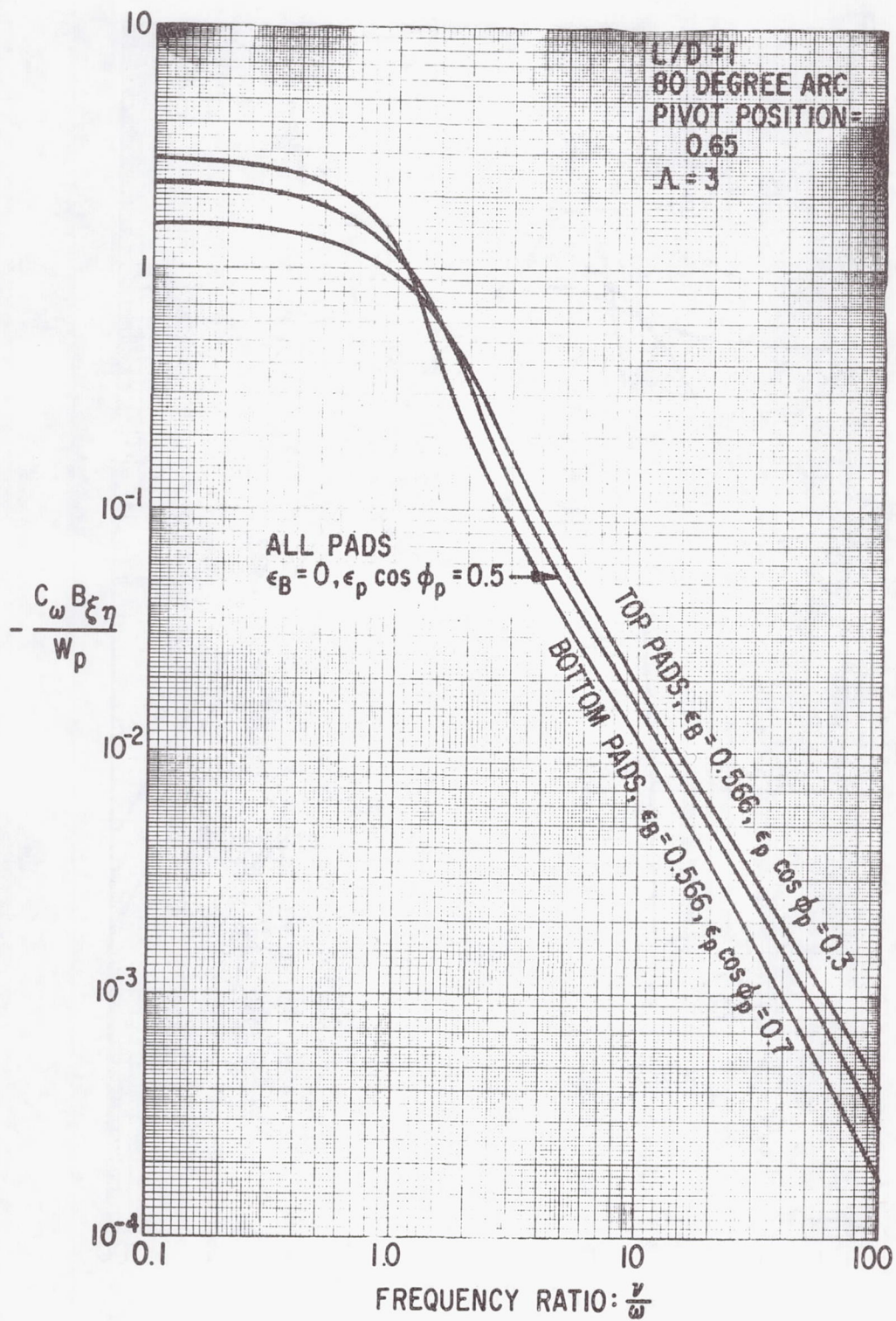


Fig. V-9 Calculated Dimensionless Pad Cross-Coupling Damping versus Frequency Ratio

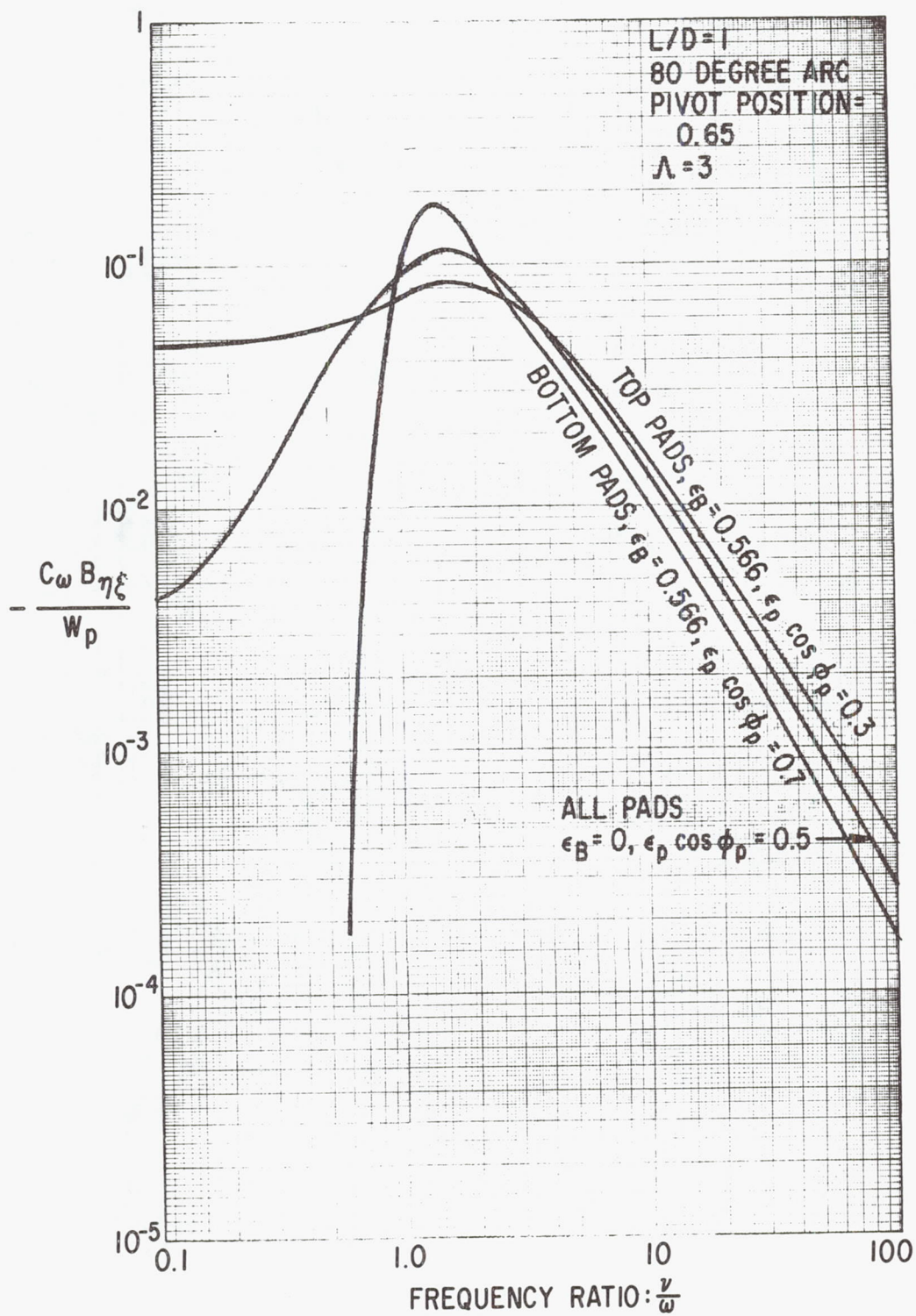


Fig. V-10 Calculated Dimensionless Pad Cross-Coupling Damping versus Frequency Ratio

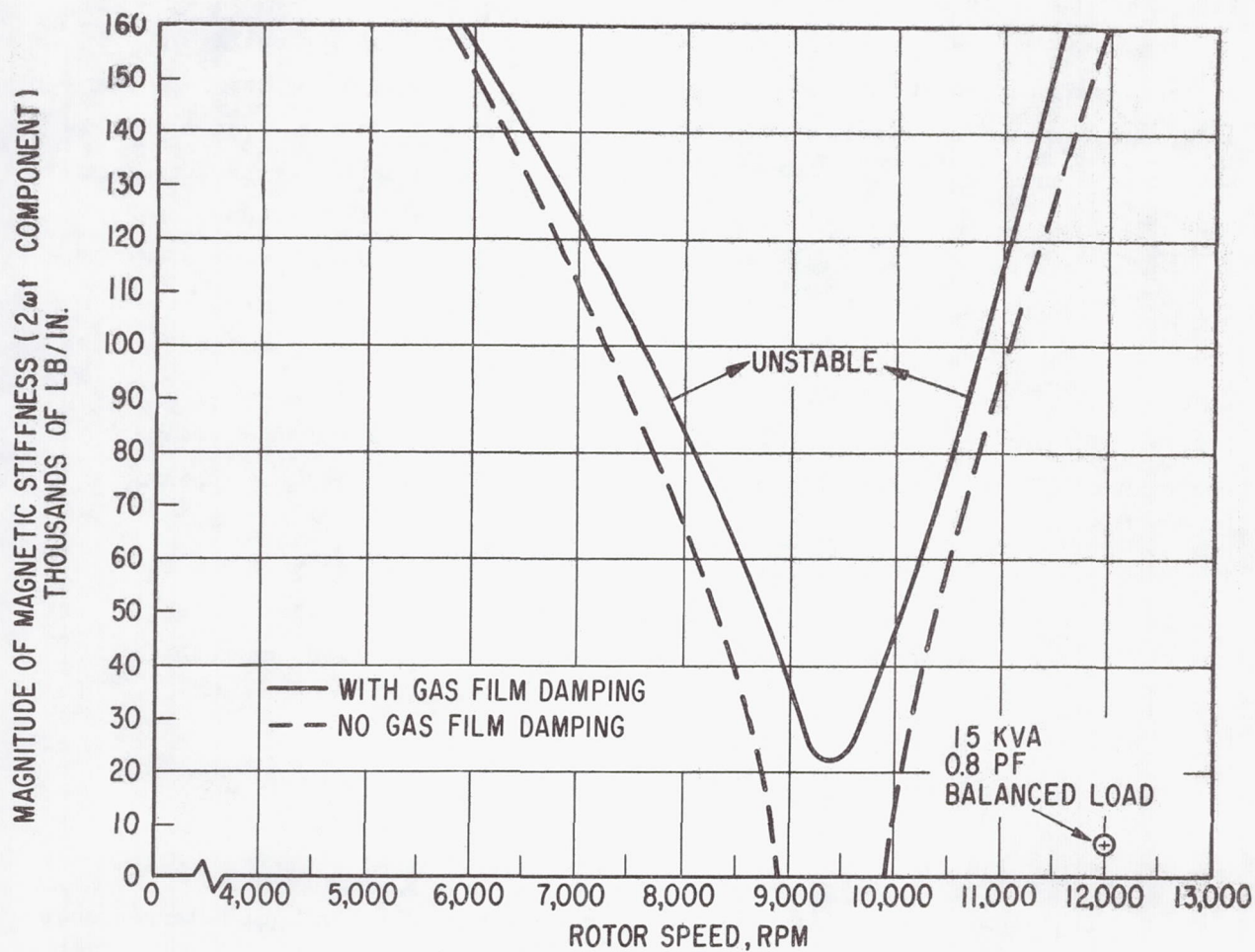


Fig. V-11 Calculated Stability Map for the Turboalternator Rotor-Bearing System

VI. DESIGN OF ROTOR BEARING SIMULATOR INCLUDING ALTERNATOR

The turboalternator bearing system design, described in Section II, was successfully tested under operating conditions which did not involve electromagnetically-induced forces on the rotor resulting from operation of the alternator under various conditions of electrical power generation. In continuance of the policy to isolate, evaluate and remedy possible problem areas by means of appropriate test programs, it was then recommended that the turboalternator bearing system should be retested under conditions which included the electromagnetic forces attendant upon the generation of electrical power. This would permit further development and acceptance testing of the rotor-bearing system in a simulator under conditions more closely representative of those which would be encountered in turboalternator operation (excluding thermal simulation) independent of, and yet parallel to development of the turboalternator aerodynamic components. Additionally, such a program would permit experimental verification of the analysis of the rotor response to electromagnetic forces as described in Section V of this report.

The recommendation to conduct this test program was approved by NASA and the necessary design modifications to the existing simulator, described in Section III of this report, commenced in April 1966. The design was carried out such that the simulator could readily be used to

1. operate over the full range of electrical power generation and electrical fault conditions,
2. evaluate design-point bearing system performance under both balanced and unbalanced rotor conditions with the rotor both horizontally and vertically orientated while operating over the range of electrical power generation and electrical fault conditions,
3. evaluate bearing performance as in (2) above under off design-point conditions such as reduced ambient pressure, maximum overspeed, and increased journal bearing clearance,

4. evaluate the rotor response to the conditions of operation in (1), (2) and (3) above ,
5. utilize the rotor shaft and stator designed for the turboalternator , and
6. identify unknown problem areas.

To conduct the extensive test program planned for the simulator at ambient pressures below atmospheric pressure, necessitated the use of air for the bearing environment rather than argon. The performance of the bearings, the rotor critical speeds, and the temperature distributions and gradients relating to operation in the air environment were calculated. The bearing calculations were based on the values of bearing clearance at design speed which were predicted for design turboalternator operation in argon. The results of these calculations were reported in Reference [24] and are, therefore, not repeated in this report.

A cross-section view of the redesigned rotor-bearing simulator including the alternator is shown in Figure VI-1. Significant features of the simulator are described in the following subsections.

Simulator Rotor

A photograph of the turboalternator rotor as delivered by the alternator manufacturer and before final machining is shown in Figure VI-2. At this stage the rotor consisted of the finally heat treated forging to which laminated pole faces have been electron-beam welded, and copper alloy amortisseur bars and stainless steel end rings welded into place. The rotor had been rough balanced, and spin tested.

The photograph in Fig. VI-3 shows the same rotor after finish machining. The finish machining consisted of the application of the electrodeposited copper heat shunt in the bore of each journal, the machining of the involute spline, the application of chrome oxide to the journal surfaces and the final machining of the critical diameters, faces and lengths. The rotor for use in the

simulator was manufactured from the turboalternator rotor detail drawings and has, therefore, the same characteristics as will be exhibited by the rotor used in the turboalternator.

The photographs shown in Figures VI-4 and VI-5 show the component parts of the simulator rotor assembly and the assembled rotor respectively. The assembly possessed the same principle dimensions, total mass, mass distribution and stiffness characteristics as exhibited by the turboalternator rotor assembly. Actual measured weight of the complete rotor assembly was 54.8 pounds.

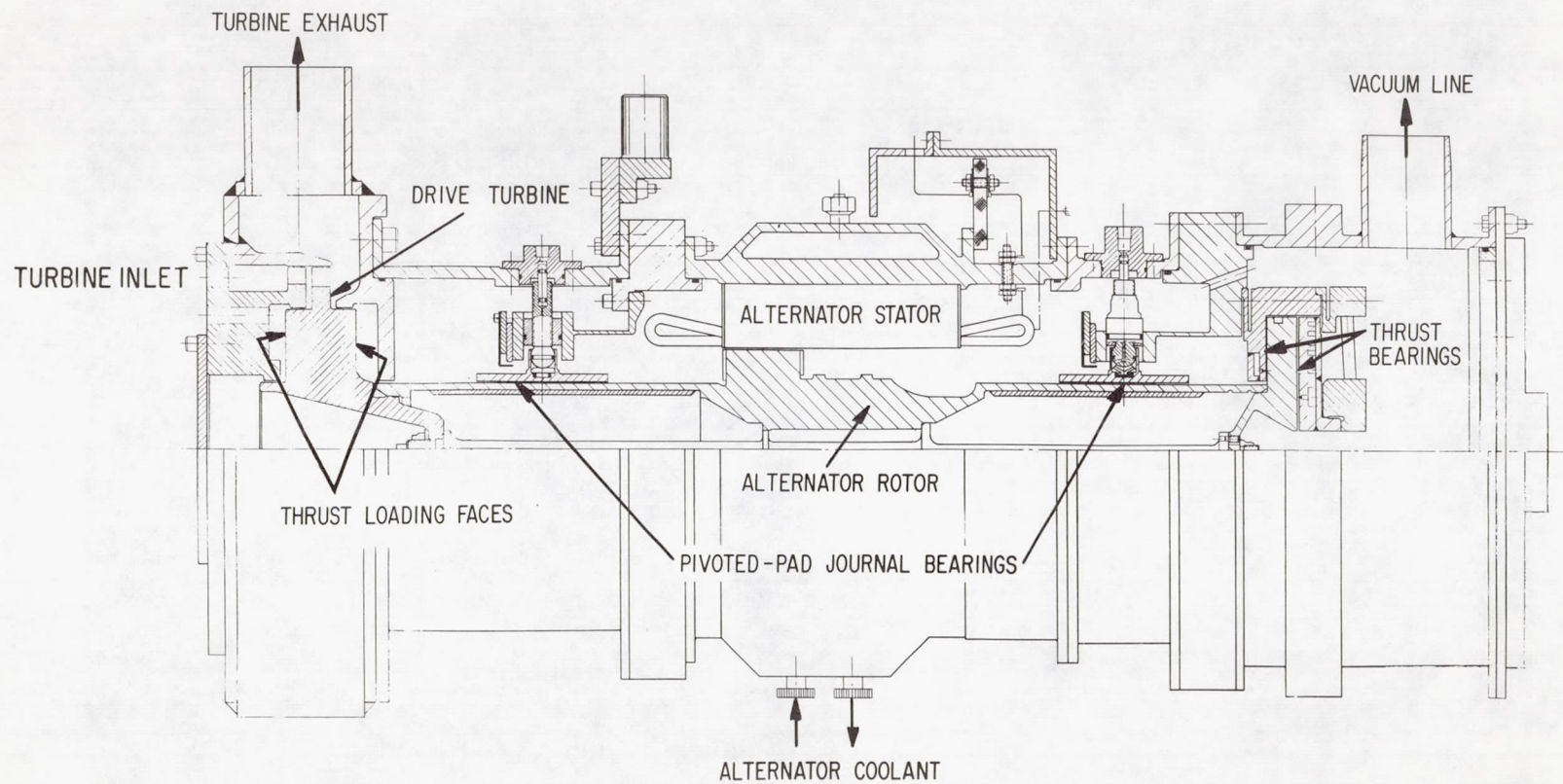


Fig. VI-1 Turboalternator Rotor-Bearing-
Alternator Simulator

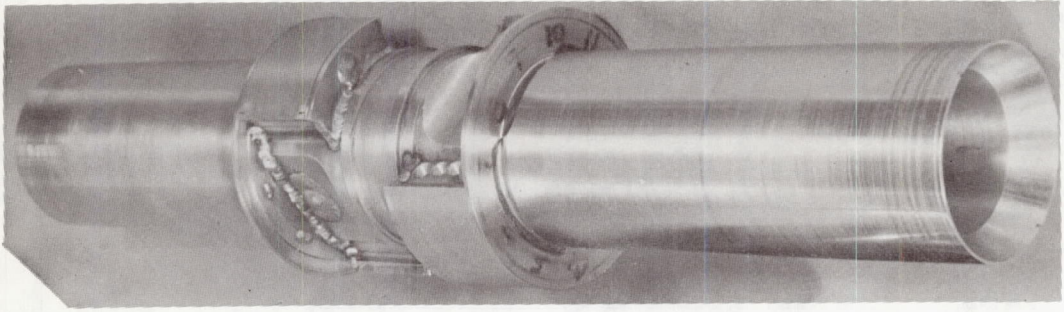


Fig. VI-2 View of Simulator Rotor Prior to Final Machining

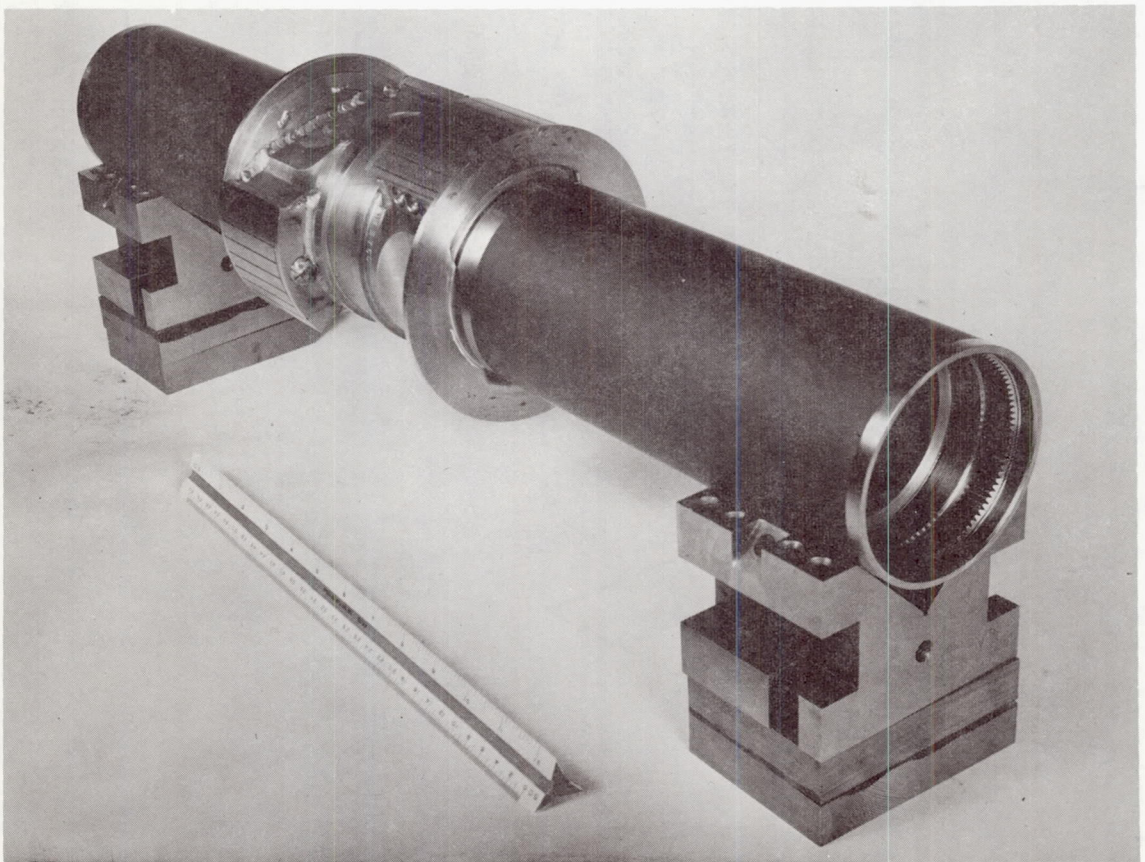


Fig. VI-3 View of the Simulator Rotor

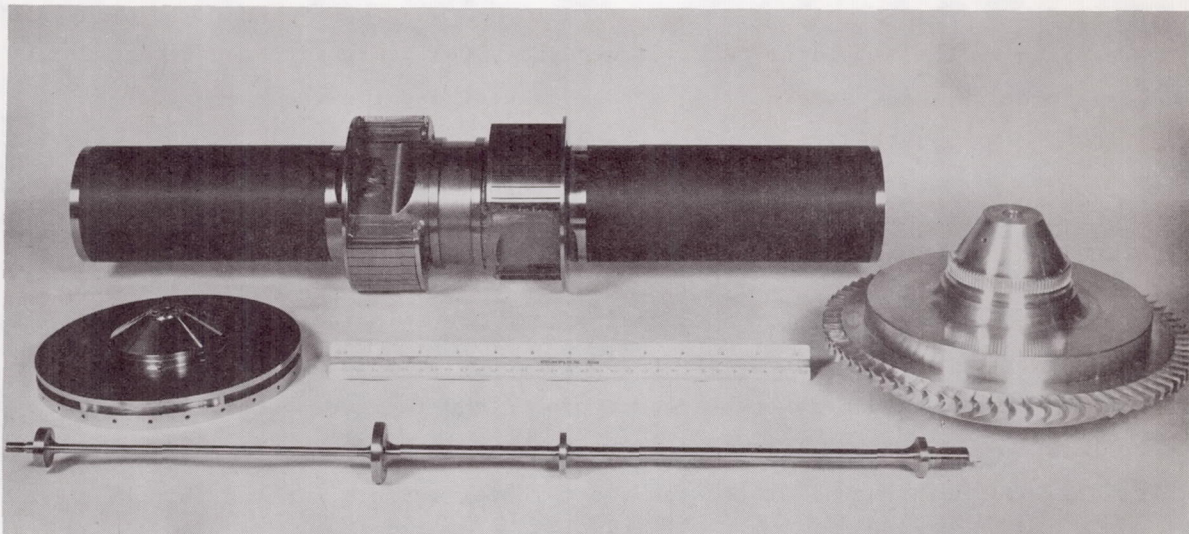


Fig. VI-4 View of the Component Parts
of the Simulator Rotor

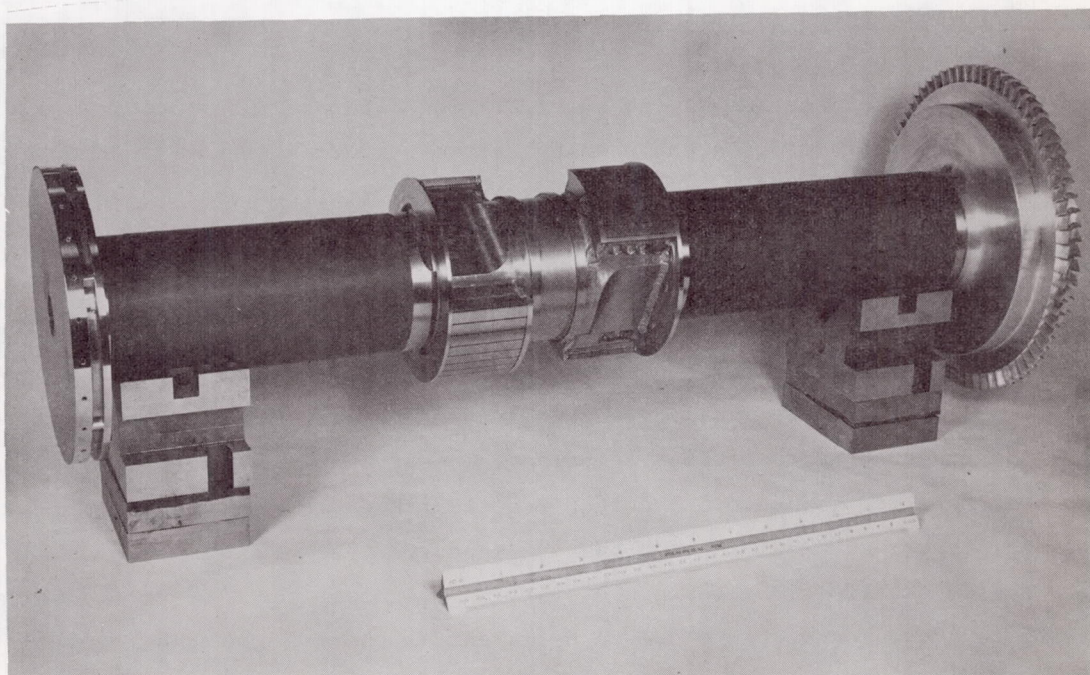


Fig. VI-5 View of the Simulator Rotor Assembly

Simulator Bearings

The redesign of the simulator that was necessary to incorporate the alternator, utilized precisely the same bearing system as designed for the turboalternator and used in the original simulator. Photographs of the journal bearing parts are shown in Figures II-7 and II-8, and the thrust bearing parts are shown in Figures II-12, II-13 and II-14.

For both the journal bearings, the bearing components included the pivoted pads, pivots, pivot support flexures, pivot "O" ring seals, and the bearing system instrumentation transducers (capacitance probes and thermocouples). These components formed two complete journal bearing assemblies which had the same interfaces for both the simulator and the turboalternator. In the thrust bearing region, the bearing components included the thrust runner, the reverse thrust bearing housing, the main thrust bearing, the thrust bearing support and the bearing system instrumentation transducers (capacitance probes and thermocouples). Again, the interface for the thrust bearing components was identical in both the simulator and the turboalternator.

Control of the Simulator Journal Bearing Clearance

One of the primary objectives of the rotor-bearing-alternator test program was to evaluate the rotor response and bearing system performance under conditions of operation designed to reduce the journal bearing friction loss. Calculations of bearing performance under the conditions pertaining to simulator operation showed that a 15% reduction in friction loss could be obtained by an increase in diametral bearing clearance from 1.75 mils to 2.28 mils. The corresponding preload values for these clearances are 0.612 and 0.491 respectively for a C_p/R ratio of 1.28×10^{-3} . To facilitate the frequent changing of clearance required by the test plan, without stopping the test and making the pivot adjustments required to achieve the required clearance value, a 600 watt resistance heater was added to each bearing support. The temperature of the support could, therefore, be changed by varying the power supplied to the heaters, resulting in a clearance change due to differential thermal expansion between

the support, bearing and journal. The initial set-up of bearing clearance performed on assembly was for operation at the minimum clearance to be tested. This condition did not, therefore, require a supply of power to the support heaters.

It should be noted that this method of changing diametral bearing clearance also results in a change of rotor eccentricity. The extent of this change, however, was considered to be within acceptable limits.

Control of Bearing Loads

Variation in journal bearing loads, from zero to full rotor weight reaction, was made possible by rotation of the complete simulator on its mounting trunnions from a vertical to a horizontal rotor orientation. Figure VI-6 and VI-7 are photographs of the complete simulator assembly in a horizontal and vertical orientation respectively.

For control of thrust load, at any orientation of the rotor, the simulator casings for and aft of the turbine wheel were extended radially inward, and labyrinth seals provided between these extensions and the rotor (see Figure VI-1). This permitted the turbine wheel to be used as a double-acting piston. Variable magnitude and direction of thrust load was obtained by control of the pressure in the cavities on each side of the turbine wheel. These cavities were connected by suitable pressure control valves to a gas supply manifold (as shown in Figure VII-4). Leakage across the labyrinths passed into the main simulator casing from where it was vented to atmosphere (via a vacuum pump when the simulator was being operated at sub-atmospheric ambient pressures).

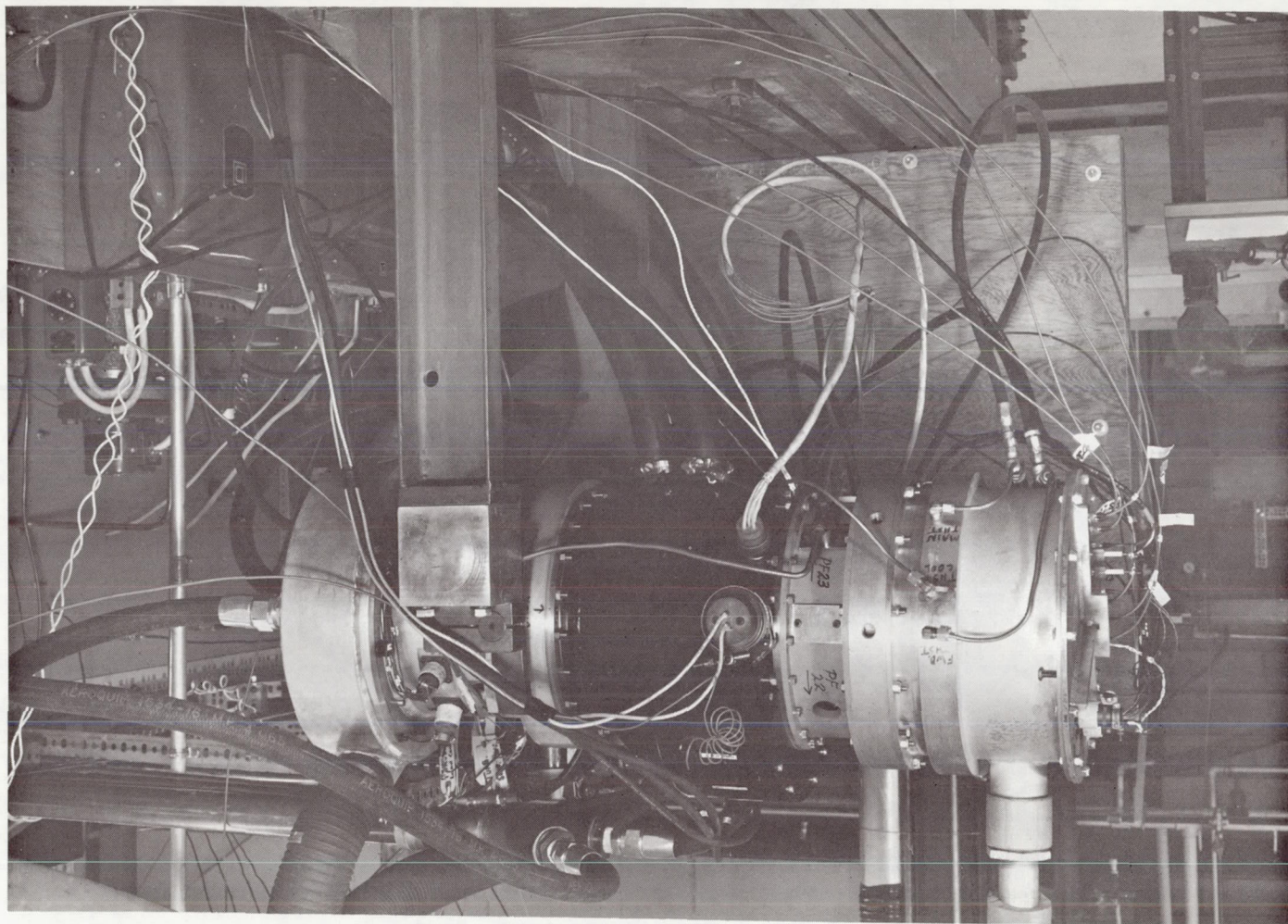


Fig. VI-6 View of Complete Simulator Installed
In a Horizontal Position on the Test Stand

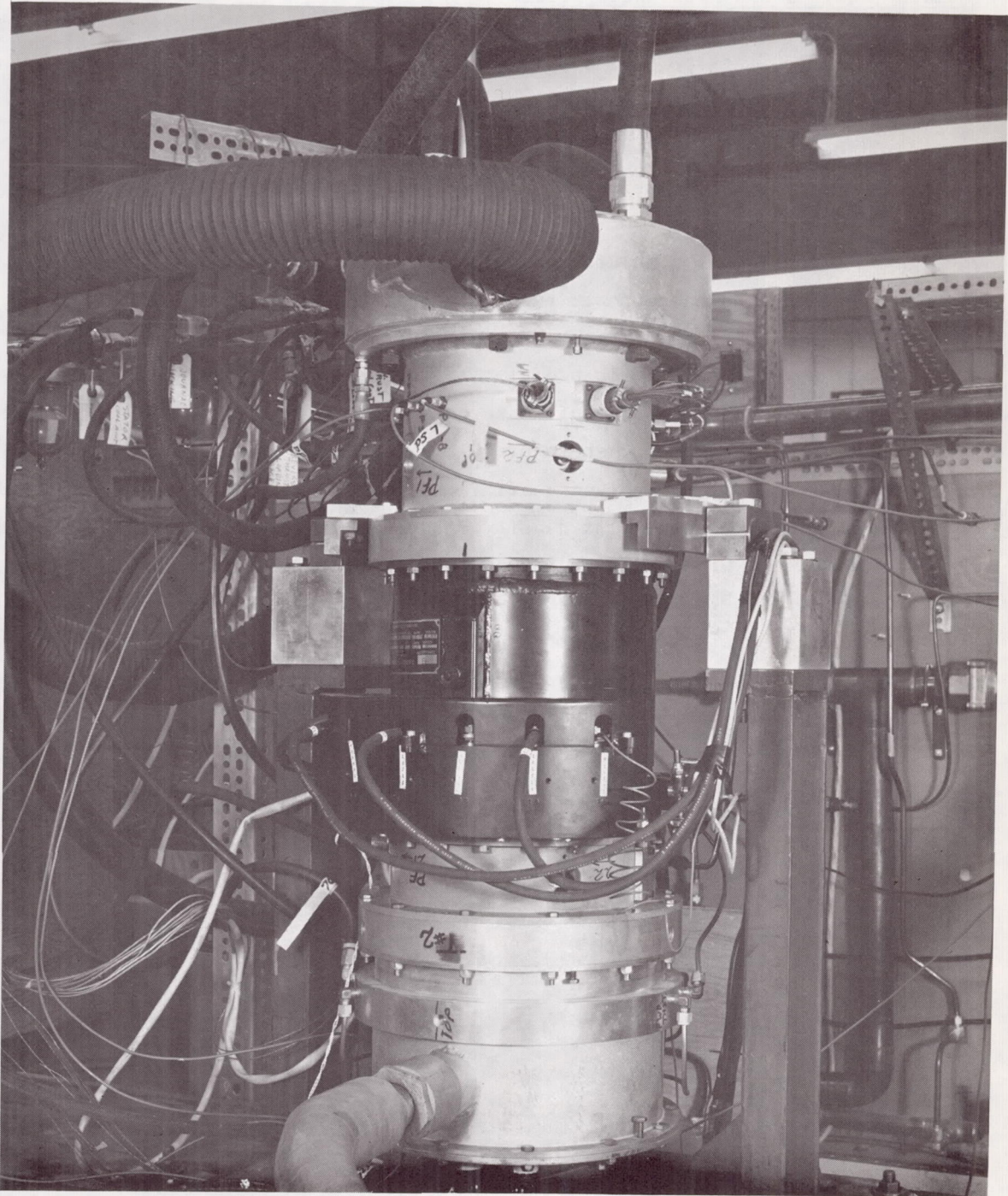


Fig. VI-7 View of Complete Simulator Installed in Vertical Position on the Test Stand

Simulator Casings and Alternator Stator

The primary function of the simulator casings were to provide an enclosure and support structure for the bearing system, alternator and turbine drive. More detailed discussion on the design of these casings is contained in Section III of this report in the subsection entitled "Simulator Casings".

Redesign of the original simulator casings was necessary to incorporate the alternator and the increased power turbine required to drive the alternator under full load conditions. Comparison of Figures III-1 and VI-1 indicates the extent of these changes. In addition to the structural changes it was necessary to introduce a section of nonmagnetic material at each end of the alternator to prevent magnetic short circuiting of the alternator flux path via the bearing support, pivot and bearing pads to the rotor journals. Such a short circuit would reduce the flux density between the alternator stator and the rotor pole faces with an attendant and unacceptable reduction in the alternator performance. The casings immediately adjacent to each end of the alternator were, therefore, manufactured from aluminum. Photographs of the alternator stator are shown in Figure VI-8.

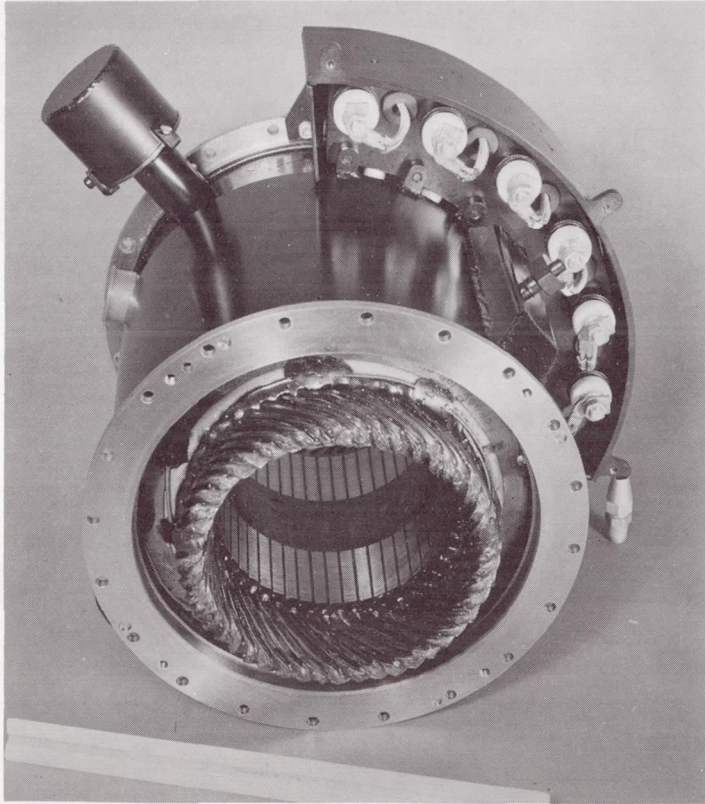


Fig. VI-8a Front View of Alternator Stator

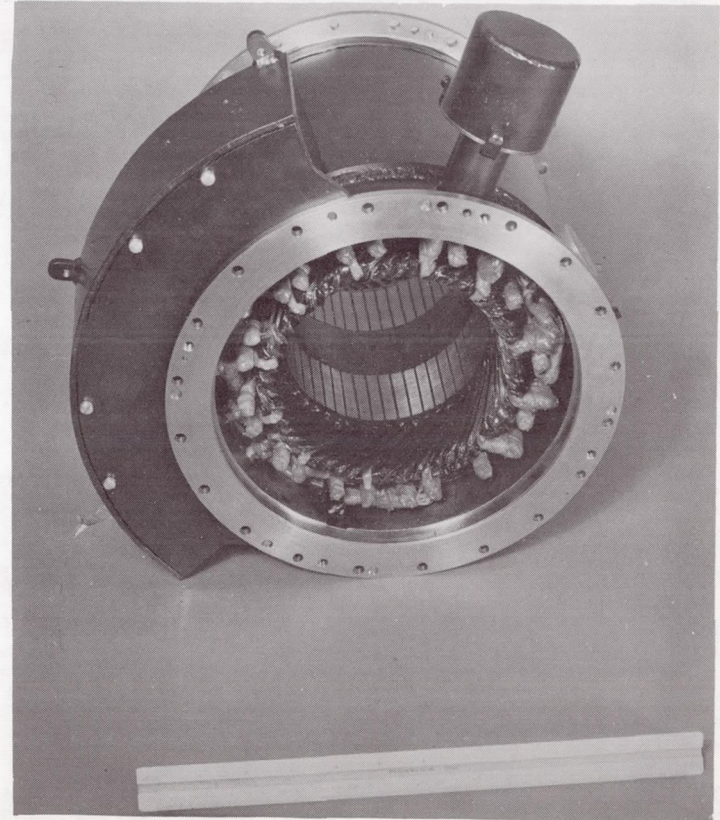


Fig. VI-8b Rear View of Alternator Stator

Simulator Turbine

To enable the alternator to generate full electrical power it was necessary to redesign the original simulator turbine which, as described in Section III of this report, was to produce approximately 1.5 HP to overcome bearing friction and windage loss at design speed. The redesigned turbine was required to develop a total power of 19.3 HP at design conditions.

In redesigning the turbine to give the increased power output, the same requirements as listed for the original simulator turbine design were taken into consideration with, of course, the exception of the power level which was increased to 19.3 HP. Again, an impulse turbine was selected to meet these requirements. The two primary factors in the design of the turbine were the requirements to correctly simulate the mass and inertia of the turboalternator turbine wheel, while maintaining the near optimum turbine parameters necessary to obtain the required power output from the available air supply system. The air supply system consisted of an existing reciprocating compressor capable of delivering 0.457 lb/sec of oil-free air at 100 PSIG and 70 F. The use of aluminum for the turbine wheel, which was possible due to the low stress levels involved with the low tip speed and also, low turbine temperature, resulted in the attainment of the mass and inertia parameters.

The predicted turbine performance was based on the methods in Reference [25] which correlates partial admission turbine performance in terms of specific speed and specific diameter which, for this turbine, are 7.14 and 5.42 respectively with an efficiency of 60%. The design is very close to optimum as regards bucket height and degree of admission. Total penalties on efficiency due to the effect of trailing edge thickness, bucket cutter diameter, bucket relative Mach number and, finally, leakage, were estimated to amount to 6%. The estimated turbine total-to-static efficiency was therefore 54%. The output power from this turbine at design point conditions is 20 HP, which leaves small margin above the 19.3 required. The calculated total temperature drop across the turbine at design condition was 172 F. To avoid the thermal problems such as unacceptable temperature gradients in the No. 1 bearing area and condensation and freezing, associated with this temperature drop, the turbine inlet temperature

was increased from 70 to 212 F by means of an air preheater. The turbine wheel would therefore operate at temperatures between 40 F and 70 F with a turbine exhaust temperature above freezing point.

The photographs in Figures VI-9 shows the turbine wheel and one of the two nozzles. Figure VI-10 shows the turbine wheel inserted into the turbine casing.

The primary performance parameters of the turbine at design point conditions are as follows.

Aerodynamic Design Point

Inlet Total Pressure (psia)	105
Exit Static Pressure (psia)	15
Inlet Total Temperature ($^{\circ}$ R)	672
Total Temperature Drop ($^{\circ}$ F)	172
Mass Flow (lb/sec)	0.38
Speed (RPM)	12,000

Nozzles

Number	2
Throat Area (in. ²)	0.090
Exit Area (in. ²)	0.563
Nozzle Height (in.)	0.45
Gas Angle	16 $^{\circ}$
Gas Exit Velocity (ft/sec)	1780
Mach No.	1.8
Efficiency (%)	92
Pitch Diameter (in.)	9.05

Blade

Number	72
Cutter Diameter (in.)	0.125
Inlet = Outlet Angle (degrees)	21.65
Trailing Edge = L.E. Thickness (in.)	0.010 - 0.015
Blade Height (in.)	0.5
Inlet Rel. Mach No.	1.35
Inlet Rel. Velocity (ft/sec)	1330
Blade Speed (ft/sec)	474
Blade Tip Diameter (in.)	9.483

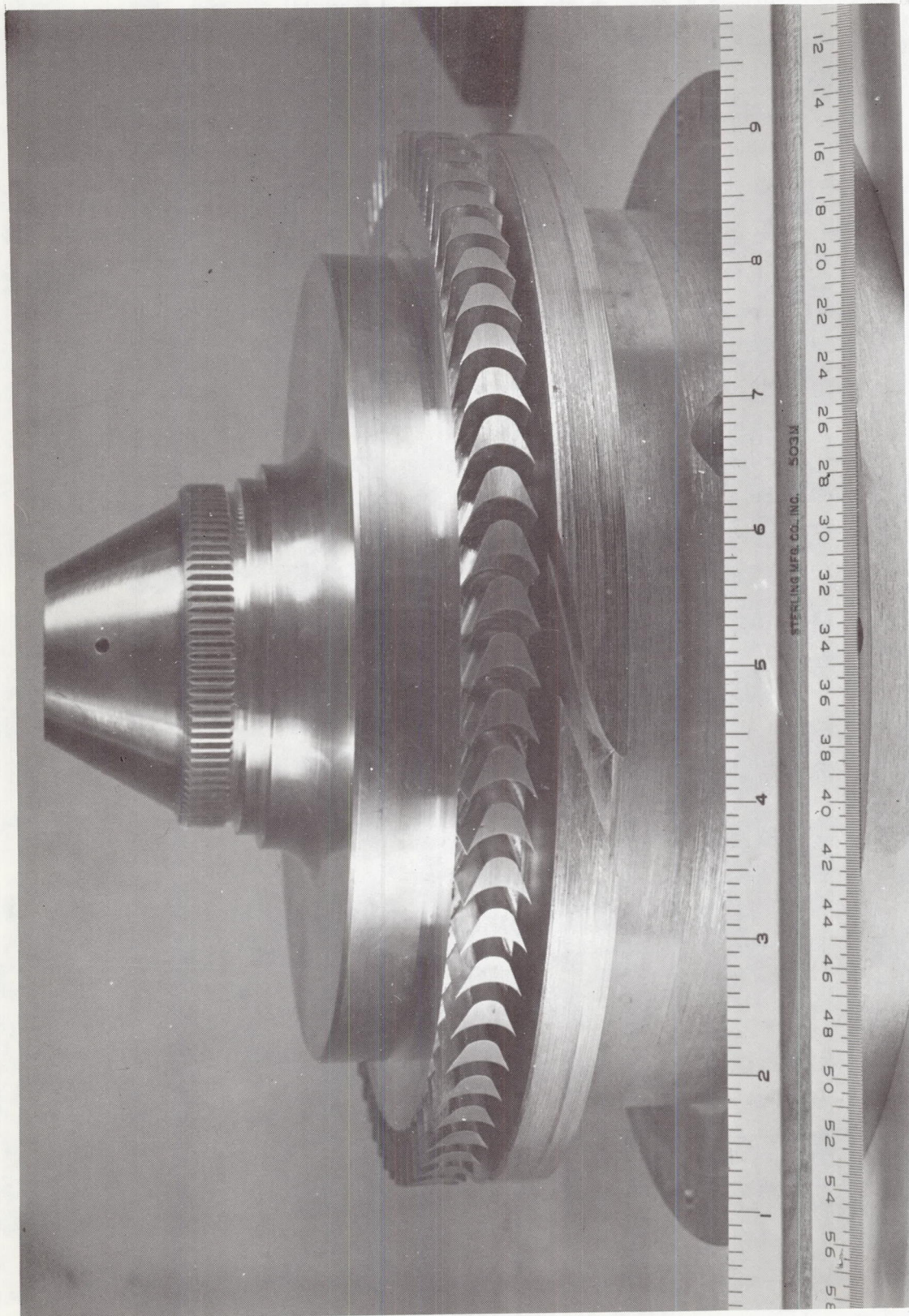


Fig. VI-9 View of Simulator Turbine Wheel and
One of Two Nozzles

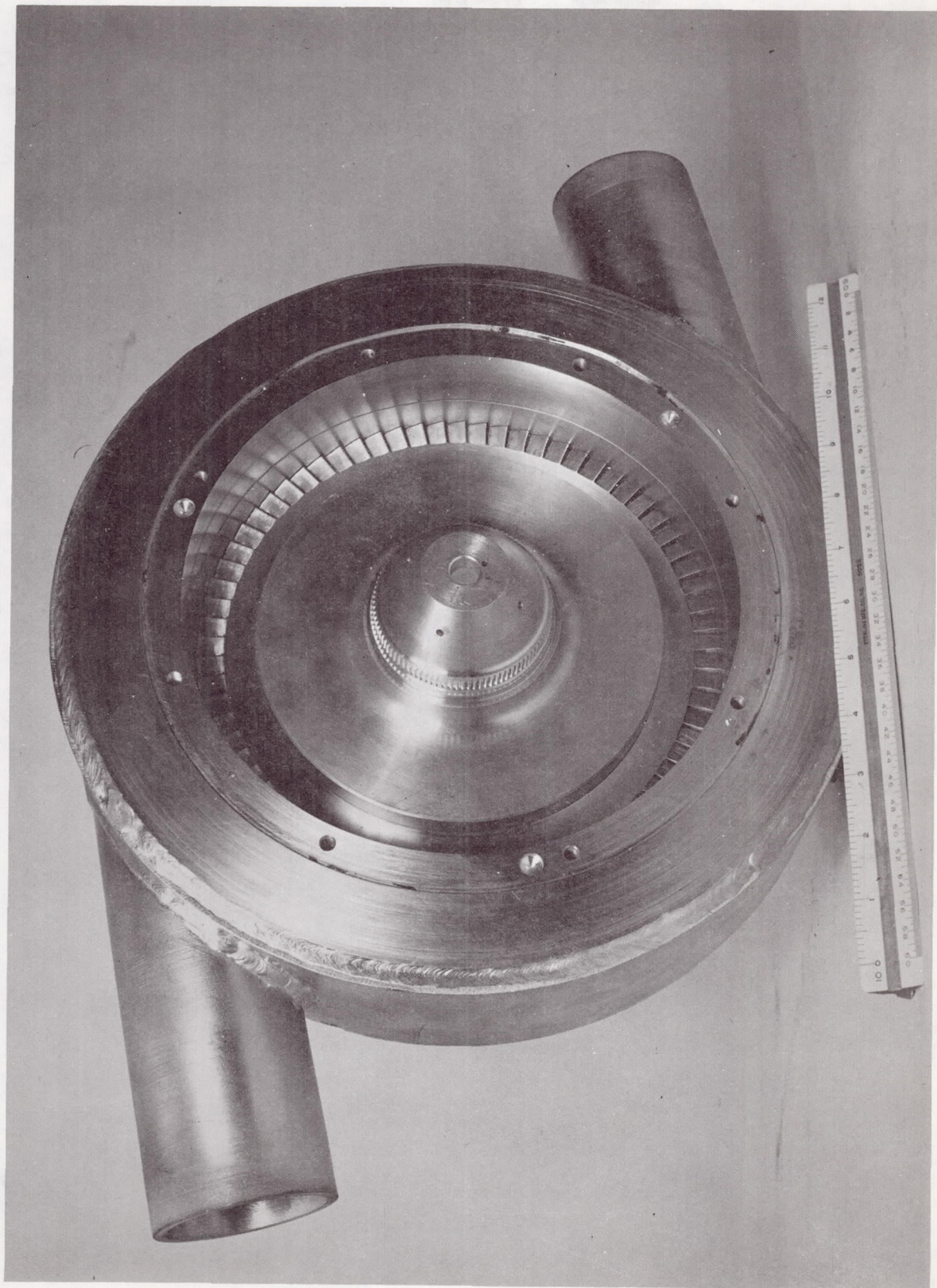


Fig. VI-10 View of Simulator Turbine Wheel and Casing

Simulator-Alternator Temperature Control

The requirement to incorporate the alternator into the simulator design and to operate under conditions involving the generation of full electrical power, results in changes in the bearing region temperature levels and gradients previously calculated for both the turboalternator and the original simulator. The differences which exist between the design and operation of the simulator, including the alternator, and the turboalternator are as follows:

1. The simulator is driven by a low temperature impulse turbine.
2. The simulator journal bearing supports are not extended, in the fore and aft directions, to form heat exchangers.
3. The coolant inlet temperature to the thrust bearing and the alternator stator is limited (by test equipment limitations) to approximately 80 F at the design flow rates of 200 lb/hr. and 600 lb/hr. for the thrust bearing and alternator respectively.

To ensure that the temperature distribution in the region of the journal bearings was satisfactory for proper operation of the bearings, a thermal analysis of the simulator was performed. The boundary conditions for this analysis were established as follows:

1. Detailed values of the alternator losses were taken from the alternator design data. An estimate was made, based on this data, that the frame temperature would be 20 F above coolant inlet temperature. Therefore, a boundary temperature of 100 F was established for the alternator stator.
2. The sink temperature in the region of the turbine wheel was taken to be 40 F. This corresponds to turbine exit temperature at the 12 KWe, 12,000 RPM operating condition. (The turbine inlet temperature at this point would be 212 F.)
3. The temperature of the thrust runner was estimated to be 100 F, i.e., 20 F above coolant inlet temperature.

4. The friction loss for each journal bearing was taken to be 342 BTU/hr. which was the maximum loss expected over the range of conditions under which the simulator was to be tested (i.e., at 12,000 RPM, 10.5 PSIA and minimum bearing clearance).

In the No. 1 bearing region thermal distortion of the journal was seen to be basically conical, with a radial height of 0.4 mils at the alternator end of the bearing. Superimposed on this cone is a crown with a radial height of 0.08 mils. The journal in No. 2 bearing region also has a conical distortion of 0.3 mils at the alternator end of the bearing. The crowning here will be 0.085 mils.

The pivots will allow the bearing pads to become aligned with the conical portion of the journals; the crowning, however, must be accommodated by the gas film. The extent of this crowning is slightly greater than the 0.075 mils crowning reported in Section II of this report but it is not expected to impair bearing performance.

Simulator Electrical Load Control

To evaluate the response of the rotor bearing system to the electromagnetic forces resulting from operation of the alternator at various levels of power generation and during a number of different electrical fault conditions, it was necessary to supply the alternator with the required excitation, absorb the power generated and provide means to initiate the required short-circuit and unbalance load conditions. The excitation requirements were met by the breadboard Voltage-Regulator-Excitor (VRE) which was built and used by the alternator manufacturer during the development and test programs associated with the alternator and the VRE. To absorb the electrical load and initiate fault conditions, a load bank was designed and supplied by the alternator manufacturer. A photograph of this load bank is shown in Figure VI-11. The design of the load bank allowed for the adjustment of load and power factor of each of the 3 phases, meters being provided for the display of phase volts, amps and watts. Provisions were also available for the ganging together of all three phases, in which case the alternator could be loaded uniformly in 3 KW increments. Loading of a single phase was achieved by the use of a switch. Short-circuit conditions, either single phase or three phase, were accomplished with the short-circuit button. The VRE was completely

automatic, excitation being supplied at speeds over 6,000-7,000 RPM. To allow acquisition of data at design speed without the effects of electromagnetic power, the VRE circuit was provided with a switch which disconnected the excitation from the alternator.

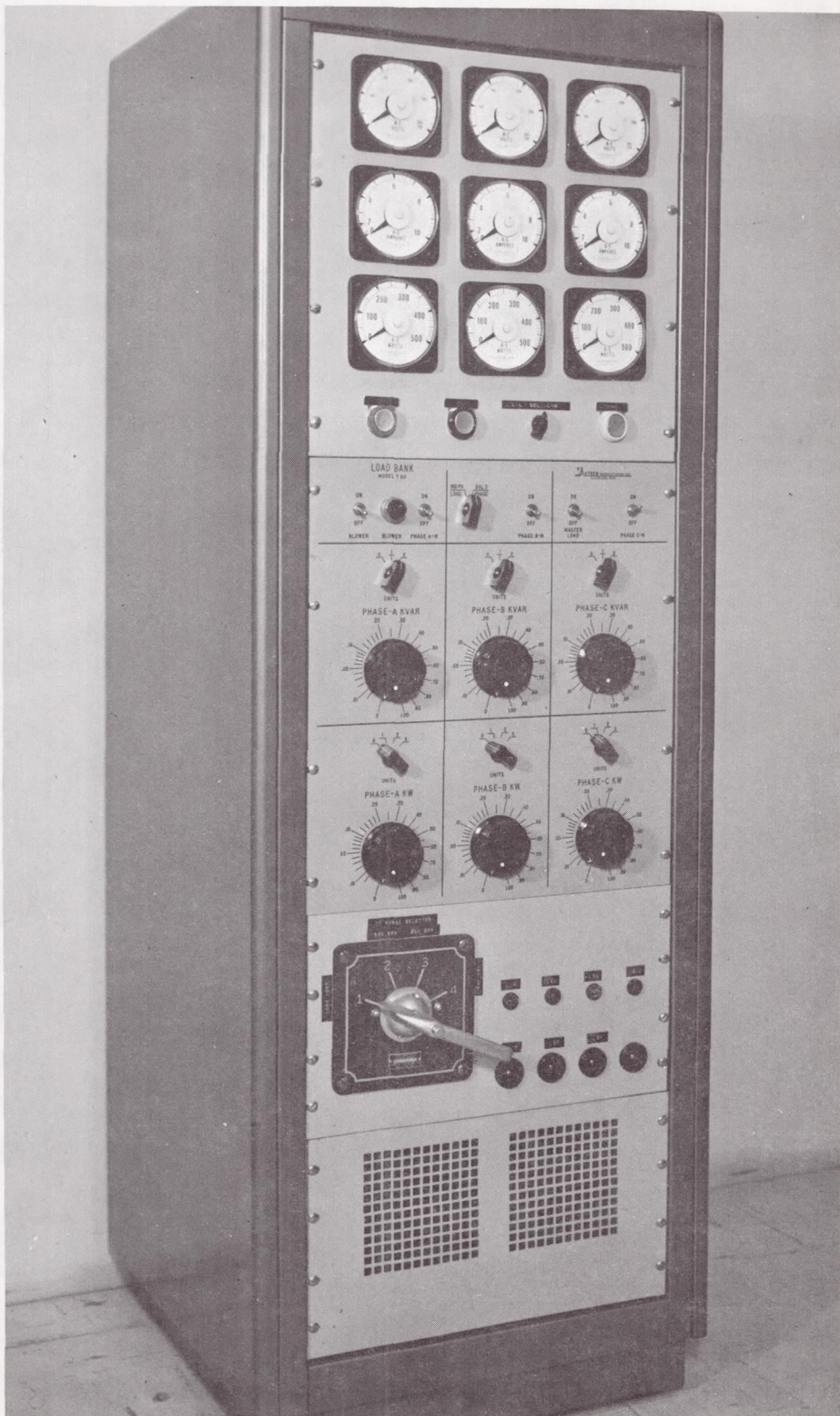


Fig. VI-11 View of the Load Bank Used to Dissipate the Power Generated During Test of the Rotor-Bearing-Alternator Simulator

Simulator-Alternator Instrumentation

As mentioned in preceding sections of this report, successful and timely development of a prototype gas-bearing machine requires extensive rotor-bearing system instrumentation for quantitative measurement of performance and for minimum risk operation. Accordingly, the rotor-bearing system intended for use in the simulator was equipped with exactly the same capacitance probe and thermocouple transducers as recommended for the prototype turboalternator design in Section II of this report.

In addition to the bearing system instrumentation, numerous additional thermocouples were installed to monitor the bearing support temperatures, turbine temperatures and coolant inlet and outlet temperatures. In addition, the thermocouples inserted into the alternator stator by the manufacturer were used to continuously monitor the temperature distribution throughout the stator.

A model 3040 Electro Products Laboratories magnetic speed pick-up was used to measure rotor speed. The pick-up sensed six notches cut in the OD of the thrust runner. Finally, the simulator was equipped with numerous pressure taps for measurement of turbine, thrust loading and bearing ambient pressures.

A description of the simulator instrumentation readout equipment, and the simulator control system is given in the next section of this report. A schematic of the control system is shown in Figure VII-4.

VII - TEST EVALUATION OF THE ROTOR BEARING SYSTEM UNDER VARIOUS CONDITIONS OF ALTERNATOR LOAD

Assembly of the bearing system and the simulator described in Section VI of this report commenced on November 8, 1966. Preliminary testing with the alternator excitation in operation was started on December 20, 1966. The planned test program commenced on January 10, 1967, and was completed on January 30, 1967. During the course of testing, approximately 90 hours of operation were accumulated in obtaining data at the 216 planned test points and during the additional tests which were performed.

The following subsections describe the simulator test facility, in which the rotor-bearing system response to electromagnetic forces was evaluated, and the specific test results pertaining to the performance of the rotor-bearing system.

Description of the Simulator Test Facility

The simulator test facility consisted of the following items:

1. the rotor-bearing-alternator system simulator (described in Section VI),
2. the voltage-regulator-excitor (VRE) and load bank,
3. the simulator control panel, and
4. the instrumentation readout and magnetic tape recording system.

Figures VI-6 and VI-7 in the preceding section of this report are photographs of the rotor-bearing-alternator simulator mounted on the test stand behind the test panel. In these photographs the simulator is mounted in the horizontal and vertical positions respectively. For operation in the vertical position, the turbine end is uppermost. In both of these photographs the simulator is shown with the pivot access holes uncovered to permit bearing clearance adjustment.

Figure VII-1 is a photograph of the left hand side of the simulator control panel and the instrument readout equipment. At far left is the CEC magnetic tape recording system which was used for data acquisition throughout the test program. This is followed by the two Microdynes used to display the motion of each journal relative to the casings. The third Microdyne and the Wayne Kerr and CRO mounted on top of the Microdynes, were used to display the thrust bearing clearances. The Hewlett-Packard electronic counter placed on top of the third Microdyne was used to continuously monitor rotor speed. The turbine inlet air heater appears as the long cylindrical section below the control panel. The temperature controls for the heater were mounted on the extension which protrudes above the main panel.

Figure VII-2 is a photograph of the right side of the simulator control panel and the instrument readout equipment. The rheostats used to adjust the journal bearing support temperatures are seen mounted on the extreme left of the panel. The two temperature recorders mounted at left center were used to continuously record the system temperatures. Below these recorders can be seen the push-button station which was used to connect or disconnect the alternator excitation as required. The ammeters shown mounted above the load bank were used to monitor the alternator excitation current during the course of testing. At the right of the figure are shown the Wayne Kerrs and CRO's which were used to display the film thickness between each bearing pad and the journal.

Figure VII-3 is a wide angle photograph taken during the course of the test program showing the complete control panel and instrumentation system.

Figure VII-4 is a schematic diagram of the simulator control system. All controls, except for heater temperatures and air-manifold supply pressure, were manually operated. It is seen from Figure VII-4 that individual control valves were supplied for

1. fine and coarse control of turbine nozzle pressure (V-4 and V-5),
2. control of main thrust loading pressure (V-6),
3. control of reverse thrust loading pressure (V-7),

4. control of main hydrostatic thrust bearing supply pressure (V-10),
5. control of reverse hydrostatic thrust bearing supply pressure (V-9),
6. control of water coolant supply pressure to the main thrust bearing stator (V-12),
7. control of jacking gas to the journal bearings (V-8),
8. control of water coolant to the alternator (V-11), and
9. control of simulator bearing region ambient pressure (V-14, V-15 and V-16).

All pertinent pressures and flows for the above listed control functions were measured via Bourdon tube pressure gages and Rotometer flowmeters mounted on the control panel, as seen in Figures VII-1, VII-2 and VII-3. Control of the bearing support heaters was obtained via manually-controlled variacs (auto transformers) also mounted on the control panel.

Shop air at 100 PSIG was used to drive the simulator turbine over the required range of speeds and electrical loads. Control of turbine inlet temperature was achieved by regulation of the heater H-1 with the set point controller.

The temperature of the gas supplied to the hydrostatic thrust bearings was controlled by regulation of the heaters H-2 and H-3. Control of the temperature of the thrust bearing and alternator coolant was achieved by regulation of the heater H-4.

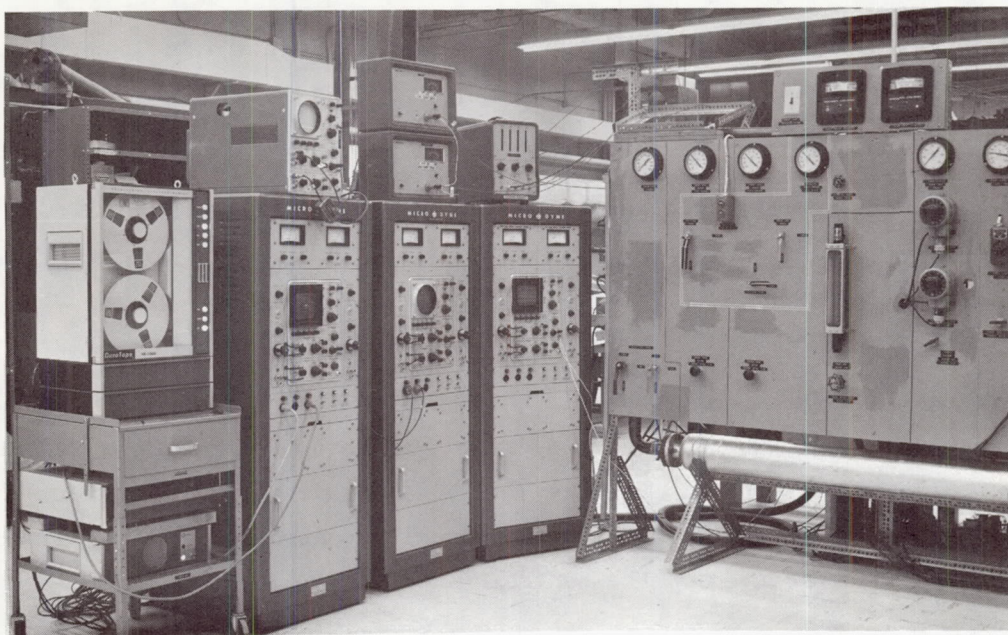


Fig. VII-1 View Showing the Left Hand Side of the Simulator Control Panel and Instrument Read-out Equipment

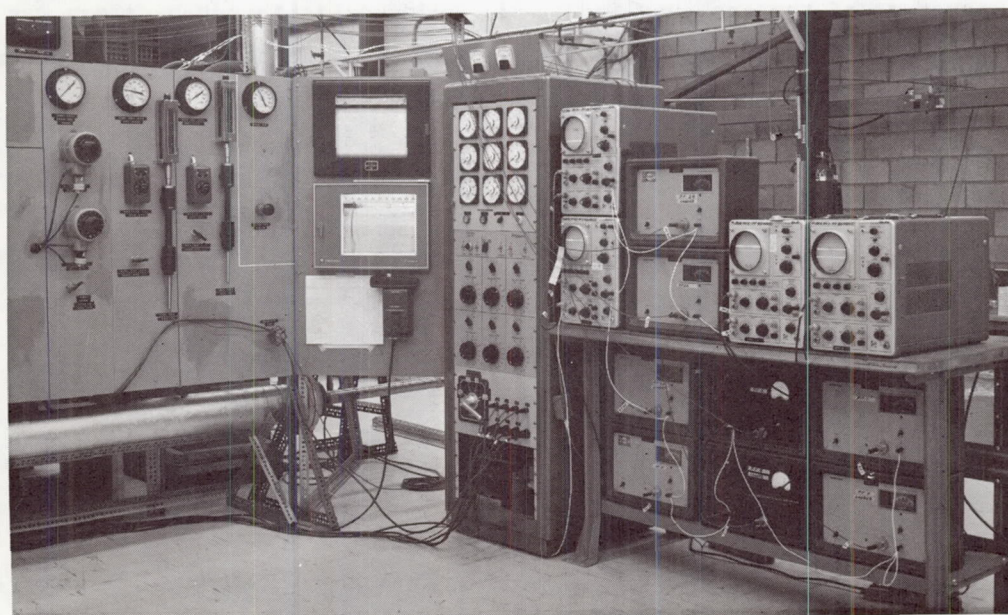


Fig. VII-2 View Showing the Right-Hand Side of the Simulator Control Panel and Instrument Read-Out Equipment

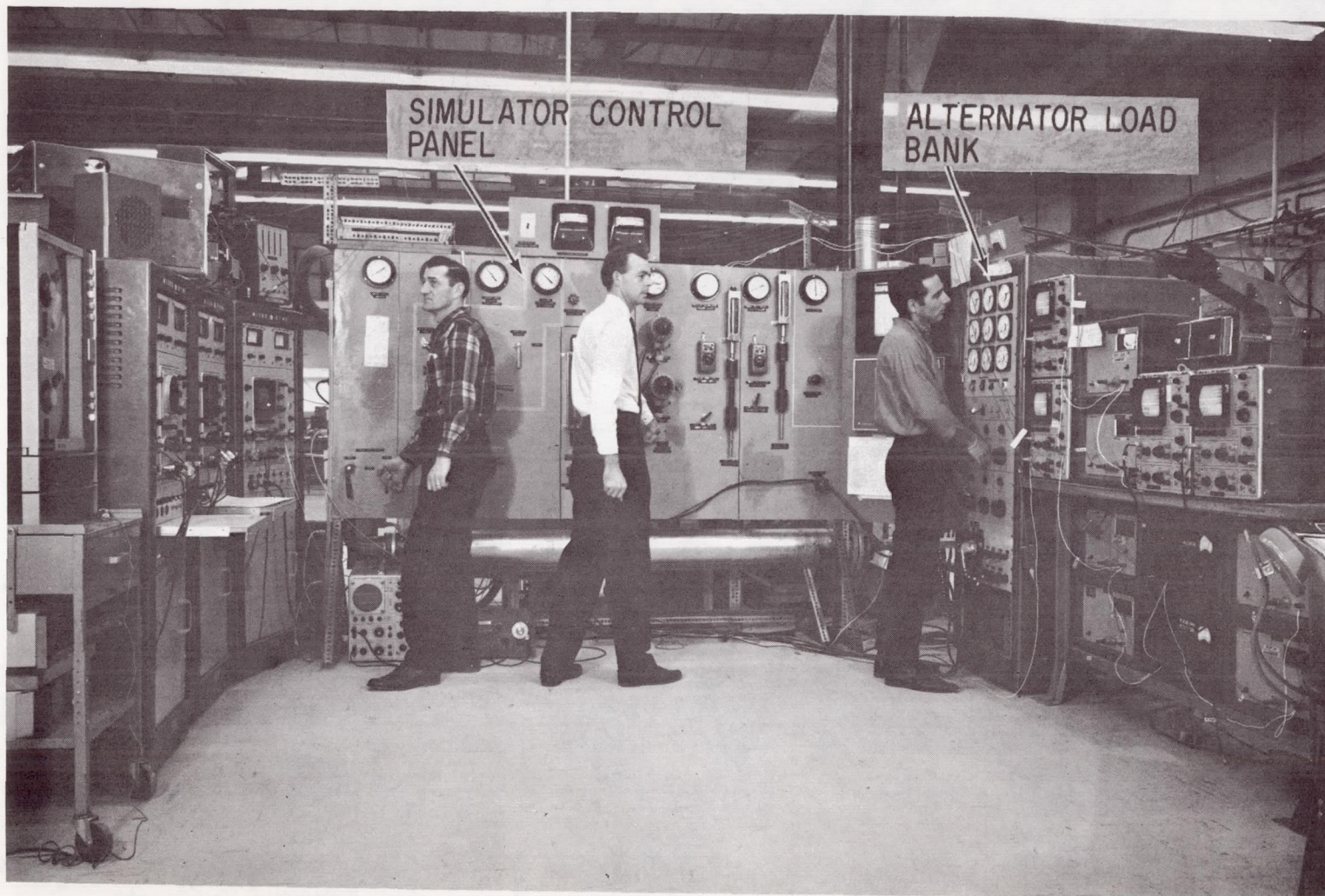


Fig. VII-3 View Showing the Simulator Control Panel and Instrument Read-out Equipment During Test

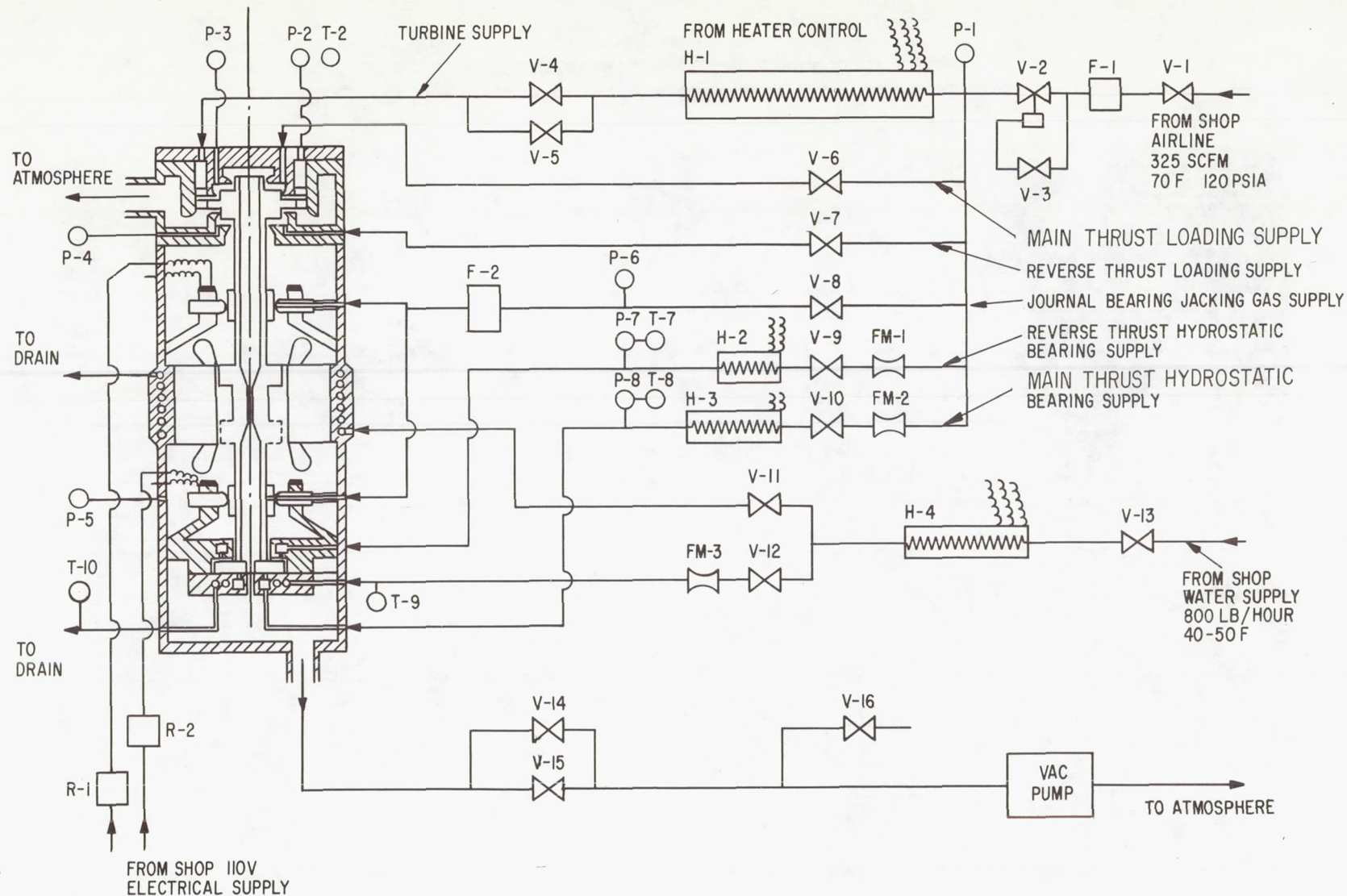


Fig. VII-4 Schematic Diagram of the Simulator Test Set-Up
for Test Evaluation of the Rotor-Bearing-Alternator
Simulator

Initial Adjustment of Simulator Rotor Concentricity and Journal Bearing Clearance

Under idealized conditions of manufacture and operation, the radial magnetic forces in a four-pole inductor alternator would cancel (i.e., the resultant radial force and transverse moment acting on the rotor would be zero). In practice, however, unavoidable variations in material and geometry of the rotor and stator, and deviations of the rotor from the exact magnetic centerline of the stator, will result in unbalanced magnetic forces (and, to a lesser extent, moments) acting on the rotor. These forces act to increase the eccentricity of the rotor which, in turn, results in further increase in the forces.

To evaluate, experimentally, the response of the rotor-bearing system to electromagnetic forces, it is necessary to conduct the appropriate tests under conditions where the eccentricity between the magnetic centers of the alternator rotor and stator is known. In practice these magnetic centers are individually indeterminate and, therefore, assembly and adjustment of the simulator must be performed by a method which does not involve determination of magnetic centers. If it is initially assumed that due to careful design and manufacture, the magnetic and geometric centers of the components are coincident, then the machine may be assembled and the bearings adjusted to permit geometrically coincident operation of the rotor and stator when operating at design conditions. The validity of this assumption and, to some extent, any discrepancy between geometric and magnetic centers may be determined if first the machine is operated at design speed in a vertical, geometrically concentric position without the alternator being excited, followed by operation with the alternator excited. Any shift in the position of the journals, as evidenced by the casing-to-journal capacitance probes, when running in these two modes of operation will be due to magnetic forces resulting from magnetic eccentricity in either, or both, the alternator rotor and stator.

Correction of any unacceptable amount of eccentricity determined by this method may be accomplished by the appropriate readjustment of the journal bearings.

The method of assembly which was chosen to ensure that the geometric eccentricity between the simulator rotor pole face diameters and the bore of the alternator stator could be selected and adjusted with an acceptable degree

of accuracy involved the use of a gage shaft and the casing to journal capacitance probes. The gage shaft consisted of a central section, which just fitted into the stator bore, with two outboard extensions. These extensions were of the same length and diameter as the rotor journals and were ground concentric with the center section. During assembly, the gage shaft was inserted into the stator bore and the casings, bearing supports and journal bearing pads assembled. The casing-to-journal capacitance probes were then inserted and connected to the instrumentation readout equipment. Moving each of the gage shaft extensions (in turn) throughout the small clearance between the central section of the gage shaft and the stator bore resulted in the establishment of approximately circular orbits in the planes of the capacitance probes, each of which was displayed on a CRO. The center of these orbits was considered to be the geometric center of the stator. The gage shaft was then centered by adjustment of the bearing pads and the distance meter reading noted. The value of these readings was used throughout the test program to describe the geometric center of the alternator stator and to determine the extent of rotor eccentricity.

Following the determination of the stator geometric center, the gage shaft was removed after withdrawing the No. 2 bearing support complete with bearing.

The rotor was then installed and the simulator fully assembled and instrumented, with the exception of the main (hydrodynamic) thrust bearing, prior to making the necessary journal bearing adjustments to permit vertical operation at design speed with the rotor concentric to the alternator stator. These adjustments were made while the rotor was in a vertical position with the thrust runner uppermost. Freedom of rotation was achieved by providing the reverse thrust bearing with a supply of jacking gas at approximately 40 PSIG. The journal bearings were adjusted to allow a diametral clearance of 0.002 inches with the geometric center of the clearance profile, as described by the ground-to-shaft probes and displayed on CRO's, positioned 0.0005 inches below the geometric center of the alternator center.

Having completed these adjustments, the simulator was prepared for preliminary testing.

Preliminary Testing

The purpose of the preliminary tests was to establish quickly and safely, the operating characteristics of the simulator, control system and instrumentation as the assembly progressed. This method of testing permits the early identification of problem areas before accessibility becomes restricted and hence, adjustments more difficult. The earliest stage at which the simulator could be rotated was attained after adjustment of the rotor concentricity, bearing clearances and assembly of the reverse thrust bearing. The first test was performed with the simulator vertical, the thrust bearing being uppermost. The main thrust bearing was not installed and the VRE and load bank were not electrically connected to the alternator. Testing commenced on December 17, 1966. A summary indicating the test configuration, purpose and observations noted during these tests is given in Table VII-1.

After the completion of Test 1, the axis of the simulator was inclined at 45° , the thrust runner remaining uppermost, and the test repeated with and without journal bearing jacking gas. For tests numbered 3 through 9, a DC power supply was used to provide excitation to the alternator field. The load bank was connected up for Test Number 7. For tests numbered 10 through 14, the DC power supply was replaced by the VRE, with an ON-OFF switch and an ammeter inserted between the VRE and the alternator for the purpose of measuring the excitation current. At the conclusion of Test Number 12, the main thrust bearing was assembled, the various access holes sealed to permit operation at lower than ambient pressures, and the instrumentation set-up completed. Tests 13 and 14 were, therefore, conducted with the complete test set-up required by the test plan.

TABLE VII-1
PRELIMINARY TEST PROGRAM

Test #	Date	Configuration Tested	Purpose of Test	Test Observations
1	12/17/67	Vertical, with rotor supported by reverse thrust bearing. No alternator excitation.	Check rotor operating concentricity, bearing clearance and standard of balance	A speed of 14,400 RPM was achieved. Rotor concentricity, bearing clearance and standard of balance were satisfactory.
2	12/20/66	45° inclination. Rotor supported by reverse thrust bearing. No alternator excitation	Check journal bearing jacking gas system and effect on bearing performance when journal jacking gas removed	At 10,000 RPM the bearing system performed satisfactorily. No apparent change in journal bearing performance when jacking gas turned off.
3	12/20/66	As Test 2 but alternator excitation supplied from DC power supply. No rotation	Ascertain the effects of excitation on rotor concentricity	At 0 RPM with rotor 0.0005 in. eccentric and supported by jacking gas, switching on the excitation increased the eccentricity by approximately 0.0005 in.
4	12/20/66	As Test 3 but simulator running at 10,000 RPM	Ascertain the effect of varying excitation current on the partially loaded rotor-bearing performance	At 10,000 RPM the excitation was increased from 0 to 5 amps. Rotor eccentricity increased from 0.0003 in. to 0.00035 in. Journal bearing film thickness was reduced by 0.0001 in.
5	12/20/66	As Test 4 but journal bearings hydrodynamic	As Test 4	Results approximately as observed in Test 4

TABLE VII-1 (Continued)

PRELIMINARY TEST PROGRAM

Test #	Date	Configuration Tested	Purpose of Test	Test Observations
6	12/21/66	As Test 5 but inclined at 5°	Ascertain the effect of varying excitation on the fully loaded rotor-bearing performance	Results approximately as observed in Tests 4 and 5
7	12/21/67	As Test 6 but load bank connected and bearings operating hydrostatically	Ascertain the effect of balanced electrical load on rotor-bearing performance	At 12,000 RPM the alternator load was slowly increased to 3KW with no noticeable effect on rotor position or bearing clearance
8	12/21/67	As Test 7	Ascertain the effect of unbalanced electrical load on rotor-bearing performance	As Test 7
9	12/21/66	As Test 7 but with hydrodynamic journal bearings	As Test 7	At 12,000 RPM the load was increased in 3 KW increments to 12.0 KW. Slight changes in orbit and bearing clearance noted.
10	12/22/66	As Test 7 with VRE installed	Ascertain the proper operation of the VRE	VRE automatically becomes operative at 7400 RPM. Performance satisfactory.

TABLE VII-1 (Concluded)

PRELIMINARY TEST PROGRAM

Test #	Date	Configuration Tested	Purpose of Test	Test Observations
11	12/22/66	As Test 10	Ascertain the effect of single and three phase short circuits on rotor-bearing performance	The short circuits, applied for varying periods up to 5 seconds resulted in orbit enlargements of less than 20 micro inches.
12	12/23/66	Simulator vertical with thrust bearing uppermost	Improve the standard of rotor balance to facilitate identification of rotor response to electromagnetic forces	To amplitude of rotor vibration at No. 2 bearing was reduced by a factor of 2. The amplitude at No. 1 bearing did not require correction
13	1/4/67	Simulator vertical with turbine uppermost	Check out main hydrodynamic thrust bearing	The main thrust bearing performed satisfactorily when operating hydrodynamically and hydrostatically
14	1/4/67	As Test 13	Check out system with bearings operating at low ambient pressures (7.2 and 10.5 PSIA)	All performance satisfactory

Conditions and Details of Simulator Test

To determine and evaluate the effects of electromagnetic forces on the turbo-alternator rotor-bearing system, a number of simulator configurations were assembled and tested. The variables involved in the definition of these configurations are

1. rotor orientation,
2. mechanical unbalance, and
3. alternator rotor eccentricity.

For each of these variables, certain conditions were selected as follows:

1. Simulator in the vertical position (turbine end up);
2. Simulator in the horizontal position (soft flexures up);
3. Rotor shaft with minimum residual unbalance;
4. Rotor shaft with 0.005 ounce inches mechanical unbalance in the plane of the turbine wheel;
5. Rotor shaft magnetically concentric with the alternator stator; and
6. Rotor shaft magnetically eccentric 0.002 ± 0.0005 inches radially with the alternator stator.

These variables were combined and the simulator assembled to form six (6) configurations (or test set-ups) as follows in Table VII-2.

Each of these six simulator configurations were subjected to the tests shown in Tables VII-3, VII-4 and VII-5.

TABLE VII-2

Simulator Configuration Variables

<u>Simulator Config.</u>	<u>Simulator Horizontal</u>	<u>Simulator Vertical</u>	<u>Mechanically Balanced</u>	<u>Mechanically Unbalanced</u>	<u>Magnetically Concentric</u>	<u>Magnetically Eccentric</u>
a		x	x		x	
b		x		x	x	
c	x			x	x	
d		x	x			x
e		x		x		x
f	x			x		x

TABLE VII-3

ZERO ELECTRICAL LOAD TEST CONDITIONS

<u>Preload</u>	<u>Test Conditions</u>		<u>Test Point Number</u>		
	<u>Pressure Psia</u>	<u>Stator*</u>	<u>10,800 RPM</u>	<u>12,000 RPM</u>	<u>14,400 RPM</u>
.612	10.5	DE	-	3	-
.612	10.5	E	1	2	4
.612	7.2	DE	-	11	-
.612	7.2	E	12	10	9
.491	10.5	DE	-	15	-
.491	10.5	E	13	14	16
.491	7.2	DE	-	23	-
.491	7.2	E	24	22	21

*Stator energized - E
 Stator de-energized - DE

TABLE VII-4

BALANCED ELECTRICAL LOAD TEST CONDITIONS AT 12,000 RPM AND 0.8 POWER FACTOR

<u>Test Conditions</u>		<u>Test Point Number</u>			
<u>Preload</u>	<u>Pressure</u>	<u>3.0 KWe</u>	<u>6.0 KWe</u>	<u>9.0 KWe</u>	<u>12.0 KWe</u>
.612	10.5	-	-	5	6
.612	7.2	8	7	-	-
.491	10.5	-	-	17	18
.491	7.2	20	19	-	-

TABLE VII-5

UNBALANCED LOADS AND SHORT CIRCUIT TEST POINTS

<u>Preload</u>	<u>Test Conditions</u>		<u>Test Point Number</u>		
	<u>Pressure</u>	<u>Power Factor</u>	<u>3.33 KVA</u>	<u>1ϕ shorted</u>	<u>3ϕ shorted</u>
.612	10.5	1	25	-	-
.612	10.5	0.8	-	33	29
.612	7.2	1	26	-	-
.612	7.2	0.8	-	34	30
.491	10.5	1	27	-	-
.491	10.5	0.8	-	35	31
.491	7.2	1	28	-	-
.491	7.2	0.8	-	36	32

Notes pertinent to Table VII-5:

- 1) 3.33 KVA, (alternator connected 1 ϕ to neutral - 2 ϕ open circuit)
- 2) 1 ϕ shorted, (alternator at 12 KWe then 1 ϕ shorted for 5 secs maximum)
- 3) 3 ϕ shorted, (alternator 12 KWe then 3 ϕ shorted for 5 secs maximum)

It should be noted that the values of preload given in Tables VII-3, VII-4 and VII-5 relate to a bearing clearance ratio (C_p/R) of 1.28×10^{-3} at design-point operating conditions. The related diametral clearances to these preload values are as follows:

<u>Preload</u>	<u>Journal Bearing Diametral Clearance</u>
0.612	1.75 MILS
0.491	2.28 MILS

During the course of the test program, the change in diametral clearance was accomplished by increasing the bearing support temperature as described in section VI of this report.

The planned sequence in which the tests were to be performed was in the order of ascending test point number. This sequence was intended to allow the accumulation of test data from all of the 'no load' and 'balanced load' conditions before proceeding with the 'unbalanced load' and 'short-circuit' conditions. These latter conditions being considered the most hazardous to uninterrupted operation due to the transients involved.

At the termination of the preliminary test program described in the preceding section, however, it was concluded that conditions involving severe transients which might prove hazardous to uninterrupted operation would not be encountered. This conclusion, permitted the revision of the test plan to allow testing under zero and balanced electrical load conditions to be immediately followed by unbalanced and short circuit testing, thereby reducing significantly the time required for simulator adjustment.

Data Acquired During Test

Testing of the rotor-bearing-alternator simulator commenced on January 10, 1967, and was completed on January 30, 1967. Test data was taken at each of the 216 prescribed test points in a total running time of 91 hours. An approximate breakdown of the running time results in 16 hours for set up and preliminary tests, 47 hours to establish reasonably stable temperature conditions for test data points, and 28 hours to obtain test data. The duration of the longest test conducted without shutdown was approximately 4 hours.

Testing of the various configurations was conducted in the sequence shown in Table VII-6. This table also shows the major variables in each configuration tested, the sequence in which journal bearing adjustments were made, and the average diametral journal bearing clearances throughout the test of each configuration.

The rotor-bearing-alternator simulator was equipped with the instrumentation described in Sections II and VI of this report. During the course of the test program, data was obtained at each test point from the instrumentation previously described, with the exception of the pad flutter probes and the main thrust stator probe. In addition to this data, magnetic tape recordings were made of the primary instrumentation signals at each data point. Polaroid photographs were also taken of the CRO displays during the configuration A and F tests involving increased journal bearing clearance.

Details concerning the data acquired and tabulated are given in Table VII-7. In this table, under the column entitled Form of 'Data Acquisition', the term tabulation refers to the data entered on the test data sheets. The position of the sensors identified in the column entitled "Sensor Designation" can be found both in this report and the referenced documentation as follows:

<u>Sensor Description</u>	<u>Report Reference Figure Nos.</u>	<u>Other References</u>
Pad to Shaft Probes and Pad Thermocouples	II-23, II-24, II-25	
Ground to Shaft and Pitch Probes	II-23, II-24	
Bearing Support Temperatures	—	
Jacking gas supply pressures and flows and bearing ambient pressures	VII-4	
Thrust bearing film thickness probes and temperatures	—	
Thrust bearing coolant flows, temperatures and loading pressures	VII-4	
Alternator Temperatures	—	
Alternator Power	VI-11	Avtron Manufacturing Operating & Installation Instructions for Model T80 Load Bank
Turbine Operation	VII-4	

Prior to evaluating the performance of the rotor-bearing-alternator simulator, the data concerning bearing film thicknesses, rotor position and dynamic motion was corrected by the appropriate calibration factor for each individual channel of instrumentation.

TABLE VII-6 SEQUENCE OF TESTING SHOWING VALUES OF PRIMARY VARIABLES OBTAINED DURING TESTS

Simulator Test Configuration	Date Tested	Rotor Orientation	Rotor Balance	Magnetic Concentricity	Journal Bearing Adjustment No	Design Bearing Diametral Clearance (Mils)	Average Journal Bearing Clearance During Test (Mils)		Sequence in Which Configurations Were Tested
							#1 Bearing	#2 Bearing	
A	1/10/67	V	B	C	1	≤ 1.75	2.17	2.36	1
A	1/26/67	V	B	C	5	≥ 2.28	2.86	2.83	12
B	1/25/67	V	UB	C	5	≤ 1.75	1.85	1.68	10
B	1/26/67	V	UB	C	5	≥ 2.28	2.90	2.84	11
C	1/24/67	H	UB	C	4	≤ 1.75	2.05	1.95	8
C	1/25/67	H	UB	C	4	≥ 2.28	2.71	2.68	9
D	1/16/67	V	B	EC	2	≤ 1.75	1.78	1.96	3
D	1/18/67	V	B	EC	2	≥ 2.28	2.67	2.80	6
E	1/13/67	V	UB	EC	2	≤ 1.75	1.89	1.89	2
E	1/18/67	V	UB	EC	2	≥ 2.28	2.54	2.81	5
F	1/17/67	H	UB	EC	2	≤ 1.75	2.01	1.81	4
F	1/23/67	H	UB	EC	3	≥ 2.28	2.43	2.57	7

V - Rotor Vertical, H-Rotor Horizontal, B-Rotor with residual unbalance

UB - Rotor with added unbalance, C-rotor concentric,

EC-Rotor eccentric

TABLE VII-7 DETAILS OF DATA ACQUIRED DURING ROTOR-BEARING
ALTERNATOR-SIMULATOR TEST PROGRAM
#1 Journal Bearing (Turbine End)

Sensor Location	Measurement	Sensor Designation	Form of Data Acquisition
Upper Pad-to-Shaft	Film Thickness	PF-1	Tabulation
"	"	PF-2	"
Lower Pad-to-Shaft	"	PF-3	Tabulation & Magnetic Tape
"	"	PF-4	Tabulation
Ground Shaft (H)	Dynamic Motion of Journal	PS-7	Tabulation & Magnetic Tape
" " (V)	"	PS-8	" " " "
One Upper Pad (See Fig. II-26).	Turbine end Temperature	TC-3	Temp. recorder Channel 1B
	Leading edge temperature	TC-4	" " " 3B
	Trailing edge temperature	TC-5	" " " 4B
	Alternator end temperature	TC-6	" " " 7B
One Lower Pad (See Fig. II-26).	Turbine end temperature	TC-7	" " " 2B
	Trailing edge temperature	TC-8	" " " 5B
	Leading edge temperature	TC-9	" " " 6B
	Alternator end temperature	TC-10	" " " 8B
Bore of Bearing Support In Plane of Pivots	Bearing Support Temperature	TC-40	" " " 10B
	" " "	TC-41	" " " 11B
	" " "	TC-42	" " " 9B
Test Panel	Jacking Gas Supply Pressure	P-6	Tabulation
Simulator	Bearing Ambient Pressure	P-5	Tabulation

TABLE VII-7 DETAILS OF DATA ACQUIRED DURING ROTOR-BEARING
ALTERNATOR-SIMULATOR TEST PROGRAM (Cont.)
#2 Journal Bearing (Thrust End)

Location	Measurement	Sensor Designation	Form of Data Acquisition
Upper Pad-To-Shaft	Film Thickness	PF-21	Tabulation
" " " "	" "	PF-22	"
Lower Pad-to-Shaft	" "	PF-23	Tabulation & Magnetic Tape
" " " "	" "	PF-24	Tabulation
Ground-to-Shaft (H)	Dynamic motion of journal	PS-27	Tabulation & Magnetic Tape
Ground-to-Shaft (V)	" " " "	PS-28	" " "
One Upper Pad	Alternator end temperature	TC-20	Temp. Recorder Channel 12B
(See Figure II-26)	Trailing edge "	TC-21	" " " 14B
	Leading " "	TC-22	" " " 15B
	Thrust end "	TC-23	" " " 18B
One Lower Pad	Alternator end temperature	TC-24	" " " 13B
(See Figure II-26)	Trailing edge "	TC-25	" " " 16B
	Leading " "	TC-26	" " " 17B
	Thrust end "	TC-27	" " " 19B
Bore of Bearing	Bearing Support Temperature	TC-45	" " " 20B
Support in Plane of		TC-46	" " " 21B
Pivots		TC-47	" " " 22B
Test Panel	Jacking Gas Supply Pressure	P-6	Tabulation
Simulator	Bearing Ambient Pressure	P-5	"

TABLE VII-7 DETAILS OF DATA ACQUIRED DURING ROTOR-BEARING
ALTERNATOR-SIMULATOR TEST PROGRAM (Cont.)
Main and Reverse Thrust Bearings

Location	Measurement	Sensor Designation	Form of Data Acquisition
Reverse Thrust Stator- to-Thrust Runner	Film Thickness	PT-29	Tabulation
Main Thrust Stator- to-Thrust Runner	Film Thickness	PT-30	Tabulation & Magnetic Tape
	Film Thickness	PT-31	Tabulation
	" "	PT-32	"
Main Thrust Stator	Outer Ring Temperature	TC-28	Temp. recorder Channel 18H
Flexible Support	Inner Ring Temperature	TC-29	" " " 19H
Main Thrust	Thrust Stator Temperature	TC-30	" " " 20H
Stator	" " "	TC-31	" " " 21H
	" " "	TC-32	" " " 22H
Main Thrust Coolant Inlet Pipe	Coolant Inlet Temperature	T -9	" " " 16H
Main Thrust Coolant Outlet Pipe	Coolant Outer Temperature	T -10	" " " 17H
Test Panel	Coolant Flow Rate	FM-3	Tabulation
Test Panel	Main Thrust Bearing Jacking gas supply pressure	P -8	"
Simulator	Main thrust bearing Loading Cavity Pressure	P -3	"
Test Panel	Main Thrust Bearing Jacking gas flow rate	FM-2	"

TABLE VII-7 DETAILS OF DATA ACQUIRED DURING ROTOR-BEARING
 ALTERNATOR-SIMULATOR TEST PROGRAM (Cont.)
 Main and Reverse Thrust Bearings (Continued)

Location	Measurement	Sensor Designation	Form of Data Acquisition
Test Panel	Reverse Thrust Bearing Jacking Gas Supply Pressure	P-7	Tabulation
Simulator	Reverse Thrust Bearing Loading Cavity Pressure	P-4	"
Test Panel	Reverse Thrust Bearing Jacking Gas Flow Rate	FM-1	"
Simulator	Main and Reverse Thrust Bearing Ambient Pressure	P-5	"

TABLE VII-7 DETAILS OF DATA ACQUIRED DURING ROTOR-BEARING
ALTERNATOR-SIMULATOR TEST PROGRAM (Cont.)

Alternator

Location	Measurement	Sensor Designation	Form of Data Acquisition
Frame I.D. Drive End	Temperature	1	Temp. Recorder Channel 1H
Stator Core " "	"	2	" " " 2H
Stator Tooth " "	"	3	" " " 3H
End Turn " "	"	4	" " " 4H
" " " "	"	5	" " " 5H
Frame I.D. Anti Drive end	"	6	" " " 6H
Bus " "	"	7	" " " 7H
" " "	"	8	" " " 8H
Stator Tooth Anti Drive End	"	9	" " " 9H
End Turn " "	"	10	" " " 10H
Coolant Inlet	"	11	" " " 11H
Coolant Outlet	"	12	" " " 12H
Load Bank	Output Volts (L-N)	VM1	Tabulation
" "	" " "	VM2	"
" "	" " "	VM3	"
" "	Output Amps "	AM1	"
" "	" " "	AM2	"
" "	" " "	AM3	"
" "	Output Watts "	WM1	"
" "	" " "	WM2	"

TABLE VII-7 DETAILS OF DATA ACQUIRED DURING ROTOR-BEARING
ALTERNATOR-SIMULATOR TEST PROGRAM (Cont.)
Alternator (Continued)

Location	Measurement	Sensor Designation	Form of Data Acquisition
Load Bank	Output Watts (L-N)	WM3	Tabulation
" "	DC Field Current	-	"
" "	DC Short Circuit Field Current	-	"
" "	Output Amps Short Circuit Current	-	"
Test Panel	Air Supply Manifold Pressure	P1	Tabulation
Simulator	Turbine Supply Pressure at Nozzle Inlet	P2	"
Simulator	Turbine Inlet Temperature	T2	Temp. Recorder Channel 13H
"	Turbine Outlet Temperature	T11	" " " 23B
"	Rotor Speed	-	Digital Counter & Magnetic Tape

Test Evaluation of Rotor Response and Stability

The primary purpose of the experimental program was to demonstrate the suitability of the rotor-bearing system under operating conditions involving the electromagnetic forces attendant on the generation of electrical power. An extensive program of testing was completed involving a wide range of operating conditions. Detailed information concerning the test conditions are contained in Tables VII-2, VII-3, VII-4 and VII-5.

The performance of the rotor-bearing system was entirely satisfactory throughout the test program. Dynamic response of the rotor and the bearing pads was in all cases but one, synchronous and of small amplitude.

The second purpose of the test program was to obtain experimental verification of the accuracy of the analytical procedures (developed in Section V of this report) for predicting rotor response and stability. Unfortunately, the accuracy of these procedures could not be established from the results of the test program. While the test results agree qualitatively with predicted results (i.e., the rotor was stable and the forced-vibration amplitudes were small), quantitative verification was not possible because (1) rotor instability could not be experimentally induced (hence, boundaries of the unstable region could not be mapped), and (2) rotor response amplitudes due to electromagnetic forces were below the noise level of the simulator instrumentation and hence not measureable.

The dynamic response of the rotor bearing system to electromagnetic forces was calculated for two sets of conditions. The first of these deals with the turbo-alternator in a vertical position and operating under the following conditions:

Speed	12,000 RPM
Bearing environment	Argon
Bearing ambient pressures	Bearing #1 - 10.5 PSIA Bearing #2 - 12.5 PSIA
Bearing temperatures	300 F
Viscosity	4.2×10^{-9} lb. sec./in. ²
Bearing diametral clearance at zero load (both bearings)	0.00175 inches

The results of the above calculations are given in Table V-2.

The second set of calculations relate to the simulator in both the vertical and horizontal positions and operating under the following conditions:

Speed	12,000 RPM
Bearing environment	Air
Bearing ambient pressure	Both bearings 10.5 PSIA
Bearing temperatures	300 F
Viscosity	3.6×10^{-9} lb. sec./in. ²
Design value of bearing diametral clearance for both horizontal and vertical operation	1.75 Mils
Increased value of bearing diametral clearance for both horizontal and vertical operation	2.28 Mils

The results of the dynamic response calculations for the conditions involved during operation of the simulator are given in Table VII-8.

It should be noted that the values of amplitude given in Tables V-2 and VII-8 are peak values arrived at by summation of the individual amplitudes at the various harmonics involved. For example, in the electrical cases numbered 1, 2, 3 and 6, the electromagnetic force components are all at the fundamental frequency which is twice synchronous. From Table V-2 for the condition entitled, "Rotor Eccentric by 0.002 Inch in Both Pole Planes, No Mechanical Unbalance", the vibration observed for these cases would only occur at the fundamental frequency of 400 CPS, there being a complete absence of vibration at synchronous frequency due to the absence of mechanical unbalance. The remaining electrical cases, 4, 5 and 7, however, all contain force components with frequencies higher than the fundamental. The observed vibration in these cases would consist of the fundamental frequency with the higher harmonics being superimposed. When mechanical unbalance is introduced without electromagnetic forces, the vibration observed would be synchronous.

In practice, other frequencies are also present; blade passing frequencies in the turbine, stator slotting and amortisseur slots in the alternator, and residual

unbalance in the rotor. Identification of specific frequencies of vibration above synchronous at the small amplitudes involved is further complicated by the out-of-roundness of the journals, and the electrical noise level present in various channels of instrumentation used to monitor the dynamic motion of the rotor and bearing pads.

The experimental data given in Table VII-9 was obtained during the test which was conducted under conditions relating to those for which the largest amplitudes of vibration were predicted by calculation, i.e., horizontal rotor eccentric by 0.002 inches in both pole planes with 0.005 ounce-inches of mechanical unbalance in the plane of the turbine (see Table VII-8). From Table VII-9 it is seen that during test the value of the parameters controlling bearing performance were in excess of the values used for calculation purposes. The diametral bearing clearance was generally larger and the viscosity lower (the latter being due to reduced bearing temperature). This results in reduced bearing stiffness, friction loss and also, (by extrapolation of the data in Table VII-8) a reduction in the amplitudes of rotor vibration. The pad pitch amplitudes would, however, be expected to increase. The rotor eccentricity in the pole planes was also in excess of the 0.002 inches used for calculation purposes. This would result in an increase in the d-c component, F_0 , of the electromagnetic forces and an increase in the amplitude of rotor and pad vibration. No attempt was made during the test of this configuration to achieve the precise parameters used in response calculations. This course of action was based on consideration of the following factors:

- 1) The demonstration of satisfactory performance of the rotor-bearing-alternator system within wide limits of bearing clearance and rotor eccentricity was considered to be of primary importance.
- 2) Data accumulated during preceding tests indicated that identification of the fundamental frequency and the higher harmonics resulting from alternator electromagnetic forces would not be possible.

TABLE VII-8
CALCULATED DYNAMIC RESPONSE OF SIMULATOR ROTOR-BEARING SYSTEM
TO ELECTROMAGNETIC ALTERNATOR FORCES

Condition	Case	Journal Brg. Diametral Clearance (Mils)	Amplitude of Rotor in Journal Bearings (Microinch)		Pitch Amplitude of Journal Bearing Shoes (Microinch/Inch)			
			Thru.Brg.End	Turbine End	Thrust Bearing End		Turbine End	
					Top Shoe	Bottom Shoe	Top Shoe	Bottom Shoe
Horizontal	2	2.27	18.89	53.0	14.15	27.92	51.43	76.41
Rotor Eccentric	2	1.75	19.59	55.75	20.33	27.8	42.75	80.16
by 0.002 In.	3	2.27	17.18	50.45	14.17	25.07	64.73	71.98
Both Pole	3	1.75	17.84	63.16	19.8	24.8	41.99	75.5
Planes;0.005	6	2.27	13.45	43.7	16.45	16.94	66.17	59.47
Oz. In., Mech- anical Unbal- ance in Turbine	6	1.75	14.00	47.1	20.17	16.19	42.4	62.5
Vertical Rotor	2	2.27	3.96	24.87	2.71	5.75	24.84	27.82
Eccentric by	3	2.27	3.74	24.5	2.94	5.3	24.83	27.19
0.002 In Both	6	2.27	3.35	23.73	3.75	3.8	25.36	25.48
Pole Planes; 0.005 Oz.In., Mechanical Unbalance in Turbine								

Note: Response amplitude values in the above table are single amplitude values measured from the static eccentricity position of the rotor resulting from the d-c component, F_o , of the electromagnetic forces, and in the case of horizontal operation, rotor weight.

Code: Case 2: 15 KVA, 0.8 power factor lagging, balanced load, saturated
Case 3: 11.25 KVA, 0.8 power factor lagging, balanced load
Case 6: No load condition, operating at 120V L-N balanced 3 ϕ , no armature current

TABLE VII-9
VALUES OF BEARING CLEARANCE, TEMPERATURE AND ROTOR ECCENTRICITY OBTAINED DURING TEST WITH ROTOR
HORIZONTAL AND MECHANICALLY UNBALANCED IN THE PLANE OF THE TURBINE WHEEL. (CONFIGURATION F)

HORIZONTAL AND MECHANICALLY UNBALANCED IN THE													
THRUST BEARING END OF ROTOR							TURBINE END OF ROTOR						
Case No	Test Data Point No.	Average Diametral Clearance Of Bearing No. 2 (Mils)		Eccentricity Of Adjacent Pole Face (Mils)		Average Temperature of 2 of Bearing No. 2 Pads (Degrees F)		Average Diametral Clearance Of Bearing No. 1 (Mils)		Eccentricity Of Adjacent Pole Face (Mils)		Average Temperature of 2 of Bearing No. 1 Pads (Degrees F)	
2	F18	2.62	(2.27)	2.62	(2.0)	123	(300)	2.34	(2.27)	3.09	(2.0)	104	(300)
2	F31	2.79	(2.27)	2.70	(2.0)	121	(300)	2.34	(2.27)	3.15	(2.0)	104	(300)
2	F35	2.65	(2.27)	2.57	(2.0)	123	(300)	2.06	(2.27)	2.98	(2.0)	115	(300)
2	F6	2.00	(1.75)	3.44	(2.0)	126	(300)	1.94	(1.75)	3.94	(2.0)	100	(300)
2	F33	1.79	(1.75)	3.42	(2.0)	122	(300)	1.85	(1.75)	3.98	(2.0)	116	(300)
3	F17	2.62	(2.27)	2.39	(2.0)	119	(300)	2.28	(2.27)	2.71	(2.0)	99	(300)
3	F5	2.15	(1.75)	3.48	(2.0)	120	(300)	2.13	(1.75)	3.99	(2.0)	88	(300)
6	F14	2.65	(2.27)	2.43	(2.0)	113	(300)	2.49	(2.27)	2.73	(2.0)	98	(300)
6	F2	1.76	(1.75)	3.29	(2.0)	107	(300)	1.88	(1.75)	3.75	(2.0)	92	(300)

Case numbers refer to the electrical cases given in Tables V-2 and VII-8.

Numbers in parenthesis are the values used in dynamic response calculation, the results of which are given in Table VII-8.

Oscilloscope photographs of the rotor-bearing performance were taken during the test related to the conditions used in calculating the dynamic response shown for the horizontal rotor, electrical Case 2 in Table VII-8. The actual values of bearing clearance, temperature and rotor eccentricity which were present during this test are shown in Table VII-9, identified by Test Point Number Fl8.

Figure VII-5 shows the performance of the turbine end bearing and journal, while Figure VII-7 shows the performance of the thrust end bearing and journal. Both figures being of the 12 KW power level condition. For purposes of comparison Figures VII-6 and VII-8 show the performance of the turbine and thrust end journal bearings respectively when operating under similar conditions, but without alternator excitation and, hence, no electrical load. Two points should be considered when examining these figures:

- 1) The dimensions given on the photographs of pad film thickness are nominal values only. The sensitivity values quoted on the figures should be used to determine accurate values of dynamic motion.
- 2) The inclined square on the photographs of journal motion represents the set-up clearance of the bearing at room temperature and zero speed. The position of the shaft orbit signal at the conditions of speed and temperature involved cannot be directly related to this clearance profile.

Figures VII-5 (A) and VII-6 (A) show the turbine bearing film thickness between one loaded pad, and the opposing unloaded pad, and the journal for 12 KW and zero excitation conditions of operation respectively. Figures VII-5 (C) and VII-6 (C) show the turbine bearing film thickness for the other loaded pad, and the opposing unloaded pad, for the same electrical conditions of operation. Figures VII-5(B) and VII-6(B) show both the orbit and the dynamic content of the turbine bearing journal motion for 12 KW and zero excitation conditions of operation.

It should be noted that in these figures the frequency is basically synchronous. There is no evidence in these traces of higher harmonics due to electromagnetic forces. The amplitude of synchronous pad vibration in the turbine end bearing is seen to be greater for the zero excitation condition (Figure VII-6) than for

the 12 KW condition (Figure VII-5). This is due to the increased film thickness involved during the zero excitation test point (F15) where the turbine end bearing diametral clearance was increased to a maximum (by increasing the bearing support temperature) to determine the point at which pad flutter would occur. Figures VII-7 and VII-8 show the performance of the thrust end journal bearing during the same two tests. In Figure VII-8 (B) (zero excitation condition) the thrust-end journal bearing diametral clearance was not adjusted during the test to determine the onset of flutter, and it can be seen that the journal amplitudes are essentially the same as those observed at the 12 KW point shown in Figure VII-7 (B). In Figures VII-7 (A and C) and VII-8 (A and C), a slight increase in the pad amplitude of vibration can be discerned at the 12 KW point. The extent of this increase is approximately 25 microinches peak-to-peak.

The experimental data contained in Figures VII-5 to VII-8 inclusive and also Table VII-9 relate to the calculated data contained in Table VII-8. This data is based on operation at an ambient pressure in the bearing cavities of 10.5 PSIA and at conditions involving the increased value of bearing diametral clearance.

Further oscilloscope photographs were taken of the bearing performance during the tests of Configuration F which are retained on file and not presented in this report. The data points at which these photographs were taken are as follows:

<u>Oscilloscope Photograph Number</u>	<u>Configuration F Test Data Point Number</u>	<u>Journal Bearing Ambient Pressure PSIA</u>
7 to 12 inc.	14	10.5
13 to 18 inc.	15	10.5
21 to 26 inc.	13	10.5
27 to 32 inc.	16	10.5
33 to 38 inc.	21	7.2
39 to 44 inc.	22	7.2
45 to 50 inc.	23	7.2
51 to 56 inc.	24	7.2
57 to 62 inc.	27	10.5
63 to 68 inc.	28	7.2
69 to 74 inc.	18	10.5
75 to 81 inc.	19	7.2
82	31	10.5
83	35	10.5

Oscilloscope photographs were also taken of bearing performance during the testing of Configuration A. (Vertical operation, residual mechanical unbalance and rotor concentric with stator). These photographs, which are also retained on file and not presented here, are identified as follows.

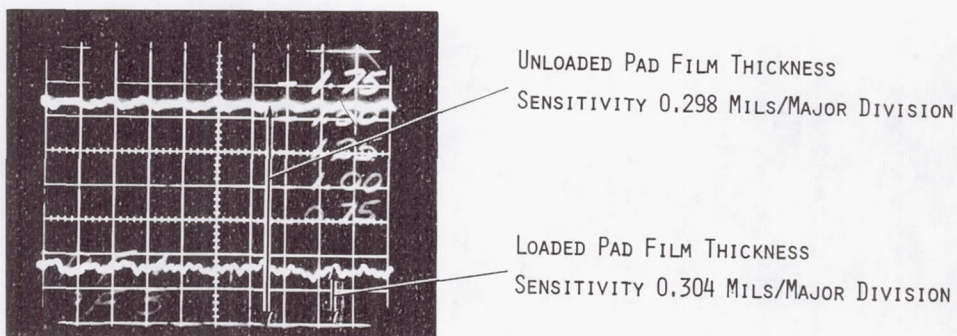
<u>Oscilloscope Photograph Number</u>	<u>Configuration A Test Data Point Number</u>	<u>Journal Bearing Ambient Pressure PSIA</u>
84 to 89 inclusive	13	10.5
90 to 95 inclusive	14	10.5
96 to 101 inclusive	15	10.5
102 to 107 inclusive	16	10.5
108 to 113 inclusive	18	10.5
114 to 119 inclusive	19	7.2
120 to 125 inclusive	21	7.2
126 to 131 inclusive	22	7.2
132 to 137 inclusive	23	7.2
138 to 143 inclusive	24	7.2
144 to 149 inclusive	28	7.2
150 to 156 inclusive	27	10.5
157	31	10.5
158	32	7.2

All of the above referenced oscilloscope photographs (Configurations A and F) are for conditions involving the increased value of bearing diametral clearances (2.28 mils).

Examination of the photographs of Configuration A bearing performance showed that the dynamic performance was almost identical to that observed during Configuration F testing, i.e., the vibration was synchronous with no evidence of the higher harmonics. The bearing pad film thicknesses for loaded and unloaded pads were approximately equal during the testing of Configuration A, (The rotor being concentric, vertical and, therefore, the pads equally loaded). A low frequency vibration of approximately 50 CPS was detected in the dynamic motion of both the journal and the pads of the turbine end bearing. This vibration which was of small amplitude, 200-300 microinches peak-to-peak, ceased when the vacuum pump (used to reduce bearing ambient pressure) was stopped. This vibration was not noted in the performance of the thrust end journal bearing. Vibration of the same frequency and amplitude was noted in the thrust bearing performance

under the same conditions of operation. This vibration also ceased on stopping the vacuum pump.

The oscilloscope photographs so far presented, or referred to, were taken during the course of the test program. Oscilloscope photographs of the bearing performance during short circuit conditions were not possible at this time due to the short duration of these conditions. During the course of the test, the data from certain channels of instrumentation were recorded on magnetic tape for each of the 216 test points, the duration of these recordings being in the order of 30 seconds for each data point. Playback of these tape recordings at the conclusions of the test program permitted the taking of further oscilloscope photographs of bearing performance at conditions of particular interest.

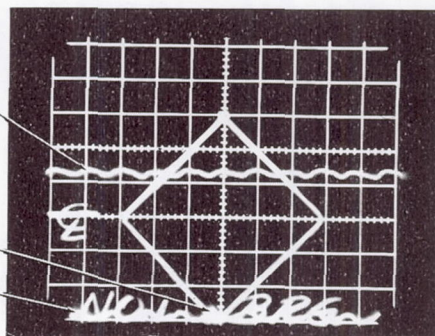


(A)

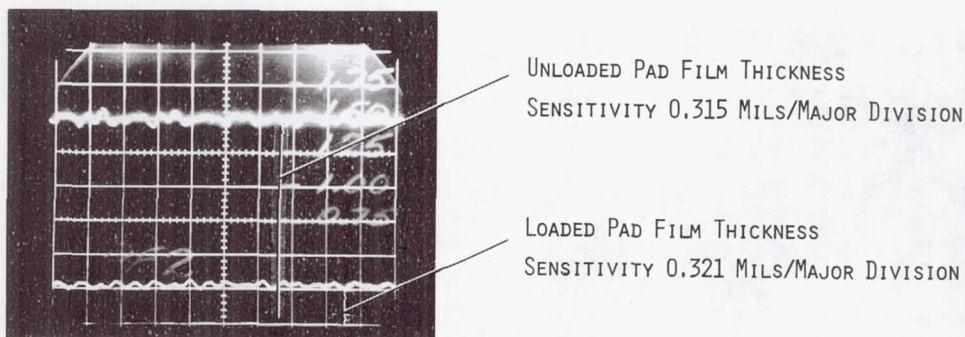
JOURNAL MOTION, HORIZONTAL PROBE
SENSITIVITY 0.665 MILS/MAJOR DIVISION

JOURNAL ORBIT

JOURNAL MOTION, VERTICAL PROBE
SENSITIVITY 0.640 MILS/MAJOR DIVISION



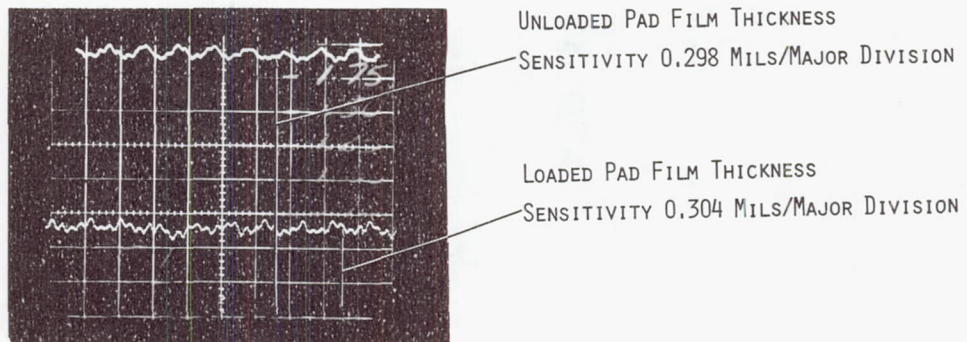
(B)



(C)

TIME BASE - ALL TRACES 5×10^{-3} SECS/MAJOR DIVISION

Fig. VII-5 Oscilloscope Photographs of the Turbine End Journal Bearing Performance at 12,000 RPM, 10.5 PSIA Ambient Pressure (Air) and a 12 KW, 0.8 PF Electrical Load (Rotor Horizontal and Eccentric-Test Point No. F 18)

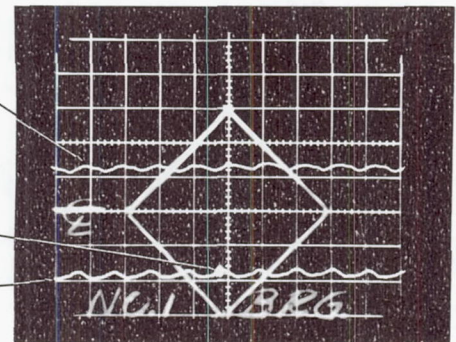


(A)

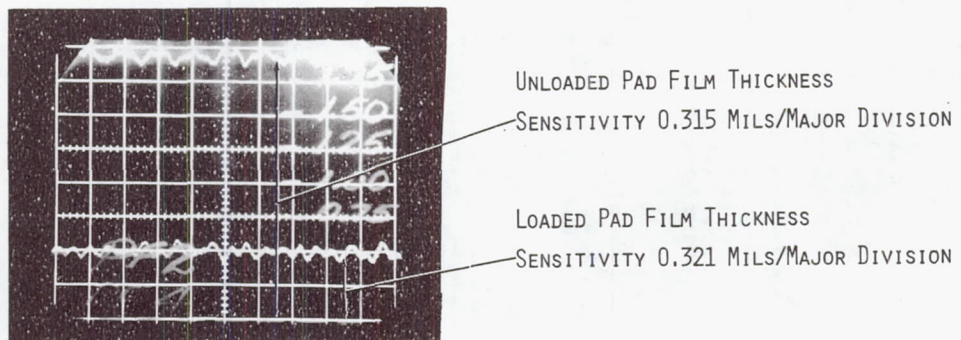
JOURNAL MOTION, HORIZONTAL PROBE
SENSITIVITY 0.665 MILS/MAJOR DIVISION

JOURNAL ORBIT

JOURNAL MOTION, VERTICAL PROBE
SENSITIVITY 0.640 MILS/MAJOR DIVISION



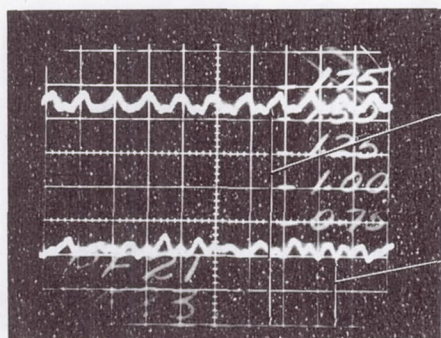
(B)



(C)

TIME BASE - ALL TRACES 5×10^{-3} SECS/MAJOR DIVISION

Fig. VII-6 Oscilloscope Photographs of the Turbine End Journal Bearing Performance at 12,000 RPM, 10.5 PSIA Ambient Pressure (Air) and Zero Alternator Excitation. (Rotor Horizontal and Eccentric - Test Point No. F 15)



UNLOADED PAD FILM THICKNESS
SENSITIVITY 0.295 MILS/MAJOR DIVISION

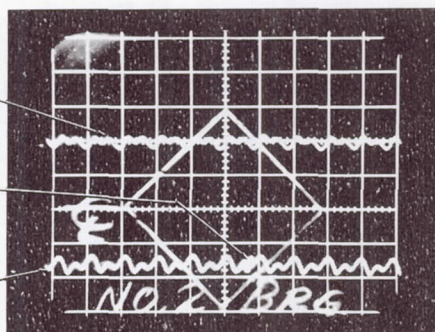
LOADED PAD FILM THICKNESS
SENSITIVITY 0.300 MILS/MAJOR DIVISION

(A)

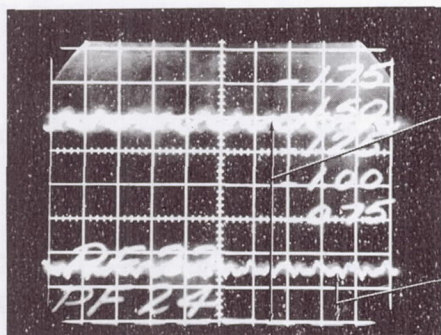
JOURNAL MOTION, HORIZONTAL PROBE
SENSITIVITY 0.45 MILS/MAJOR DIVISION

JOURNAL ORBIT

JOURNAL MOTION, VERTICAL PROBE
SENSITIVITY 0.47 MILS/MAJOR DIVISION



(B)



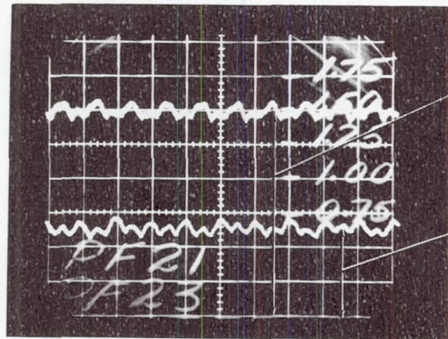
UNLOADED PAD FILM THICKNESS
SENSITIVITY 0.287 MILS/MAJOR DIVISION

LOADED PAD FILM THICKNESS
SENSITIVITY 0.31 MILS/MAJOR DIVISION

(C)

TIME BASE - ALL TRACES 5×10^{-3} SECS/MAJOR DIVISION

Fig. VII-7 Oscilloscope Photographs of the Thrust End Journal Bearing Performance at 12,000 RPM 10.5 PSIA Ambient Pressure (Air) and a 12 KW, 0.8 PF Electrical Load. (Rotor Horizontal and Eccentric - Test Point No. F 18)



UNLOADED PAD FILM THICKNESS

SENSITIVITY 0.295 MILS/MAJOR DIVISION

LOADED PAD FILM THICKNESS

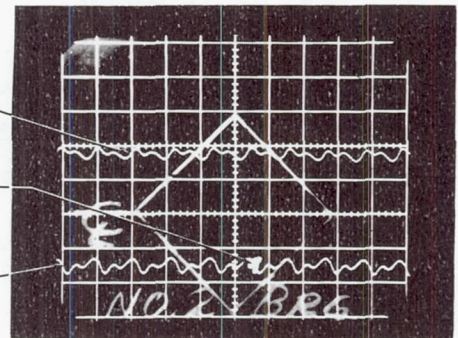
SENSITIVITY 0.300 MILS/MAJOR DIVISION

(A)

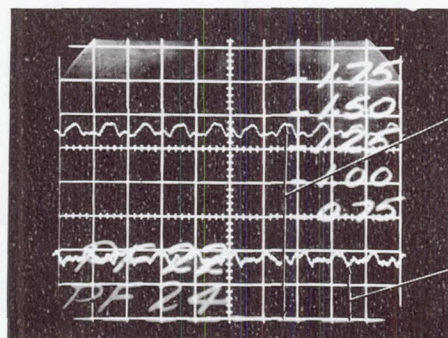
JOURNAL MOTION, HORIZONTAL PROBE
SENSITIVITY 0.45 MILS/MAJOR DIVISION

JOURNAL ORBIT

JOURNAL MOTION, VERTICAL PROBE
SENSITIVITY 0.47 MILS/MAJOR DIVISION



(B)



UNLOADED PAD FILM THICKNESS

SENSITIVITY 0.287 MILS/MAJOR DIVISION

LOADED PAD FILM THICKNESS

SENSITIVITY 0.31 MILS/MAJOR DIVISION

(C)

TIME BASE - ALL TRACES 5×10^{-3} SECS/MAJOR DIVISION

Fig. VII-8 Oscilloscope Photographs of the Thrust End Journal Bearing Performance at 12,000 RPM, 10.5 PSIA Ambient Pressure (Air) and Zero Alternator Excitation. (Rotor Horizontal and Eccentric - Test Point No. F 15)

Oscilloscope photographs of the turbine bearing performance, taken from a playback of the magnetic tape recording made during test of the simulator, with the rotor vertical, eccentric, and with residual mechanical unbalance, (Configuration D) are shown in Figures VII-9 and VII-10. Figure VII-9 shows the effect on the journal and on the pivoted-pad film thickness, of applying alternator field excitation at no-load conditions of operation. Figure VII-10 shows the effect of imposing both single-phase and 3-phase short circuits on the alternator when operating at a 12 KW balanced-load condition.

The upper traces on the photographs in Figures VII-9 and VII-10 indicate that journal vibration is largely synchronous and that the amplitude is virtually unaffected by the various conditions of alternator electrical load and short circuit. The cause of this synchronous vibration, the peak-to-peak amplitude of which is approximately 0.19 mils, is attributed primarily to residual unbalance, and, to a lesser extent, to out-of-roundness of the journal. There is no evidence in these traces of any two-per-rev or higher harmonic response due to electromagnetic forces. It should be noted, however, that the predicted amplitude of journal vibration at the higher harmonics was, as shown in Table V-2, in the order of a few microinches with the rotor vertical and mechanically balanced. Under such small amplitude conditions, the associated instrumentation signals would be masked by the residual electrical noise level which was present on all channels of instrumentation.

The lower traces on the photographs in Figures VII-9 and VII-10 show the film thickness of one of the lower bearing pads and indicate an increase in dynamic film variation when an electrical load is applied. The largest peak-to-peak variation in the pad film thickness, approximately 0.26 mils, occurred during the single-phase short, as shown on Figure VII-10 (B). As noted above, the amplitude of journal vibration was essentially unaffected by the electrical conditions of alternator operation. Consequently, the apparent increase in dynamic variation of film thickness must have been due to vibration of the pad-flexure assembly relative to the journal.

The high-frequency content of the lower (film thickness) traces seen in Figures VII-9 and VII-10 is attributed to electrical noise in the particular channel of

instrumentation. However, during single-phase shorting of the alternator (while operating under conditions of 12 KW load), a clear indication of two-per-rev variation in film thickness did emerge from the background noise level as shown in Figure VII-10 (B).

The low frequency pad vibration referred to in previous paragraphs can be seen in Figure VII-9 (A) and (C).

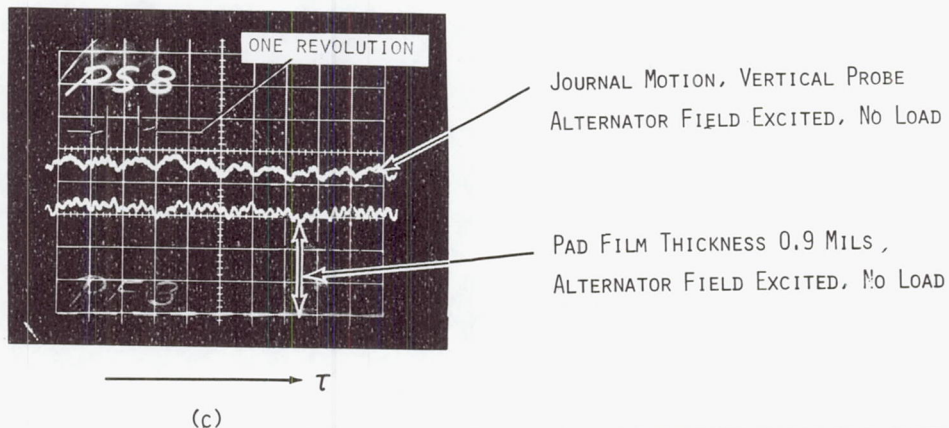
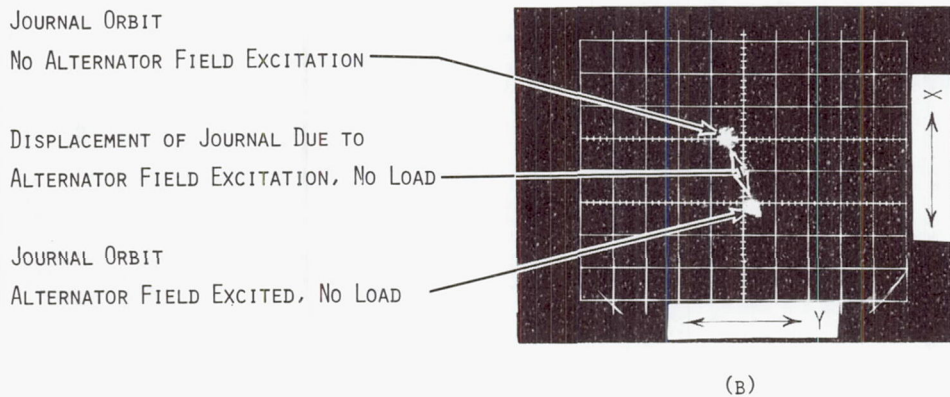
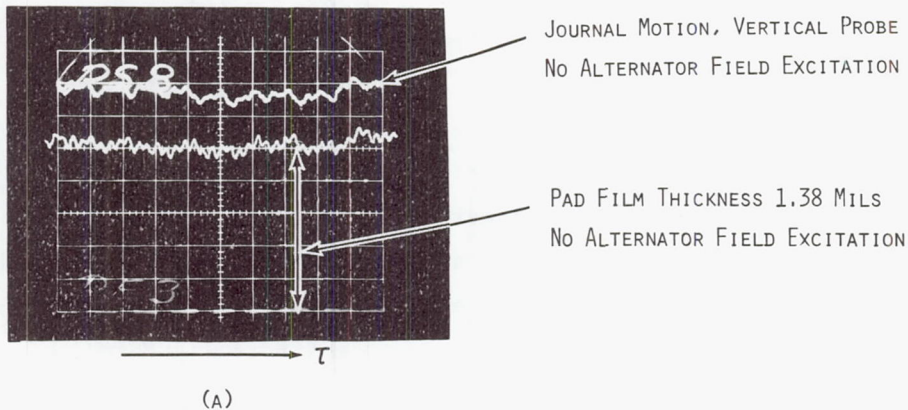
Oscilloscope photographs of the turbine bearing performance, taken from a playback of the magnetic tape recording made during test of the simulator with the rotor horizontal, eccentric, and mechanically unbalanced by 0.005 ounce-inches in the plane of the turbine wheel (Configuration F), are shown in Figures VII-11, VII-12 and VII-13. Figure VII-11 shows the effect on bearing performance of applying the alternator field excitation at no-load conditions of operation. Figure VII-12 shows the effect of 12 KW balanced load and single-phase short circuit conditions. The effect of a 3-phase short-circuit condition and a resulting labyrinth rub, due to excessive rotor eccentricity, is shown in Figure VII-11 (A). The peak-to-peak amplitude increases to 0.3 mils under the single-phase short condition shown in Figure VII-12C. Again, it is not possible to detect, with any certainty, the presence of the predicted higher harmonics

The lower traces on Figures VII-11 and VII-12, showing pad film thickness, have similar characteristics to those described for vertical operation with residual unbalance. The peak-to-peak amplitudes of vibration of both the journal and the pad film thickness, however, are seen to be somewhat larger in the case of horizontal and unbalanced operation. This trend was predicted by analysis as is shown in Table VII-8.

During the 3-phase short circuit tests on the horizontal rotor, the turbine wheel rubbed on a labyrinth when the short was initiated. This incident is clearly seen from the bearing orbit photographs on Figure VII-13 (B). The right hand orbit was photographed immediately prior to the short being applied. On applying the short, the rotor moved vertically downward which caused contact with the labyrinth. The rotor then bounced vertically upward. The situation returned

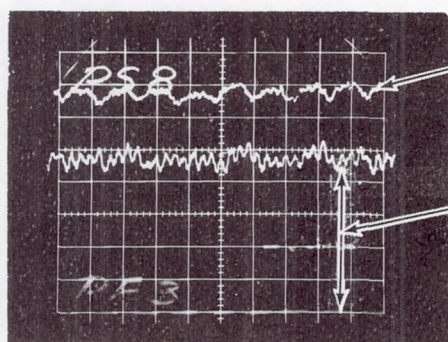
to normal on removal of the short condition. Figure VII-13 (A) shows time-base traces from the X and Y journal probes during the labyrinth rub, while Figure VII-13 (C) shows simultaneous traces from the X journal probe and the loaded-pad film thickness probe.

The rub, which occurred on the large diameter turbine wheel labyrinth seal, was the result of operating at alternator eccentricities in excess of 4 mils at the alternator pole adjacent to the turbine bearing, and 3.5 mils at the pole plane adjacent to the thrust-end bearing. The eccentricity at the plane of the turbine was calculated to be in excess of 6 mils. During assembly of the simulator the clearance at this plane was checked, with shim stock, to be 7 mils. From these figures it can be seen that the small increase in eccentricity which resulted from initiating the 3-phase short circuit was sufficient to cause the rub. This short-circuit test was repeated several times and on each occasion a labyrinth rub occurred. However, no bearing rubs were detected and, as can be seen from the lower trace on Figure VII-13C, adequate film thickness between the journal and the pad was retained throughout the incident.



SENSITIVITY - JOURNAL TRACES AND ORBITS 0.38×10^{-3} INCHES/MAJOR DIVISION
 SENSITIVITY - PAD TRACES 0.36×10^{-3} INCHES/MAJOR DIVISION
 TIME BASE - ALL TRACES 5×10^{-3} SECS/MAJOR DIVISION

Fig. VII-9 Oscilloscope Photographs of the Turbine End Journal Bearing Performance at 12,000 RPM and 7.2 PSIA Ambient Pressure (Air). (Rotor Vertical and Eccentric by 0.002-0.003 inches-Test Point No's. D22 and D23)



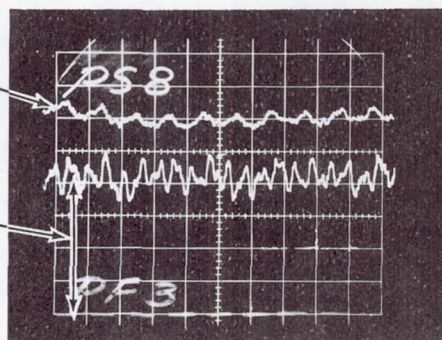
JOURNAL MOTION, VERTICAL PROBE
12 KW - 3 PHASE - 0.8 PF

PAD FILM THICKNESS 0.6 MILS
12 KW - 3 PHASE - 0.8 PF

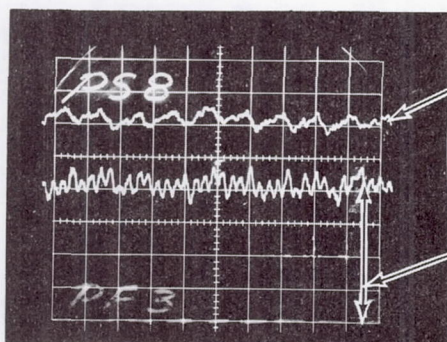
(A)

JOURNAL MOTION, VERTICAL PROBE
DURING A SINGLE PHASE SHORT CIRCUIT

PAD FILM THICKNESS 0.56 MILS
DURING A SINGLE PHASE SHORT CIRCUIT



(B)



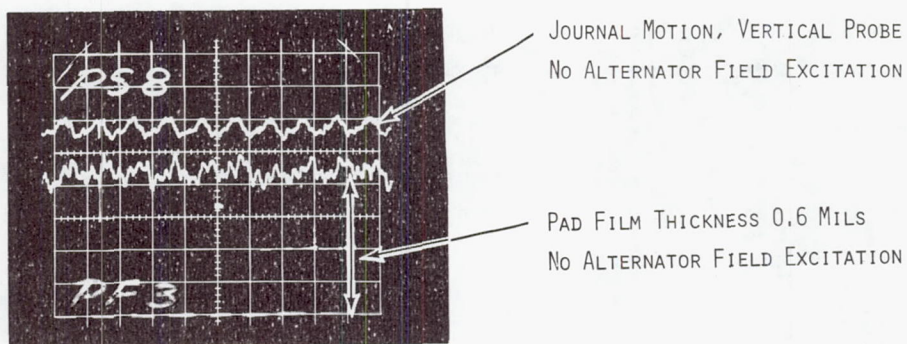
JOURNAL MOTION, VERTICAL PROBE
DURING A THREE PHASE SHORT CIRCUIT

PAD FILM THICKNESS 0.52 MILS
DURING A THREE PHASE SHORT CIRCUIT

(C)

SENSITIVITY - JOURNAL TRACES AND ORBITS 0.38×10^{-3} INCHES/MAJOR DIVISION
SENSITIVITY - PAD TRACES 0.180×10^{-3} INCHES/MAJOR DIVISION
TIME BASE - ALL TRACES 5×10^{-3} SECS/MAJOR DIVISION

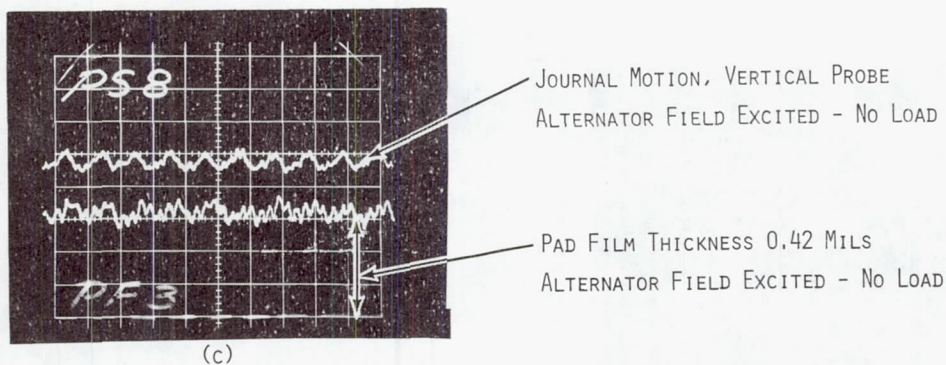
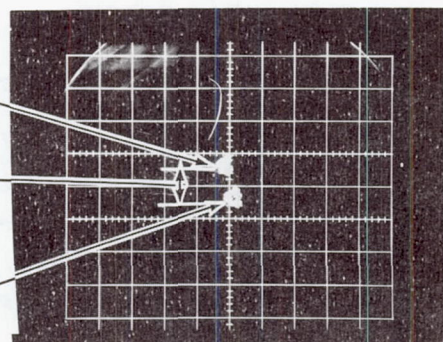
Fig. VII-10 Oscilloscope Photographs of the Turbine End Journal Bearing Performance at 12,000 RPM and 72 PSIA Ambient Pressure (Air) (Rotor Vertical and Eccentric by 0.002 - 0.003 Inches - Test-Point No's D32 and D36)



JOURNAL ORBIT
NO ALTERNATOR FIELD EXCITATION

DISPLACEMENT OF JOURNAL DUE TO
ALTERNATOR FIELD EXCITATION, NO LOAD

JOURNAL ORBIT
ALTERNATOR FIELD EXCITED, NO LOAD

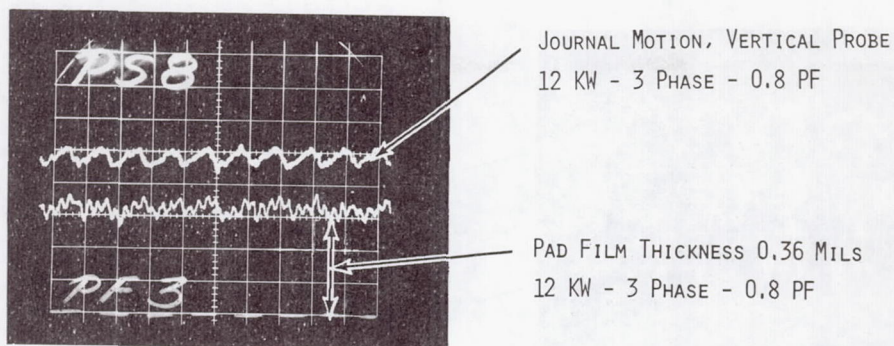


SENSITIVITY - JOURNAL TRACES AND ORBITS 0.38×10^{-3} INCHES/MAJOR DIVISION

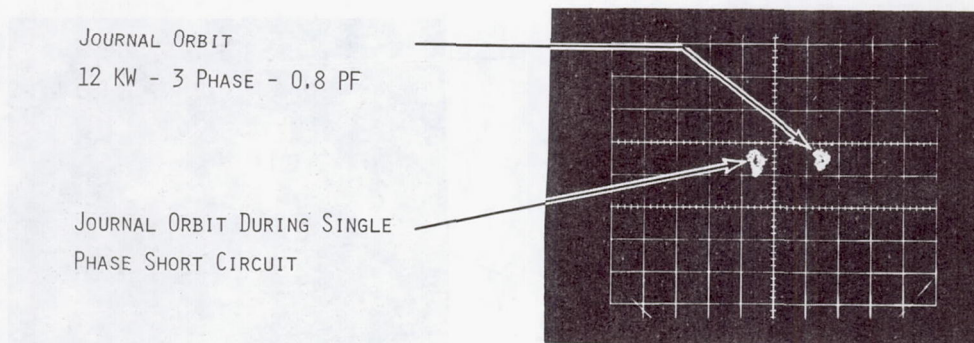
SENSITIVITY - PAD TRACES 0.180×10^{-3} INCHES/MAJOR DIVISION

TIME BASE - ALL TRACES 5×10^{-3} SECS/MAJOR DIVISION

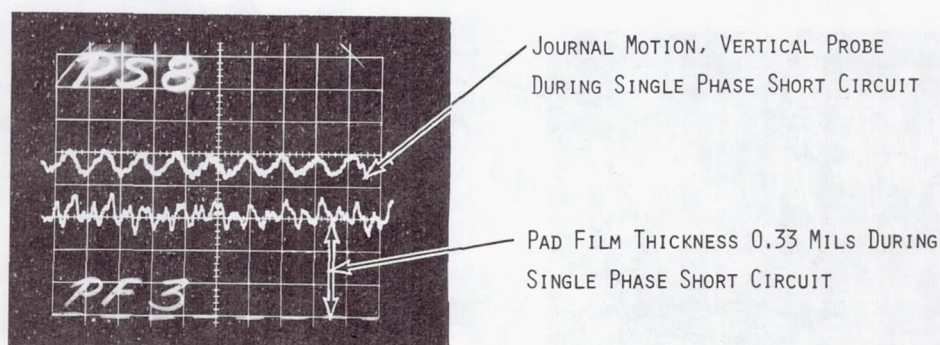
Fig. VII-11 Oscilloscope Photographs of the Turbine End Journal Bearing Performance at 12,000 RPM and 7.2 PSIA Ambient Pressure (Air) (Rotor Horizontal and Eccentric by 0.003-0.004 Inches - Test Point No's F10 and F11)



(A)



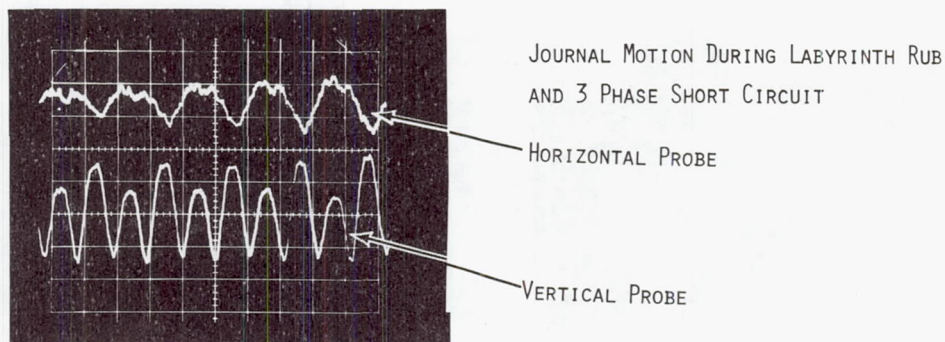
(B)



(C)

SENSITIVITY - JOURNAL TRACES AND ORBITS 0.38×10^{-3} INCHES/MAJOR DIVISION
SENSITIVITY - PAD TRACES 0.18×10^{-3} INCHES/MAJOR DIVISION
TIME BASE - ALL TRACES 5×10^{-3} SECS/MAJOR DIVISION

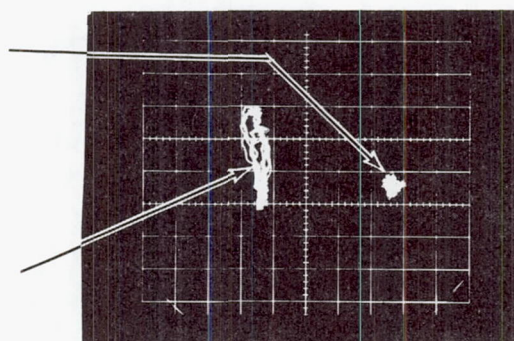
Fig. VII-12 Oscilloscope Photographs of the Turbine End Journal Bearing Performance at 12,000 RPM and 7.2 PSIA Ambient Pressure (Air) (Rotor Horizontal and Eccentric by 0.003-0.004 Inches - Test Point No. F34)



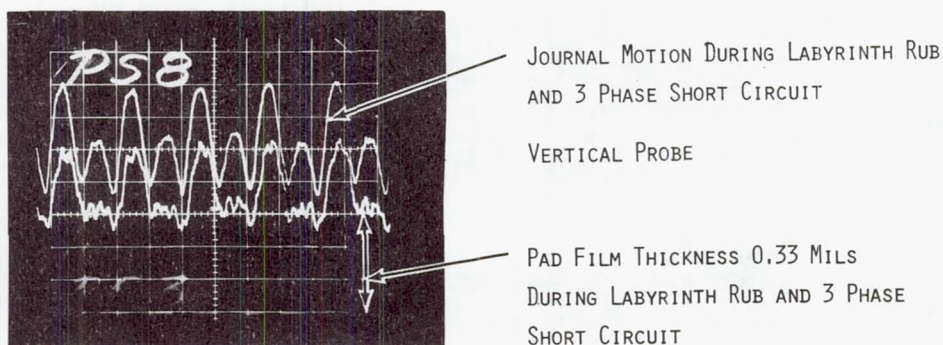
(A)

JOURNAL ORBIT BEFORE LABYRINTH RUB
12 KW - 3 PHASE - 0.8 PF

JOURNAL ORBIT DURING LABYRINTH RUB
AND 3 PHASE SHORT CIRCUIT



(B)



(C)

SENSITIVITY - JOURNAL TRACES AND ORBITS - 0.38×10^{-3} INCHES/MAJOR DIVISION
SENSITIVITY - PAD TRACES 0.18×10^{-3} INCHES/MAJOR DIVISION
TIME BASE - ALL TRACES 5×10^{-3} SECS/MAJOR DIVISION

Fig. VII-13 Oscilloscope Photographs of the Turbine End Journal Bearing Performance at 12,000 RPM and 7.2 PSIA Ambient Pressure (Air) (Rotor Horizontal and Eccentric by 0.003-0.004 Inches - Test Point No. F29)

Additional Test Program

In addition to performing the tests prescribed in the test plan, six additional tests were performed. The purpose of these tests is defined as follows:

- Test 1: Observe the effects of increasing the journal bearing clearance, and establish values of maximum diametral clearance which would permit safe operation with the simulator in a horizontal position.
- Test 2: Repeat the above tests with the simulator in a vertical position.
- Test 3: Observe the performance with the simulator inclined at 45°
- Test 4: Observe the journal orbits during coastdown of the simulator from the overspeed condition of 14,400 RPM to 5,000 RPM with and without alternator excitation to demonstrate both the standard of balance attained and the extent of any discrepancy between geometric and magnetic concentricity.
- Test 5: Determine the extent of the back leakage through the journal bearing jacking supply system with the simulator running in a vertical position.
- Test 6: Observe the performance with the simulator vertical and the rotor eccentric and misaligned, i.e., eccentricity in the pole plane adjacent to the turbine in a direction toward the loaded pads and eccentricity in the pole plane adjacent to the thrust end in a direction toward the unloaded pads.

The additional Test Number 1 was conducted as an extension of the test of Configuration F at Data Points 14 and 15 (with and without alternator excitation). To achieve the required conditions, the temperature of the turbine end journal bearing support was increased, thereby increasing the bearing diametral clearance. The clearance of the thrust end journal bearing was not increased during this test.

Figure VII-14, photographs (A) through (D), show the performance of the turbine end journal bearing at the threshold and during instability of one of the

unloaded bearing pads. Fig. VII-14 (A) shows the film thicknesses of one loaded and one unloaded pad immediately prior to the onset of instability. Figure VII-14 (B) shows the form of the instability and, in particular, that adequate film thickness existed during this phenomena which has a frequency of 40 CPS. It is shown in Figure VII-14 (C) that the journal motion was unaffected by instability of the unloaded pad. The performance shown in Figures VII-14 A, B and C were (with the exception of bearing clearance) obtained during testing at data point F 14, i.e., with alternator excitation but no electrical load. Figure VII-14 (D) shows the effect on instability of removing the excitation (Test Point F 15). From this figure it is seen that the instability ceased and that the film thickness of both loaded and unloaded pads was increased. The cessation of the instability coupled with the increase in film thickness on removal of the alternator excitation suggests that the observed instability resulted from a magnetic short circuit around the alternator stator, the bearing pads, and other magnetic parts of the simulator design forming part of this circuit. The occurrence of this phenomena in the turboalternator is improbable as the bearing support system is, unlike the simulator, manufactured from non-magnetic materials. During this test, the other pads (one loaded and one unloaded) did not exhibit any tendencies to become unstable.

From the observed test results, it is concluded that safe operation of the turboalternator in a horizontal position will be obtained while the film thickness of the unloaded pads is less than 1.8 mils. (Stable operation of both bearings at this clearance while operating at 12 KW can be seen in Figures VII-5 and VII-7.)

The additional Test Number 2 was conducted as extension of the test on Configuration A (rotor vertical, concentric and mechanically balanced). The test was performed, without alternator excitation throughout, at three values of ambient pressure, 14.7 PSIA, 10.5 PSIA and 7.2 PSIA. Like additional Test Number 1, the turbine journal bearing clearance was increased by raising the temperature of the bearing support. Throughout the test the thrust end journal bearing clearances were maintained at normal levels. Figure 15 shows the journal bearing performance at the maximum values of clearance attained during the test which was performed at an ambient pressure of 7.2 PSIA. Figures VII-15 (A & B) show the motion of the journal (time base traces and orbit) with a predominant

vibration frequency of 40 CPS. It should be noted that increasing the ambient pressure to 14.7 PSIA from 7.2 PSIA did not significantly reduce the amplitude of the 40 CPS vibration. Stopping the vacuum pump, however, resulted in the disappearance of this mode of vibration. Figure VII-15 (B & C) show the pad film thickness. Again the 40 CPS vibration can be clearly seen. From these figures it is seen that film thicknesses of approximately 1.7 mils were attained on both loaded and unloaded pads, a situation where the bearing preload is approaching zero. It was shown during the course of this test that at large clearances, the journal and pads became noticeably responsive to forced vibrations emanating from associated auxiliary equipment, in this case the vacuum pump. Operation under such conditions, while not shown to be harmful, is not recommended. Insufficient time curtailed further testing at these increased values of bearing clearance in conjunction with the various electrical load and fault conditions to which the other configurations were subjected. From examination of the test data, it is concluded that for safe operation of the turboalternator in a vertical position the maximum bearing film thickness on any pad should be limited to 1.5 mils.

Satisfactory simulator operation at 7.2 PSIA over the full range of electrical conditions involved was previously demonstrated during testing of Configuration B at an average film thickness of 1.44 mils.

Additional Test Number 3 was also conducted as an extension of the test of Configuration A. The axis of the simulator was inclined at 45° and the test performed at three values of bearing ambient pressure (14.7 PSIA, 10.5 PSIA and 7.2 PSIA) without alternator excitation. Oscilloscope photographs which were taken of the bearing performance are not presented in this report. The rotor-bearing system performance was satisfactory throughout the course of the test.

Additional Test Number 4 was also conducted as an extension of the tests of Configuration A. This test was performed at one value of bearing ambient pressure (14.7 PSIA) both with and without alternator excitation.

The test consisted of accelerating the rotor to 14,400 RPM, closing the turbine supply valve and permitting the rotor to coast down. The main thrust bearing was supplied with jacking gas throughout the test. Oscilloscope photographs of both journal orbits were taken during coastdown as shown in Figure VII-16. These photographs, which are multi-exposures, were obtained by repositioning the orbit after each exposure. Figures VII-16 (A) and VII-16 (B) show the turbine end journal orbit with and without alternator excitation respectively. Figures VII-16 (C) and VII-16 (C) show the thrust end journal orbits under the same conditions. These orbits indicate the combined effect of the residual unbalance in the rotor system and the out-of-roundness which was present in the thrust end journal. Figures VII-16 (A and B) do not exhibit any noticeable effects of either alternator excitation or the rigid body modes of vibration. Figures VII-16 (C and D) do exhibit a slight orbit enlargement between 7,000 and 8,000 RPM, this being the speed range in which the increased amplitudes of vibration associated with the rigid body criticals were predicted.

This test was conducted with the rotor positioned geometrically concentric to the bore of the alternator stator. From Figure VII-16, it can be seen that excitation of the alternator field had no effect on the concentricity of the rotor. It should be noted that the repositioning of the orbit necessary to obtain the multi-exposure photographs was accomplished by adjustment of the CRO beam used to display the signals from the horizontal ground-to-shaft probes, the relative positions of the orbits at each speed are, therefore, a correct representation of journal position in the vertical direction. It is concluded that the geometric and magnetic centers of the alternator rotor and stator used in this test program are either closely coincident or the static forces involved in operation with excitation, but zero power, are too small to effect the bearing performance.

During the course of the test program on Configurations A through F, it became evident that some back leakage from the loaded pads was occurring. When the bearings were operating in an ambient pressure of 14.7 PSIA, it was noted that the pressure gage normally used to measure journal bearing jacking gas supply pressure was indicating pressures of up to 9.0 PSIG, the exact pressure being dependent on simulator orientation. A check on the system showed that the gas

in the bearing film, which is at a pressure higher than ambient pressure, was leaking back through the jacking-gas orifices, past the "O" ring-type check valves built into the pivot seats and pressurizing the supply pipe lines up to the test panel.

Additional Test Number 5 was introduced as an extension of the test on Configuration A, to determine the extent of back leakage. The test was performed with the simulator in a vertical position and with a bearing ambient pressure of 14.7 PSIA. The jacking-gas supply line was disconnected at the test panel and a flowmeter inserted, the downstream side of the flowmeter being left open to atmosphere. At a speed of 12,000 RPM a total leakage flow from the four pads was noted to be 0.06425 CFM. The leakage from the individual pads was as follows:

<u>Pad (identified by the capacity probe #)</u>	<u>Pad Leakage (SCFM)</u>
PF3	.0264
PF4	.0246
PF23	0
PF24	.0132

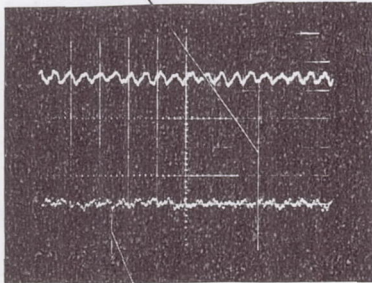
Due to the difference in back pressure existing across the check valve during normal operation and during the course of the leakage tests, the magnitude of pad leakage as determined by these tests will be considerably in excess of the leakage rates occurring under normal conditions of operation. However, conducting the tests in the manner described allows the introduction of a simple flow test of the bearings to be installed in the turboalternator. Bearing performance during the leak test was considered satisfactory with adequate film thickness at all times. Therefore, no further attempts were made to correlate flow, backpressure and bearing film thickness. The appropriate manufacturing drawing of the bearing parts was revised to include a reverse flow leakage test with a supply pressure of 10 PSIG, the resulting leakage flow not to exceed 750 CC/min., this being equivalent to the maximum pad leakage observed during the test.

Additional Test Number 6 was introduced to permit observation of the dynamic response of the journals and bearing pads when the rotor was eccentric and misaligned. The misalignment was achieved by adjusting the journal bearings to

obtain an eccentricity in the direction of the loaded pads at the turbine end and, simultaneously, eccentricity in the direction of the unloaded pads at the thrust bearing end. In addition, the opportunity was taken to observe the thrust bearing performance under operating conditions involving misalignment between the thrust runner and stator, a condition which occurs when the rotor alignment is changed after the thrust bearing adjustments have been made. This test was conducted as an extension of the tests on Configuration A, the only adjustments made being to change the rotor eccentricity. The thrust bearing adjustment was not corrected to maintain the parallelism between runner and stator. Three bearing ambient pressure levels were used during the test (14.7, 10.5 and 7.2 PSIA).

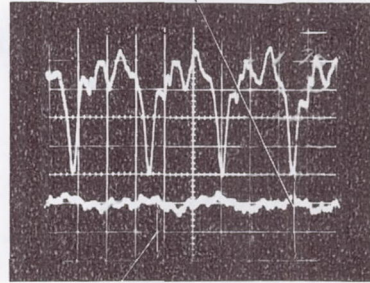
Throughout the test, the hydrodynamic bearing performance was satisfactory, the journal and pad response to electromagnetic alternator forces being synchronous and of similar magnitudes to those previously described in this report. The eccentricity in the plane of the pole face adjacent to the turbine end bearing was approximately 0.7 mils in the direction of the loaded pads and the eccentricity in the plane of the pole face adjacent to the thrust end bearing was approximately 0.3 mils in the direction of the unloaded pads. This represents an angular misalignment of the rotor and the thrust plate of 0.013 degrees. The performance of the hydrodynamic thrust bearing under these conditions was acceptable throughout, a minimum film thickness of approximately 1.0 mil being observed at one capacitance probe simultaneously with a film thickness of 1.5 mils at a probe positioned at 180° .

UNLOADED PAD FILM THICKNESS
AT THRESHOLD OF INSTABILITY.
ALTERNATOR EXCITED - NO LOAD
SENSITIVITY 0.298 MILS/MAJOR DIVISION



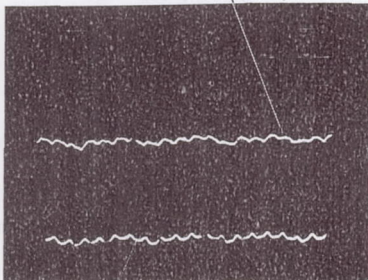
(A)
LOADED PAD FILM THICKNESS AT
THRESHOLD OF INSTABILITY.
ALTERNATOR EXCITED - NO LOAD
SENSITIVITY 0.304 MILS/MAJOR DIVISION

UNLOADED PAD FILM THICKNESS
DURING INSTABILITY. ALTERNATOR
EXCITED - NO LOAD
SENSITIVITY 0.298 MILS/MAJOR DIVISION



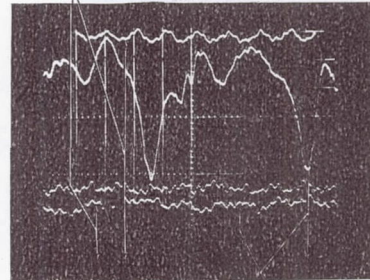
(B)
LOADED PAD FILM THICKNESS
DURING INSTABILITY ALTERNATOR
EXCITED - NO LOAD
SENSITIVITY 0.304 MILS/MAJOR DIVISION

JOURNAL MOTION, HORIZONTAL PROBE
DURING INSTABILITY.
SENSITIVITY 0.665 MILS/MAJOR DIVISION



(C)
JOURNAL MOTION, VERTICAL PROBE
DURING INSTABILITY.
SENSITIVITY 0.640 MILS/MAJOR DIVISION

LOADED AND UNLOADED PAD FILM
THICKNESSES ON REMOVAL OF ALTERNATOR
EXCITATION
SENSITIVITIES:
UPPER TRACES 0.298 MILS/MAJOR DIVISION
LOWER TRACES 0.304 MILS/MAJOR DIVISION

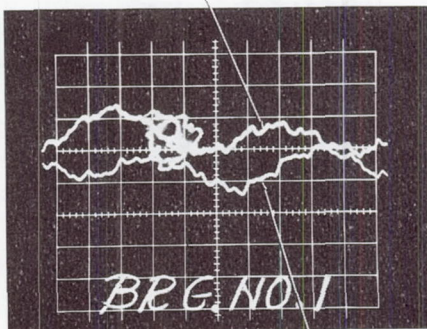


(D)
LOADED AND UNLOADED PAD FILM
THICKNESSES DURING INSTABILITY
AND PRIOR TO REMOVING ALTERNATOR
EXCITATION

TIME BASE - FIGURE A, B AND C - 10×10^{-3} SECS/MAJOR DIVISION
FIGURE D - 5×10^{-3} SECS/MAJOR DIVISION

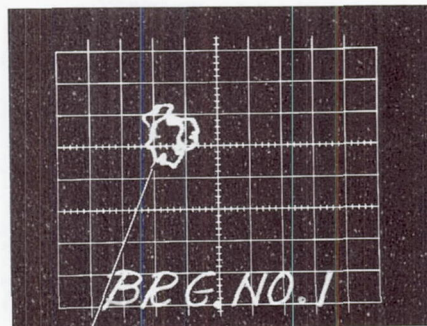
Fig. VII-14 Oscilloscope Photographs of the Turbine End Journal Bearing Performance During Tests to Determine the Maximum Permissible Bearing Clearance. Speed 12,000 RPM, 10.5 PSIA Ambient Pressure (Air). Rotor Horizontal, Eccentric and Mechanically Unbalanced. (Configuration F Test Points 14 and 15)

JOURNAL MOTION, HORIZONTAL PROBE
 SENSITIVITY 0.266 MILS/MAJOR DIVISION



(A)

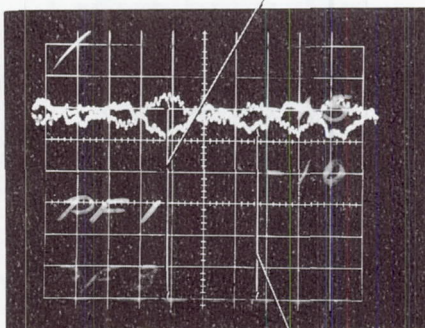
JOURNAL MOTION, VERTICAL PROBE
 SENSITIVITY 0.256 MILS/MAJOR DIVISION



(B)

JOURNAL ORBIT
 SENSITIVITY:-
 VERTICAL PROBE 0.256 MILS/MAJOR DIVISION
 HORIZONTAL PROBE 0.266 MILS/MAJOR DIVISION

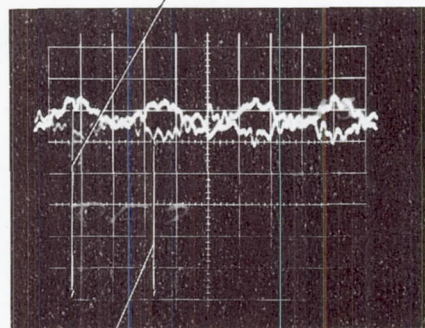
UNLOADED PAD FILM THICKNESS
 SENSITIVITY 0.298 MILS/MAJOR DIVISION



(C)

LOADED PAD FILM THICKNESS
 SENSITIVITY 0.304 MILS/MAJOR DIVISION

UNLOADED PAD FILM THICKNESS
 SENSITIVITY 0.315 MILS/MAJOR DIVISION

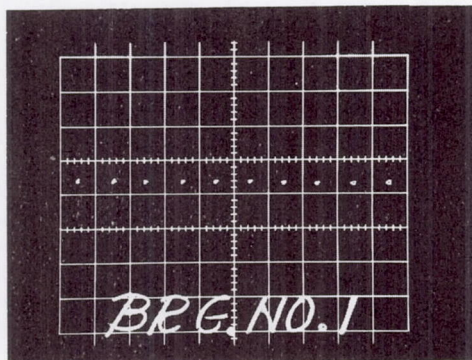


(D)

LOADED PAD FILM THICKNESS
 SENSITIVITY 0.321 MILS/MAJOR DIVISION

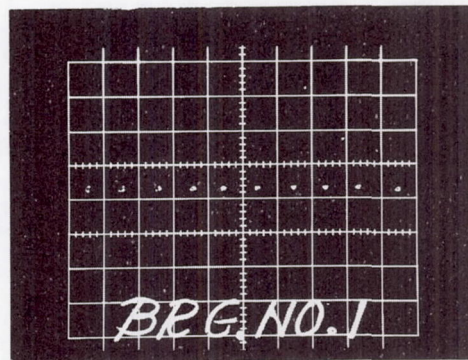
TIME BASE - FIGURE A	5×10^{-3} SECS/MAJOR DIVISION
FIGURES C AND D 10×10^{-3} SECS/MAJOR DIVISION	

Fig. VII-15 Oscilloscope Photographs of the Turbine End Journal Bearing Performance During Tests to Determine the Maximum Permissible Bearing Clearance. Speed 12,000 RPM, 10.5 PSIA Ambient Pressure (Air), Rotor Vertical, Concentric and Balanced. (Configuration A Test Point 23)



(A)

NO ALTERNATOR EXCITATION



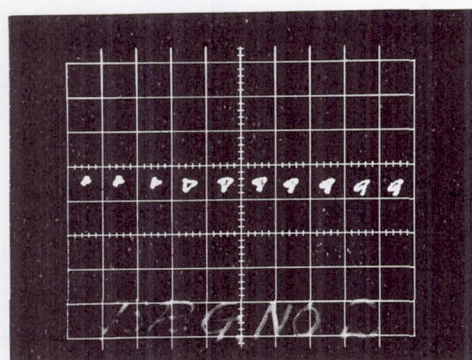
(B)

WITH ALTERNATOR EXCITATION

TURBINE END JOURNAL ORBITS

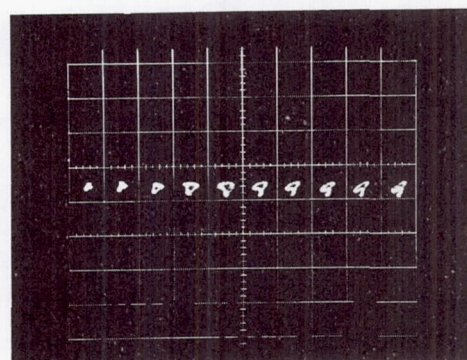
SENSITIVITY: HORIZONTAL - 0.665 MILS/MAJOR DIVISION

VERTICAL - 0.640 MILS/MAJOR DIVISION



(C)

NO ALTERNATOR EXCITATION



(D)

WITH ALTERNATOR EXCITATION

THRUST END JOURNAL ORBITS

SENSITIVITY: HORIZONTAL 0.45 MILS/MAJOR DIVISION

VERTICAL 0.47 MILS/MAJOR DIVISION

SPEEDS IN RPM READING FROM LEFT TO RIGHT ON EACH FIGURE ARE 5,000, 6,000, 7,000, 8,000, 9,000, 10,000, 11,000, 12,000, 13,000 AND 14,400

Fig. VII-16 Oscilloscope Photographs of Journal Orbits Showing the Residual Unbalance, Out-of-Roundness and Effect of Excitation Over the Speed Range 5,000-14,400 RPM Rotor Vertical and Concentric Bearing Ambient Pressure 14.7 PSIA (Air)

Test Evaluation of Journal Bearing Performance and Alternator Magnetic Force Gradients

The effect of the static electromagnetic force, F_o , on journal position and pad film thickness resulting from operation with an eccentric rotor can be clearly seen on Figures VII-9, VII-10, VII-11 and VII-12. In Figure VII-9 (B), the vertical distance of 0.83 mils separating the two orbits indicates the movement of the journal resulting from switching on the alternator excitation with the rotor in a vertical position. The lower traces on Figures VII-9 (A) and VII-9 (C) show the effect on the pad film thickness.

Figure VII-11 (B) again shows the effect of switching on the excitation. In this case the rotor was horizontal and, as a result of the increased stiffness of the loaded bearings, the journal movement is considerably reduced. The reduction in pad film thickness is, for the same reason, also less. Similar trends can be seen as a consequence of initiating both the single-and three-phase short (Figures VII-12 and VII-13).

From the observed steady-state movements of the journal and changes in pad film thickness which resulted from each change in the condition of alternator operation, it is possible to estimate the static electromagnetic force, F_o , which caused these changes. In order to make such estimates, it is necessary to have experimental data showing the pad film thickness for each of the four pads in the bearing, and also experimental data showing the eccentricity of the rotor pole-planes relative to the bore of the alternator stator. As described previously, the simulator was equipped with the instrumentation required to make these measurements.

Following acquisition of the experimental data, the recorded probe readings were corrected for differential thermal expansion effects between journal, pads, bearing supports and capacitance probes and also instrumentation calibration effects. The data were then superimposed on plots of calculated bearing performance. The calculated bearing performance was plotted as curves of film thickness versus bearing preload ratio for selected values of bearing load. In order to plot the experimental data, the value of bearing preload ratios (m) were calculated from the following geometric relationship:

$$m = 1 - \frac{h_p(\text{avg.})}{C_p}$$

The value of static magnetic load was then obtained by linear interpolation of the experimental points relative to the two adjacent calculated load curves.

Three representative curves are shown in Figures VII-17, VII-18 and VII-19. The experimental data plotted on Figures VII-17 and VII-18 are for the journal bearing located adjacent to the thrust bearing, the rotor being vertically oriented with residual mechanical unbalance. The experimental data plotted on Figure VII-19 is likewise for the same bearing. In this case, however, the rotor is horizontal and also unbalanced by 0.005 ounce-inches in the plane of the turbine wheel.

Under alternator operating conditions of zero excitation (therefore, no load), the electromagnetic force is zero and the corresponding experimental data point should fall on the zero load line for vertical operation, and on the load line representing 1-g bearing load for horizontal operation which, in this case, is 28 pounds. The fact that the experimental data points for zero excitation condition are not coincident with the appropriate load lines is attributed to radial forces on the rotor resulting from eccentric operation of the turbine labyrinth seals and also to variations in bearing geometry. For example, the analysis of bearing performance does not take into account the effect of the 0.2 mil deep pocket which is cut into the surface of each of the loaded pads for the purposes of hydrostatic lift-off. A further potential loss in film thickness for a given load exists as a consequence of back-leakage from the bearing film through the lift-off bearing orifice in the loaded pads. Although check valves were used to limit this backflow, some leakage was, as described in preceeding paragraphs, detected during the tests.

Examination of the calculated bearing performance plotted on Figures VII-17 and VII-18 shows that the load change associated with a given change in film thickness is greater in the regions of high loads than it is for the same film thickness change in the regions of low loads. Considering then the experimental

data obtained during alternator operation in a vertical orientation, it is reasonable to describe the zero excitation test point as the zero load point. The bearing loads at other conditions of alternator electrical operation can then be determined.

If it is assumed that the electromagnetic force gradients are the same for each of the two alternator pole pairs, and that for small eccentricities the force gradients are linear, then the calculated and experimental bearing performance data can be used to calculate the static electromagnetic gradients. The change in radial force on the rotor which results from a change in eccentricity at the turbine labyrinth is accounted for in the calculations of the electromagnetic gradients. Values of bearing load and pole-plane eccentricity under various conditions of alternator operation are given in Table VII-10 together with values of the experimentally-determined and analytically-predicted average static force gradient for each pole pair. From examination of the force gradient values, it is seen that those obtained from experimental data are lower than the predicted values. The spread in the experimentally-determined gradient values at any given alternator operating condition is due to (1) experimental error, and (2) small viscosity changes due to 30 to 40 F variations in temperature from the 110 F value used for the bearing performance calculations.

The experimentally-determined gradients for zero load and for 3.33 KVA alternator operation are approximately 50 percent of the predicted values; whereas the gradients at 12 KW alternator output are 55 to 65 percent of the predicted values.

The corrected values of rotor eccentricity in the planes of the turbine wheel, turbine journal bearing, pole face adjacent to turbine journal bearing, pole face adjacent to thrust end journal bearing, and thrust end journal bearing at each of the 216 data points are given in Appendix K. The corrected values of journal bearing film thickness at each of the 216 data points are given in Appendix J. Curves showing the calculated and experimental performance of both journal bearings similar to those presented in Figures VII-17, VII-18 and VII-19 were plotted from the data obtained during the testing of each configuration (A through F). These curves, while retained on file are not presented in this report.

TABLE NO. VII-10 - Calculated and Experimentally Determined Static
Electromagnetic Force Gradient Per Alternator Pole Pair

Alternator Operating Condition	Turbine Journal Bearing and Adjacent Pole Pair		Thrust-End Journal Bearing and Adjacent Pole Pair		Average Static Force Gradient Per Pole Pair (Lb./Mil)	
	Force on Brg. Due to F_o (lb) *	Eccentricity of Poles (Mils) *	Force on Brg. Due to F_o (lb) *	Eccentricity of Poles (Mils) *	From Test Results *	Predicted by Analysis
No Excitation	0	2.64	0	2.30	0	0
No Excitation	0	2.81	0	2.42	0	0
Excitation only	8.0	2.84	4.6	2.46	2.01	3.82
Excitation only	10.0	3.16	4.0	2.67	1.82	3.82
3KW, 3-phase, 0.8 PF	11.0	2.87	4.4	2.47	2.19	-
3KW, 3-phase, 0.8 PF	13.5	3.22	5.5	2.70	2.45	-
6KW, 3-phase, 0.8 PF	11.0	2.88	6.6	2.46	2.83	-
6KW, 3-phase, 0.8 PF	16.5	3.23	5.5	2.71	2.67	-
12KW, 3-phase, 0.8 PF	17.0	3.01	7.5	2.56	3.44	5.625
12KW, 3-phase, 0.8 PF	16.0	3.00	6.4	2.57	3.05	5.625
12KW, 3-phase, 0.8 PF	22.0	3.45	6.8	2.87	3.22	5.625
12KW, 3-phase, 0.8 PF	22.0	3.42	7.7	2.82	3.48	5.625
3.33KVA, 1-phase, 1.0 PF	8.0	2.73	4.1	2.28	1.98	3.93
3.33KVA, 1-phase, 1.0 PF	11.0	3.23	3.4	2.73	1.70	3.93

* The experimental data was obtained during test with the rotor oriented vertically and rotating at 12,000 rpm.

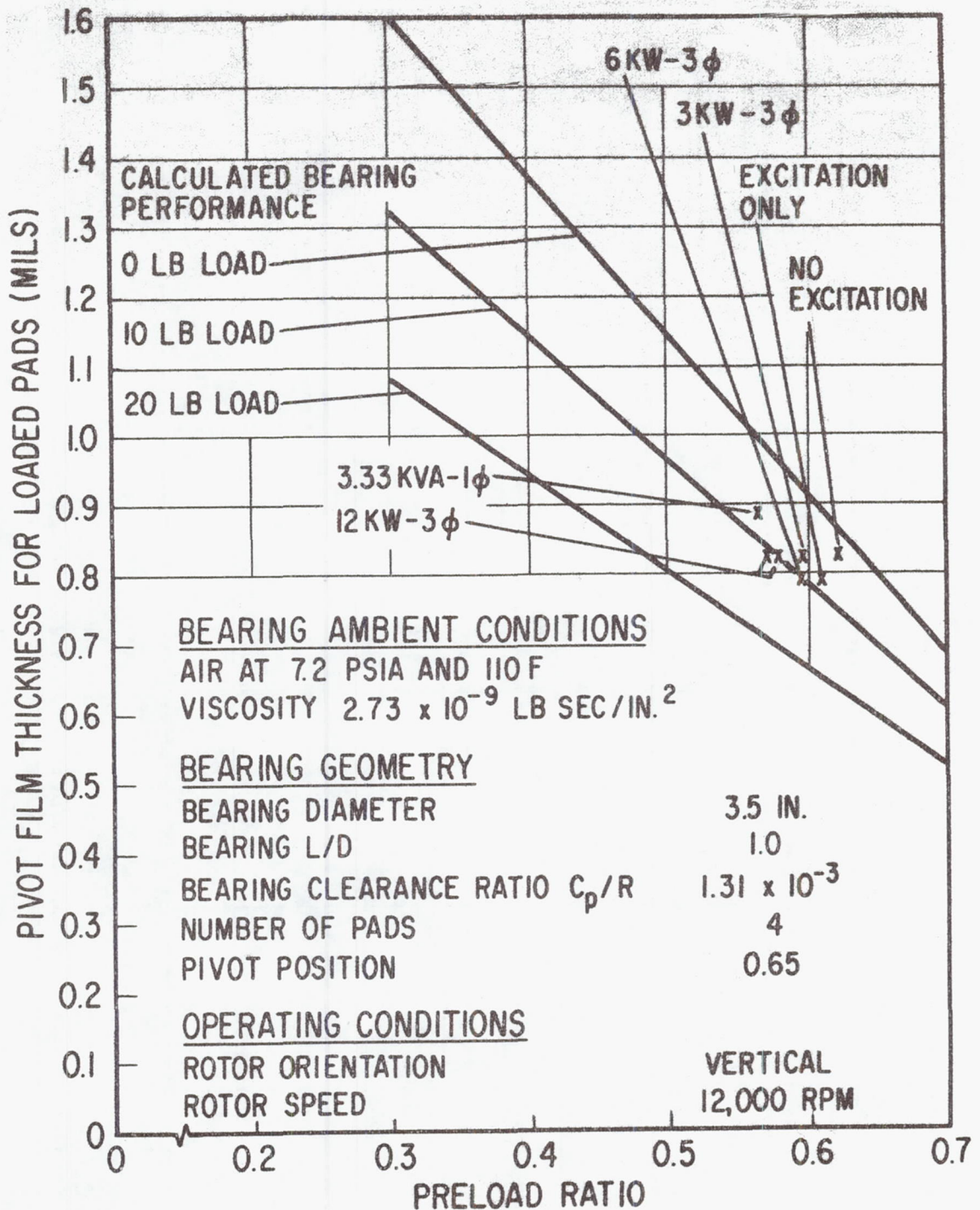


Fig. VII-17 Calculated and Experimental Performance of the Journal Bearing Adjacent to the Thrust Bearing at High Preloads (Rotor Vertical)

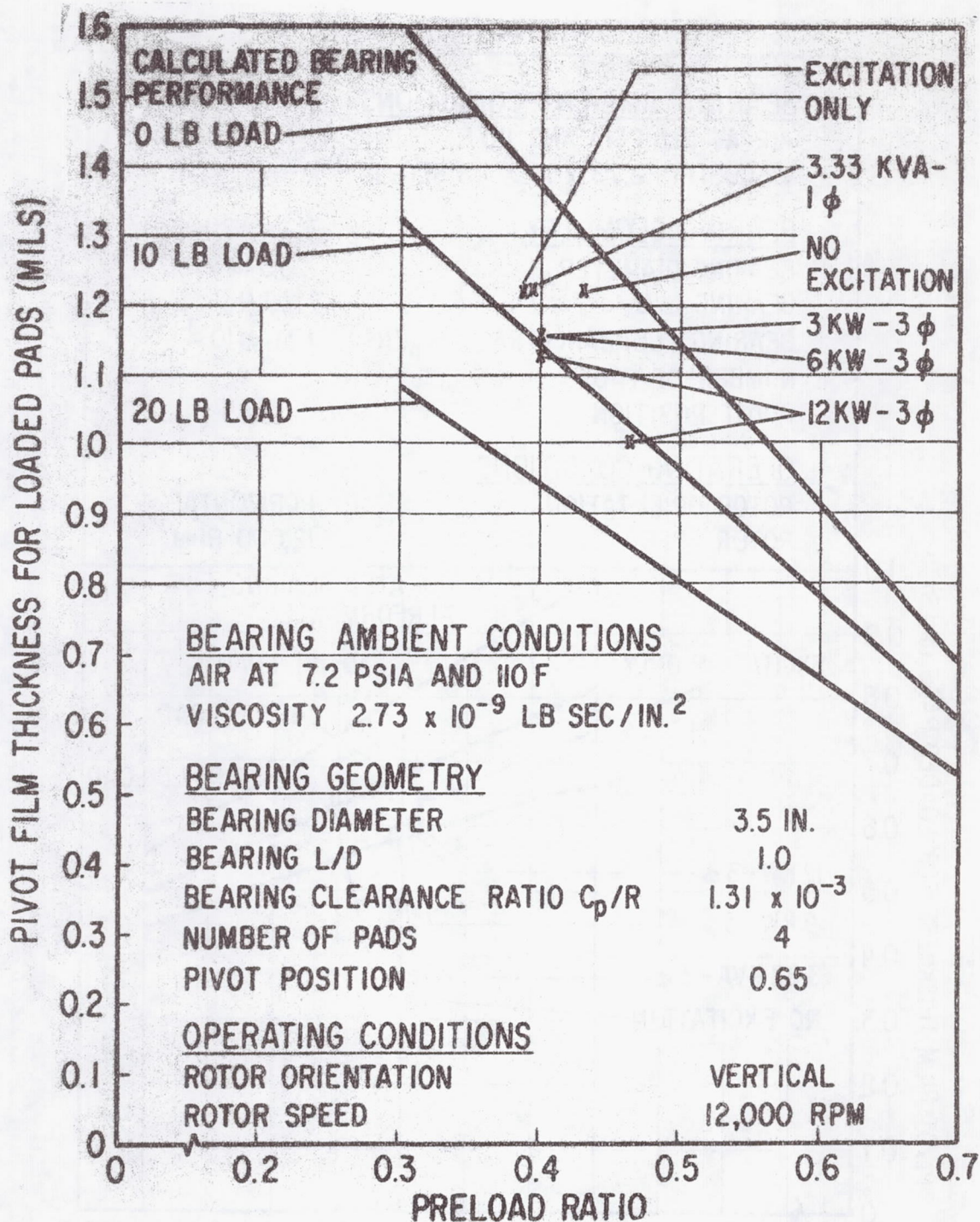


Fig. VII-18 Calculated and Experimental Performance of the Journal Bearing Adjacent to the Thrust Bearing at Low Preloads (Rotor Vertical)

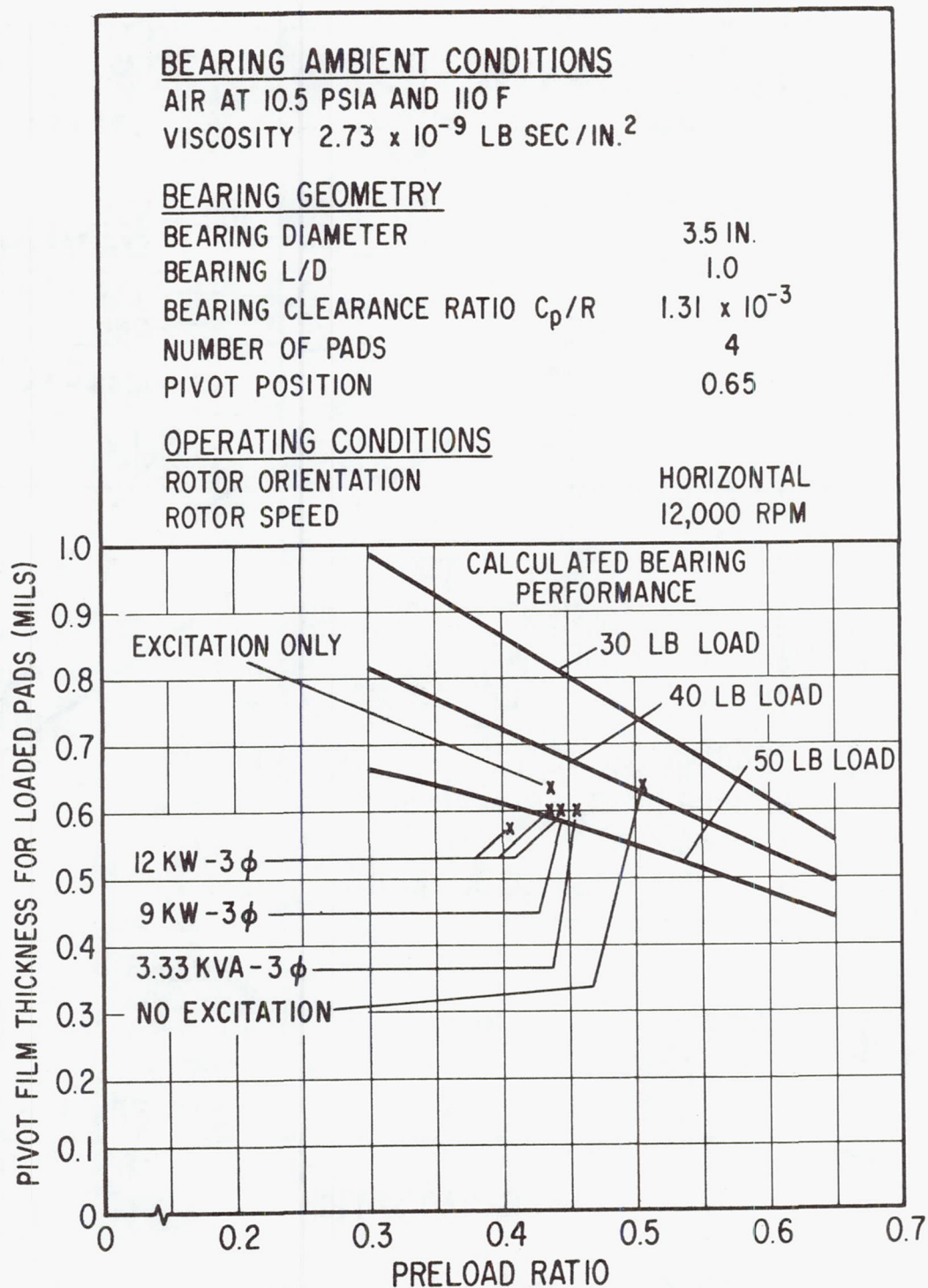


Fig. VII-19 Calculated and Experimental Performance of the Journal Bearing Adjacent to the Thrust Bearing at Low Preloads (Rotor Horizontal)

Test Evaluation of Hydrodynamic Thrust Bearing Performance

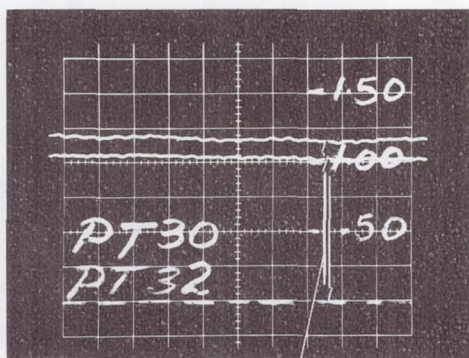
During the course of the test program which, as previously described, was primarily designed to evaluate rotor-bearing response to electromagnetic forces the thrust bearing performance was continuously monitored. The rotor-bearing response analysis and calculations which were performed yielded values of amplitude and frequency in a radial direction, the assumption being made that geometric centers and magnetic centers would be coincident in the axial direction and, therefore, axial magnetically induced loads would not be experienced.

The 216 data points in the test plan involved operation at bearing ambient pressures of 10.5 PSIA and 7.2 PSIA. During these tests the hydrodynamic thrust bearing film thickness was maintained at approximately 1.0 mil by adjusting the pressure levels in the two cavities positioned fore and aft of the turbine wheel. A qualitative indication was obtained during test which showed that film thickness increased with increased electrical load.

Dynamic variations in film thickness were of negligible proportions, approximately 50 microinches, and no detectable variations occurred over the range of conditions involved during the test program.

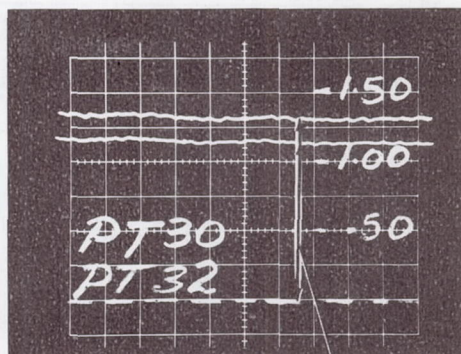
Resulting from the previously described indication of a thrust load change associated with a change in electrical power output, an additional test (Number 7) was instituted. For this test the simulator casings and the cavities fore and aft of the turbine were vented to atmosphere. With the simulator in a vertical position (turbine end uppermost), the load on the thrust bearing is then the weight of the rotor (54.87 pounds). This load can be modified by two different conditions: primarily, a change in the pressure distribution upstream and downstream of the turbine buckets, this condition occurring as a result of operating the impulse turbine at off design point conditions; and, secondly, electromagnetically induced forces due to the axial displacement of the geometric and magnetic centers of the alternator rotor and stator.

The oscilloscope photographs taken of thrust bearing film thickness during this test are shown in Figure VII-20. Figure VII-20 (A) shows the bearing film thickness at 12,000 RPM and zero excitation. The Figure VII-20 (B) (C) and (D) shows the bearing film thickness at 12,000 RPM and electrical loads of 3KW, 6KW, and 12 KW (0.8 PF) respectively. From Figure III-20 and the data taken from the third probe (PT31) used to ascertain thrust bearing film thickness, it was determined that a film thickness variation of 0.2 mils existed between the three capacitance probe positions during each test, and that the film thickness increased by 0.2 mils between the zero excitation and 12 KW test points. This change represents at the film thicknesses involved, a reduction in load of approximately 12 pounds. Due to the more than adequate film thicknesses observed, no further attempts were made to identify the source of the forces involved, i.e., alternator axial magnetic forces or turbine wheel pressure distribution.



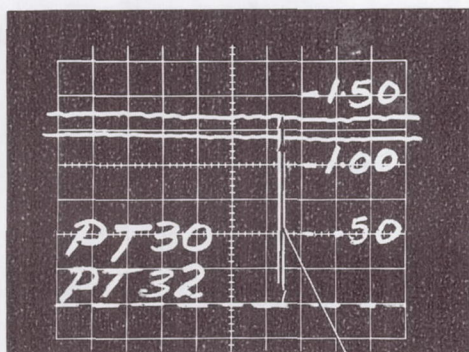
(A)

*AVERAGE FILM THICKNESS AT CONDITIONS
OF ZERO EXCITATION 1.42 MILS



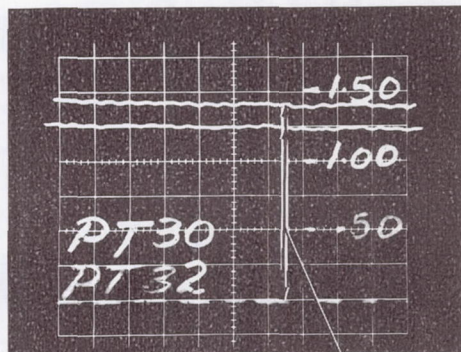
(B)

*AVERAGE FILM THICKNESS AT CONDITIONS
OF 3 KW ELECTRICAL LOAD 1.59 MILS



(C)

*AVERAGE FILM THICKNESS AT CONDITIONS
OF 6.0 KW ELECTRICAL LOAD 1.64 MILS



(D)

*AVERAGE FILM THICKNESS AT CONDITIONS
OF 12.0 KW ELECTRICAL LOAD 1.68 MILS

SENSITIVITY	UPPER TRACES (PT-30) 0.302 MILS/MAJOR DIVISION
	LOWER TRACES (PT-32) 0.317 MILS/MAJOR DIVISION
TIME BASE	ALL TRACES - 5×10^{-3} SECS/MAJOR DIVISION

*NOTE: FILM THICKNESS VALUES ARE THE AVERAGE OF THE 3 CAPACITANCE PROBE READINGS. THE SIGNALS FROM 2 OF THESE PROBES ARE SHOWN IN THESE FIGURES.

Fig. VII-20 Oscilloscope Photographs of the Hydrodynamic Thrust Bearing Performance Over a Range of Electrical Load Conditions. Rotor Vertical, Concentric and Mechanically Balanced. Speed 12,000 RPM, 14.7 PSIA Ambient Pressure (Air)

VIII. CONCLUSIONS AND RECOMMENDATIONS

A gas-bearing rotor support system has been designed, built and tested by MTI for the NASA Brayton Cycle axial-flow turboalternator developed by P&WA under prime contract from the NASA-Lewis Research Center. The design was experimentally evaluated in two full-scale rotor-bearing system test rigs, the first of which

- 1) exactly simulated the design of the turboalternator bearing system,
- 2) very closely simulated the mechanical configuration and physical parameters of the turboalternator rotor (the actual turbine and alternator components were not, however, used), and
- 3) permitted testing of the rotor-bearing system under operating and environmental conditions similar to those which would exist in the turboalternator.

The design of the first test rig did not utilize a high-temperature turbine or introduce the facilities required to generate electrical power.

The rotor-bearing system design performed satisfactorily and successfully passed the required P&WA acceptance tests.

Analyses, performed to determine the rotor-bearing system response and stability under conditions involving the electromagnetic forces attendant upon the generation of electrical power, showed that the rotor would be stable and the amplitudes of vibration small.

The test rig was then rebuilt to incorporate the turboalternator rotor shaft and alternator stator. The tests conducted in this, the second test rig, involved both the generation of electrical power and the demonstration of electrical fault conditions. The rotor-bearing system performed satisfactorily and demonstrated that, as predicted by analysis, the system was stable and the amplitudes of vibration small. In addition, the rotor-bearing system was successfully operated at increased values of journal bearing clearance, thereby reducing the bearing friction loss. Further tests were conducted to determine the safe boundaries of rotor-bearing system operation. At no time did operation

become marginal or hazardous to uninterrupted operation. The rotor-bearing system proved to be both flexible and rugged.

Specific Conclusions

Following is a list of specific conclusions relating to the design of the turbo-alternator rotor-bearing system as documented in Section II of this report. These conclusions are, of course, substantiated by the test results documented in Sections IV and VII.

1) Hydrodynamic Journal Bearings

Performance of the journal bearings was excellent throughout the test program and in reasonably good agreement with predicted performance. At no time within the design range of operation was either instability of the journals or pivoted pads, or simple resonance of the pads or flexures detected. Attempts to initiate instability by increasing bearing clearance were unsuccessful; however, a low frequency pad resonance was discovered on an unloaded pad when operating at a diametral clearance of 2.5 mils with the simulator horizontally oriented. This clearance represents a 28 percent increase in the design point clearance. A low frequency pad and journal resonance was also noted during vertical operation at a diametral bearing clearance of 3.42 mils. This clearance represents a 95 percent increase in the design point clearance. At no time during the test program was the performance of the rotor-bearing system noticeably affected by the electromagnetic forces resulting from either the generation of electrical power or the short-circuit and unbalance-load conditions of operation. Similarly, addition of the prescribed amounts of turbine unbalance did not unduly affect bearing performance.

Rotor-bearing system performance under conditions involving 0 to 4.0 mils eccentricity between the alternator rotor and stator was satisfactory at all times.

Rotor-bearing system performance, in both the horizontal and vertical orientations, was satisfactory under conditions of operation involving the increased value of bearing clearance required to achieve a calculated 15 percent reduction in the design-point value of friction loss given in Table II-2.

2) Hydrostatic Lift-Off Journal Bearings

Performance of the hydrostatic lift-off journal bearings was satisfactory at all times. The lift-off bearings should be used during startup and shutdown of the turboalternator whenever there is a radial component of rotor weight acting on the lower pads. The supply of gas to the bearings can be discontinued at rotor speeds in excess of 8,000 rpm. The use of excessive supply pressures should be avoided as the lift-off bearings are capable of lifting the rotor shaft until contact is made with the upper pads. The selection of the value of supply pressure appropriate to any particular rotor orientation in a 1-g gravitational field should be based on the attainment of a loaded-pad film thickness of 0.4-0.7 mils. In a zero-g gravitational field or in a vertical position, the lift-off journal bearings should not be used.

3) Hydrodynamic Thrust Bearing

Performance of the hydrodynamic thrust bearing was satisfactory throughout the test program, the test results being in quite good agreement with predicted results at design-point conditions. Under off-design-point conditions of operation, the performance at low loads was in excess of the predicted performance; whereas, at high loads the performance was less than predicted. An overload capacity of 40 percent at adequate film thickness was demonstrated during the test program. Performance of the thrust bearing liquid-cooling mechanism was excellent, even at coolant flow rates less than 150 pounds per hour. Dimensional stability of the aluminum thrust plate over the 14-month test period was, from all operating indications, excellent.

4) Main and Reverse Hydrostatic Thrust Bearings

Performance of the main hydrostatic thrust bearing is slightly better than predicted, while performance of the reverse thrust bearing falls slightly short of design values. Nonetheless, film thickness of the reverse thrust bearing at the required startup load condition is more than adequate for safe, reliable operation.

General Conclusions

Successful development of a reliable turboalternator gas-bearing rotor-support system, at least for static environmental conditions, appears to have been achieved to the point where generation of electrical power was demonstrated. However, extensive testing of the actual turboalternator, under both static and dynamic environmental conditions, will be required before final substantiation of reliability can be made.

The technological advancements directly related to gas-bearing turbomachinery which have been incorporated into the design of the turboalternator were, for the main part, conceived and developed during the previously completed NASA program to develop a high-performance axial-flow turbocompressor, Reference 22. A further advancement, appearing for the first time, which has been incorporated into the turboalternator journal bearing design, is the introduction of hydrostatic lift-off capability into the hydrodynamic pivoted-pad bearing. This feature was accomplished without imposing unacceptable restraint on the freedom of motion of the pads, without interruption of the highly stressed pivot/seat contact zone and without the use of fatigue-prone gas supply piping.

Initial startup of the simulator took place in November 1966. The final test took place in January 1967. The entire test program was conducted without a single bearing rub or failure.

Recommendations

The following recommendations are made based on the results of the work reported herein.

- 1) During the course of the test program, the occurrence of back-leakage via the hydrostatic lift-off journal bearing check valve was noted. No serious deterioration in bearing performance resulted from this occurrence. It is concluded that bearing performance may well prove adequate without the check valve; therefore, tests should be conducted to confirm this point.
- 2) The turboalternator bearing system should be experimentally evaluated under the various operating, and non-operating, vibration and shock conditions designated in NASA Specification P0055-1 (see Appendix H). The rotor-bearing system simulator would be an excellent vehicle with which to make the necessary evaluations.

REFERENCES

1. Curwen, P. W., "Operational Experience With Gas-Bearing Turbomachinery", presented at a panel discussion on Gas Bearing Applications held on November 30, 1966 at the ASME 1966 Winter Annual Meeting, New York, New York.
2. Corcoran, C.S., and Yeager, L.J., "Development of Electric Components for a 400 Hertz Brayton Cycle Energy Conversion System", Proceedings of the 1967 Intersociety Energy Conversion Engineering Conference, published by ASME, August 1967.
3. Pinkus, O. and B. Sternlicht, "Theory of Hydrodynamic Lubrication", McGraw Hill Book Co., 1960.
4. Gross, W. A., "Gas Film Lubrication", John Wiley & Sons, 1962.
5. "First International Symposium on Gas Lubricated Bearings" (1959), edited by D. D. Fuller, ACR-49, Office of Naval Research, Department of the Navy, Washington, D. C.
6. Grassam, N. S. and J. W. Powell, "Gas Lubricated Bearings", Butterworth & Co., (London) 1964.
7. Wernick, R.J. and C.H.T. Pan, "Static and Dynamic Characteristics of Self Acting, Partial-Arc, Gas Journal Bearing", ASME Paper 63-Lub-5.
8. Malanoski, S.B. and C.H.T. Pan, "The Static and Dynamic Characteristics of the Spiral Grooved Thrust Bearing", ASME Paper 64-Lub-9.
9. Lund, J.W., "A Theoretical Analysis of Whirl Instability and Pneumatic Hammer for A Rigid Rotor in Pressurized Gas Journal Bearings", (submitted for Publication in ASME).
10. Pan, C.H.T., "Spectral Analysis of Gas Bearing Systems for Stability Studies", MTI Report 64TR58.
11. Gunter, E.J., Jr., J.G. Hinkle and D.D. Fuller, "The Effects of Speed, Load and Film Thickness on the Performance of Gas Lubricated, Tilting Pad, Journal Bearings", Trans. ASLE, Vol. 7, No. 4, October 1964.
12. Muijderland, E.A., "Spiral Grooved Bearings", Phillips Research Laboratories (Netherlands), 1964.
13. Sternlicht, B., and E. B. Arwas, "State-of-the-Art of Gas-Lubricated Turbomachinery", MTI Report 65TR5-I.
14. Cheng, G., C. Y. Chow and S.F. Murray, "The Hydrodynamic Gas Journal Bearing and the Hydrodynamic Gas Thrust Bearing", MTI Report 65TR5-II, Vol. 1.

REFERENCES (Continued)

15. Lund, J.W., "The Hydrostatic Gas Journal Bearing and the Hydrostatic Gas Thrust Bearing", MTI Report 65TR5-II, Vol. 2.
16. Lund, J. and T. Chiang, "The Influence of Electromagnetic Forces on the Stability and Response of an Alternator Rotor", Mechanical Technology Report MTI 67TR34, issued under contract No. 33(615)-3238 with Wright Patterson Air Force Base, Ohio, May 1967.
17. Castelli, V. and J. Pirvics, "Equilibrium Characteristics of Axial-Groove Gas-Lubricated Bearings", Journal of Lubrication Technology, TRANS. ASME, Series F. Vol. 89, 1967, pp. 177-196.
18. Whittaker, E.T., and G. N. Watson, "Modern Analysis", Cambridge, New York, 1927.
19. Timoshenko, S., "Vibration Problems in Engineering", 3rd Edition, D. Van Nostrand Company, Inc., New York, 1956.
20. den Hartog, J.D., "Mechanical Vibrations", McGraw-Hill Book Company, 1956.
21. Stoker, J.J., "Non-Linear Vibrations", Interscience Publishers, New York, 1950.
22. Curwen, P.W., "Research and Development of High-Performance Axial Flow Turbomachinery", Volume 2 - Design of Gas Bearings, NASA Report CR-801.
23. Dryer, A.M., F.M. Kirkpatrick; E. F. Russell, J. M. Wimsatt and L. J. Yeager, "Alternator and Voltage Regulator - Exciter Design and Development", Volume 1 of Final Report, June 9, 1967.
24. Frost, A., Submittal of Gas Bearing and Magnetic Interaction Simulator Design Data for NASA Solar Brayton Cycle Axial Flow Turbine Alternator, December 5, 1966, MTI Report No. 66TR63.
25. Balje, O.E., "A Study on Design Criteria and Matching of Turbomachines", ASME Paper No. 60-WA-230, January 10, 1961.

NOMENCLATURE

C, C_p	Pad clearance (radius of curvature of pad minus radius of curvature of journal) - inches
C_B	Difference between the dimension from the bearing geometric center to the pad surface (at the pivot point) and the journal radius at design speed.
D	Diameter of journal or thrust bearing - inches
FHP	Friction horsepower
h	Heat transfer film coefficient - $\frac{\text{BTU}}{\text{hr.} \cdot \text{ft.}^2 \cdot \text{F}}$
h	Bearing film thickness - inches
h_{pivot}, h_p	Pivoted-pad film thickness at pivot location - inches
k	Thermal conductivity - $\frac{\text{BTU}}{\text{hr.} \cdot \text{ft.} \cdot \text{F}}$
K_A	Axial stiffness of thrust bearing gas film - lb./in.
K_{flex}	Stiffness of pivot-support flexure - lb./in.
K_R, K_{film}	Radial stiffness of journal bearing gas film - lb./in.
K_T	Angular stiffness of thrust bearing gas film - lb./in.
L	Length of journal bearing - inches
m	Journal bearing preload ratio -- $1 - \frac{C_B/R}{C_p/R}$
N	Rotor speed - revolutions per second
N_p	Resonant frequency of a journal bearing pivoted-pad in the pitch direction - revolutions per second
N_R	Resonant frequency of a journal bearing pivoted-pad in the roll direction - revolutions per second
P_a	Bearing ambient pressure - psia
P_s	Hydrostatic bearing supply pressure - psia
Q	Bearing heat generation rate - $\frac{\text{BTU}}{\text{hr.}}$
R	Radius of journal or thrust bearing - inches
t	Thickness of journal bearing pivoted-pad - inches.

T_h	Temperature of bearing housing - $^{\circ}\text{F}$
T_o	Reference temperature of bearing system (taken as 70 F in this report) - $^{\circ}\text{F}$
T_p	Average temperature of pivoted-pad - $^{\circ}\text{F}$
T_s	Average temperature of journal - $^{\circ}\text{F}$
W	Bearing load - pounds
β	Total angular arc of one pivoted-pad - degrees
ϵ_b	Bearing eccentricity ratio
ϵ_p	Pad eccentricity ratio
θ_p	Angular distance from the leading edge of a pad to its pivot point - degrees
Λ	Compressibility number
μ	Viscosity - lb.-sec./in. ²
ϕ	Pad attitude angle - degrees
ψ	Pivot-to-bearing-load angle - degrees
ω	Angular velocity - radians/second

APPENDIX A: The Load-Carrying Capacity and Dynamic Coefficients for a Partial Arc Gas Journal Bearing

The pressures, p , generated by the hydrodynamic action in a gas journal bearing film, are determined from Reynolds' equation [3]:

$$\frac{\partial}{R \partial \theta} \left(\frac{\rho h^3}{12 \mu} \frac{\partial p}{R \partial \theta} \right) + \frac{\partial}{\partial z} \left(\frac{\rho h^3}{12 \mu} \frac{\partial p}{\partial z} \right) = \frac{1}{2} R \omega \frac{d(\rho h)}{R \partial \theta} + \frac{d(\rho h)}{dt} \quad (A1)$$

Here, ρ is the gas density, μ is the viscosity, ω is the angular speed of rotation, h is the film thickness, R is the journal radius, t is time, θ is the angular coordinate and z is the axial coordinate. Under isothermal conditions, ρ can be replaced by p assuming that the gas obeys the perfect gas law. The equation is made dimensionless by introducing the symbols

$$P = \frac{p}{p_a} \quad (A2)$$

$$H = \frac{h}{C} \quad (A3)$$

$$\zeta = \frac{z}{R} \quad (A4)$$

$$\tau = i \nu t \quad (A5)$$

where p_a is the ambient pressure, C is the radial clearance, ν is the whirl frequency and $i = \sqrt{-1}$. Furthermore, introduce the parameters

$$\text{Compressibility number: } \Lambda = \frac{6 \mu \omega}{p_a} \left(\frac{R}{C} \right)^2 \quad (A6)$$

$$\text{Whirl frequency ratio: } \gamma = \frac{\nu}{\omega} \quad (A7)$$

By means of these definitions, Eq. (A1) can be written as

$$\frac{\partial}{\partial \theta} \left(H^3 \frac{\partial P^2}{\partial \theta} \right) + \frac{\partial}{\partial \zeta} \left(H^3 \frac{\partial P^2}{\partial \zeta} \right) = 2 \Lambda \frac{\partial(PH)}{\partial \theta} + i 4 \gamma \Lambda \frac{\partial(PH)}{\partial \tau} \quad (A8)$$

The dimensionless film thickness is expressed by

$$H = 1 + \epsilon \cos(\theta - \varphi) \quad (A9)$$

where ϵ is the eccentricity ratio (the ratio between the journal center eccentricity and the radial clearance C) and φ is the attitude angle, which is the angle measured from the pad load line to the line connecting the bearing and journal centers. The angular coordinate θ is also measured from the load line.

For convenience in the numerical evaluation of Eq. (A8), define

$$Q = (PH)^2 \quad (\text{A-10})$$

whereby Eq. (A8) becomes

$$\frac{\partial}{\partial \theta} \left(H \frac{\partial Q}{\partial \theta} - 2Q \frac{\partial H}{\partial \theta} \right) + \frac{\partial}{\partial \zeta} \left(H \frac{\partial Q}{\partial \zeta} - 2Q \frac{\partial H}{\partial \zeta} \right) = 2\Lambda \frac{\partial \sqrt{Q}}{\partial \theta} + i4\gamma\Lambda \frac{\partial \sqrt{Q}}{\partial \tau} \quad (\text{A-11})$$

This equation is to be solved for both static and dynamic conditions but such that the amplitude of the dynamic motion is kept small. Let the journal center operate at a steady-state eccentricity ratio ϵ_0 with a corresponding attitude angle φ_0 . The corresponding dimensionless film pressure is P_0 and the dimensionless film thickness is

$$H_0 = 1 + \epsilon_0 \cos(\theta - \varphi_0) \quad (\text{A-12})$$

Assume that this steady-state position is perturbed by a harmonic, small amplitude motion with frequency ν . At the bearing centerplane, let the amplitudes be ϵ_1 and φ_1 where both quantities are complex;

$$\epsilon_i = \epsilon_{ir} + i\epsilon_{ic} \quad (\text{A-13})$$

and similarly for φ_1 . This symbolism is an abbreviation of

$$\epsilon_i = \text{Re} \{ (\epsilon_{ir} + i\epsilon_{ic}) e^{i\nu t} \} = \epsilon_{ir} \cos(\nu t) - \epsilon_{ic} \sin(\nu t) \quad (\text{A-14})$$

In addition, the axis of the journal performs a harmonic, small angular motion described by the angle $\bar{\alpha}_r$, which is a rotation around the tangential direction, and by the angle $\bar{\alpha}_t$, which is a rotation around the negative radial direction. Thus, at the axial distance ζ from the bearing centerplane, the eccentricity ratio ϵ and the attitude angle φ are given by

$$\epsilon = \epsilon_0 + \epsilon_i + \zeta \alpha_r \quad (\text{A-15})$$

where

$$\varphi = \varphi_0 + \varphi_1 + \frac{1}{\varepsilon_0} \int \alpha_t \quad (\text{A-16})$$

$$\alpha_r = \frac{R}{C} \bar{\alpha}_r$$

$$\alpha_t = \frac{R}{C} \bar{\alpha}_t \quad (\text{A17})$$

By substitution from Eqs. (A15) and (A16), Eq. (A9) becomes

$$H = H_0 + \varepsilon_1 \cos(\theta - \varphi_0) + \varepsilon_0 \varphi_1 \sin(\theta - \varphi_0) + \alpha_r \int \cos(\theta - \varphi_0) + \alpha_t \int \sin(\theta - \varphi_0) \quad (\text{A18})$$

The resulting perturbation in the dimensionless film pressure can be written

$$P = P_0 + \varepsilon_1 P_1 + \varepsilon_0 \varphi_1 P_2 + \alpha_r P_3 + \alpha_t P_4 \quad (\text{A19})$$

where P_1 to P_4 are complex quantities and independent of time. With these two equations, Eq. (A10) becomes

$$Q = Q_0 + 2\varepsilon_1 Q_1 + 2\varepsilon_0 \varphi_1 Q_2 + 2\alpha_r Q_3 + 2\alpha_t Q_4 \quad (\text{A20})$$

where

$$Q_0 = (P_0 H_0)^2 \quad (\text{A21})$$

$$Q_1 = H_0 \sqrt{Q_0} \left(P_1 + \frac{\sqrt{Q_0}}{H_0^2} \cos(\theta - \varphi_0) \right) \quad (\text{A22})$$

$$Q_2 = H_0 \sqrt{Q_0} \left(P_2 + \frac{\sqrt{Q_0}}{H_0^2} \sin(\theta - \varphi_0) \right) \quad (\text{A23})$$

$$Q_3 = H_0 \sqrt{Q_0} \left(P_3 + \frac{\sqrt{Q_0}}{H_0^2} \int \cos(\theta - \varphi_0) \right) \quad (\text{A24})$$

$$Q_4 = H_0 \sqrt{Q_0} \left(P_4 + \frac{\sqrt{Q_0}}{H_0^2} \int \sin(\theta - \varphi_0) \right) \quad (\text{A25})$$

Introducing Eqs. (A18) and (A20) into Eq. (A11), and collecting terms in accordance with the perturbation variables, results in the following sets of equations:

$$\frac{\partial^2 Q_0}{\partial \theta^2} + \frac{\partial^2 Q_0}{\partial \zeta^2} - \frac{1}{H_0} \left(\frac{\partial H_0}{\partial \theta} + \frac{\Lambda}{\sqrt{Q_0}} \right) \frac{\partial Q_0}{\partial \theta} - \frac{2}{H_0} \frac{\partial^2 H_0}{\partial \theta^2} Q_0 = 0 \quad (A26)$$

$$\begin{aligned} \frac{\partial^2 Q_1}{\partial \theta^2} + \frac{\partial^2 Q_1}{\partial \zeta^2} - \frac{1}{H_0} \left(\frac{\partial H_0}{\partial \theta} + \frac{\Lambda}{\sqrt{Q_0}} \right) \frac{\partial Q_1}{\partial \theta} - \frac{1}{H_0} \left(2 \frac{\partial^2 H_0}{\partial \theta^2} - \frac{\Lambda}{2 Q_0^{3/2}} \frac{\partial Q_0}{\partial \theta} + i \frac{2 \gamma \Lambda}{\sqrt{Q_0}} \right) Q_1 = \\ - \frac{1}{2 H_0^2} \left(\frac{\Lambda}{\sqrt{Q_0}} (\cos(\theta - \phi_0) + \sin(\theta - \phi_0)) \right) \frac{\partial Q_0}{\partial \theta} - \frac{\cos(\theta - \phi_0)}{H_0^2} Q_0 \end{aligned} \quad (A27)$$

$$\begin{aligned} \frac{\partial^2 Q_2}{\partial \theta^2} + \frac{\partial^2 Q_2}{\partial \zeta^2} - \frac{1}{H_0} \left(\frac{\partial H_0}{\partial \theta} + \frac{\Lambda}{\sqrt{Q_0}} \right) \frac{\partial Q_2}{\partial \theta} - \frac{1}{H_0} \left(2 \frac{\partial^2 H_0}{\partial \theta^2} - \frac{\Lambda}{2 Q_0^{3/2}} \frac{\partial Q_0}{\partial \theta} + i \frac{2 \gamma \Lambda}{\sqrt{Q_0}} \right) Q_2 = \\ - \frac{1}{2 H_0^2} \left(\frac{\Lambda}{\sqrt{Q_0}} \sin(\theta - \phi_0) - \epsilon_0 - \cos(\theta - \phi_0) \right) \frac{\partial Q_0}{\partial \theta} - \frac{\sin(\theta - \phi_0)}{H_0^2} Q_0 \end{aligned} \quad (A28)$$

$$\begin{aligned} \frac{\partial^2 Q_3}{\partial \theta^2} + \frac{\partial^2 Q_3}{\partial \zeta^2} - \frac{1}{H_0} \left(\frac{\partial H_0}{\partial \theta} + \frac{\Lambda}{\sqrt{Q_0}} \right) \frac{\partial Q_3}{\partial \theta} - \frac{1}{H_0} \left(2 \frac{\partial^2 H_0}{\partial \theta^2} - \frac{\Lambda}{2 Q_0^{3/2}} \frac{\partial Q_0}{\partial \theta} + i \frac{2 \gamma \Lambda}{\sqrt{Q_0}} \right) Q_3 = \\ - \frac{5}{2 H_0^2} \left(\frac{\Lambda}{\sqrt{Q_0}} (\cos(\theta - \phi_0) + \sin(\theta - \phi_0)) \right) \frac{\partial Q_0}{\partial \theta} + \frac{\cos(\theta - \phi_0)}{2 H_0} \frac{\partial Q_0}{\partial \zeta} - \frac{5 \cos(\theta - \phi_0)}{H_0^2} Q_0 \end{aligned} \quad (A29)$$

$$\begin{aligned} \frac{\partial^2 Q_4}{\partial \theta^2} + \frac{\partial^2 Q_4}{\partial \zeta^2} - \frac{1}{H_0} \left(\frac{\partial H_0}{\partial \theta} + \frac{\Lambda}{\sqrt{Q_0}} \right) \frac{\partial Q_4}{\partial \theta} - \frac{1}{H_0} \left(2 \frac{\partial^2 H_0}{\partial \theta^2} - \frac{\Lambda}{2 Q_0^{3/2}} \frac{\partial Q_0}{\partial \theta} + i \frac{2 \gamma \Lambda}{\sqrt{Q_0}} \right) Q_4 = \\ - \frac{5}{2 H_0^2} \left(\frac{\Lambda}{\sqrt{Q_0}} \sin(\theta - \phi_0) - \epsilon_0 - \cos(\theta - \phi_0) \right) \frac{\partial Q_0}{\partial \theta} + \frac{\sin(\theta - \phi_0)}{2 H_0} \frac{\partial Q_0}{\partial \zeta} - \frac{5 \sin(\theta - \phi_0)}{H_0^2} Q_0 \end{aligned} \quad (A30)$$

Of these equations, the first is the conventional, steady-state equation. It is non-linear and is solved numerically in finite difference form by an iterative procedure developed by Castelli and Pirvics [17]. It is described for reference in Appendix B. The last four equations depend on the steady-state solution, Q_0 , and its derivatives. They are linear equations but with complex, independent variables. The solution is obtained numerically from finite difference equations as described in Appendix C.

The boundary conditions for Reynolds' equation, Eq. (A1), are that the pressure is equal to ambient along the periphery of the pad:

$$\left. \begin{array}{l} \text{for } z = \pm \frac{1}{2} L \text{ (at sides)} \\ \text{for } \theta = \theta_1 \text{ (at leading edge)} \\ \text{for } \theta = \theta_2 \text{ (at trailing edge)} \end{array} \right\} p = p_a$$

In terms of the dimensionless variable Q , these conditions can be expressed by

$$\left. \begin{array}{l} \text{at } \zeta = \frac{1}{D} \\ \text{at } \theta = \theta_1 \\ \text{at } \theta = \theta_2 \end{array} \right\} : \left\{ \begin{array}{l} Q_0 = H_0^2 \\ Q_1 = H_0 \cos(\theta - \phi_0) \\ Q_2 = H_0 \sin(\theta - \phi_0) \\ Q_3 = \zeta H_0 \cos(\theta - \phi_0) \\ Q_4 = \zeta H_0 \sin(\theta - \phi_0) \end{array} \right. \quad (\text{A31})$$

$$\text{at } \zeta = 0 : \left\{ \begin{array}{l} \frac{\partial Q_0}{\partial \zeta} = \frac{\partial Q_1}{\partial \zeta} = \frac{\partial Q_2}{\partial \zeta} = 0 \\ Q_3 = Q_4 = 0 \end{array} \right. \quad (\text{A32})$$

(Note: Q_0 , Q_1 and Q_2 are even functions of ζ whereas Q_3 and Q_4 are odd functions of ζ).

Once Q has been obtained, the resulting hydrodynamic force is computed by integration of the film pressure. The force is given a radial component F_r and tangential component F_t with respect to the steady-state position of the journal center:

$$\left. \begin{array}{l} F_r \\ F_t \end{array} \right\} = \int_{-\frac{1}{2}}^{\frac{1}{2}} \int_{\theta_1}^{\theta_2} (p - p_a) \left\{ \begin{array}{l} -\cos(\theta - \phi_0) \\ \sin(\theta - \phi_0) \end{array} \right\} R d\theta dz \quad (\text{A33})$$

or, in dimensionless form, making use of Eq. (A19):

$$\left. \begin{aligned} f_r &= \frac{\bar{F}_r}{p_a L D} \\ f_t &= \frac{\bar{F}_t}{p_a L D} \end{aligned} \right\} = \frac{1}{2 \frac{L}{D}} \int_0^{\frac{L}{D}} \int_{\theta_1}^{\theta_2} [P_0 - 1 + \varepsilon_1 P_1 + \varepsilon_0 \phi_1 P_2] \begin{Bmatrix} -\cos(\theta - \phi_0) \\ \sin(\theta - \phi_0) \end{Bmatrix} d\theta d\zeta \quad (A34)$$

This equation defines a first order Taylor series expansion of f_r and f_t around the steady-state position. For abbreviation, write

$$\begin{aligned} f_r &= f_{r0} + Z_{rr} \varepsilon_1 + Z_{rt} \varepsilon_0 \phi_1 \\ f_t &= f_{t0} + Z_{tr} \varepsilon_1 + Z_{tt} \varepsilon_0 \phi_1 \end{aligned} \quad (A35)$$

By comparing Eqs.(A34) and (A35), and making use of Eqs. (A21) to (A23), the coefficients become

$$\left. \begin{aligned} f_{r0} \\ f_{t0} \end{aligned} \right\} = \frac{1}{2 \frac{L}{D}} \int_0^{\frac{L}{D}} \int_{\theta_1}^{\theta_2} \left[\frac{\sqrt{Q_0}}{H_0} - 1 \right] \begin{Bmatrix} -\cos(\theta - \phi_0) \\ \sin(\theta - \phi_0) \end{Bmatrix} d\theta d\zeta \quad (A36)$$

$$\left. \begin{aligned} Z_{rr} \\ Z_{tr} \end{aligned} \right\} = \frac{1}{2 \frac{L}{D}} \int_0^{\frac{L}{D}} \int_{\theta_1}^{\theta_2} \frac{1}{H_0} \left[\frac{Q_1}{\sqrt{Q_0}} - \frac{\sqrt{Q_0}}{H_0} \cos(\theta - \phi_0) \right] \begin{Bmatrix} -\cos(\theta - \phi_0) \\ \sin(\theta - \phi_0) \end{Bmatrix} d\theta d\zeta \quad (A37)$$

$$\left. \begin{aligned} Z_{rt} \\ Z_{tt} \end{aligned} \right\} = \frac{1}{2 \frac{L}{D}} \int_0^{\frac{L}{D}} \int_{\theta_1}^{\theta_2} \frac{1}{H_0} \left[\frac{Q_2}{\sqrt{Q_0}} - \frac{\sqrt{Q_0}}{H_0} \sin(\theta - \phi_0) \right] \begin{Bmatrix} -\cos(\theta - \phi_0) \\ \sin(\theta - \phi_0) \end{Bmatrix} d\theta d\zeta \quad (A38)$$

The restoring hydrodynamic moment has the two components T_r and T_t which can be expressed in dimensionless form similar to the dimensionless force components:

$$\left. \begin{aligned} t_r &= \frac{T_r}{2p_a L^3} \\ t_t &= \frac{T_t}{2p_a L^3} \end{aligned} \right\} = \frac{1}{8\left(\frac{L}{D}\right)^3} \int_0^{\frac{L}{D}} \int_{\theta_1}^{\theta_2} (\alpha_r P_3 + \alpha_t P_4) \begin{Bmatrix} -\cos(\theta - \varphi_0) \\ \sin(\theta - \varphi_0) \end{Bmatrix} d\theta d\xi \quad (A39)$$

Noting, that the hydrodynamic moment is zero under static conditions, the restoring moment can be expressed as a first order Taylor series as

$$\begin{aligned} t_r &= Y_{rr} \alpha_r + Y_{rt} \alpha_t \\ t_t &= Y_{tr} \alpha_r + Y_{tt} \alpha_t \end{aligned} \quad (A40)$$

Comparing Eqs.(A39) and (A40), and making use of Eqs. (A24) and (A25), yields

$$\left. \begin{aligned} Y_{rr} \\ Y_{tr} \end{aligned} \right\} = \frac{1}{8\left(\frac{L}{D}\right)^3} \int_0^{\frac{L}{D}} \int_{\theta_1}^{\theta_2} \frac{1}{H_0} \left[\frac{Q_3}{\sqrt{Q_0}} - \frac{\sqrt{Q_0}}{H_0} \xi \cos(\theta - \varphi_0) \right] \begin{Bmatrix} -\cos(\theta - \varphi_0) \\ \sin(\theta - \varphi_0) \end{Bmatrix} d\theta d\xi \quad (A41)$$

$$\left. \begin{aligned} Y_{rt} \\ Y_{tt} \end{aligned} \right\} = \frac{1}{8\left(\frac{L}{D}\right)^3} \int_0^{\frac{L}{D}} \int_{\theta_1}^{\theta_2} \frac{1}{H_0} \left[\frac{Q_4}{\sqrt{Q_0}} - \frac{\sqrt{Q_0}}{H_0} \xi \sin(\theta - \varphi_0) \right] \begin{Bmatrix} -\cos(\theta - \varphi_0) \\ \sin(\theta - \varphi_0) \end{Bmatrix} d\theta d\xi \quad (A42)$$

In order to refer the dynamic coefficients to a coordinate system whose orientation is independent of a particular steady-state journal center position, a ξ - η coordinate system is introduced with origin at (ϵ_0, φ_0) and with the ξ -axis along the line of the static load on the pad (i.e. for a tilting pad, the ξ -axis passes through the pivot point). Let the journal center amplitudes, normalized with respect to the radial clearance, be ξ and η at the centerplane of the bearing. Hence, the transformation of the motion becomes

$$\begin{aligned}
(\varepsilon_0 + \varepsilon_1) \cos(\varphi_0 + \varphi_1) &= \varepsilon_0 \cos \varphi_0 + \xi \\
(\varepsilon_0 + \varepsilon_1) \sin(\varphi_0 + \varphi_1) &= \varepsilon_0 \sin \varphi_0 + \eta
\end{aligned}
\tag{A43}$$

or

$$\begin{aligned}
\varepsilon_1 &= \xi \cos \varphi_0 + \eta \sin \varphi_0 \\
\varepsilon_0 \varphi_1 &= -\xi \sin \varphi_0 + \eta \cos \varphi_0
\end{aligned}
\tag{A44}$$

Similarly, the dimensionless components of the total force acting on the journal are

$$f_\xi = \frac{F_\xi}{W} = 1 - \frac{f_r}{W} \cos \varphi_0 - \frac{f_t}{W} \sin \varphi_0 \tag{A45}$$

$$f_\eta = \frac{F_\eta}{W} = -\frac{f_r}{W} \sin \varphi_0 + \frac{f_t}{W} \cos \varphi_0 \tag{A46}$$

where W is the static pad load and $\bar{W} = W/p_a LD$

Expand f_ξ and f_η in first order Taylor series around the steady-state position:

$$\begin{aligned}
f_\xi &= -Z_{\xi\xi} \xi - Z_{\xi\eta} \eta \\
f_\eta &= -Z_{\eta\xi} \xi - Z_{\eta\eta} \eta
\end{aligned}
\tag{A47}$$

Substituting Eqs. (A35) and (A44) into Eqs. (A45) and (A46) and comparing with Eq. (A47), results in

$$\bar{W} = \frac{W}{p_a LD} = f_{r0} \cos \varphi_0 + f_{t0} \sin \varphi_0 = \sqrt{f_{r0}^2 + f_{t0}^2} \tag{A48}$$

$$\varphi_0 = \tan^{-1} \left(\frac{f_{t0}}{f_{r0}} \right) \tag{A49}$$

$$Z_{\xi\xi} = \frac{1}{\bar{W}} \left[(Z_{rr} \cos \varphi_0 + Z_{tr} \sin \varphi_0) \cos \varphi_0 - (Z_{rt} \cos \varphi_0 + Z_{tt} \sin \varphi_0) \sin \varphi_0 \right]$$

$$\begin{aligned}
Z_{\xi\eta} &= \frac{1}{W} [(Z_{rr} \cos \phi_0 + Z_{tr} \sin \phi_0) \sin \phi_0 + (Z_{rt} \cos \phi_0 + Z_{tt} \sin \phi_0) \cos \phi_0] \\
Z_{\eta\xi} &= \frac{1}{W} [(Z_{rr} \sin \phi_0 - Z_{tr} \cos \phi_0) \cos \phi_0 - (Z_{rt} \sin \phi_0 - Z_{tt} \cos \phi_0) \sin \phi_0] \\
Z_{\eta\eta} &= \frac{1}{W} [(Z_{rr} \sin \phi_0 - Z_{tr} \cos \phi_0) \sin \phi_0 + (Z_{rt} \sin \phi_0 - Z_{tt} \cos \phi_0) \cos \phi_0]
\end{aligned} \tag{A50}$$

Set

$$Z_{\xi\xi} = K_{\xi\xi} + i\gamma B_{\xi\xi} \tag{A51}$$

and similarly for $Z_{\xi\eta}$, $Z_{\eta\xi}$ and $Z_{\eta\eta}$. Next, let the actual journal center amplitudes be $\bar{\xi} = C\xi$ and $\bar{\eta} = C\eta$ and express the actual forces in their Taylor series expansion:

$$\begin{aligned}
F_{\xi} &= -\bar{K}_{\xi\xi} \bar{\xi} - \bar{B}_{\xi\xi} \frac{d\bar{\xi}}{dt} - \bar{K}_{\xi\eta} \bar{\eta} - \bar{B}_{\xi\eta} \frac{d\bar{\eta}}{dt} \\
F_{\eta} &= -\bar{K}_{\eta\xi} \bar{\xi} - \bar{B}_{\eta\xi} \frac{d\bar{\xi}}{dt} - \bar{K}_{\eta\eta} \bar{\eta} - \bar{B}_{\eta\eta} \frac{d\bar{\eta}}{dt}
\end{aligned} \tag{A52}$$

Since $\bar{\xi}$ and $\bar{\eta}$ are amplitudes of a harmonic motion with frequency ν , $\frac{d\bar{\xi}}{dt} = i\nu\bar{\xi}$ and $\frac{d\bar{\eta}}{dt} = i\nu\bar{\eta}$. Thus, comparing Eqs. (A47) and (A52) and making use of Eq. (A51), the dimensionless coefficients can be expressed as

$$K_{\xi\xi} = \frac{C\bar{K}_{\xi\xi}}{W} \tag{A53}$$

$$B_{\xi\xi} = \frac{C\omega\bar{B}_{\xi\xi}}{W} \tag{A54}$$

and analogously for $K_{\xi\eta}$, $B_{\xi\eta}$, etc.

The derivation of the dynamic moment coefficients follows the same lines. Let the moment acting on the journal in the ξ -plane be T_{ξ} and in the η -plane T_{η} . Then,

$$\begin{aligned}
t_{\xi} &= \frac{RT_{\xi}}{WL^3} = -\frac{t_r}{W} \cos \phi_0 - \frac{t_t}{W} \sin \phi_0 \\
t_{\eta} &= \frac{RT_{\eta}}{WL^3} = -\frac{t_r}{W} \sin \phi_0 + \frac{t_t}{W} \cos \phi_0
\end{aligned} \tag{A55}$$

The angular displacements of the journal axis are $\frac{d\bar{\xi}}{dz}$ and $\frac{d\bar{\eta}}{dz}$. In dimensionless form they are related to the angular displacements α_r and α_t by relationships similar to Eq. (A44):

$$\begin{aligned}\alpha_r &= \frac{d\bar{\xi}}{d\bar{\zeta}} \cos \phi_0 + \frac{d\bar{\eta}}{d\bar{\zeta}} \sin \phi_0 \\ \alpha_t &= -\frac{d\bar{\xi}}{d\bar{\zeta}} \sin \phi_0 + \frac{d\bar{\eta}}{d\bar{\zeta}} \cos \phi_0\end{aligned}\quad (\text{A56})$$

Thus, if t_ξ and t_η are expanded in Taylor series as

$$\begin{aligned}t_\xi &= -Y_{\xi\xi} \frac{d\bar{\xi}}{d\bar{\zeta}} - Y_{\xi\eta} \frac{d\bar{\eta}}{d\bar{\zeta}} \\ t_\eta &= -Y_{\eta\xi} \frac{d\bar{\xi}}{d\bar{\zeta}} - Y_{\eta\eta} \frac{d\bar{\eta}}{d\bar{\zeta}}\end{aligned}\quad (\text{A57})$$

the Y-coefficients can be determined by substituting Eqs. (A40) and (A56) into Eq. (A55) and comparing with Eq. (A57). The resulting expressions are identical to Eqs. (A50) with Z everywhere replaced by Y.

Define

$$Y_{\xi\xi} = G_{\xi\xi} + i\gamma D_{\xi\xi} \quad (\text{A58})$$

and similarly for $Y_{\xi\eta}$, $Y_{\eta\xi}$ and $Y_{\eta\eta}$. To express these dimensionless coefficients in terms of actual coefficients, expand the moments T_ξ and T_η into Taylor series:

$$\begin{aligned}T_\xi &= -\bar{G}_{\xi\xi} \left(\frac{d\bar{\xi}}{dz} \right) - \bar{D}_{\xi\xi} \frac{d}{dt} \left(\frac{d\bar{\xi}}{dz} \right) - \bar{G}_{\xi\eta} \left(\frac{d\bar{\eta}}{dz} \right) - \bar{D}_{\xi\eta} \frac{d}{dt} \left(\frac{d\bar{\eta}}{dz} \right) \\ T_\eta &= -\bar{G}_{\eta\xi} \left(\frac{d\bar{\xi}}{dz} \right) - \bar{D}_{\eta\xi} \frac{d}{dt} \left(\frac{d\bar{\xi}}{dz} \right) - \bar{G}_{\eta\eta} \left(\frac{d\bar{\eta}}{dz} \right) - \bar{D}_{\eta\eta} \frac{d}{dt} \left(\frac{d\bar{\eta}}{dz} \right)\end{aligned}\quad (\text{A59})$$

For a harmonic motion $\frac{d}{dt} \left(\frac{d\bar{\xi}}{dz} \right) = i\nu \frac{d\bar{\xi}}{dz}$ and similarly for $\frac{d\bar{\eta}}{dz}$. Hence, by comparing Eqs. (A57) and (A59), the dimensionless coefficients become

$$G_{\xi\xi} = \frac{C \bar{G}_{\xi\xi}}{W L^2} \quad (A60)$$

$$D_{\xi\xi} = \frac{C \omega \bar{D}_{\xi\xi}}{W L^2} \quad (A61)$$

and analogously for $G_{\xi\eta}$, $D_{\xi\eta}$, etc.

APPENDIX B: The Numerical Solution of the Steady-State Gas Film Pressures
by Finite Difference Equations

Reynolds' equation for steady-state operating conditions is derived in Appendix A where it is given in dimensionless form by Eq. (A26). The independent variable is Q_0 which defines the film pressure by means of Eq. (A21). It is seen, that Reynolds' equation is non-linear since $\sqrt{Q_0}$ appears in the coefficient to $\frac{\partial Q_0}{\partial \theta}$. Thus, the equation is solved by iteration. An initial guess of $\sqrt{Q_0} = H_0$ is made after which Reynolds' equation becomes linear and can be solved as described in the following. Having obtained a first approximation to the solution, a new value of $\sqrt{Q_0}$ can be computed and used for a second calculation of Reynolds' equation. This process is repeated until the difference between two successive iterations is smaller than an arbitrarily specified error.

With $\sqrt{Q_0}$ given for any one particular calculation, Reynolds' equation is converted into a finite difference equation and solved numerically. Set

$$f_4 = -\frac{1}{H_0} \left(\frac{\partial H_0}{\partial \theta} + \frac{1}{\sqrt{Q_0}} \right) \quad (B1)$$

$$f_5 = -\frac{2}{H_0} \frac{\partial^2 H_0}{\partial \theta^2} \quad (B2)$$

whereby Eq. (A26) can be written as

$$\frac{\partial^2 Q_0}{\partial \theta^2} + \frac{\partial^2 Q_0}{\partial \xi^2} + f_4 \frac{\partial Q_0}{\partial \theta} + f_5 Q_0 = 0 \quad (B3)$$

Introduce a finite difference grid with j-axis along the θ -direction and with i-axis in the negative ξ -direction such that $j = 1$ at the leading edge, $j = M$ at the trailing edge, $i = 1$ at the side of the pad and $i = N$ at the centerplane of the bearing. There are m increments in the j-direction and n increments in the i-direction where

$$\begin{aligned} m &= M - 1 \\ n &= N - 1 \end{aligned} \quad (B4)$$

The length of the increments are given by

$$\Delta\theta = \frac{\theta_2 - \theta_1}{m} \quad (\text{B5})$$

$$\Delta\zeta = \left(\frac{L}{D}\right)/n \quad (\text{B6})$$

Hence, dropping the subscript 0 for Q_0 , Eq. (B3) can be written in finite difference form as

$$\begin{aligned} \frac{1}{\Delta\zeta^2} Q_{i-1,j} + \left((f_5)_{ij} - \frac{2}{\Delta\zeta^2} - \frac{2}{\Delta\theta^2} \right) Q_{ij} + \frac{1}{\Delta\zeta^2} Q_{i+1,j} + \left(\frac{1}{\Delta\theta^2} - \frac{1}{2\Delta\theta} (f_4)_{ij} \right) Q_{i,j-1} \\ + \left(\frac{1}{\Delta\theta^2} + \frac{1}{2\Delta\theta} (f_4)_{ij} \right) Q_{i,j+1} = 0 \end{aligned} \quad (\text{B7})$$

For a particular value of j this equation can be written in matrix form as

$$A_j \phi_j + B_j \phi_{j-1} + C_j \phi_{j+1} = F_j \quad (\text{B8})$$

where A_j , B_j and C_j are square matrices, and F_j and ϕ_j are column vectors. To set up these matrices, introduce the boundary conditions given in Appendix A in Eqs. (A31) and (A32). In finite difference form, the conditions for Q_0 in the i -direction are

$$\underline{i=1 \quad (\zeta = \frac{L}{D})} : \quad Q_{1,j} = H_0^2 \quad (\text{note: } H_0 \text{ is independent of } i) \quad (\text{B9})$$

$$\underline{i=N \quad (\zeta = 0)} : \quad Q_{N+1,j} = Q_{N-1,j} \quad (\text{B10})$$

With these conditions, Eqs. (B7) and (B8) can be used to determine the matrix elements. The matrices become

$$\phi_j = \begin{Bmatrix} Q_{2,j} \\ Q_{3,j} \\ \vdots \\ Q_{N,j} \end{Bmatrix}_n \quad (\text{B11})$$

$$A_j = \left\{ \begin{array}{cccccc} ((f_5)_{2,j} - \frac{2}{\Delta f^2} - \frac{2}{\Delta \theta^2}) & \frac{1}{\Delta f^2} & 0 & 0 & \cdots & 0 \\ \frac{1}{\Delta f^2} & ((f_5)_{3,j} - \frac{2}{\Delta f^2} - \frac{2}{\Delta \theta^2}) & \frac{1}{\Delta f^2} & 0 & \cdots & 0 \\ \vdots & \vdots & \vdots & \vdots & \ddots & \vdots \\ 0 & \cdots & 0 & \frac{2}{\Delta f^2} & ((f_5)_{N,j} - \frac{2}{\Delta f^2} - \frac{2}{\Delta \theta^2}) & \end{array} \right\}_{n \times n} \quad (B12)$$

$$B_j = \left\{ \begin{array}{cccccc} (\frac{1}{\Delta \theta^2} - \frac{1}{2\Delta \theta} (f_4)_{2,j}) & 0 & 0 & \cdots & \cdots & 0 \\ 0 & (\frac{1}{\Delta \theta^2} - \frac{1}{2\Delta \theta} (f_4)_{3,j}) & 0 & \cdots & \cdots & 0 \\ \vdots & \vdots & \vdots & \ddots & \vdots & \vdots \\ 0 & \cdots & 0 & (\frac{1}{\Delta \theta^2} - \frac{1}{2\Delta \theta} (f_4)_{N,j}) & \end{array} \right\}_{n \times n} \quad (B13)$$

$$C_j = \left\{ \begin{array}{cccccc} (\frac{1}{\Delta \theta^2} + \frac{1}{2\Delta \theta} (f_4)_{2,j}) & 0 & 0 & \cdots & \cdots & 0 \\ 0 & (\frac{1}{\Delta \theta^2} + \frac{1}{2\Delta \theta} (f_4)_{3,j}) & 0 & \cdots & \cdots & 0 \\ \vdots & \vdots & \vdots & \ddots & \vdots & \vdots \\ 0 & \cdots & 0 & (\frac{1}{\Delta \theta^2} + \frac{1}{2\Delta \theta} (f_4)_{N,j}) & \end{array} \right\}_{n \times n} \quad (B14)$$

$$F_j = \left\{ \begin{array}{c} -\frac{1}{\Delta f^2} H_{0j}^2 \\ 0 \\ \vdots \\ 0 \end{array} \right\}_n \quad (B15)$$

Hence, ϕ_j is the independent variable whereas the other matrices are known. To solve Eq. (B8), define a recurrence relationship:

$$\phi_{j-1} = D_{j-1} \phi_j + E_{j-1} \quad (\text{B16})$$

where D_j is an $n \times n$ square matrix and E_j is a column vector. Letting this equation define D_j and E_j , substitute Eq. (B16) into Eq. (B8) to get

$$D_j = -(A_j + B_j D_{j-1})^{-1} C_j \quad (\text{B17})$$

$$E_j = (A_j + B_j D_{j-1})^{-1} (F_j - B_j E_{j-1}) \quad (\text{B18})$$

These two equations establish recurrence relationships for the D-matrices and the E-vectors. Before they can be used, however, the boundary conditions in the j-direction must be introduced. They derive from Eq. (A31) in Appendix A.

$$\underline{j=1 \quad (\theta=\theta_1)}: \quad Q_{i,1} = H_{0,1}^2 \quad (\text{B19})$$

$$\underline{j=M \quad (\theta=\theta_2)}: \quad Q_{i,M} = H_{0,M}^2 \quad (\text{B20})$$

Eq. (B19) can be satisfied by setting (see Eq. (B8)):

$$A_1 = \text{identity matrix}$$

$$B_1 = C_1 = 0$$

$$F_1 = \begin{Bmatrix} H_{0,1}^2 \\ \vdots \\ H_{0,1}^2 \end{Bmatrix}_n = \phi_1 \quad (\text{B21})$$

Hence, from Eq. (B17) and (B18),

$$D_1 = 0$$

$$E_1 = F_1 = \phi_1$$

(B22)

Thus, Eqs. (B17) and (B18) can be used to compute D_j and E_j step by step, letting j go from $j = 2$ to $j = m = M-1$. Since from Eq. (B20),

$$\phi_M = \begin{Bmatrix} H_{o,M}^2 \\ \vdots \\ H_{c,M}^2 \end{Bmatrix} \quad (\text{B23})$$

Eq. (B16) allows computing ϕ_{j-1} by letting j go from $j = M$ to $j = 3$. In this way, all the vectors ϕ_j have been obtained and, thereby, Q_o is known at all gridpoints.

The convergence of the iterative procedure, iterating on $\sqrt{Q_o}$, is achieved when

$$\max. \left\{ \frac{|Q_{ij}^{(k)} - Q_{ij}^{(k-1)}|}{Q_{ij}^{(k)}} \right\} \leq \text{specified error} \quad (\text{B24})$$

where k gives the iteration number.

Once Q_o is computed, the static load on the pad is calculated by integrating the film pressures. The dimensionless force components, f_{ro} and f_{to} , are given in Appendix A, Eq. (A36). The integration is performed numerically, using Simpson's rule of integration. The dimensionless pad load $\bar{W} = W/p_a LD$ and the steady-state attitude angle φ_o are then found from Eqs. (A48) and (A49).

APPENDIX C: The Numerical Calculation of the Dynamic Coefficients for the Pad Gas Journal Bearing

To compute the dynamic coefficients for the pad, it is necessary to solve for the four perturbed, dimensionless pressures (Q_1, Q_2, Q_3 , and Q_4) as described in Appendix A. The four variables are given by Eqs. (A27) to (A30). These equations have the common form,

$$\frac{\partial^2 q}{\partial \theta^2} + \frac{\partial^2 q}{\partial \zeta^2} + f_4 \frac{\partial q}{\partial \theta} + (f_5 + if_6) q = f_7 \quad (C1)$$

where

$$f_4 = -\frac{1}{H_0} \left(\frac{\partial H_0}{\partial \theta} + \frac{\Lambda}{\sqrt{Q_0}} \right) \quad (C2)$$

$$f_5 = -\frac{1}{H_0} \left(2 \frac{\partial^2 H_0}{\partial \theta^2} - \frac{\Lambda}{2 Q_0^{3/2}} \frac{\partial Q_0}{\partial \theta} \right) \quad (C3)$$

$$f_6 = -\frac{1}{H_0} \frac{2\gamma\Lambda}{\sqrt{Q_0}} \quad (C4)$$

and f_7 stands for the right-hand side of Eqs. (A27) to (A30). It is seen that f_7 is a function of Q_0 .

Introduce a finite difference grid with j -axis along the θ -direction and i -axis in the negative ζ -direction such that $j = 1$ at the leading edge ($\theta = \theta_1$), $j = M$ at the trailing edge ($\theta = \theta_2$), $i = 1$ at the side of the pad ($\zeta = \frac{L}{D}$) and $i = N$ at the centerplane of the bearing ($\zeta = 0$). There are $m = (M-1)$ increments in the j -direction and $n = (N-1)$ increments in the i -direction. The increments are

$$\Delta \theta = \frac{\theta_2 - \theta_1}{m} \quad (C5)$$

$$\Delta \zeta = \left(\frac{L}{D} \right) / n \quad (C6)$$

Thereby Eq. (C1) can be written on finite difference form as

$$\begin{aligned} \frac{1}{\Delta \zeta^2} q_{i-1,j} + (f_{5ij} + i f_{6ij} - \frac{2}{\Delta \zeta^2} - \frac{2}{\Delta \theta^2}) q_{ij} + \frac{1}{\Delta \zeta^2} q_{i+1,j} + (\frac{1}{\Delta \theta^2} - \frac{1}{2\Delta \theta} f_{4ij}) q_{i,j-1} \\ + (\frac{1}{\Delta \theta^2} + \frac{1}{2\Delta \theta} f_{4ij}) q_{i,j+1} = f_{7ij} \end{aligned} \quad (C7)$$

For a particular value of j , this equation can be written in matrix form as

$$[U_j + iV_j] \phi_j + B_j \phi_{j-1} + C_j \phi_{j+1} = F_j \quad (C8)$$

where U_j , V_j , B_j , and C_j are square matrices, and F_j and ϕ_j are column vectors. ϕ_j is complex:

$$\phi_j = \varphi_j + i\psi_j \quad (C9)$$

where φ_j and ψ_j are column vectors.

To set up the matrices in Eq. (C8), the boundary conditions given by Eqs. (A31) and (A32), Appendix A, are used. These equations specify the values of q along the periphery of the pad such that q_{1j} , q_{i1} and q_{iM} are known. Furthermore, from Eq. (A32),

$$\text{for } Q_1 \text{ and } Q_2: \quad q_{N+1,j} = q_{N-1,j}$$

$$\text{for } Q_3 \text{ and } Q_4: \quad q_{Nj} = 0$$

Thus, the matrices can be determined from Eqs. (C7) and (C8):

$$\varphi_j = \text{Re} \left\{ \begin{matrix} q_{2j} \\ q_{3j} \\ \vdots \\ q_{Nj} \end{matrix} \right\}_n \quad (C10)$$

$$\psi_j = \text{Im} \left\{ \begin{matrix} q_{2j} \\ q_{3j} \\ \vdots \\ q_{Nj} \end{matrix} \right\}_n \quad (C11)$$

For $q = Q_1$ and $q = Q_2$,

$$\bar{F}_j = \left\{ \begin{array}{c} (f_7)_{2,j} - \frac{1}{\Delta \gamma^2} q_{1,j} \\ (f_7)_{3,j} \\ \vdots \\ (f_7)_{N,j} \end{array} \right\}_n \quad (C12)$$

$$U_j = \left\{ \begin{array}{cccccc} ((f_5)_{2,j} - \frac{2}{\Delta \gamma^2} - \frac{2}{\Delta \theta^2}) & \frac{1}{\Delta \gamma^2} & 0 & \cdots & \cdots & 0 \\ \frac{1}{\Delta \gamma^2} & ((f_5)_{3,j} - \frac{2}{\Delta \gamma^2} - \frac{2}{\Delta \theta^2}) & \frac{1}{\Delta \gamma^2} & \cdots & \cdots & 0 \\ \vdots & \vdots & \vdots & \ddots & \ddots & \vdots \\ 0 & \cdots & 0 & \frac{2}{\Delta \gamma^2} & ((f_5)_{N,j} - \frac{2}{\Delta \gamma^2} - \frac{2}{\Delta \theta^2}) & \end{array} \right\}_{n \times n} \quad (C13)$$

$$V_j = \left\{ \begin{array}{cccc} (f_6)_{2,j} & 0 & \cdots & 0 \\ 0 & (f_6)_{3,j} & \cdots & 0 \\ \vdots & \vdots & \ddots & \vdots \\ 0 & \cdots & \cdots & (f_6)_{N,j} \end{array} \right\}_{n \times n} \quad (C14)$$

$$B_j = \left\{ \begin{array}{cccc} (\frac{1}{\Delta \theta^2} - \frac{1}{2\Delta \theta} (f_4)_{2,j}) & 0 & \cdots & 0 \\ 0 & (\frac{1}{\Delta \theta^2} - \frac{1}{2\Delta \theta} (f_4)_{3,j}) & \cdots & 0 \\ \vdots & \vdots & \ddots & \vdots \\ 0 & \cdots & \cdots & (\frac{1}{\Delta \theta^2} - \frac{1}{2\Delta \theta} (f_4)_{N,j}) \end{array} \right\}_{n \times n} \quad (C15)$$

$$C_j = \left\{ \begin{array}{cccc} (\frac{1}{\Delta \theta^2} + \frac{1}{2\Delta \theta} (f_4)_{2,j}) & 0 & \cdots & 0 \\ 0 & (\frac{1}{\Delta \theta^2} + \frac{1}{2\Delta \theta} (f_4)_{3,j}) & \cdots & 0 \\ \vdots & \vdots & \ddots & \vdots \\ 0 & \cdots & \cdots & (\frac{1}{\Delta \theta^2} + \frac{1}{2\Delta \theta} (f_4)_{N,j}) \end{array} \right\}_{n \times n} \quad (C16)$$

For $q = Q_3$ and $q = Q_4$, reduce the size of the U_j , V_j , B_j and C_j matrices to $(n-1) \times (n-1)$ by deleting the last row and the last column in each matrix. Furthermore, reduce F_j to a $(n-1)$ -vector by deleting the last element.

In this way, Eq. (C8) establishes a matrix equation for determining the unknown $\phi_j = \varphi_j + i\psi_j$. Define the recurrence relationships:

$$\phi_{j-1} = D_{j-1} \phi_j - G_{j-1} \psi_j + E_{j-1} \quad (C17)$$

$$\psi_{j-1} = G_{j-1} \phi_j + D_{j-1} \psi_j + H_{j-1}$$

where D_j and G_j are square matrices, and E_j and H_j are column vectors. Letting these equations define D_j , G_j , E_j and H_j , substitute Eq. (C17) into Eq. (C8) to get

$$D_j = -L_{j-1} C_j \quad (C18)$$

$$G_j = K_{j-1} C_j \quad (C19)$$

$$E_j = L_{j-1} [F_j - B_j E_{j-1}] - K_{j-1} B_j H_{j-1} \quad (C20)$$

$$H_j = -K_{j-1} [F_j - B_j E_{j-1}] - L_{j-1} B_j H_{j-1} \quad (C21)$$

where

$$K_{j-1} = (T_{j-1}^{-1} S_{j-1} + S_{j-1}^{-1} T_{j-1})^{-1} S_{j-1}^{-1} \quad (C22)$$

$$L_{j-1} = (T_{j-1}^{-1} S_{j-1} + S_{j-1}^{-1} T_{j-1})^{-1} T_{j-1}^{-1} \quad (C23)$$

$$S_{j-1} = U_j + B_j D_{j-1} \quad (C24)$$

$$T_{j-1} = V_j + B_j G_{j-1} \quad (C25)$$

Eqs. (C18) to (C21) establish recurrence formulas for calculating D_j , G_j , E_j and H_j . Since q_{i1} is on the leading edge and known from Eq. (A31), Eq. (C17) shows that

$$D_i = G_i = H_i = 0 \quad (C26)$$

$$E_i = \begin{Bmatrix} q_{2,i} \\ q_{3,i} \\ \vdots \\ q_{N,i} \end{Bmatrix} = \phi_i \quad (C27)$$

Thus Eqs. (C18) to (C21) can be used to calculate D_j , G_j , E_j and H_j , letting j go from $j = 2$ to $j = m = M-1$. Next, with q_{iM} given by Eq. (A31), the condition at the trailing edge is

$$\phi_M = \begin{Bmatrix} q_{2,M} \\ q_{3,M} \\ \vdots \\ q_{N,M} \end{Bmatrix} \quad \psi_M = 0 \quad (C28)$$

Thereby Eq. (C17) can be employed to compute ϕ_{j-1} and ψ_{j-1} , letting j go from $j = M$ to $j = 3$, and in this way q_{ij} is obtained at all gridpoints as a complex quantity. Finally, the 8 dynamic coefficients are calculated by a numerical integration of q as defined by Eqs. (A37), (A38), (A41) and (A42), Appendix A.

APPENDIX D: The Dynamic Coefficients and the Response of the Shoes in a Tilting Pad Journal Bearing

When the static bearing reaction is known and the rotor speed is specified, the corresponding static inclination of each shoe in the tilting-pad bearing can be determined. Hence, the steady-state operating eccentricity ratio is known for each shoe and also the corresponding dynamic gas film coefficients as shown in Appendix A, i.e., $\bar{Z}_{\xi\xi}$, $\bar{Z}_{\xi\eta}$, $\bar{Z}_{\eta\xi}$ and $\bar{Z}_{\eta\eta}$ are known. These coefficients, however, must be modified to account for the dynamic motion of the shoe where the shoe pitches on its pivot and is flexibly mounted in the radial direction.

Consider as previously done in Appendix A, a ξ - η -coordinate system with origin in the steady-state journal center position and with the ξ -axis passing through the pivot point. The journal center dynamic amplitudes are $\bar{\xi}$ and $\bar{\eta}$, the center of the pad arc has the amplitude $\bar{\eta}_p$ and the pad has the radial amplitude $\bar{\xi}_p$. When the pad mass is m_p , the mass moment of inertia of the pad is I_p around an axial axis passing through the pivot point (the pitch axis) and the stiffness of the flexible mount is K_p , the equations of motion for the pad are

$$m_p \frac{d^2 \bar{\xi}_p}{dt^2} = \bar{K}_{\xi\xi} (\bar{\xi} - \bar{\xi}_p) + \bar{B}_{\xi\xi} \frac{d}{dt} (\bar{\xi} - \bar{\xi}_p) + \bar{K}_{\xi\eta} (\bar{\eta} - \bar{\eta}_p) + \bar{B}_{\xi\eta} \frac{d}{dt} (\bar{\eta} - \bar{\eta}_p) - K_p \bar{\xi}_p \quad (D1)$$

$$\frac{I_p}{R^2} \frac{d^2 \bar{\eta}_p}{dt^2} = \bar{K}_{\eta\xi} (\bar{\xi} - \bar{\xi}_p) + \bar{B}_{\eta\xi} \frac{d}{dt} (\bar{\xi} - \bar{\xi}_p) + \bar{K}_{\eta\eta} (\bar{\eta} - \bar{\eta}_p) + \bar{B}_{\eta\eta} \frac{d}{dt} (\bar{\eta} - \bar{\eta}_p) \quad (D2)$$

where R is the pad radius. Assume the motion to be harmonic with frequency ν and define a complex notation by

$$\bar{\xi} = \bar{\xi}_r + i \bar{\xi}_i \quad (D-3)$$

which is an abbreviated form of

$$\bar{\xi} = \text{Re} \{ (\bar{\xi}_r + i \bar{\xi}_i) e^{i\nu t} \} = \bar{\xi}_r \cos(\nu t) - \bar{\xi}_i \sin(\nu t) \quad (D-4)$$

and similarly for $\bar{\eta}, \bar{\eta}_P$ and $\bar{\xi}_P$. Thus, Eqs. (D-1) and (D-2) can be written:

$$(K_P - \nu^2 m_P) \bar{\xi}_P = \bar{Z}_{\xi\xi} (\bar{\xi} - \bar{\xi}_P) + \bar{Z}_{\xi\eta} (\bar{\eta} - \bar{\eta}_P) \quad (D-5)$$

$$-\nu^2 \frac{I_P}{R^2} \bar{\eta}_P = \bar{Z}_{\eta\xi} (\bar{\xi} - \bar{\xi}_P) + \bar{Z}_{\eta\eta} (\bar{\eta} - \bar{\eta}_P) \quad (D-6)$$

where $\bar{Z}_{\xi\xi}, \bar{Z}_{\xi\eta}$, etc., are defined as

$$\bar{Z}_{\xi\xi} = \bar{K}_{\xi\xi} + i\nu \bar{B}_{\xi\xi} \quad (D-7)$$

etc., These equations are readily solved to get:

$$\begin{aligned} \bar{\xi} - \bar{\xi}_P &= \alpha_{\xi\xi} \bar{\xi} + \alpha_{\xi\eta} \bar{\eta} \\ \bar{\eta} - \bar{\eta}_P &= \alpha_{\eta\xi} \bar{\xi} + \alpha_{\eta\eta} \bar{\eta} \end{aligned} \quad (D-8)$$

where:

$$\begin{aligned} \alpha_{\xi\xi} &= \frac{1}{A} (K_P - \nu^2 m_P) (\bar{Z}_{\eta\eta} - \nu^2 \frac{I_P}{R^2}) \\ \alpha_{\xi\eta} &= \frac{1}{A} \nu^2 \frac{I_P}{R^2} \bar{Z}_{\xi\eta} \\ \alpha_{\eta\xi} &= -\frac{1}{A} (K_P - \nu^2 m_P) \bar{Z}_{\eta\xi} \\ \alpha_{\eta\eta} &= -\frac{1}{A} \nu^2 \frac{I_P}{R^2} (\bar{Z}_{\xi\xi} + K_P - \nu^2 m_P) \\ A &= (\bar{Z}_{\xi\xi} + K_P - \nu^2 m_P) (\bar{Z}_{\eta\eta} - \nu^2 \frac{I_P}{R^2}) - \bar{Z}_{\xi\eta} \bar{Z}_{\eta\xi} \end{aligned} \quad (D-9)$$

The forces acting on the journal are of course the same as the ones acting on the pad, see eqs. (D-5) and (D-6). Hence,

$$\begin{aligned} F_{\xi} &= -\bar{Z}_{\xi\xi}(\bar{\xi}-\bar{\xi}_p) - \bar{Z}_{\xi\eta}(\bar{\eta}-\bar{\eta}_p) = -\bar{Z}'_{\xi\xi}\bar{\xi} - \bar{Z}'_{\xi\eta}\bar{\eta} \\ F_{\eta} &= -\bar{Z}_{\eta\xi}(\bar{\xi}-\bar{\xi}_p) - \bar{Z}_{\eta\eta}(\bar{\eta}-\bar{\eta}_p) = -\bar{Z}'_{\eta\xi}\bar{\xi} - \bar{Z}'_{\eta\eta}\bar{\eta} \end{aligned} \quad (D-10)$$

where the coefficients on the right hand side are found by substitution from Eqs. (D-8) as:

$$\begin{aligned} \bar{Z}'_{\xi\xi} &= \alpha_{\xi\xi}\bar{Z}_{\xi\xi} + \alpha_{\eta\xi}\bar{Z}_{\xi\eta} \\ \bar{Z}'_{\xi\eta} &= \alpha_{\xi\eta}\bar{Z}_{\xi\xi} + \alpha_{\eta\eta}\bar{Z}_{\xi\eta} \\ \bar{Z}'_{\eta\xi} &= \alpha_{\xi\xi}\bar{Z}_{\eta\xi} + \alpha_{\eta\xi}\bar{Z}_{\eta\eta} \\ \bar{Z}'_{\eta\eta} &= \alpha_{\xi\eta}\bar{Z}_{\eta\xi} + \alpha_{\eta\eta}\bar{Z}_{\eta\eta} \end{aligned} \quad (D-11)$$

These coefficients then make it possible to express the pad reactions F_{ξ} and F_{η} directly in terms of the journal center amplitudes $\bar{\xi}$ and $\bar{\eta}$ by means of Eqs. (D-10). However, the coefficients from all the pads must be combined in order to represent the composite bearing by a single set of coefficients. For this purpose, introduce an x-y-coordinate system with origin in the steady-state position of the journal center, the x-axis in the load direction and the y-axis perpendicular to this direction. When the angle between the negative x-axis and the ξ -axis for the k 'th pad is ψ_k , the transformation equations are

$$\begin{Bmatrix} \bar{\xi} \\ \bar{\eta} \end{Bmatrix} = - \begin{Bmatrix} \cos\psi_k & \sin\psi_k \\ -\sin\psi_k & \cos\psi_k \end{Bmatrix} \begin{Bmatrix} \bar{x} \\ \bar{y} \end{Bmatrix} \quad \begin{Bmatrix} F_{xk} \\ F_{yk} \end{Bmatrix} = - \begin{Bmatrix} \cos\psi_k & -\sin\psi_k \\ \sin\psi_k & \cos\psi_k \end{Bmatrix} \begin{Bmatrix} F_{\xi} \\ F_{\eta} \end{Bmatrix} \quad (D-12)$$

where \bar{x} and \bar{y} are the journal center amplitudes, and F_{xk} and F_{yk} are the dynamic forces by which the pad film acts on the journal. When the total bearing reactions are F_x and F_y , they can be written

$$\begin{aligned} F_x &= \sum_k F_{xk} = -\bar{Z}_{xx}\bar{x} - \bar{Z}_{xy}\bar{y} \\ F_y &= \sum_k F_{yk} = -\bar{Z}_{yx}\bar{x} - \bar{Z}_{yy}\bar{y} \end{aligned} \quad (D-13)$$

where \bar{z}_{xx} , \bar{z}_{xy} , etc., then represent the complete tilting pad bearing. They are found by substituting Eqs. (D-10) and (D-12) into Eq. (D-13) to get:

$$\begin{aligned}\bar{z}_{xx} &= \sum_k [\bar{z}'_{ff} \cos^2 \psi_k + \bar{z}'_{\eta\eta} \sin^2 \psi_k - (\bar{z}'_{f\eta} + \bar{z}'_{\eta f}) \cos \psi_k \sin \psi_k]_k \\ \bar{z}_{xy} &= \sum_k [\bar{z}'_{f\eta} \cos^2 \psi_k - \bar{z}'_{\eta f} \sin^2 \psi_k + (\bar{z}'_{ff} - \bar{z}'_{\eta\eta}) \cos \psi_k \sin \psi_k]_k \\ \bar{z}_{yx} &= \sum_k [\bar{z}'_{\eta f} \cos^2 \psi_k - \bar{z}'_{f\eta} \sin^2 \psi_k + (\bar{z}'_{ff} - \bar{z}'_{\eta\eta}) \cos \psi_k \sin \psi_k]_k \\ \bar{z}_{yy} &= \sum_k [\bar{z}'_{\eta\eta} \cos^2 \psi_k + \bar{z}'_{ff} \sin^2 \psi_k + (\bar{z}'_{f\eta} + \bar{z}'_{\eta f}) \cos \psi_k \sin \psi_k]_k\end{aligned}\quad (D-14)$$

These coefficients can be used directly in the calculation of rotor response and rotor stability as discussed later.

Once the rotor amplitudes \bar{x} and \bar{y} have been calculated, they can be transformed into $\bar{\xi}$ and $\bar{\eta}$ components by Eqs. (D-12) for each pad, and Eqs. (D-8) can then be used to determine the pad motion represented by the radial amplitude $\bar{\xi}_p$ and the pitch amplitude $\bar{\eta}_p$.

Similarly, in the rotor response calculation the slope amplitudes $d\bar{x}/dz$ and $d\bar{y}/dz$ are computed. By means of Eqs. (D-12) they can be transformed into $d\bar{\xi}/dz$ and $d\bar{\eta}/dz$, and the moments acting on the pad become (see Appendix A, Eqs. (A-58) and (A-59)):

$$T_{\bar{\xi}} = Y_{ff} \left[\frac{d\bar{\xi}}{dz} - \left(\frac{d\bar{\xi}}{dz} \right)_p \right] + Y_{f\eta} \left[\frac{d\bar{\eta}}{dz} - \left(\frac{d\bar{\eta}}{dz} \right)_p \right] \quad (D-15)$$

$$T_{\bar{\eta}} = Y_{\eta f} \left[\frac{d\bar{\xi}}{dz} - \left(\frac{d\bar{\xi}}{dz} \right)_p \right] + Y_{\eta\eta} \left[\frac{d\bar{\eta}}{dz} - \left(\frac{d\bar{\eta}}{dz} \right)_p \right]$$

where the Y-coefficients are calculated as shown in Appendix A, and $\left(\frac{d\bar{\xi}}{dz} \right)_p$ and $\left(\frac{d\bar{\eta}}{dz} \right)_p$ are the roll and yaw amplitudes of the pad, respectively. The roll and yaw axes pass through the pivot point, the roll axis is tangential to the pad and the yaw axis is in the radial direction. The corresponding mass moments of inertia of the pad are I_{η} and $I_{\bar{\xi}}$, respectively. Hence, the equations of motion can be derived similarly to Eqs. (D-5) and (D-6) and become

$$\begin{aligned}-\nu^2 I_{\eta} \left(\frac{d\bar{\xi}}{dz} \right)_p &= T_{\bar{\xi}} \\ -\nu^2 I_{\bar{\xi}} \left(\frac{d\bar{\eta}}{dz} \right)_p &= T_{\bar{\eta}}\end{aligned}\quad (D-16)$$

Introducing T_{ξ} and T_{η} from Eq. (D-15) the solution can be expressed analogously to Eqs. (D-8) as

$$\begin{aligned}\frac{d\bar{\xi}}{dz} - \left(\frac{d\bar{\xi}}{dz}\right)_p &= \alpha'_{\xi\xi} \frac{d\bar{\xi}}{dz} + \alpha'_{\xi\eta} \frac{d\bar{\eta}}{dz} \\ \frac{d\bar{\eta}}{dz} - \left(\frac{d\bar{\eta}}{dz}\right)_p &= \alpha'_{\eta\xi} \frac{d\bar{\xi}}{dz} + \alpha'_{\eta\eta} \frac{d\bar{\eta}}{dz}\end{aligned}\quad (D-17)$$

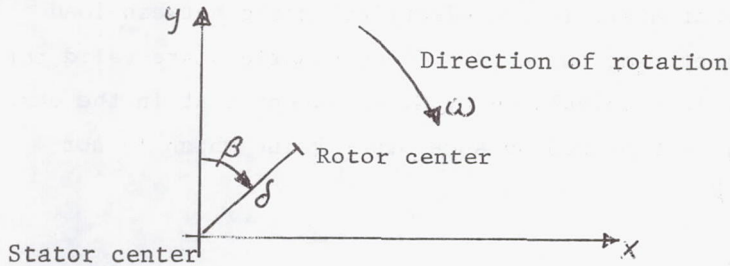
where

$$\begin{aligned}\alpha'_{\xi\xi} &= -\frac{1}{A'} (\bar{Y}_{\eta\eta} - \nu^2 I_{\xi}) \nu^2 I_{\eta} \\ \alpha'_{\xi\eta} &= \frac{1}{A'} \nu^2 I_{\xi} \bar{Y}_{\xi\eta} \\ \alpha'_{\eta\xi} &= \frac{1}{A'} \nu^2 I_{\eta} \bar{Y}_{\eta\xi} \\ \alpha'_{\eta\eta} &= -\frac{1}{A'} (\bar{Y}_{\xi\xi} - \nu^2 I_{\eta}) \nu^2 I_{\xi} \\ A' &= (\bar{Y}_{\xi\xi} - \nu^2 I_{\eta})(\bar{Y}_{\eta\eta} - \nu^2 I_{\xi}) - \bar{Y}_{\xi\eta} \bar{Y}_{\eta\xi}\end{aligned}\quad (D-18)$$

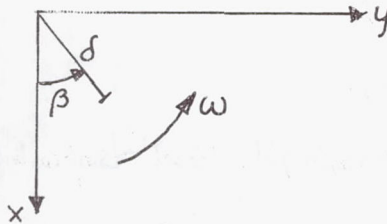
Thus, the roll and yaw amplitudes can be determined from Eqs. (D-17) once the rotor response has been computed.

APPENDIX E - Reduction of the Magnetic Force data from the General Electric Company

The magnetic forces imposed on the rotor by the alternator are calculated by the General Electric Company. The coordinate system chosen by G.E. has the y-axis vertical and the x-axis horizontal with origin in the magnetic center, and the rotor position is measured by the eccentricity δ and the angle β between the y-axis and the direction of eccentricity:



G.E. gives the results for the components $F(y)$ and $F(x)$ of the force acting on the stator. The force acting on the rotor has then the opposite sign. Furthermore, in the analysis of rotor response and stability the coordinate system is different:



Thus, the forces acting on the rotor are F_x and F_y which are related to the forces $F(y)$ and $F(x)$ obtained by G.E. by

$$F_x = -F(y) \quad F_y = -F(x) \quad (E-1)$$

In their general form, the forces can be written

$$F_x = \delta \sum_{n=0}^N \sum_{m=0}^M \left\{ a'_{nm} \cos(2n\omega t + \beta + m\phi) + b'_{nm} \cos(2n\omega t + \beta - m\phi) + a_{nm} \cos(2n\omega t - \beta + m\phi) + b_{nm} \cos(2n\omega t - \beta - m\phi) \right\} \quad (E-2)$$

$$F_y = \delta \sum_{n=0}^N \sum_{m=0}^M \left\{ a'_{nm} \sin(2n\omega t + \beta + m\phi) + b'_{nm} \sin(2n\omega t + \beta - m\phi) \right. \\ \left. + a_{nm} \sin(2n\omega t - \beta + m\phi) + b_{nm} \sin(2n\omega t - \beta - m\phi) \right\} \quad (E-3)$$

where ω is the angular speed of the rotor in radians/sec, t is time and $\phi = \pi$ -power angle (the power angle is the electrical angle between load current and direct axis magnetizing current). These equations are valid for all the six operating conditions calculated by G. E. except that in the case of a single phase fault, $m\phi$ is replaced by some other value which is not necessarily a multiple of ϕ .

For use in the rotor analysis, Eqs. (E-2) and (E-3) are rewritten by introducing the expressions

$$\begin{aligned} D_n &= \sum_{m=0}^M (a'_{nm} + b'_{nm}) \cos(m\phi) \\ E_n &= \sum_{m=0}^M (a'_{nm} - b'_{nm}) \sin(m\phi) \\ G_n &= \sum_{m=0}^M (a_{nm} + b_{nm}) \cos(m\phi) \\ H_n &= \sum_{m=0}^M (a_{nm} - b_{nm}) \sin(m\phi) \end{aligned} \quad (E-4)$$

By means of the trigonometric identities

$$\cos(2n\omega t + \beta + m\phi) = [\cos\beta \cdot \cos(m\phi) - \sin\beta \cdot \sin(m\phi)] \cos(2n\omega t) - [\sin\beta \cos(m\phi) + \cos\beta \sin(m\phi)] \sin(2n\omega t)$$

$$\sin(2n\omega t + \beta + m\phi) = [\sin\beta \cdot \cos(m\phi) + \cos\beta \cdot \sin(m\phi)] \cos(2n\omega t) + [\cos\beta \cdot \cos(m\phi) - \sin\beta \sin(m\phi)] \sin(2n\omega t)$$

and the analogous ones for the other trigonometric functions, and noting from the figure above that

$$x = \delta \cos\beta \quad y = \delta \sin\beta \quad (E-5)$$

Eqs. (E-2) and (E-3) can be expressed as

$$F_x = \sum_{n=0}^N \left\{ [(D_n + G_n)x - (E_n - H_n)y] \cos(2n\omega t) - [(E_n + H_n)x + (D_n - G_n)y] \sin(2n\omega t) \right\} \quad (E-6)$$

$$F_y = \sum_{n=0}^N \left\{ [(E_n + H_n)x + (D_n - G_n)y] \cos(2n\omega t) + [(D_n + G_n)x - (E_n - H_n)y] \sin(2n\omega t) \right\} \quad (E-7)$$

or

$$\begin{aligned} F_x &= \sum_{n=0}^N \{ A_n \cos(2n\omega t) + B_n \sin(2n\omega t) \} \\ F_y &= \sum_{n=0}^N \{ -B_n \cos(2n\omega t) + A_n \sin(2n\omega t) \} \end{aligned} \quad (E-8)$$

where the definition of A_n and B_n is obvious by comparing Eqs. (E-8) with Eqs. (E-6) and (E-7). It is seen, that in the general case, A_n and B_n depend on x and y such that even if $\delta = \sqrt{x^2 + y^2}$ is kept constant, A_n and B_n varies when β is changed. This is true in the three "short circuit" cases analyzed by G.E. However, in the other three cases where the load is balanced, it is found that

$$\text{for } n=0 : a_{0m} = b_{0m} = 0$$

balanced load

$$\text{for } n \geq 1 : a'_{nm} = b'_{nm} = 0$$

Thereby Eqs. (E-4) yields

$$\text{for } n=0 : G_0 = H_0 = 0$$

balanced load

$$\text{for } n \geq 1 : D_n = E_n = 0$$

Furthermore, it will be found that $E_0 = 0$. The forces become

$$\begin{aligned} F_x &= D_0 x + \sum_{n=1}^N \{ [G_n x + H_n y] \cos(2n\omega t) - [H_n x - G_n y] \sin(2n\omega t) \} \\ F_y &= D_0 y + \sum_{n=1}^N \{ [H_n x - G_n y] \cos(2n\omega t) + [G_n x + H_n y] \sin(2n\omega t) \} \end{aligned} \quad (E-9)$$

balanced load

or by making use of Eqs. (E-5)

$$F_x = D_0 x + \sum_{n=1}^N \delta \sqrt{G_n^2 + H_n^2} \cdot \cos(2n\omega t - \beta + \tan^{-1}(\frac{H_n}{G_n}))$$

(E-10)

$$F_y = D_0 y + \sum_{n=1}^N \delta \sqrt{G_n^2 + H_n^2} \cdot \sin(2n\omega t - \beta + \tan^{-1}(\frac{H_n}{G_n}))$$

balanced load

Hence, as would be expected for a balanced alternator load, each frequency component of the forces has a magnitude which only depends on the eccentricity. The phase angle between the frequency components, however, depends on β , but in the present case this is of no importance since in all the three balanced load cases there is only one frequency (i.e., $n=1$). Thereby, a change in β simply means a change in time base which, of course, in no way influences the rotor response results. On the other hand, in the three "short circuit" cases it is not possible to obtain expressions similar to Eqs. (E-10) and for those conditions the response of the rotor depends, at least theoretically, on β . In the present calculations, it is assumed that this dependency is of little physical significance and β has been set equal to zero. (i.e. $x=\delta, y=0$).

For the analysis of rotor stability it is necessary to use the gradients of the magnetic forces. They can be obtained directly from Eqs. (E-6) and (E-7):

$$\begin{aligned}
 \frac{\partial F_x}{\partial x} &= \sum_{n=0}^N [(D_n + G_n) \cos(2n\omega t) - (E_n + H_n) \sin(2n\omega t)] = - \sum_{n=0}^N [Q_{xxn} \cos(2n\omega t) - q_{xxn} \sin(2n\omega t)] \\
 \frac{\partial F_x}{\partial y} &= - \sum_{n=0}^N [(E_n - H_n) \cos(2n\omega t) + (D_n - G_n) \sin(2n\omega t)] = - \sum_{n=0}^N [Q_{xy_n} \cos(2n\omega t) - q_{xy_n} \sin(2n\omega t)] \\
 \frac{\partial F_y}{\partial x} &= \sum_{n=0}^N [(E_n + H_n) \cos(2n\omega t) + (D_n + G_n) \sin(2n\omega t)] = - \sum_{n=0}^N [Q_{yx_n} \cos(2n\omega t) - q_{yx_n} \sin(2n\omega t)] \\
 \frac{\partial F_y}{\partial y} &= \sum_{n=0}^N [(D_n - G_n) \cos(2n\omega t) - (E_n - H_n) \sin(2n\omega t)] = - \sum_{n=0}^N [Q_{yy_n} \cos(2n\omega t) - q_{yy_n} \sin(2n\omega t)]
 \end{aligned} \tag{E-11}$$

where the Q 's and q 's are defined by these equations. It is seen that

$$\begin{aligned}
 Q_{xxn} &= -q_{yx_n} = -(D_n + G_n) = Q_{xn} \\
 q_{xxn} &= Q_{yx_n} = -(E_n + H_n) = q_{xn} \\
 Q_{yy_n} &= q_{xy_n} = -(D_n - G_n) = Q_{yn} \\
 q_{yy_n} &= -Q_{xy_n} = -(E_n - H_n) = q_{yn}
 \end{aligned} \tag{E-12}$$

In the three balanced load cases the expressions become

$$\begin{aligned}
 \text{for } n=0: \quad Q_{xx0} &= Q_{yy0} = D_0 \\
 Q_{xy0} &= Q_{yx0} = 0
 \end{aligned} \tag{E-13}$$

for $n \geq 1$:

$$Q_{xxn} = -Q_{yy_n} = -G_n$$

$$Q_{xy_n} = Q_{yx_n} = -H_n$$

$$q_{xxn} = -q_{yy_n} = -H_n$$

$$q_{xy_n} = q_{yx_n} = G_n$$

(E-14)

Therefore, for balanced load,

$$\frac{\partial F_x}{\partial x} = D_0 + \sum_{n=1}^N \sqrt{G_n^2 + H_n^2} \cdot \cos(2n\omega t + \tan^{-1}(\frac{H_n}{G_n}))$$

$$\frac{\partial F_x}{\partial y} = \frac{\partial F_y}{\partial x} = \sum_{n=1}^N \sqrt{G_n^2 + H_n^2} \cdot \sin(2n\omega t + \tan^{-1}(\frac{H_n}{G_n}))$$

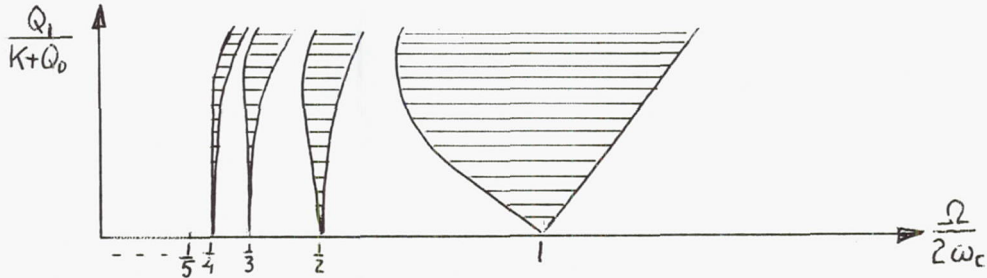
$$\frac{\partial F_y}{\partial y} = D_0 - \sum_{n=1}^N \sqrt{G_n^2 + H_n^2} \cdot \cos(2n\omega t + \tan^{-1}(\frac{H_n}{G_n}))$$

APPENDIX F: Analysis of Rotor Stability with Magnetic Forces

To illustrate the stability problem for a rotor with magnetic forces, consider first a simplified model, namely a symmetric, rigid rotor supported in two identical bearings. Let the rotor mass be M , the combined bearing stiffness K , the rotor amplitude x , and let the magnetic force be represented by $-[Q_0 + Q_1 \cos(\Omega t)]x$ where Ω is the frequency of the magnetic force. Then the equation of motion is

$$M \frac{d^2 x}{dt^2} = -[K + Q_0 + Q_1 \cos(\Omega t)]x \quad (F-1)$$

where any bearing damping has been ignored. This equation is the standard Mathieu equation which has been treated extensively in the literature (References 18 through 21). It has an infinite number of instability zones which may be shown graphically as



where ω_c is the critical speed of the rotor,

$$\omega_c = \sqrt{\frac{K + Q_0}{M}} \quad (F-2)$$

The shaded regions are the instability zones. They are centered in $\frac{\Omega}{2\omega_c} = 1, \frac{1}{2}, \frac{1}{3}, \dots$.

The frequency Ω of the magnetic force is a multiple of the angular speed ω of the rotor and usually $\Omega = 2\omega$ such that the abscissa becomes $\frac{\Omega}{2\omega_c} = \frac{\omega}{\omega_c}$. Hence, for a given rotor the abscissa simply represents the speed of the rotor. In the present investigation the rotor operates above its first critical speed and it is, therefore, only necessary to consider the first instability zone (i.e., the zone centered at $\frac{\Omega}{2\omega_c} = 1$). Furthermore, in all the six cases for which the magnetic forces have been computed, Q_0 and Q_1 are much smaller than K such that $Q_1/(K+Q_0) \ll 1$. This makes it possible to employ a method, called the Method of Averaging, to determine the instability zones as discussed in the following. Before this method is described, however, the exact solution shall be discussed for the purpose of comparison.

The usual method for determining the instability zones centered at $\frac{\Omega}{2\omega_c} = 1, \frac{1}{3}, \frac{1}{5}, \frac{1}{7}, \frac{1}{9}$, etc., is to expand x in a Fourier series:

$$x = \sum_{n=1}^{\infty} \left[x_{cn} \cos\left((2n-1)\frac{\Omega}{2}t\right) - x_{sn} \sin\left((2n-1)\frac{\Omega}{2}t\right) \right] \quad (F-3)$$

Substitution of this expansion into Eqs. (F-1) results in an infinite set of homogenous equations. The threshold of instability is then obtained by equating the determinant of the coefficient matrix to zero:

$$\begin{vmatrix} \left(1 - \left(\frac{\Omega}{2\omega_c}\right)^2 + \frac{1}{2} \frac{Q_1}{K+Q_0}\right) & 0 & \frac{1}{2} \frac{Q_1}{K+Q_0} & 0 & \cdots \\ 0 & \left(1 - \left(\frac{\Omega}{2\omega_c}\right)^2 - \frac{1}{2} \frac{Q_1}{K+Q_0}\right) & 0 & \frac{1}{2} \frac{Q_1}{K+Q_0} & \cdots \\ \frac{1}{2} \frac{Q_1}{K+Q_0} & 0 & \left(1 - q\left(\frac{\Omega}{2\omega_c}\right)^2\right) & 0 & \cdots \\ 0 & \frac{1}{2} \frac{Q_1}{K+Q_0} & 0 & \left(1 - q\left(\frac{\Omega}{2\omega_c}\right)^2\right) & \cdots \\ \vdots & \vdots & \vdots & \vdots & \ddots \end{vmatrix} = 0 \quad (F-4)$$

Truncating the infinite determinant after the first two rows yields the solution,

$$\frac{Q_1}{K+Q_0} = \pm 2 \left[1 - \left(\frac{\Omega}{2\omega_c}\right)^2 \right] \quad (F-5)$$

If the determinant is truncated after the four first rows the result becomes

$$\frac{Q_1}{K+Q_0} = \pm \left[1 - q \left(\frac{\Omega}{2\omega_c} \right)^2 \pm \sqrt{\left(1 - q \left(\frac{\Omega}{2\omega_c} \right)^2 \right)^2 + 4 \left(1 - q \left(\frac{\Omega}{2\omega_c} \right)^2 \right) \left(1 - \left(\frac{\Omega}{2\omega_c} \right)^2 \right)} \right] \quad (F-6)$$

The results for the first instability zone from these equations may be compared:

$Q_1/(K+Q_0)$ from:		
$\frac{\Omega}{2\omega_c}$	2 x 2 Determinant Eq . (F-5)	4 x 4 Determinant Eq . (F-6)
.7	1.02	1.25
.8	.72	.78
1	0	0
1.2	0.88	0.85
1.4	1.92	1.83

It is seen that the simpler equation, Eq . (F-5), gives sufficiently accurate results for $Q_1/(K+Q_0) < 1$, especially for that branch of the instability zone where $\Omega/2\omega_c > 1$ which is also the branch of interest. The simpler solution only makes use of the first term in the Fourier expansion for x and is, therefore, based on a single frequency oscillation.

To solve Eq . (F-1) by the Method of Averaging, set

$$X = X_c \cos \psi - X_s \sin \psi \quad (F-7)$$

where

$$\psi = \nu t \quad (F-8)$$

and ν is the unknown frequency of the motion. Then define

$$\ddot{X} = -\nu X_c \sin \psi - \nu X_s \cos \psi \quad (F-9)$$

where \dot{x} means $\frac{dx}{dt}$. However, it cannot a priori be assumed that x_c and x_s are constant. Hence, in actuality

$$\ddot{x} = -\nu x_c \sin \psi - \nu x_s \cos \psi + \dot{x}_c \cos \psi - \dot{x}_s \sin \psi \quad (F-10)$$

For Eqs. (F-9) and (F-10) to be compatible, it is necessary that

$$\dot{x}_c \cos \psi - \dot{x}_s \sin \psi = 0 \quad (F-11)$$

If this condition is imposed, Eqs. (F-1) and (F-9) yield:

$$\ddot{x} = -\nu^2 x_c \cos \psi + \nu^2 x_s \sin \psi - \nu \dot{x}_c \sin \psi - \nu \dot{x}_s \cos \psi = \frac{1}{M} [K + Q_0 + Q_1 \cos \Omega t] (x_c \cos \psi - x_s \sin \psi) \quad (F-12)$$

Multiply Eqs. (F-11) by $\cos \psi$, Eqs. (F-12) by $-\frac{1}{\nu} \sin \psi$ and add

$$\dot{x}_c = x_c \left[\frac{K+Q_0}{M\nu} - \nu + \frac{Q_1}{M\nu} \cos \Omega t \right] \cos \psi \sin \psi - x_s \left[\frac{K+Q_0}{M\nu} - \nu + \frac{Q_1}{M\nu} \cos \Omega t \right] \sin^2 \psi \quad (F-13)$$

Multiply Eq. (F-11) by $-\sin \psi$, Eq. (F-12) by $-\frac{1}{\nu} \cos \psi$ and add

$$\dot{x}_s = x_c \left[\frac{K+Q_0}{M\nu} - \nu + \frac{Q_1}{M\nu} \cos \Omega t \right] \cos^2 \psi - x_s \left[\frac{K+Q_0}{M\nu} - \nu + \frac{Q_1}{M\nu} \cos \Omega t \right] \cos \psi \sin \psi \quad (F-14)$$

In this way the second order differential Eq. (F-1) has been transformed into two first order equations.

On the threshold of instability, x_c and x_s are bounded.

Hence,

$$\lim_{T \rightarrow \infty} \left[\frac{1}{T} \int_0^T \dot{x}_c dt \right] = 0 \quad \lim_{T \rightarrow \infty} \left[\frac{1}{T} \int_0^T \dot{x}_s dt \right] = 0 \quad (F-15)$$

The righthand side of Eqs. (F-13) and (F-14) can be averaged in the same way. In performing the integrations, it shall be assumed that x_c and x_s are sufficiently slowly varying functions that they can be kept constant in the integration process. Then the following integrals are encountered:

$$\lim_{T \rightarrow \infty} \left[\frac{1}{T} \int_0^T \cos' \psi dt \right] = \lim_{T \rightarrow \infty} \left[\frac{1}{T} \int_0^T \frac{1}{2} (1 + \cos 2\psi) dt \right] = \frac{1}{2} \quad (F-16)$$

$$\lim_{T \rightarrow \infty} \left[\frac{1}{T} \int_0^T \sin^2 \psi dt \right] = \lim_{T \rightarrow \infty} \left[\frac{1}{T} \int_0^T \frac{1}{2} (1 - \cos 2\psi) dt \right] = \frac{1}{2} \quad (F-17)$$

$$\lim_{T \rightarrow \infty} \left[\frac{1}{T} \int_0^T \cos \psi \sin \psi dt \right] = \lim_{T \rightarrow \infty} \left[\frac{1}{T} \int_0^T \frac{1}{2} \sin 2\psi dt \right] = 0 \quad (F-18)$$

$$\begin{aligned} \lim_{T \rightarrow \infty} \left[\frac{1}{T} \int_0^T \cos \Omega t \cdot \cos^2 \psi dt \right] &= \lim_{T \rightarrow \infty} \left[\frac{1}{2T} \int_0^T \cos \Omega t (1 + \cos 2\psi) dt \right] \\ &= 0 + \lim_{T \rightarrow \infty} \left[\frac{1}{4T} \int_0^T [\cos(2\psi(1 + \frac{\Omega}{2\nu})) + \cos(2\psi(1 - \frac{\Omega}{2\nu}))] dt \right] = \begin{cases} 0 & \text{if } \frac{\Omega}{2\nu} \neq \pm 1 \\ \frac{1}{4} & \text{if } \frac{\Omega}{2\nu} = \pm 1 \end{cases} \end{aligned} \quad (F-19)$$

$$\lim_{T \rightarrow \infty} \left[\frac{1}{T} \int_0^T \cos \Omega t \cdot \sin^2 \psi dt \right] = \lim_{T \rightarrow \infty} \left[\frac{1}{2T} \int_0^T \cos \Omega t (1 - \cos 2\psi) dt \right] = \begin{cases} 0 & \text{if } \frac{\Omega}{2\nu} \neq \pm 1 \\ -\frac{1}{4} & \text{if } \frac{\Omega}{2\nu} = \pm 1 \end{cases} \quad (F-20)$$

$$\lim_{T \rightarrow \infty} \left[\frac{1}{T} \int_0^T \cos \Omega t \cdot \cos \psi \cdot \sin \psi dt \right] = \lim_{T \rightarrow \infty} \left[\frac{1}{4T} \int_0^T [\sin(2\psi(1 + \frac{\Omega}{2\nu})) + \sin(2\psi(1 - \frac{\Omega}{2\nu}))] dt \right] = 0 \quad (F-21)$$

Thus, only by setting $\frac{\Omega}{2\nu} = 1$ does a non-trivial solution exist. By averaging Eqs. (F-13) and (F-14) in this way, two equations are obtained:

$$\frac{K + Q_0}{M\nu} - \nu - \frac{Q_1}{2M\nu} = 0$$

$$\frac{K + Q_0}{M\nu} - \nu + \frac{Q_1}{2M\nu} = 0$$

By introducing the critical speed ω_c from Eq . (F-2), these equations can be written

$$\frac{Q_1}{K+Q_0} = \pm 2 \left[1 - \left(\frac{\omega}{\omega_c} \right)^2 \right] = \pm 2 \left[1 - \left(\frac{\Omega}{2\omega_c} \right)^2 \right] \quad (F-22)$$

which is the same solution as obtained in Eq . (F-5). It can therefore be concluded that the Method of Averaging determines the first instability zone and even if the solution is approximate, the error is negligible when $Q_1/(K+Q_0) < 2$ for $\Omega/2\omega_c > 1$ and when $Q_1/(K+Q_0) \lesssim 0.7$ for $\Omega/2\omega_c < 1$.

For those three operating conditions where the alternator operates with balanced load, the magnetic forces have only one frequency component ($\Omega = 2\omega$) in which case the above analysis can be applied without any further discussion. For the three "short circuit" conditions, however, there are additional higher frequency components ($\Omega = 2\omega, 4\omega, 6\omega$, etc.). Since the Method of Averaging eliminates all frequencies except one, namely $\Omega/2$, it is necessary to investigate what effect the higher harmonics in the magnetic forces have on the instability threshold. Therefore, assume that both a second and a third harmonic are present whereby Eq . (F-1) becomes

$$M \frac{d^2 x}{dt^2} = - \left[K + Q_0 + Q_1 \cos(\Omega t) + Q_2 \cos(2\Omega t) + Q_3 \cos(3\Omega t) \right] x \quad (F-23)$$

Expanding x in a Fourier series, and collecting terms in $\cos(\Omega t)$, $\sin(\Omega t)$, $\cos(2\Omega t)$, $\sin(2\Omega t)$, etc. yields a determinant in analogy to the one given by Eq . (F-4):

$$\begin{vmatrix} (K+Q_0 - M(\frac{\Omega}{2})^2 + \frac{1}{2}Q_1) & 0 & \frac{1}{2}(Q_1+Q_2) & 0 & - & - & - \\ 0 & (K+Q_0 - M(\frac{\Omega}{2})^2 - \frac{1}{2}Q_1) & 0 & \frac{1}{2}(Q_1-Q_2) & - & - & - \\ \frac{1}{2}(Q_1+Q_2) & 0 & (K+Q_0 - 9M(\frac{\Omega}{2})^2 + \frac{1}{2}Q_3) & 0 & - & - & - \\ 0 & \frac{1}{2}(Q_1-Q_2) & 0 & (K+Q_0 - 9M(\frac{\Omega}{2})^2 - \frac{1}{2}Q_3) & - & - & - \\ \vdots & \vdots & \vdots & \vdots & & & \end{vmatrix} = 0 \quad (F-24)$$

If the determinant is truncated at 2×2 , the same solution is obtained as before, see Eq . (F-5). However, if the determinant is truncated at 4×4 , the solution

differs from the one obtained with only one frequency component as given in Eq. (F-6). To illustrate the difference, assume first that $Q_2=Q_1$ and $Q_3=0$, i.e., the magnetic force has two equal frequency components. The corresponding solution becomes

$$\frac{\Omega}{2\omega_c} \geq 1 \quad \frac{Q_1}{K+Q_0} = \frac{1}{4} \left(1 - 9 \left(\frac{\Omega}{2\omega_c} \right)^2 \right) + \sqrt{\frac{1}{16} \left(1 - 9 \left(\frac{\Omega}{2\omega_c} \right)^2 \right)^2 + \left(1 - 9 \left(\frac{\Omega}{2\omega_c} \right)^2 \right) \left(1 - \left(\frac{\Omega}{2\omega_c} \right)^2 \right)} \quad (F-25)$$

$$Q_2 = Q_1, \quad Q_3 = 0$$

Next, assume that all three frequency components are present and that $Q_2=Q_3=Q_1$. The solution becomes

$$\frac{\Omega}{2\omega_c} \geq 1 \quad \frac{Q_1}{K+Q_0} = \frac{2}{3} \left(1 - 5 \left(\frac{\Omega}{2\omega_c} \right)^2 \right) + \frac{2}{3} \sqrt{\left(1 - 5 \left(\frac{\Omega}{2\omega_c} \right)^2 \right)^2 + 3 \left(1 - 9 \left(\frac{\Omega}{2\omega_c} \right)^2 \right) \left(1 - \left(\frac{\Omega}{2\omega_c} \right)^2 \right)} \quad (F-26)$$

$$Q_2 = Q_3 = Q_1$$

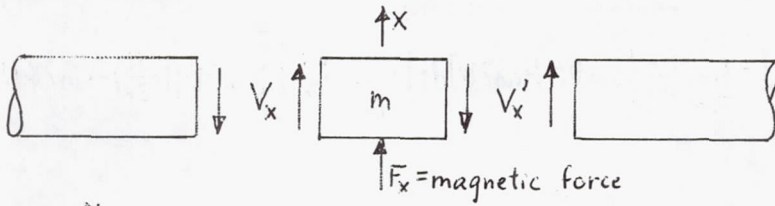
The four solutions may be compared numerically as shown in the following table:

$\frac{\Omega}{2\omega_c}$	Method of Aver. Eq. (F-22)	One Frequency Eq. (F-6)	Two Frequencies Eq. (F-25)	Three Frequencies Eq. (F-26)
1.05	0.205	0.202	0.194	0.194
1.1	0.42	0.41	0.39	0.39
1.2	0.88	0.85	0.78	0.78
1.4	1.92	1.83	1.61	1.60

It is seen that of the higher harmonics, only the second is of any significance, and even its influence is not too pronounced. Furthermore, when $Q_2 > Q_1$ it is found that the stability threshold increases again such that the results from the Method of Averaging in most cases gives the lowest threshold. On this basis the Method of Averaging can be accepted as giving results with sufficiently good accuracy for the present purpose. The next step, therefore, is to apply this method to the complete rotor analysis.

Consider a small segment of the shaft where the magnetic forces are applied. The shear forces to the left are V_x and V_y , and the shear forces to the right are V'_x and V'_y . The rotor amplitudes are x and y , and the mass of the shaft

section is m . With the electrical forces given as shown in Appendix E, the equations of motion become



$$m\ddot{x} = V_x - V_x' - x \sum_{n=0}^N [Q_{xxn} \cos(2n\omega t) - q_{xxn} \sin(2n\omega t)] - y \sum_{n=0}^N [Q_{xy_n} \cos(2n\omega t) - q_{xy_n} \sin(2n\omega t)] = -f_x \quad (\text{F-27})$$

$$m\ddot{y} = V_y - V_y' - x \sum_{n=0}^N [Q_{yx_n} \cos(2n\omega t) - q_{yx_n} \sin(2n\omega t)] - y \sum_{n=0}^N [Q_{yy_n} \cos(2n\omega t) - q_{yy_n} \sin(2n\omega t)] = -f_y \quad (\text{F-28})$$

Let the frequency of the vibration be ν and set

$$x = x_c \cos \psi - x_s \sin \psi \quad (\text{F-29})$$

$$V_x = V_{xc} \cos \psi - V_{xs} \sin \psi$$

where

$$\psi = \nu t$$

Similar equations hold for the y -components. Following exactly the same procedure as used to derive Eqs. (F-13) and (F-14), four equations are obtained:

$$\begin{aligned} \dot{x}_c &= \left[\frac{1}{\nu m} f_x - \nu x \right] \sin \psi \\ \dot{x}_s &= \left[\frac{1}{\nu m} f_x - \nu x \right] \cos \psi \\ \dot{y}_c &= \left[\frac{1}{\nu m} f_y - \nu y \right] \sin \psi \\ \dot{y}_s &= \left[\frac{1}{\nu m} f_y - \nu y \right] \cos \psi \end{aligned} \quad (\text{F-30})$$

These equations are averaged as defined by Eqs. (F-15) and in this process it is necessary to set $\nu = \omega$ to get a non-trivial solution. Hence, only the magnetic force components with $n = 0$ and $n = 1$ remain in the averaged equations. In performing the required integration, the integrals from Eqs. (F-16) to (F-21)

are used, and in addition the following integrals are encountered:

$$\lim_{T \rightarrow \infty} \left[\frac{1}{T} \int_0^T \sin \Omega t \cos^2 \psi dt \right] = \lim_{T \rightarrow \infty} \left[\frac{1}{2T} \int_0^T \sin \Omega t [1 + \cos 2\psi] dt \right] = \lim_{T \rightarrow \infty} \left[\frac{1}{4T} \int_0^T [\sin 2\psi (1 + \frac{\Omega}{2\nu}) - \sin 2\psi (1 - \frac{\Omega}{2\nu})] dt \right] = 0 \quad (F-31)$$

$$\lim_{T \rightarrow \infty} \left[\frac{1}{T} \int_0^T \sin \Omega t \sin^2 \psi dt \right] = \lim_{T \rightarrow \infty} \left[\frac{1}{2T} \int_0^T \sin \Omega t [1 - \cos 2\psi] dt \right] = 0 \quad (F-32)$$

$$\begin{aligned} \lim_{T \rightarrow \infty} \left[\frac{1}{T} \int_0^T \sin \Omega t \cos \psi \sin \psi dt \right] &= \lim_{T \rightarrow \infty} \left[\frac{1}{2T} \int_0^T \sin \Omega t \sin 2\psi dt \right] \\ &= \lim_{T \rightarrow \infty} \left[\frac{1}{4T} \int_0^T [\cos 2\psi (1 - \frac{\Omega}{2\nu}) - \cos 2\psi (1 + \frac{\Omega}{2\nu})] dt \right] = \begin{cases} 0 & \text{for } \frac{\Omega}{2\nu} \neq 1 \\ -\frac{1}{4} & \text{for } \frac{\Omega}{2\nu} = -1 \\ \frac{1}{4} & \text{for } \frac{\Omega}{2\nu} = 1 \end{cases} \quad (F-33) \end{aligned}$$

where Ω is the lowest magnetic force frequency, i.e. $\Omega = 2\omega$. Thus, $\frac{\Omega}{2\nu} = 1$ as a requirement results in $\nu = \omega$. By means of these integrals, averaging Eqs. (F-30) yields

$$V'_{xc} = V_{xc} + (\nu^2 m - Q_{xx0} - \frac{1}{2} Q_{xx1}) x_c - \frac{1}{2} q_{xx1} x_s - (Q_{xy0} + \frac{1}{2} Q_{xy1}) y_c - \frac{1}{2} q_{xy1} y_s \quad (F-34)$$

$$V'_{xs} = V_{xs} - \frac{1}{2} q_{xx1} x_c + (\nu^2 m - Q_{xx0} + \frac{1}{2} Q_{xx1}) x_s - \frac{1}{2} q_{xy1} y_c - (Q_{xy0} - \frac{1}{2} Q_{xy1}) y_s \quad (F-35)$$

$$V'_{yc} = V_{yc} - (Q_{yx0} + \frac{1}{2} Q_{yx1}) x_c - \frac{1}{2} q_{yx1} x_s + (\nu^2 m - Q_{yy0} - \frac{1}{2} Q_{yy1}) y_c - \frac{1}{2} q_{yy1} y_s \quad (F-36)$$

$$V'_{ys} = V_{ys} - \frac{1}{2} q_{yx1} x_c - (Q_{yx0} - \frac{1}{2} Q_{yx1}) x_s - \frac{1}{2} q_{yy1} y_c + (\nu^2 m - Q_{yy0} + \frac{1}{2} Q_{yy1}) y_s \quad (F-37)$$

These equations can be used directly in the rotor stability analysis as described in Appendix G.

APPENDIX G: Method for Calculating Rotor response and Stability

The method employed to compute the response and the stability threshold of a rotor with magnetic forces is an extension of the conventional Holzer method for lateral vibrations (Prohl-Myklestad Method). The rotor is divided up into smaller sections such that each section has uniform diameter and the mass of each section is lumped at the two end points of the section. In this way the rotor is represented by a series of mass points, called rotor stations, connected by weightless shaft sections of uniform stiffness. This idealized rotor model can be brought as close to the actual rotor as desired by choosing a large number of stations, but in practice a high degree of accuracy can be obtained with a rather limited number of stations.

The described subdivision of the rotor necessitates that there are rotor stations at each location where the shaft diameter changes, and at the two endpoints of the rotor. Furthermore, stations are introduced where the rotor has concentrated masses such as wheels, impellers, collars, etc.; at all bearing locations, at all mechanical unbalance locations and at the locations where the magnetic forces are applied. Thus, an arbitrary rotor station, can be assigned a mass m_j , a transverse and a polar mass moment of inertia: I_{Tj} and I_{pj} , respectively, 8 dynamic bearing coefficients: K_{xxj} , B_{xxj} , K_{xyj} , etc., a mechanical unbalance and magnetic forces. For any particular station, any or all of these quantities may be zero.

The rotor vibrates with frequency ν radians/sec. and the amplitudes at station j are x_j and y_j :

$$x_j = x_{cj} \cos(\nu t) - x_{sj} \sin(\nu t) \quad (G-1)$$

$$y_j = y_{cj} \cos(\nu t) - y_{sj} \sin(\nu t) \quad (G-2)$$

The slopes of the vibrating rotor at station j are

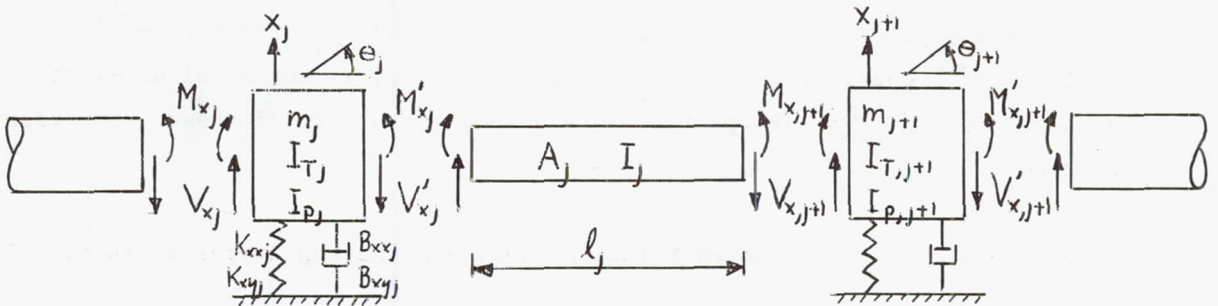
$$\theta_j = \left(\frac{dx}{dz} \right)_j = \theta_{cj} \cos(\nu t) - \theta_{sj} \sin(\nu t) \quad (G-3)$$

$$\phi_j = \left(\frac{dy}{dz} \right)_j = \phi_{cj} \cos(\nu t) - \phi_{sj} \sin(\nu t) \quad (G-4)$$

The bending moment is M with components M_x and M_y , and the shear force is V with components V_x and V_y which can be expressed as

$$M_x = M_{xc} \cos(\nu t) - M_{xs} \sin(\nu t) \quad (G-5)$$

and similarly for M_y , V_x and V_y . The quantities to the left of station j are called M_{xj} , M_{yj} , V_{xj} , and V_{yj} and the quantities to the right of the station are called M'_{xj} , M'_{yj} , V'_{xj} and V'_{yj} . Thus, a force balance and a moment balance can be set up for station j :



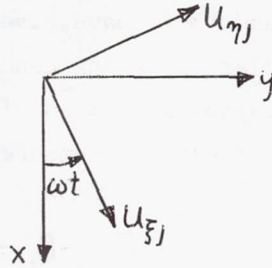
$$m_j \ddot{x}_j = V_{xj} - V'_{xj} - K_{xxj} x_j - B_{xxj} \dot{x}_j - K_{xyj} y_j - B_{xyj} \dot{y}_j + (F_{xj})_{unbal.} + (F_{xj})_{Magn.} \quad (G-6)$$

$$m_j \ddot{y}_j = V_{yj} - V'_{yj} - K_{yxj} x_j - B_{yxj} \dot{x}_j - K_{yyj} y_j - B_{yyj} \dot{y}_j + (F_{yj})_{unbal.} + (F_{yj})_{Magn.} \quad (G-7)$$

$$I_{Tj} \ddot{\theta}_j + \omega I_{Pj} \dot{\theta}_j = M'_{xj} - M_{xj} \quad (G-8)$$

$$I_{Tj} \ddot{\phi}_j - \omega I_{Pj} \dot{\phi}_j = M'_{yj} - M_{yj} \quad (G-9)$$

In order to express the unbalance force, let the mechanical unbalance at Station j have the components $U_{\xi j}$ and $U_{\eta j}$ (lbs-sec²) with respect to a ξ - η -coordinate system which is fixed in the rotor. Thus, the ξ - η -system rotates with respect to the x-y-system:



The unbalance forces become

$$(F_{xj})_{unbal} = \omega^2 U_{\xi j} \cos(\omega t) - \omega^2 U_{\eta j} \sin(\omega t) \quad (G-10)$$

$$(F_{yj})_{unbal} = \omega^2 U_{\xi j} \sin(\omega t) + \omega^2 U_{\eta j} \cos(\omega t)$$

where ω is the angular speed of the rotor.

The expressions for the magnetic forces depend on which frequency the vibration has, and whether the calculation is for response or stability. Let the forces be expressed as

$$(F_x)_{Mag} = F_{xc} \cos(\nu t) - F_{xs} \sin(\nu t) \quad (G-11)$$

$$(F_y)_{Mag} = F_{yc} \cos(\nu t) - F_{ys} \sin(\nu t) \quad (G-12)$$

If $\nu = \omega$ as in a stability calculation or when calculating the response caused by a mechanical unbalance, the magnetic forces have been derived in Appendix F as Eqs. (F-34) to (F-37), i.e.,:

For $\nu = \omega$

$$F_{xc} = -(Q_{xx0} + \frac{1}{2} Q_{xx1}) x_c - \frac{1}{2} q_{xx1} x_s - (Q_{xy0} + \frac{1}{2} Q_{xy1}) y_c - \frac{1}{2} q_{xy1} y_s \quad (G-13)$$

$$F_{xs} = -\frac{1}{2} q_{xx1} x_c - (Q_{xx0} - \frac{1}{2} Q_{xx1}) x_s - \frac{1}{2} q_{xy1} y_c - (Q_{xy0} - \frac{1}{2} Q_{xy1}) y_s \quad (G-14)$$

$$F_{yc} = -(Q_{yx0} + \frac{1}{2} Q_{yx1}) x_c - \frac{1}{2} q_{yx1} x_s - (Q_{yy0} + \frac{1}{2} Q_{yy1}) y_c - \frac{1}{2} q_{yy1} y_s \quad (G-15)$$

$$F_{ys} = -\frac{1}{2} q_{yx1} x_c - (Q_{yx0} - \frac{1}{2} Q_{yx1}) x_s - \frac{1}{2} q_{yy1} y_c - (Q_{yy0} - \frac{1}{2} Q_{yy1}) y_s \quad (G-16)$$

If $\nu \neq \omega$ (i.e., $\nu = 2\omega, 4\omega$, etc.) as in the calculation of response due to the magnetic forces, the forces are derived in Appendix E as Eqs. (E-8) and (E-9). For a selected, fixed steady-state eccentricity between the alternator stator and the rotor (i.e., x and y in Eqs. (E-6) and (E-7) have given constant values), A_n and B_n can be computed for a particular operating condition of the alternator. Setting $\nu = 2n\omega, n=1, 2, \dots$, and the corresponding values of A_n and B_n equal to A_ν and B_ν , respectively, a particular frequency component of $(F_x)_{Magn}$ and $(F_y)_{Magn}$ can be written

$$\begin{aligned} \underline{\nu = 2n\omega} \quad F_{xc} &= A_n = A_\nu & F_{xs} &= -B_n = -B_\nu \\ F_{yc} &= -B_n = -B_\nu & F_{ys} &= -A_n = -A_\nu \end{aligned} \quad (G-17)$$

Having determined the mechanical unbalance forces and the magnetic forces, Eqs. (G-6) to (G-9) can be written, leaving out the index j :

$$V'_{xc} = V_{xc} - (K_{xx} - (\frac{\nu}{\omega})^2 m \omega^2) x_c + (\frac{\nu}{\omega}) \omega B_{xx} x_s - K_{xy} y_c + (\frac{\nu}{\omega}) \omega B_{xy} y_s + \omega^2 U_\xi + F_{xc} \quad (G-18)$$

$$V'_{xs} = V_{xs} - (\frac{\nu}{\omega}) \omega B_{xx} x_c - (K_{xx} - (\frac{\nu}{\omega})^2 m \omega^2) x_s - (\frac{\nu}{\omega}) \omega B_{xy} y_c - K_{xy} y_s + \omega^2 U_\eta + F_{xs} \quad (G-19)$$

$$V'_{yc} = V_{yc} - K_{yx} x_c + (\frac{\nu}{\omega}) \omega B_{yx} x_s - (K_{yy} - (\frac{\nu}{\omega})^2 m \omega^2) y_c + (\frac{\nu}{\omega}) \omega B_{yy} y_s + \omega^2 U_\xi + F_{yc} \quad (G-20)$$

$$V'_{ys} = V_{ys} - (\frac{\nu}{\omega}) \omega B_{yx} x_c - K_{yx} x_s - (\frac{\nu}{\omega}) \omega B_{yy} y_c - (K_{yy} - (\frac{\nu}{\omega})^2 m \omega^2) y_s - \omega^2 U_\eta + F_{ys} \quad (G-21)$$

$$M'_{xc} = M_{xc} - (\frac{\nu}{\omega})^2 \omega^2 I_T \theta_c - (\frac{\nu}{\omega}) \omega^2 I_P \phi_s \quad (G-22)$$

$$M'_{xs} = M_{xs} - (\frac{\nu}{\omega})^2 \omega^2 I_T \theta_s + (\frac{\nu}{\omega}) \omega^2 I_P \phi_c \quad (G-23)$$

$$M'_{yc} = M_{yc} + (\frac{\nu}{\omega}) \omega^2 I_P \theta_s - (\frac{\nu}{\omega})^2 \omega^2 I_T \phi_c \quad (G-24)$$

$$M'_{ys} = M_{ys} - (\frac{\nu}{\omega}) \omega^2 I_P \theta_c - (\frac{\nu}{\omega})^2 \omega^2 I_T \phi_s \quad (G-25)$$

These equations establish the change in shear force and bending moment across a rotor station. They apply to a single frequency ν . In a stability analysis, $\nu = \omega$ (i.e., $\frac{\nu}{\omega} = 1$) and F_{xc} , F_{xs} , F_{yc} and F_{ys} are given by Eqs. (G-13) to (G-16). For such a calculation, U_ξ and $U_\eta = 0$. In a mechanical unbalance response calculation, U_ξ and U_η have specified values and the frequency ν is equal to ω (i.e., $\frac{\nu}{\omega} = 1$) so that F_{xc} , F_{xs} , F_{yc} and F_{ys} are given by Eqs. (G-13) to (G-16).

In a magnetic force response calculation, the magnetic eccentricity is specified and F_{xc} , F_{xs} , F_{yc} , and F_{ys} are taken from Eqs. (G-17) where A_n and B_n are computed as shown in Appendix E. In this type of calculation, $\nu = 2n\omega$ (i.e. $\nu/\omega = 2n, n=1, 2, \dots$) and $U_f = U_g = 0$. It should be noted, that in performing the calculations, the 8 bearing coefficients depend on the particular frequency.

Referring to the above figure, the shaft section connecting station j and station $(j+1)$ is considered next. The section has the length ℓ_j , the cross sectional area A_j , the cross-sectional transverse moment of inertia I_j and the shaft material has a Young's modulus E . From conventional beam theory, the relationships between the amplitudes, the slopes, the shear forces and the bending moments at the ends of the section become

$$X_{j+1} = X_j + \ell_j \theta_j + \frac{\ell_j^2}{2EI_j} M'_{xj} + \frac{\ell_j^3}{6EI_j} V'_{xj} \quad (G-26)$$

$$\theta_{j+1} = \theta_j + \frac{\ell_j}{EI_j} M'_{xj} + \frac{\ell_j^2}{2EI_j} V'_{xj} \quad (G-27)$$

$$M_{j+1} = M_j + \ell_j V'_j \quad (G-28)$$

$$V_{j+1} = V'_j \quad (G-29)$$

These equations together with Eqs. (G-18) to (G-25) establish a set of recurrence relationships by which the calculation can be performed step-by-step, starting from the left rotor end where

$$M_1 = V_1 = 0$$

or

$$M_{xc1} = M_{xs1} = M_{yc1} = M_{ys1} = V_{xc1} = V_{xs1} = V_{yc1} = V_{ys1} = 0 \quad (G-30)$$

For a given frequency, several calculations are performed. In the first calculation, set $X_{c1} = 1$ and $X_{s1} = Y_{c1} = Y_{s1} = \theta_{c1} = \theta_{s1} = \phi_{c1} = \phi_{s1} = 0$ and use the

recurrence relationships to obtain the bending moments and the shear force at the last rotor station (station m):

$$M'_{xcm} = \alpha_{11}, M'_{xsm} = \alpha_{21}, M'_{ycm} = \alpha_{31}, M'_{ysm} = \alpha_{41}, V'_{xcm} = \alpha_{51}, \text{ etc.}$$

next set $x_{s1} = 1$ and $x_{c1} = y_{c1} = y_{s1} = \theta_{c1} = \theta_{s1} = \phi_{c1} = \phi_{s1} = 0$ and compute the quantities at the last station:

$$M'_{xcm} = \alpha_{12}, M'_{xsm} = \alpha_{22}, M'_{ycm} = \alpha_{32}, \text{ etc.}$$

In the same way, calculations are performed for $y_{c1} = 1, y_{s1} = 1, \theta_{c1} = 1$, etc., i.e., a total of 8 calculations. In all these calculations, all the station forces in Eqs. (G-18) to (G-25) which are independent of x and y , are ignored, i.e., set $U_f = U_g = 0$, and set $F_{xc} = F_{xs} = F_{yc} = F_{ys} = 0$ when performing a magnetic response calculation (but not in a stability calculation or a mechanical unbalance calculation where the magnetic forces are proportional to x and y).

As a result of these 8 calculations, the influence coefficients have been obtained which relate the bending moment and shear force at the last rotor station to the amplitudes and slopes at the first station:

$$\begin{Bmatrix} \alpha_{11} & \alpha_{12} & \dots & \alpha_{18} \\ \alpha_{21} & \alpha_{22} & \dots & \alpha_{28} \\ \vdots & \vdots & & \vdots \\ \alpha_{81} & \alpha_{82} & \dots & \alpha_{88} \end{Bmatrix} \begin{Bmatrix} x_{c1} \\ x_{s1} \\ \vdots \\ \phi_{s1} \end{Bmatrix} \sim \begin{Bmatrix} M'_{xcm} \\ M'_{xsm} \\ \vdots \\ V'_{ysm} \end{Bmatrix} \quad (\text{G-31})$$

This influence coefficient matrix is valid for one particular value of the frequency ν .

In the further discussion, it is necessary to separate the stability calculation and the response calculations.

In the stability calculation there is only one frequency value, namely $\nu = \omega$. Thus, there is only one influence coefficient matrix. Since at the last rotor station,

$$M'_{xcm} = M'_{xsm} = M'_{ycm} = M'_{ysm} = V'_{xcm} = V'_{xsm} = V'_{ycm} = V'_{ysm} = 0 \quad (\text{G-32})$$

the right hand side of Eqs. (G-31) is zero. Hence, a non-trivial solution for $x_{c1}, x_{s1}, \dots, \phi_{s1}$ only exists if the determinant Δ of the matrix vanishes.

$$\Delta = \begin{vmatrix} \alpha_{11} & \alpha_{12} & - & - & - & - & - & \alpha_{18} \\ \alpha_{21} & \alpha_{22} & - & - & - & - & - & \alpha_{28} \\ \vdots & \vdots & & & & & & \vdots \\ \alpha_{81} & \alpha_{82} & - & - & - & - & - & \alpha_{88} \end{vmatrix} \quad (G-33)$$

Thus, when $\Delta = 0$ the rotor is on the threshold of instability. Now, for a particular rotor-alternator system operating at specified conditions, the determinant will usually have a non-zero value. One way to establish if the rotor then is stable or unstable is to determine if the rotor operates below or above the instability threshold. This requires finding the threshold. To this end, normalize the eight magnetic force coefficients with respect to $\sqrt{Q_{xx1}^2 + q_{xx1}^2}$:

$$\begin{aligned} Q_{xx1} &= \left[\frac{Q_{xx1}}{\sqrt{Q_{xx1}^2 + q_{xx1}^2}} \right] \sqrt{Q_{xx1}^2 + q_{xx1}^2} \\ q_{xx1} &= \left[\frac{q_{xx1}}{\sqrt{Q_{xx1}^2 + q_{xx1}^2}} \right] \sqrt{Q_{xx1}^2 + q_{xx1}^2} \\ Q_{xy1} &= \left[\frac{Q_{xy1}}{\sqrt{Q_{xx1}^2 + q_{xx1}^2}} \right] \sqrt{Q_{xx1}^2 + q_{xx1}^2} \\ q_{xy1} &= \left[\frac{q_{xy1}}{\sqrt{Q_{xx1}^2 + q_{xx1}^2}} \right] \sqrt{Q_{xx1}^2 + q_{xx1}^2} \end{aligned} \quad (G-34)$$

and the same for Q_{yx1} , q_{yx1} , Q_{yy1} , and q_{yy1} . Then vary $\sqrt{Q_{xx1}^2 + q_{xx1}^2}$ starting from zero, in steps, keeping the ratios in the brackets in Eqs. (G-34) constant and maintaining the same rotor speed. For each value of $\sqrt{Q_{xx1}^2 + q_{xx1}^2}$, the value of the determinant can be computed as described above and where the determinant changes sign, is the instability threshold. If the actual value of $\sqrt{Q_{xx1}^2 + q_{xx1}^2}$ is less than the threshold value, the rotor is stable, otherwise it is unstable. In passing, it should be noted that this assumes the rotor to be stable when $\sqrt{Q_{xx1}^2 + q_{xx1}^2} = 0$, i.e. in the absence of any magnetic forces, but this is already known to be the case for the rotor presently investigated.

Turning next to the mechanical unbalance response calculation where the frequency ν is equal to ω , the 8 by 8 influence coefficient matrix of Eqs. (G-31) is first computed as previously described. Thereafter, a ninth rotor calculation is performed in which the mechanical unbalances $U_{\xi j}$ and $U_{\eta j}$ are assigned

their actual values, and the amplitudes and slopes at the first rotor station are set equal to zero ($x_{c1} = x_{s1} = y_{c1} = \dots = \phi_{s1} = 0$). The corresponding bending moments and shear forces at the last rotor station are computed as

$$M'_{xcm} = \alpha_{19}, M'_{xsm} = \alpha_{29}, M'_{ycm} = \alpha_{39}, \dots, V'_{ysm} = \alpha_{89} \quad (G-35)$$

Then, in total,

$$\begin{Bmatrix} \alpha_{11} & \alpha_{12} & \dots & \alpha_{18} \\ \alpha_{21} & \alpha_{22} & \dots & \alpha_{28} \\ \vdots & \vdots & & \vdots \\ \alpha_{81} & \alpha_{82} & \dots & \alpha_{88} \end{Bmatrix} \begin{Bmatrix} x_{c1} \\ x_{s1} \\ \vdots \\ \phi_{s1} \end{Bmatrix} + \begin{Bmatrix} \alpha_{19} \\ \alpha_{29} \\ \vdots \\ \alpha_{89} \end{Bmatrix} = \begin{Bmatrix} M'_{xcm} \\ M'_{xsm} \\ \vdots \\ V'_{ysm} \end{Bmatrix} = 0 \quad (G-36)$$

These 8 simultaneous equations can be solved for $x_{c1}, x_{s1}, \dots, \phi_{s1}$, and by back substitution the amplitudes at each rotor station can be computed from the relationships:

$$\begin{Bmatrix} x_{cj} \\ x_{sj} \\ y_{cj} \\ y_{sj} \end{Bmatrix} = \begin{Bmatrix} \beta_{11} & \beta_{12} & \dots & \beta_{18} \\ \beta_{21} & \beta_{22} & \dots & \beta_{28} \\ \beta_{31} & \beta_{32} & \dots & \beta_{38} \\ \beta_{41} & \beta_{42} & \dots & \beta_{48} \end{Bmatrix} \begin{Bmatrix} x_{c1} \\ x_{s1} \\ \vdots \\ \phi_{s1} \end{Bmatrix} + \begin{Bmatrix} \beta_{19} \\ \beta_{29} \\ \beta_{39} \\ \beta_{49} \end{Bmatrix} \quad (G-37)$$

where the β 's have been obtained in the process of performing the nine rotor calculations.

The calculation of the response of the rotor to the magnetic forces caused by a magnetic eccentricity is analogous to the unbalance response calculation. However, a complete calculation must be performed for each frequency present ($\nu = 2\omega, 4\omega, \dots, 2N\omega$). At any given frequency, the 8 calculations previously described are first performed in which $u_{\xi j} = u_{\eta j} = F_{xc} = F_{xs} = F_{yc} = F_{ys} = 0$. Thereby, the 8 by 8 influence coefficient matrix of Eqs. (G-31) is obtained. Then a ninth rotor calculation is performed where $F_{xc}, F_{xs}, F_{yc}, F_{ys}$ are assigned their actual values at the selected frequency as defined by Eqs. (G-17) ($u_{\xi j}$ and $u_{\eta j}$ are of course, zero). Thus, the coefficients $\alpha_{19}, \alpha_{29}, \dots, \alpha_{89}$ are obtained similar to Eq. (G-35), and the corresponding

values of $x_{c1}, x_{s1}, \dots, \phi_1$ can be found from Eqs. (G-36). Finally, the rotor amplitudes are obtained from Eqs. (G-37). Performing similar calculations for all frequencies, $n=1, 2, \dots, N$, the total rotor amplitudes can be found by superposition:

$$x_j = \sum_{n=1}^N [x_{cjn} \cos(2n\omega t) - x_{sjn} \sin(2n\omega t)] \quad (G-38)$$

By plotting the equations, the maximum amplitudes can be found.

APPENDIX H

SPECIFICATION NO. P0055-1 (NASA)

July 15, 1963

SOLAR BRAYTON CYCLE SPACE POWER SYSTEM ENVIRONMENTAL SPECIFICATION

1.0 SCOPE

- 1.1 This specification covers the anticipated environmental conditions listed below to which the Solar Brayton Cycle Space Power System and components shall be designed to withstand without malfunction or performance degradation.

This specification does not cover development and/or acceptance tests.

1.2 Environments

Environmental conditions specified are applicable to each of the components and the complete solar space power system through manufacture, storage, transportation, lift-off, boost, orbit, and orbital transfer.

2.0 Environmental Conditions

2.1 Storage and Transportation

The components and their associated equipment shall be capable of withstanding without performance impairment the following loads applied along each of three mutually perpendicular axes of its container.

2.1.1 Shock - 4 G shock within one of the following times and wave shape:

2.1.1.1 Triangular pulse of 10 milliseconds.

2.1.1.2 Half-sine pulse of 8 milliseconds.

2.1.1.3 Rectangular pulse of 5 milliseconds.

2.1.2 Vibration:

2.1.2.1 2 - 10 cps 0.40 inches double amplitude

2.1.2.2 10 - 500 cps 2.0 G peak

2.2 Launch, Lift-Off, Boost

The non-operation system and components shall be capable of withstanding without performance impairment the following simultaneous

launch loads applied at the system mounting points and in the directions and magnitudes specified:

2.2.1 Shock

35 G shock along each of three mutually perpendicular axes within one of the wave shape and pulse times in 2.1.1. above.

2.2.2 Vibration

Sinusoidal input applied at the system mounting points along each of three mutually perpendicular axes

16 - 100 cps	at 6 G peak
100 - 180 cps	at 0.0118" double amplitude
180 - 2000 cps	at 19 G peak

2.2.3 Acceleration

The non-operating system and its accessory components shall be capable of withstanding the following launch accelerations for five (5) minutes duration:

- 2.2.3.1 7 G - along boost vehicle lift-off axis.
3 G - along boost vehicle lift-off axis in opposite direction.
4.5 G - all directions in plane normal to lift-off axis.

2.2.4 Acoustic Noise

The non-operating system and its components shall be capable of withstanding the induced vibrations while subjected to an acoustic noise field with an integrated level of 148 d.b., Re 0.0002 micro-bar.

2.3 Orbital Operation

The equipment shall be designed to be capable of start-up and continuous operation at rated power in earth orbits of from 300 to 20,000 nautical miles without malfunction for 10,000 hours time.

2.3.1 Shock

Prior to system startup and deployment, the components shall sustain up to 7 G shock (course correction) along the lift-off or flight axis with one of the wave forms and time durations indicated in paragraph 2.1.1.

2.3.2 Vibration

The system and components will sustain vibrations in orbit while in operation of 0.25 G peak over a frequency range of 5 to 2000 cps for a time period of five minutes for each occurrence.

2.3.3 Acceleration

2.3.3.1 Undeployed

The undeployed system and components will sustain accelerations of $3\frac{1}{2}$ G in one direction along the lift-off axis, and plus or minus 1 G in all directions in the plane normal to the lift-off axis. These accelerations will be sustained individually for a period of five minutes maximum for each occurrence.

2.3.3.2 Deployed

The deployed operating system will also be required to be capable of sustaining a continuous, unidirectional acceleration arising from a 4 RPM spin rate of the spacecraft. The G loading on the system components will be a function of their radial location with respect to the spin axis. For the purposes of this application, the centerline axis of the collector and system is located at a radius of 33 feet from the spin axis and experiences an 0.18 G acceleration.

APPENDIX I

SPECIFICATION NO. 6359-A

November 5, 1965

PRATT & WHITNEY AIRCRAFT SPECIFICATION FOR ACCEPTANCE TESTING A TURBOALTERNATOR ROTOR DYNAMIC SIMULATOR

1. SCOPE

This specification covers the acceptance test for a turboalternator rotor dynamic simulator incorporating hydrodynamic gas bearings.

2. REQUIREMENTS

2.1 General

The test specified below is intended to demonstrate satisfactory operation of the dynamic simulator incorporating hydrodynamic gas bearings.

2.2 Data

The following data within the accuracy shown, shall be continuously monitored and any condition which indicates that the limits of paragraph 3 have been exceeded shall be recorded.

- a. Time of day -----
- b. Rotation speed ----- ± 100 rpm
- c. Position of shaft relative
to bearing ----- ± 0.00005 inch
- d. Dynamic displacement of at least
one bearing pad in each bearing ----- ± 0.00005 inch
- e. Journal bearing, housings and pad
and thrust bearing stator
temperatures ----- ± 2 Farenheit degrees
- f. Ambient gas pressure at each bearing ----- ± 0.3 psi
- g. Vibration at each bearing support- ± 0.0005 inch

2.3 Acceptance Test

The acceptance test shall consist of runs a. through f. of Table I. The test runs need not be conducted in the order listed. The applicable test cycles are defined in paragraph 2.3.1. The forward direction is defined as the axial direction from the thrust bearing toward the turbine.

TABLE I
ACCEPTANCE TEST

Test Run	Position of Rotor Axis	Rotor Unbalance	Location of Rotor Unbalance	Applicable Test Cycle	Number of Test Cycles Applied
a.	horizontal	Less than 0.001 oz-in	Not specified	I	3
b.	horizontal	0.005 oz-in	5.75 inches overhung forward of front bearing centerline	I	3
c.	vertical	Less than 0.001 oz-in	Not specified	I	3
d.	vertical	0.005 oz-in	5.75 inches overhung forward of front bearing centerline	I	3
e.	horizontal	Less than 0.001 oz-in	Not specified	II	1
f.	vertical	0.005 oz-in	5.75 inches overhung forward of front bearing centerline	II	1

2.3.1 Test Cycles

During each of the test cycles the bearing lubricant shall be dry, oil free air or inert gas. Ambient pressure at the bearing shall be equal to or less than 10.5 pounds per square inch absolute. Gas at pressure above ambient may be supplied to the bearings during acceleration, deceleration or as specified herein. The following test cycles shall apply as specified herein:

2.3.1.1 Test Cycle I

- a. Accelerate rotor to 12,000 RPM and maintain $12,000 \pm 200$ RPM for a period of 10 minutes.
- b. Accelerate rotor to 14,400 RPM and maintain $14,400 \pm 200$ RPM for a period of 5 minutes.
- c. Decelerate rotor to a complete stop.

2.3.1.2 Test Cycle II

- a. Accelerate the rotor to 12,000 RPM and maintain $12,000 \text{ RPM} \pm 500$ RPM for a period of at least 10 minutes. While the rotor is maintained at $12,000 \pm 500$ RPM and while gas at pressure above ambient is applied to the thrust bearing, apply the following thrust loads: 100 ± 10 pounds forward or reversed, 0 ± 5 pounds and 250 ± 25 pounds rearward.

While the rotor is maintained at $12,000 \pm 500$ RPM and while no gas at pressure above 10.5 psia is applied directly to the bearings, apply the following thrust loads in the rearward direction, 85 ± 5 , 55 ± 5 and 30 ± 5 pounds.

- b. Decelerate rotor to a complete stop.

3. ACCEPTANCE

The tests shall be satisfactorily completed when the entire acceptance test has been completed without changes to the configuration, except as authorized by the Pratt & Whitney Aircraft program manager, and the following conditions have been met.

- a. There shall be no indication of bearing seizure or contact between the rotor shaft and bearing at 12,000 RPM or above with no gas at pressure above ambient supplied. With gas supplied at a pressure above ambient there is no indication of bearing seizure or contact above 600 RPM.
- b. Vibration at the bearing mounts does not exceed 0.002 inches double amplitude.
- c. Maximum rotor excursion does not exceed 0.005 inch axially or 0.002 inch radially.
- d. Bearing pad motion does not exceed 0.0005 inch double amplitude at the free end furthest removed from the pivot.
- e. The thrust bearing axial vibratory motion at the outer rim shall not exceed 0.0006 inch double amplitude.

APPENDIX J: REDUCTION OF BEARING DATA ACQUIRED DURING ROTOR-BEARING-ALTERNATOR TESTING

During the course of the rotor-bearing alternator test program to determine the rotor-bearing system response to electromagnetic forces, values of bearing film thickness and temperature were tabulated for each of the 216 test points involved. For each of the journal bearings, the data acquired consisted of a film thickness dimension for each of the four pads which constitute a bearing and eight temperatures. The film thickness dimensions were obtained from capacitance probes mounted in the pads as shown in Figures II-23 and II-24, readout being obtained from CRO's. Temperatures were obtained from chromel-alumel thermocouples, four of which were attached to one unloaded and one loaded pad in each bearing in the positions shown in Figure II-26, readout of temperature being obtained from temperature recorders.

During the course of the test program, it was not found convenient to permit the temperature of the journal bearings to reach the values for which theoretical bearing performance calculations had been made. To allow comparison of experimental performance with calculated performance it was, therefore, necessary to perform further calculations using as an input parameter the reduced value of viscosity associated with the temperatures which were experienced during testing. The value of viscosity used in these calculations was determined from the average temperature (110F) of the 16 bearing pad thermocouples (8 per bearing) over the 216 data points involved. The maximum and minimum values of bearing temperature observed during testing were as follows.

<u>Bearing Identity</u>	<u>Maximum Temperature Degrees F</u>	<u>Minimum Temperature Degrees F</u>
Turbine end Journal Bearing	128.5	79
Thrust End Journal Bearing	143	90

The change in viscosity over this range of temperatures is $\pm 4.4\%$ of the average value used for the purposes of calculation.

Further parameters used in both the theoretical calculations of bearing performance and the evaluation of experimental data are the values of journal and pad radii. The values used were obtained from the inspection records of the components and are given as follows:

Component	Inspection Dimension (inches)	Radii Used In Evaluation of test data (inches)
Turbine end journal in plane of pivots	3.49617/3.49613 Dia.	1.748075
Thrust end journal in plane of pivots	3.49603/3.49591 Dia.	1.747985
Bearing Pad (1 from each bearing)	1.7505	1.7505

To reduce the number of calculations of theoretical bearing performance, an average value of journal radius was used, i.e., 1.74803, the results being approximately applicable to both journal bearings. The clearance ratio C_p/R at design speed becomes.

$$\frac{C_p}{R} = \frac{R_p - R}{R}$$

$$C_p/R = 1.31 \times 10^{-3}$$

where C_p = Radial difference between the machined radius of the bearing pad and the radius of the journal at design speed.

R_p = Machined radius of bearing pad

R = Machined radius of journal + radial centrifugal growth.

The effect of differential thermal expansion on this ratio is negligible and is, therefore, ignored.

The theoretical bearing performance was calculated using a viscosity of 2.73×10^{-9} lb.sec./in.² and a clearance ratio of 1.31×10^{-3} , for a selected range of bearing loads and diametral clearance values (preload), one set of calculations being required at each ambient pressure involved, i.e., 10.5 PSIA and 7.2 PSIA. The results of the theoretical calculations are shown plotted in the form of loaded-pad film thickness versus preload in Figures VII-17, VII-18 and VII-19.

To superimpose the experimentally obtained data on the curves of theoretical bearing performance it was necessary to determine an average value of preload for the complete bearing. This was accomplished from the geometrical relationship

$$m = 1 - \frac{HP}{C_p}$$

where m = Preload ratio

HP = Average film thickness of 4 pads

C_p = Radial difference between the machined radius of the bearing pads and the radius of the journal at design speed.

Also required was an average value of loaded-pad film thickness. To reduce the considerable amount of experimental data accumulated during test a computer program was written which performed the following calculations:

- a. Modified the experimentally obtained readings of film thickness to allow for instrumentation calibration factors.
- b. Calculated the average film thickness HP for each bearing from

$$HP = \frac{hp1 + hp2 + hp3 + hp4}{4}$$

where $hp1$ $hp4$ are the corrected values of film thickness for the 4 pads comprising each bearing.

- c. Calculated the average film thickness HPL of the two loaded pads from

$$HPL = \frac{hp3 + hp4}{2}$$

- d. Calculated the value of preload m from

$$m = 1 - \frac{HP}{C_p}$$

where C_p values of 2.26×10^{-3} and 2.35×10^{-3} were given the turbine end and thrust bearing end respectively, these values being determined from the inspection records of the journal and pads.

In addition to the calculation of the above quantities, calculations were performed to permit comparison of the sum of the film thicknesses in one loaded and one diametrically opposed unloaded pad, with the sum of the film thicknesses of the remaining two pads comprising a bearing. Also performed were calculations to determine the eccentricity and the change of eccentricity of the journal within the bearing assembly. These calculations are described as follows:

- e. Calculate the average film thickness of the two unloaded pads from

$$HPU = \frac{hp1 + hp2}{2}$$

- f. Calculate the sum of the film thicknesses of one loaded and one unloaded pad

$$HPUL1 = hp1 + hp3$$

- g. Calculate the sum of the film thicknesses for the remaining loaded and unloaded pads

$$HPUL2 = hp2 + hp4$$

- h. Compare the sum of the pad film thicknesses of one loaded pad and one unloaded pad with that of the sum of the remaining pad film thicknesses from

$$HPULD = HPUL1 - HPUL2$$

- i. Calculate and define the direction of the eccentricity of the journal within the bearing assembly.

Eccentricity in the direction between the loaded pads EBL from

$$EBL = \frac{HP - HPL}{.707}$$

Eccentricity in the direction between the unloaded pads (EBU) from

$$EBU = \frac{HP-HPU}{.707}$$

- j. Calculate the change and direction of change in eccentricity from the eccentricity observed at the zero excitation test point.

An increase in eccentricity (ΔEBL) denoted +VE

A decrease in eccentricity (ΔEBL) denoted -VE

An increase in eccentricity (ΔEBU) denoted +VE

A decrease in eccentricity (ΔEBU) denoted -VE

The results of these calculations for each of the 216 test points are contained in Table J-1.

Certain of the experimentally obtained values of film thickness and preload are shown superimposed on the curves of theoretical performance shown in Figures VII-17, VII-18 and VII-19. The experimental data in these plots were obtained from the tests of Configuration D (Figures VII-17 and VII-18) and Configuration F (Figure VII-19). The experimental data for the remaining test points were also plotted.

The test conditions relating to the configuration and test point numbers referred to on these pages can be obtained from Tables VII-2 through VII-5 inclusive. It should be noted that the first test point number in each group is the zero excitation test point number. The duration of the short circuits (5 secs. max.) did not permit the acquisition of data; therefore, the data contained in those lines identified by a test point number which relates to a single or three phase short circuit condition are for conditions immediately prior to the initiation of the short circuit.

Table J-1

Tabulation of Bearing Performance Data Acquired
During Rotor-Bearing-Alternator
Simulator Testing

BRG. NO. 1 CONFIGURATION A AMBIENT PRESS 10.5PSIA											
TEST POINT	HP	HPU	HPL	HPUL1	HPUL2	HPULD	M	EBL	EBU	DELTA EBL	DELTA EBU
3	1.314	1.440	1.187	2.647	2.608	0.040	0.419	0.179			
1	1.175	1.319	1.032	2.286	2.416	-0.130	0.480	0.203		0.025	
2	1.175	1.319	1.032	2.286	2.416	-0.130	0.480	0.203		0.025	
4	1.144	1.256	1.032	2.286	2.290	-0.004	0.494	0.159		-0.020	
5	1.067	1.165	0.969	2.106	2.162	-0.056	0.528	0.139		-0.040	
6	1.006	1.044	0.967	1.988	2.035	-0.047	0.555	0.054		-0.125	
25	1.191	1.162	1.221	2.408	2.358	0.050	0.473		0.042	0.221	
29	1.050	1.037	1.062	2.287	1.911	0.376	0.536		0.017	0.196	
33	1.021	0.978	1.064	2.107	1.976	0.131	0.548		0.061	0.240	

BRG. NO. 1 CONFIGURATION A AMBIENT PRESS 7.2PSIA											
TEST POINT	HP	HPU	HPL	HPUL1	HPUL2	HPULD	M	EBL	EBU	DELTA EBL	DELTA EBU
11	1.190	1.288	1.092	2.408	2.353	0.055	0.473	0.138			
7	0.990	1.044	0.935	1.988	1.971	0.017	0.562	0.077		-0.061	
8	1.005	1.074	0.937	1.987	2.035	-0.048	0.555	0.097		-0.041	
9	1.036	1.104	0.967	2.107	2.035	0.072	0.542	0.097		-0.042	
10	1.021	1.074	0.967	2.048	2.035	0.013	0.548	0.075		-0.063	
12	1.051	1.135	0.967	2.107	2.098	0.009	0.535	0.119		-0.019	
26	1.159	1.162	1.157	2.408	2.229	0.178	0.487	0.000		0.138	
30	0.973	0.978	0.969	2.046	1.847	0.199	0.569	0.006		-0.132	
34	0.975	0.948	1.001	1.987	1.911	0.075	0.569		0.038	0.176	

BRG. NO. 2 CONFIGURATION A AMBIENT PRESS 10.5PSIA											
TEST POINT	HP	HPU	HPL	HPUL1	HPUL2	HPULD	M	EBL	EBU	DELTA EBL	DELTA EBU
3	1.144	1.222	1.067	2.138	2.439	-0.301	0.513	0.110			
1	1.248	1.338	1.158	2.376	2.616	-0.240	0.469	0.128		0.018	
2	1.248	1.338	1.158	2.376	2.616	-0.240	0.469	0.128		0.018	
4	1.143	1.251	1.036	2.138	2.435	-0.297	0.514	0.152		0.042	
5	1.278	1.367	1.188	2.376	2.735	-0.359	0.456	0.126		0.017	
6	1.247	1.367	1.128	2.316	2.673	-0.357	0.469	0.169		0.060	
25	1.247	1.367	1.128	2.316	2.673	-0.357	0.469	0.169		0.060	
29	1.232	1.367	1.097	2.316	2.612	-0.296	0.476	0.191		0.081	
33	1.201	1.367	1.036	2.256	2.550	-0.294	0.489	0.234		0.125	

BRG. NO. 2 CONFIGURATION A AMBIENT PRESS 7.2PSIA											
TEST POINT	HP	HPU	HPL	HPUL1	HPUL2	HPULD	M	EBL	EBU	DELTA EBL	DELTA EBU
11	1.054	1.164	0.945	1.959	2.258	-0.299	0.551	0.155			
7	1.187	1.308	1.067	2.138	2.612	-0.473	0.495	0.171		0.016	
8	1.158	1.279	1.036	2.138	2.492	-0.354	0.507	0.172		0.018	
9	1.039	1.163	0.914	1.900	2.254	-0.353	0.558	0.176		0.021	
10	1.113	1.251	0.975	2.078	2.373	-0.295	0.526	0.195		0.040	
12	1.218	1.308	1.128	2.198	2.673	-0.475	0.482	0.128		-0.027	
26	1.158	1.279	1.036	2.138	2.492	-0.354	0.507	0.172		0.018	
30	1.142	1.308	0.975	2.078	2.488	-0.410	0.514	0.236		0.081	
34	1.157	1.308	1.006	2.078	2.550	-0.472	0.508	0.214		0.059	

BRG. NO. 1 CONFIGURATION A AMBIENT PRESS 10.5PSIA										DELTA	DELTA
TEST POINT										EBU	EBU
NO.	HP	HPU	HPL	HPUL1	HPUL2	HPULD	M	EBL			
15	1.657	1.656	1.659	3.191	3.438	-0.247	0.267	0.000			
13	1.363	1.412	1.314	2.589	2.863	-0.274	0.397	0.069	0.069		
14	1.425	1.442	1.407	2.770	2.928	-0.157	0.370	0.025	0.025		
16	1.503	1.503	1.502	3.191	3.438	-0.229	0.335	0.000	0.000		
17	1.363	1.353	1.373	2.652	2.799	-0.147	0.397		0.015	0.015	
18	1.379	1.384	1.373	2.652	2.862	-0.210	0.390	0.008	0.008		
35	1.348	1.353	1.343	2.592	2.799	-0.208	0.404	0.007	0.007		
27	1.518	1.535	1.502	2.891	3.182	-0.292	0.328	0.023	0.023		
31	1.285	1.321	1.250	2.470	2.672	-0.202	0.431	0.050	0.050		

BRG. NO. 1 CONFIGURATION A AMBIENT PRESS 7.2PSIA										DELTA	DELTA
TEST POINT										EBU	EBU
NO.	HP	HPU	HPL	HPUL1	HPUL2	HPULD	M	EBL			
23	1.765	1.840	1.690	3.431	3.628	-0.197	0.219	0.106			
36	1.301	1.323	1.280	2.471	2.735	-0.264	0.424	0.030	-0.076		
19	1.316	1.353	1.280	2.531	2.735	-0.204	0.418	0.051	-0.055		
20	1.362	1.412	1.312	2.650	2.799	-0.149	0.397	0.071	-0.036		
21	1.441	1.505	1.377	2.709	3.054	-0.344	0.362	0.091	-0.015		
22	1.440	1.503	1.377	2.769	2.991	-0.222	0.363	0.090	-0.017		
24	1.487	1.565	1.409	2.829	3.118	-0.289	0.342	0.110	0.004		
28	1.518	1.596	1.439	2.890	3.181	-0.292	0.328	0.111	0.005		
32	1.301	1.321	1.282	2.470	2.736	-0.266	0.424	0.028	-0.079		

BRG. NO. 2 CONFIGURATION A AMBIENT PRESS 10.5PSIA										DELTA	DELTA
TEST POINT										EBU	EBU
NO.	HP	HPU	HPL	HPUL1	HPUL2	HPULD	M	EBL			
15	1.247	1.309	1.185	2.557	2.431	0.126	0.469	0.088			
13	1.425	1.484	1.366	2.973	2.727	0.247	0.394	0.083	-0.005		
14	1.380	1.455	1.306	2.914	2.607	0.306	0.413	0.106	0.018		
16	1.277	1.338	1.215	2.676	2.431	0.245	0.457	0.087	-0.000		
17	1.425	1.513	1.336	2.972	2.727	0.246	0.394	0.125	0.037		
18	1.425	1.513	1.336	2.972	2.727	0.246	0.394	0.125	0.037		
35	1.484	1.571	1.397	3.091	2.846	0.245	0.368	0.123	0.035		
27	1.484	1.571	1.397	3.091	2.846	0.245	0.368	0.123	0.035		
31	1.529	1.630	1.428	3.150	2.965	0.185	0.349	0.142	0.055		

BRG. NO. 2 CONFIGURATION A AMBIENT PRESS 7.2PSIA										DELTA	DELTA
TEST POINT										EBU	EBU
NO.	HP	HPU	HPL	HPUL1	HPUL2	HPULD	M	EBL			
23	1.291	1.368	1.215	2.735	2.431	0.304	0.451	0.108			
36	1.438	1.571	1.306	3.031	2.722	0.309	0.388	0.188	0.080		
19	1.409	1.513	1.306	2.972	2.665	0.308	0.400	0.147	0.038		
20	1.395	1.484	1.306	2.914	2.665	0.249	0.407	0.126	0.018		
21	1.306	1.397	1.215	2.735	2.488	0.247	0.444	0.129	0.020		
22	1.395	1.484	1.306	2.914	2.665	0.249	0.407	0.126	0.018		
24	1.544	1.629	1.458	3.151	3.023	0.129	0.343	0.121	0.012		
28	1.529	1.600	1.458	3.151	2.965	0.186	0.349	0.100	-0.008		
32	1.513	1.630	1.397	3.150	2.903	0.247	0.356	0.164	0.056		

BRG. NO. 1 CONFIGURATION B AMBIENT PRESS 10.5PSIA

TEST POINT	NO.	HP	HPU	HPL	HPUL1	HPUL2	HPULD	M	EBL	EBU	DELTA EBL	DELTA EBU
	3	1.024	0.951	1.096	1.928	2.166	-0.238	0.547		0.102		
	1	0.838	0.767	0.908	1.567	1.784	-0.217	0.629		0.100		-0.003
	2	0.884	0.829	0.939	1.688	1.847	-0.160	0.609		0.078		-0.025
	4	0.899	0.860	0.939	1.688	1.910	-0.223	0.602		0.055		-0.047
	5	0.837	0.767	0.906	1.628	1.720	-0.092	0.630		0.098		-0.004
	6	0.822	0.738	0.906	1.568	1.720	-0.151	0.636		0.119		0.017
	33	0.760	0.676	0.844	1.448	1.592	-0.145	0.664		0.119		0.016
	25	1.009	0.922	1.096	1.869	2.166	-0.297	0.554		0.123		0.021
	29	0.992	0.951	1.033	1.868	2.102	-0.234	0.561		0.058		-0.044

BRG. NO. 1 CONFIGURATION B AMBIENT PRESS 7.2PSIA

TEST POINT	NO.	HP	HPU	HPL	HPUL1	HPUL2	HPULD	M	EBL	EBU	DELTA EBL	DELTA EBU
	11	1.179	1.106	1.251	2.230	2.484	-0.254	0.479		0.103		
	34	0.714	0.646	0.781	1.327	1.528	-0.201	0.684		0.095		-0.008
	7	0.791	0.738	0.844	1.507	1.656	-0.148	0.650		0.075		-0.028
	8	0.915	0.860	0.969	1.748	1.910	-0.162	0.595		0.077		-0.026
	9	1.008	0.983	1.033	1.868	2.165	-0.297	0.554		0.036		-0.068
	10	0.977	0.922	1.033	1.808	2.102	-0.294	0.567		0.079		-0.024
	12	1.023	0.983	1.064	1.928	2.165	-0.236	0.547		0.057		-0.046
	26	1.024	0.983	1.065	1.868	2.229	-0.362	0.547		0.058		-0.045
	30	0.946	0.922	0.971	1.747	2.038	-0.290	0.581		0.035		-0.068

BRG. NO. 2 CONFIGURATION B AMBIENT PRESS 10.5PSIA

TEST POINT	NO.	HP	HPU	HPL	HPUL1	HPUL2	HPULD	M	EBL	EBU	DELTA EBL	DELTA EBU
	3	0.787	0.814	0.760	1.546	1.604	-0.058	0.665	0.038			
	1	0.817	0.843	0.790	1.606	1.662	-0.056	0.652	0.037		-0.001	
	2	0.832	0.873	0.790	1.665	1.662	0.003	0.646	0.058		0.020	
	4	0.615	0.501	0.730	0.862	1.600	-0.738	0.738		0.161	0.200	
	5	0.846	0.901	0.790	1.665	1.719	-0.055	0.640	0.078		0.040	
	6	0.846	0.901	0.790	1.665	1.719	-0.055	0.640	0.078		0.040	
	33	0.816	0.873	0.760	1.665	1.600	0.065	0.653	0.080		0.042	
	25	0.905	0.960	0.851	1.783	1.838	-0.055	0.615	0.077		0.038	
	29	1.054	1.134	0.973	2.080	2.134	-0.054	0.552	0.114		0.076	

BRG. NO. 2 CONFIGURATION B AMBIENT PRESS 7.2PSIA

TEST POINT	NO.	HP	HPU	HPL	HPUL1	HPUL2	HPULD	M	EBL	EBU	DELTA EBL	DELTA EBU
	11	0.832	0.873	0.790	1.665	1.662	0.003	0.646	0.058			
	34	0.742	0.814	0.669	1.486	1.480	0.005	0.684	0.103		0.045	
	7	0.742	0.814	0.669	1.486	1.480	0.005	0.684	0.103		0.045	
	8	0.816	0.873	0.760	1.665	1.600	0.065	0.653	0.080		0.022	
	9	0.801	0.873	0.730	1.605	1.600	0.005	0.659	0.101		0.043	
	10	0.861	0.931	0.790	1.724	1.719	0.004	0.634	0.099		0.041	
	12	0.920	0.960	0.881	1.843	1.838	0.005	0.608	0.055		-0.003	
	26	0.890	0.960	0.820	1.783	1.777	0.007	0.621	0.098		0.040	
	30	1.038	1.134	0.942	2.080	2.073	0.008	0.558	0.136		0.078	

BRG. NO. 1 CONFIGURATION B AMBIENT PRESS 10.5PSIA												
TEST POINT		HP	HPU	HPL	HPUL1	HPUL2	HPULD	M	EBL	EBU	DELTA EBL	DELTA EBU
15		1.781	1.810	1.752	3.432	3.692	-0.260	0.212	0.041			
13		1.472	1.503	1.441	2.769	3.119	-0.350	0.349	0.044		0.003	
14		1.518	1.535	1.502	2.891	3.182	-0.292	0.328	0.023		-0.018	
16		1.565	1.565	1.564	3.011	3.247	-0.236	0.308	0.000		0.041	
17		1.379	1.382	1.375	2.651	2.863	-0.212	0.390	0.005		-0.036	
18		1.380	1.353	1.407	2.592	2.928	-0.336	0.389		0.039	0.079	
31		1.364	1.353	1.375	2.592	2.863	-0.272	0.397		0.016	0.057	
27		1.426	1.412	1.439	2.711	2.992	-0.281	0.369		0.019	0.060	
35		1.271	1.230	1.312	2.411	2.673	-0.262	0.438		0.058	0.099	

BRG. NO. 1 CONFIGURATION B AMBIENT PRESS 7.2PSIA												
TEST POINT		HP	HPU	HPL	HPUL1	HPUL2	HPULD	M	EBL	EBU	DELTA EBL	DELTA EBU
23		1.858	1.899	1.816	3.611	3.820	-0.210	0.178	0.059			
32		1.349	1.323	1.375	2.532	2.863	-0.332	0.403		0.037	0.096	
19		1.410	1.414	1.407	2.651	2.991	-0.340	0.376	0.005		-0.054	
20		1.472	1.474	1.470	2.831	3.055	-0.224	0.349	0.000		0.059	
21		1.214	0.926	1.502	1.609	3.246	-1.636	0.463		0.407	0.466	
22		1.518	1.565	1.471	2.890	3.182	-0.293	0.328	0.066		0.007	
24		1.410	1.503	1.316	2.647	2.991	-0.343	0.376	0.133		0.074	
28		1.363	1.442	1.284	2.588	2.863	-0.276	0.397	0.112		0.053	
36		1.379	1.353	1.405	2.652	2.863	-0.211	0.390		0.037	0.096	

BRG. NO. 2 CONFIGURATION B AMBIENT PRESS 10.5PSIA												
TEST POINT		HP	HPU	HPL	HPUL1	HPUL2	HPULD	M	EBL	EBU	DELTA EBL	DELTA EBU
15		1.308	1.309	1.306	2.677	2.554	0.123	0.444	0.000			
13		1.455	1.512	1.397	2.973	2.846	0.128	0.381	0.081		0.081	
14		1.440	1.484	1.397	2.973	2.788	0.185	0.387	0.061		0.061	
16		1.321	1.367	1.276	2.736	2.550	0.186	0.438	0.065		0.065	
17		1.455	1.513	1.397	3.032	2.788	0.244	0.381	0.082		0.082	
18		1.410	1.484	1.336	2.914	2.727	0.187	0.400	0.104		0.104	
31		1.410	1.484	1.336	2.914	2.727	0.187	0.400	0.104		0.104	
27		1.515	1.542	1.489	3.092	2.970	0.123	0.355	0.037		0.037	
35		1.574	1.630	1.519	3.270	3.027	0.243	0.330	0.078		0.078	

BRG. NO. 2 CONFIGURATION B AMBIENT PRESS 7.2PSIA												
TEST POINT		HP	HPU	HPL	HPUL1	HPUL2	HPULD	M	EBL	EBU	DELTA EBL	DELTA EBU
23		1.262	1.309	1.215	2.617	2.431	0.186	0.463	0.067			
32		1.395	1.484	1.306	2.914	2.665	0.249	0.407	0.126		0.059	
19		1.365	1.425	1.306	2.855	2.607	0.247	0.419	0.085		0.018	
20		1.410	1.484	1.336	2.914	2.727	0.187	0.400	0.104		0.037	
21		1.306	1.397	1.215	2.735	2.488	0.247	0.444	0.129		0.062	
22		1.365	1.425	1.306	2.855	2.607	0.247	0.419	0.085		0.018	
24		1.529	1.600	1.458	3.151	2.965	0.186	0.349	0.100		0.034	
28		1.500	1.542	1.458	3.092	2.908	0.185	0.362	0.059		-0.007	
36		1.514	1.600	1.427	3.151	2.903	0.248	0.356	0.122		0.056	

BRG. NO 1 CONFIGURATION C AMBIENT PRESS 10.5PSIA

TEST
POINT

NO.	HP	HPU	HPL	HPUL1	HPUL2	HPULD	M	EBL	EBU	DELTA EBL	DELTA EBU
3	1.174	1.754	0.594	2.098	2.596	-0.498	0.481	0.821			
1	1.004	1.477	0.531	1.799	2.217	-0.418	0.556	0.669		-0.152	
2	1.019	1.507	0.531	1.859	2.217	-0.358	0.549	0.690		-0.130	
4	1.034	1.507	0.561	1.920	2.217	-0.297	0.542	0.669		-0.152	
5	0.988	1.475	0.501	1.798	2.154	-0.356	0.563	0.689		-0.131	
6	1.004	1.507	0.501	1.798	2.217	-0.419	0.556	0.712		-0.109	
25	1.019	1.507	0.531	1.859	2.217	-0.358	0.549	0.690		-0.130	
29	0.881	1.293	0.468	1.560	1.963	-0.404	0.610	0.583		-0.237	
33	0.957	1.477	0.438	1.678	2.152	-0.475	0.576	0.735		-0.086	

BRG. NO. 1 CONFIGURATION C AMBIENT PRESS 7.2PSIA

TEST
POINT

NO.	HP	HPU	HPL	HPUL1	HPUL2	HPULD	M	EBL	EBU	DELTA EBL	DELTA EBU
11	1.311	2.060	0.561	2.396	2.847	-0.451	0.420	1.060			
7	0.988	1.538	0.438	1.737	2.215	-0.478	0.563	0.778		-0.282	
8	1.065	1.661	0.468	1.917	2.342	-0.424	0.529	0.843		-0.217	
9	1.157	1.784	0.531	2.097	2.532	-0.435	0.488	0.886		-0.174	
10	1.080	1.691	0.468	1.977	2.342	-0.365	0.522	0.864		-0.196	
12	1.065	1.661	0.468	1.917	2.342	-0.424	0.529	0.843		-0.217	
26	1.018	1.568	0.468	1.858	2.215	-0.358	0.549	0.778		-0.282	
30	0.849	1.354	0.343	1.497	1.898	-0.400	0.624	0.715		-0.345	
34	0.879	1.416	0.343	1.557	1.961	-0.404	0.611	0.758		-0.302	

BRG. NO. 2 CONFIGURATION C AMBIENT PRESS 10.5PSIA

TEST
POINT

NO.	HP	HPU	HPL	HPUL1	HPUL2	HPULD	M	EBL	EBU	DELTA EBL	DELTA EBU
3	0.927	1.338	0.517	1.777	1.932	-0.154	0.605	0.580			
1	1.059	1.571	0.547	2.073	2.162	-0.089	0.549	0.724		0.144	
2	1.030	1.512	0.547	2.014	2.104	-0.090	0.562	0.683		0.102	
4	0.928	1.308	0.547	1.778	1.932	-0.153	0.605	0.538		-0.042	
5	1.001	1.454	0.547	1.955	2.047	-0.092	0.574	0.642		0.061	
6	0.971	1.425	0.517	1.895	1.989	-0.094	0.587	0.642		0.062	
25	0.986	1.425	0.547	1.955	1.989	-0.034	0.580	0.621		0.041	
29	1.059	1.571	0.547	2.073	2.162	-0.089	0.549	0.724		0.144	
33	1.044	1.542	0.547	2.073	2.104	-0.031	0.556	0.704		0.123	

BRG. NO. 2 CONFIGURATION C AMBIENT PRESS 7.2PSIA

TEST
POINT

NO.	HP	HPU	HPL	HPUL1	HPUL2	HPULD	M	EBL	EBU	DELTA EBL	DELTA EBU
11	0.941	1.425	0.456	1.835	1.928	-0.092	0.600	0.686			
7	0.912	1.367	0.456	1.776	1.870	-0.094	0.612	0.644		-0.041	
8	0.897	1.367	0.426	1.717	1.870	-0.154	0.618	0.666		-0.020	
9	0.839	1.221	0.456	1.600	1.755	-0.155	0.643	0.541		-0.144	
10	0.941	1.425	0.456	1.835	1.928	-0.092	0.600	0.686		0.000	
12	1.115	1.745	0.486	2.131	2.330	-0.199	0.525	0.890		0.205	
26	1.014	1.542	0.486	2.013	2.043	-0.029	0.569	0.747		0.061	
30	0.954	1.513	0.395	1.893	1.923	-0.030	0.594	0.791		0.105	
34	0.925	1.455	0.395	1.834	1.866	-0.031	0.606	0.749		0.064	

BRG. NO. 1 CONFIGURATION C AMBIENT PRESS 10.5PSIA												
TEST POINT		HP	HPU	HPL	HPUL1	HPUL2	HPULD	M	EBL	EBU	DELTA EBL	DELTA EBU
15	1.696	2.674	0.719	3.114	3.671	-0.556	0.249	1.383				
13	1.294	1.994	0.594	2.516	2.659	-0.144	0.428	0.990			-0.392	
14	1.373	2.152	0.594	2.516	2.975	-0.459	0.393	1.102			-0.281	
16	1.465	2.244	0.687	2.697	3.165	-0.468	0.352	1.102			-0.281	
17	1.232	1.903	0.561	2.396	2.532	-0.135	0.455	0.949			-0.434	
18	1.185	1.903	0.467	2.336	2.403	-0.068	0.476	1.016			-0.367	
31	1.234	1.938	0.531	2.216	2.721	-0.505	0.454	0.995			-0.388	
27	1.542	2.460	0.624	2.815	3.353	-0.538	0.318	1.298			-0.084	
35	1.264	2.029	0.499	2.336	2.720	-0.384	0.441	1.082			-0.300	

BRG. NO. 1 CONFIGURATION C AMBIENT PRESS 7.2PSIA												
TEST POINT		HP	HPU	HPL	HPUL1	HPUL2	HPULD	M	EBL	EBU	DELTA EBL	DELTA EBU
23	1.632	2.703	0.561	3.052	3.478	-0.426	0.278	1.515				
32	1.062	1.750	0.374	2.035	2.213	-0.178	0.530	0.974			-0.541	
19	1.217	2.029	0.406	2.214	2.656	-0.442	0.461	1.148			-0.367	
20	1.279	2.152	0.406	2.333	2.782	-0.449	0.434	1.235			-0.280	
21	1.372	2.244	0.499	2.514	2.972	-0.458	0.393	1.234			-0.280	
22	1.356	2.244	0.468	2.454	2.972	-0.519	0.400	1.256			-0.259	
24	1.418	2.367	0.468	2.573	3.098	-0.525	0.373	1.343			-0.172	
28	1.479	2.460	0.499	2.693	3.224	-0.531	0.345	1.387			-0.128	
36	1.279	2.152	0.406	2.333	2.782	-0.449	0.434	1.235			-0.280	

BRG. NO. 2 CONFIGURATION C AMBIENT PRESS 10.5PSIA												
TEST POINT		HP	HPU	HPL	HPUL1	HPUL2	HPULD	M	EBL	EBU	DELTA EBL	DELTA EBU
15	1.221	1.804	0.639	2.369	2.515	-0.146	0.480	0.824				
13	1.382	2.126	0.639	2.841	2.688	0.153	0.412	1.052			0.228	
14	1.338	2.036	0.639	2.605	2.745	-0.141	0.431	0.988			0.165	
16	1.280	1.891	0.669	2.547	2.573	-0.026	0.455	0.865			0.041	
17	1.468	2.298	0.639	2.841	3.033	-0.192	0.375	1.174			0.350	
18	1.396	2.154	0.639	2.782	2.803	-0.021	0.406	1.071			0.248	
31	1.381	2.124	0.639	2.723	2.803	-0.080	0.412	1.050			0.227	
27	1.381	2.124	0.639	2.723	2.803	-0.080	0.412	1.050			0.227	
35	1.353	2.067	0.639	2.723	2.688	0.035	0.424	1.010			0.186	

BRG. NO. 2 CONFIGURATION C AMBIENT PRESS 7.2PSIA												
TEST POINT		HP	HPU	HPL	HPUL1	HPUL2	HPULD	M	EBL	EBU	DELTA EBL	DELTA EBU
23	1.233	1.920	0.547	2.427	2.507	-0.080	0.475	0.971				
32	1.291	2.095	0.486	2.603	2.560	0.043	0.451	1.138			0.167	
19	1.277	2.037	0.517	2.544	2.564	-0.021	0.457	1.075			0.104	
20	1.335	2.154	0.517	2.662	2.679	-0.018	0.432	1.157			0.186	
21	1.233	1.949	0.517	2.426	2.507	-0.081	0.475	1.013			0.042	
22	1.335	2.154	0.517	2.662	2.679	-0.018	0.432	1.157			0.186	
24	1.510	2.473	0.547	2.957	3.082	-0.124	0.358	1.362			0.391	
28	1.437	2.327	0.547	2.781	2.967	-0.186	0.389	1.259			0.288	
36	1.305	2.154	0.456	2.602	2.618	-0.016	0.445	1.200			0.229	

BRG. NO. 1 CONFIGURATION D AMBIENT PRESS 10.5PSIA

TEST POINT	NO.	HP	HPU	HPL	HPUL1	HPUL2	HPULD	M	EBL	EBU	DELTA EBL	DELTA EBU
	3	1.144	1.163	1.125	2.348	2.228	0.120	0.494	0.027			
	1	0.957	1.071	0.844	1.984	1.845	0.140	0.576	0.160		0.133	
	2	0.989	1.071	0.906	2.045	1.909	0.136	0.563	0.116		0.089	
	4	1.004	1.102	0.906	2.045	1.972	0.073	0.556	0.138		0.111	
	5	0.926	1.041	0.812	1.925	1.780	0.144	0.590	0.162		0.135	
	6	0.833	0.950	0.717	1.745	1.589	0.156	0.631	0.165		0.137	
	25	0.989	1.072	0.906	1.986	1.972	0.014	0.562	0.117		0.090	
	29	0.818	0.950	0.687	1.684	1.589	0.095	0.638	0.186		0.159	
	33	0.802	0.918	0.687	1.684	1.526	0.158	0.645	0.164		0.136	

BRG. NO. 1 CONFIGURATION D AMBIENT PRESS 7.2PSIA

TEST POINT	NO.	HP	HPU	HPL	HPUL1	HPUL2	HPULD	M	EBL	EBU	DELTA EBL	DELTA EBU
	11	0.989	1.041	0.937	2.046	1.909	0.137	0.562	0.073			
	7	0.803	0.950	0.656	1.623	1.589	0.034	0.645	0.208		0.134	
	8	0.804	0.950	0.658	1.562	1.653	-0.091	0.644	0.206		0.133	
	9	0.834	0.950	0.719	1.684	1.653	0.031	0.631	0.163		0.090	
	10	0.818	0.950	0.687	1.684	1.589	0.095	0.638	0.186		0.113	
	12	0.895	1.041	0.749	1.864	1.716	0.148	0.604	0.206		0.133	
	26	0.927	1.072	0.781	1.864	1.843	0.020	0.590	0.206		0.132	
	30	0.756	0.950	0.561	1.562	1.460	0.102	0.666	0.275		0.201	
	34	0.787	0.979	0.594	1.622	1.524	0.097	0.652	0.273		0.199	

BRG. NO. 2 CONFIGURATION D AMBIENT PRESS 10.5PSIA

TEST POINT	NO.	HP	HPU	HPL	HPUL1	HPUL2	HPULD	M	EBL	EBU	DELTA EBL	DELTA EBU
	3	0.951	1.018	0.884	1.723	2.081	-0.359	0.595	0.095			
	1	0.979	1.105	0.853	1.781	2.134	-0.353	0.583	0.178		0.083	
	2	0.994	1.105	0.884	1.781	2.196	-0.415	0.577	0.156		0.062	
	4	0.950	1.047	0.853	1.723	2.077	-0.354	0.596	0.137		0.042	
	5	0.994	1.134	0.854	1.722	2.254	-0.532	0.577	0.198		0.103	
	6	1.038	1.192	0.884	1.840	2.311	-0.471	0.558	0.218		0.123	
	25	1.024	1.163	0.884	1.840	2.254	-0.413	0.564	0.197		0.103	
	29	1.038	1.192	0.884	1.840	2.311	-0.471	0.558	0.218		0.123	
	33	1.038	1.192	0.884	1.840	2.311	-0.471	0.558	0.218		0.123	

BRG. NO. 2 CONFIGURATION D AMBIENT PRESS 7.2PSIA

TEST POINT	NO.	HP	HPU	HPL	HPUL1	HPUL2	HPULD	M	EBL	EBU	DELTA EBL	DELTA EBU
	11	0.891	0.960	0.823	1.604	1.962	-0.358	0.621	0.096			
	7	0.949	1.105	0.793	1.662	2.134	-0.473	0.596	0.220		0.124	
	8	0.949	1.075	0.823	1.663	2.134	-0.472	0.596	0.178		0.082	
	9	0.875	0.988	0.762	1.544	1.958	-0.414	0.628	0.160		0.063	
	10	0.920	1.047	0.793	1.603	2.077	-0.474	0.609	0.179		0.083	
	12	1.024	1.163	0.884	1.840	2.254	-0.413	0.564	0.197		0.101	
	26	1.024	1.163	0.884	1.840	2.254	-0.413	0.564	0.197		0.101	
	30	1.007	1.192	0.823	1.780	2.249	-0.469	0.571	0.261		0.164	
	34	0.993	1.162	0.823	1.722	2.249	-0.528	0.578	0.240		0.143	

BRG. NO. 1 CONFIGURATION D AMBIENT PRESS 10.5PSIA											
TEST POINT											
NO.	HP	HPU	HPL	HPUL1	HPUL2	HPULD	M	EBL	EBU	DELTA EBL	DELTA EBU
15	1.652	1.805	1.500	3.428	3.181	0.247	0.269	0.215			
13	1.388	1.743	1.033	2.821	2.732	0.089	0.386	0.502		0.287	
14	1.389	1.714	1.064	2.822	2.732	0.090	0.386	0.460		0.244	
16	1.497	1.743	1.251	3.065	2.925	0.139	0.337	0.348		0.132	
17	1.310	1.682	0.939	2.701	2.541	0.160	0.420	0.526		0.310	
18	1.249	1.623	0.876	2.521	2.476	0.044	0.447	0.528		0.312	
27	1.420	1.745	1.094	2.883	2.795	0.088	0.372	0.460		0.245	
31	1.264	1.682	0.846	2.579	2.476	0.103	0.441	0.592		0.376	
35	1.172	1.530	0.813	2.400	2.286	0.114	0.482	0.507		0.291	

BRG. NO. 1 CONFIGURATION D AMBIENT PRESS 7.2PSIA											
TEST POINT											
NO.	HP	HPU	HPL	HPUL1	HPUL2	HPULD	M	EBL	EBU	DELTA EBL	DELTA EBU
23	1.606	1.805	1.407	3.307	3.117	0.190	0.289	0.281			
19	1.202	1.621	0.783	2.459	2.349	0.110	0.468	0.592		0.311	
20	1.233	1.621	0.846	2.519	2.413	0.106	0.454	0.548		0.267	
21	1.296	1.591	1.001	2.642	2.542	0.100	0.427	0.417		0.136	
22	1.295	1.652	0.939	2.641	2.541	0.100	0.427	0.505		0.223	
24	1.356	1.805	0.908	2.759	2.667	0.092	0.400	0.634		0.353	
28	1.373	1.775	0.971	2.760	2.731	0.029	0.393	0.569		0.287	
32	1.186	1.682	0.690	2.396	2.348	0.049	0.475	0.702		0.420	
36	1.186	1.682	0.690	2.396	2.348	0.049	0.475	0.702		0.420	

BRG. NO. 2 CONFIGURATION D AMBIENT PRESS 10.5PSIA											
TEST POINT											
NO.	HP	HPU	HPL	HPUL1	HPUL2	HPULD	M	EBL	EBU	DELTA EBL	DELTA EBU
15	1.277	1.366	1.188	2.317	2.793	-0.476	0.456	0.126			
13	1.513	1.715	1.310	2.732	3.319	-0.587	0.356	0.286		0.160	
14	1.484	1.657	1.310	2.673	3.261	-0.589	0.369	0.245		0.119	
16	1.291	1.453	1.128	2.316	2.846	-0.530	0.451	0.230		0.105	
17	1.438	1.657	1.219	2.553	3.200	-0.647	0.388	0.309		0.184	
18	1.423	1.657	1.189	2.493	3.200	-0.707	0.394	0.331		0.205	
27	1.379	1.569	1.189	2.375	3.142	-0.767	0.413	0.269		0.143	
31	1.452	1.686	1.219	2.553	3.257	-0.704	0.382	0.330		0.204	
35	1.377	1.627	1.128	2.434	3.076	-0.642	0.414	0.353		0.228	

BRG. NO. 2 CONFIGURATION D AMBIENT PRESS 7.2PSIA											
TEST POINT											
NO.	HP	HPU	HPL	HPUL1	HPUL2	HPULD	M	EBL	EBU	DELTA EBL	DELTA EBU
23	1.336	1.453	1.219	2.376	2.970	-0.594	0.431	0.166			
19	1.408	1.657	1.158	2.493	3.138	-0.645	0.401	0.352		0.187	
20	1.408	1.657	1.158	2.493	3.138	-0.645	0.401	0.352		0.187	
21	1.291	1.453	1.128	2.316	2.846	-0.530	0.451	0.230		0.065	
22	1.438	1.657	1.219	2.553	3.200	-0.647	0.388	0.309		0.144	
24	1.572	1.802	1.341	2.791	3.496	-0.705	0.331	0.326		0.160	
28	1.424	1.627	1.220	2.434	3.261	-0.827	0.394	0.288		0.122	
32	1.407	1.686	1.128	2.493	3.133	-0.641	0.401	0.395		0.229	
36	1.258	1.511	1.006	2.196	2.837	-0.641	0.465	0.357		0.192	

BRG. NO. 1 CONFIGURATION E AMBIENT PRESS 10.5PSIA											
TEST POINT											
NO.	HP	HPU	HPL	HPUL1	HPUL2	HPULD	M	EBL	EBU	DELTA EBL	DELTA EBU
3	1.067	1.134	0.999	2.167	2.099	0.067	0.528	0.095			
1	0.958	1.072	0.844	1.925	1.908	0.017	0.576	0.162		0.067	
2	0.974	1.072	0.876	1.925	1.972	-0.047	0.569	0.139		0.044	
4	0.989	1.072	0.906	1.986	1.972	0.014	0.562	0.117		0.022	
5	0.943	1.104	0.781	1.864	1.906	-0.043	0.583	0.228		0.133	
6	0.864	1.011	0.717	1.804	1.652	0.152	0.618	0.208		0.113	
25	1.096	1.286	0.906	2.224	2.161	0.063	0.515	0.268		0.174	
29	0.782	1.072	0.492	1.864	1.265	0.599	0.654	0.410		0.316	
33	0.849	1.011	0.687	1.743	1.652	0.092	0.624	0.229		0.135	

BRG. NO. 1 CONFIGURATION E AMBIENT PRESS 7.2PSIA											
TEST POINT											
NO.	HP	HPU	HPL	HPUL1	HPUL2	HPULD	M	EBL	EBU	DELTA EBL	DELTA EBU
11	1.128	1.256	0.999	2.286	2.225	0.061	0.501	0.182			
7	0.657	0.981	0.333	1.562	1.067	0.495	0.709	0.458		0.277	
8	0.972	1.163	0.781	1.983	1.906	0.077	0.570	0.270		0.089	
9	0.988	1.163	0.813	1.983	1.971	0.012	0.563	0.248		0.066	
10	0.988	1.163	0.813	1.983	1.971	0.012	0.563	0.248		0.066	
12	1.035	1.256	0.813	2.043	2.097	-0.054	0.542	0.313		0.132	
26	1.081	1.286	0.876	2.163	2.161	0.002	0.522	0.290		0.108	
30	0.849	1.072	0.626	1.681	1.715	-0.034	0.624	0.316		0.134	
34	0.802	1.011	0.594	1.622	1.587	0.034	0.645	0.295		0.114	

BRG. NO. 2 CONFIGURATION E AMBIENT PRESS 10.5PSIA											
TEST POINT											
NO.	HP	HPU	HPL	HPUL1	HPUL2	HPULD	M	EBL	EBU	DELTA EBL	DELTA EBU
3	0.846	0.960	0.732	1.484	1.900	-0.416	0.640	0.161			
1	0.905	1.047	0.763	1.543	2.077	-0.534	0.615	0.200		0.040	
2	0.920	1.047	0.793	1.603	2.077	-0.474	0.609	0.179		0.018	
4	0.831	0.960	0.701	1.484	1.838	-0.355	0.647	0.183		0.022	
5	1.052	1.221	0.884	1.840	2.369	-0.528	0.552	0.238		0.077	
6	0.978	1.162	0.794	1.602	2.311	-0.710	0.584	0.260		0.100	
25	0.919	1.075	0.763	1.543	2.134	-0.592	0.609	0.221		0.060	
29	0.965	1.075	0.854	1.663	2.196	-0.534	0.589	0.156		-0.004	
33	1.008	1.163	0.853	1.840	2.192	-0.352	0.571	0.219		0.058	

BRG. NO. 2 CONFIGURATION E AMBIENT PRESS 7.2PSIA											
TEST POINT											
NO.	HP	HPU	HPL	HPUL1	HPUL2	HPULD	M	EBL	EBU	DELTA EBL	DELTA EBU
11	0.921	1.017	0.824	1.544	2.139	-0.595	0.608	0.136			
7	0.978	1.162	0.794	1.602	2.311	-0.710	0.584	0.260		0.124	
8	1.053	1.191	0.915	1.781	2.431	-0.649	0.552	0.195		0.059	
9	0.935	1.075	0.794	1.543	2.196	-0.654	0.602	0.199		0.062	
10	0.950	1.075	0.824	1.603	2.196	-0.594	0.596	0.178		0.041	
12	1.038	1.191	0.885	1.722	2.431	-0.709	0.558	0.216		0.080	
26	0.934	1.104	0.763	1.543	2.192	-0.649	0.603	0.241		0.105	
30	0.888	1.075	0.701	1.543	2.011	-0.468	0.622	0.264		0.128	
34	0.933	1.134	0.732	1.602	2.130	-0.529	0.603	0.284		0.147	

BRG. NO. 1 CONFIGURATION E AMBIENT PRESS 10.5PSIA

TEST POINT										EBU	DELTA EBL	DELTA EBU
NO.	HP	HPU	HPL	HPUL1	HPUL2	HPULD	M	EBL				
15	1.668	1.836	1.500	3.428	3.244	0.184	0.262	0.238				
13	1.358	1.745	0.971	2.701	2.731	-0.030	0.399	0.548		0.310		
14	1.404	1.745	1.064	2.822	2.795	0.027	0.379	0.482		0.244		
16	1.481	1.743	1.219	3.065	2.861	0.204	0.345	0.371		0.133		
17	1.266	1.593	0.939	2.522	2.541	-0.019	0.440	0.463		0.225		
18	1.203	1.561	0.844	2.461	2.349	0.112	0.468	0.507		0.270		
27	1.312	1.593	1.032	2.644	2.605	0.039	0.419	0.397		0.159		
31	1.126	1.439	0.813	2.281	2.223	0.058	0.502	0.442		0.204		
35	1.126	1.439	0.813	2.281	2.223	0.058	0.502	0.442		0.204		

BRG. NO. 1 CONFIGURATION E AMBIENT PRESS 7.2PSIA

TEST POINT										EBU	DELTA EBL	DELTA EBU
NO.	HP	HPU	HPL	HPUL1	HPUL2	HPULD	M	EBL				
23	1.452	1.623	1.282	2.947	2.862	0.084	0.357	0.241				
19	1.141	1.500	0.783	2.280	2.286	-0.006	0.495	0.507		0.266		
20	1.188	1.500	0.876	2.401	2.350	0.051	0.474	0.441		0.200		
21	1.245	1.530	0.969	2.583	2.415	0.168	0.447	0.396		0.156		
22	1.203	1.530	0.876	2.461	2.350	0.111	0.468	0.462		0.221		
24	1.249	1.623	0.876	2.521	2.476	0.044	0.447	0.528		0.287		
28	1.281	1.623	0.939	2.582	2.541	0.041	0.433	0.484		0.243		
32	1.125	1.500	0.751	2.280	2.222	0.058	0.502	0.530		0.289		
36	1.079	1.500	0.658	2.158	2.157	0.001	0.523	0.595		0.355		

BRG. NO. 2 CONFIGURATION E AMBIENT PRESS 10.5PSIA

TEST POINT										EBU	DELTA EBL	DELTA EBU
NO.	HP	HPU	HPL	HPUL1	HPUL2	HPULD	M	EBL				
15	1.322	1.425	1.219	2.376	2.912	-0.536	0.437	0.145				
13	1.513	1.716	1.310	2.791	3.261	-0.471	0.356	0.287		0.142		
14	1.484	1.657	1.310	2.673	3.261	-0.589	0.369	0.245		0.100		
16	1.321	1.483	1.158	2.375	2.908	-0.533	0.438	0.229		0.084		
17	1.438	1.657	1.219	2.553	3.200	-0.647	0.388	0.309		0.164		
18	1.438	1.657	1.219	2.553	3.200	-0.647	0.388	0.309		0.164		
27	1.424	1.628	1.219	2.553	3.142	-0.589	0.394	0.289		0.144		
31	1.454	1.657	1.250	2.553	3.261	-0.709	0.381	0.288		0.142		
35	1.423	1.657	1.189	2.493	3.200	-0.707	0.394	0.331		0.185		

BRG. NO. 2 CONFIGURATION E AMBIENT PRESS 7.2PSIA

TEST POINT										EBU	DELTA EBL	DELTA EBU
NO.	HP	HPU	HPL	HPUL1	HPUL2	HPULD	M	EBL				
23	1.277	1.396	1.158	2.316	2.793	-0.477	0.457	0.158				
19	1.380	1.570	1.189	2.434	3.085	-0.651	0.413	0.269		0.101		
20	1.397	1.605	1.188	2.553	3.034	-0.481	0.406	0.295		0.127		
21	1.305	1.483	1.128	2.375	2.846	-0.471	0.445	0.251		0.083		
22	1.380	1.570	1.189	2.434	3.085	-0.651	0.413	0.269		0.101		
24	1.498	1.686	1.310	2.732	3.261	-0.530	0.362	0.266		0.098		
28	1.469	1.657	1.280	2.613	3.261	-0.649	0.375	0.266		0.098		
32	1.408	1.657	1.158	2.493	3.138	-0.645	0.401	0.352		0.185		
36	1.392	1.657	1.128	2.493	3.076	-0.583	0.408	0.374		0.206		

BRG. NO. 1 CONFIGURATION F AMBIENT PRESS 10.5PSIA

TEST POINT	NO.	HP	HPU	HPL	HPUL1	HPUL2	HPULD	M	EBL	EBU	DELTA EBL	DELTA EBU
	3	1.080	1.503	0.656	2.100	2.219	-0.120	0.522	0.599			
	1	0.972	1.410	0.533	1.858	2.029	-0.171	0.570	0.621		0.022	
	2	0.941	1.349	0.533	1.798	1.966	-0.168	0.584	0.577		-0.022	
	4	1.003	1.381	0.626	1.920	2.093	-0.173	0.556	0.534		-0.065	
	5	1.064	1.596	0.533	1.977	2.281	-0.304	0.529	0.752		0.153	
	6	0.971	1.442	0.501	1.858	2.028	-0.170	0.570	0.666		0.067	
	25	1.065	1.565	0.565	1.977	2.282	-0.305	0.529	0.707		0.108	
	29	0.000	0.000	0.000	0.000	0.000	0.000	1.000	0.000		0.599	
	33	0.926	1.381	0.472	1.676	2.029	-0.353	0.590	0.643		0.044	

BRG. NO. 1 CONFIGURATION F AMBIENT PRESS 7.2PSIA

TEST POINT	NO.	HP	HPU	HPL	HPUL1	HPUL2	HPULD	M	EBL	EBU	DELTA EBL	DELTA EBU
	11	1.173	1.721	0.626	2.158	2.534	-0.376	0.481	0.774			
	7	0.956	1.442	0.470	1.797	2.028	-0.231	0.577	0.687		-0.087	
	8	0.987	1.503	0.470	1.856	2.091	-0.234	0.563	0.731		-0.044	
	9	1.018	1.503	0.533	1.917	2.155	-0.238	0.550	0.686		-0.088	
	10	0.956	1.442	0.470	1.797	2.028	-0.231	0.577	0.687		-0.087	
	12	1.017	1.565	0.470	1.916	2.154	-0.238	0.550	0.774		-0.000	
	26	1.095	1.721	0.470	1.976	2.406	-0.430	0.515	0.884		0.110	
	34	0.910	1.381	0.440	1.676	1.965	-0.288	0.597	0.665		-0.109	

BRG. NO. 2 CONFIGURATION F AMBIENT PRESS 10.5PSIA

TEST POINT	NO.	HP	HPU	HPL	HPUL1	HPUL2	HPULD	M	EBL	EBU	DELTA EBL	DELTA EBU
	3	0.795	1.132	0.457	1.304	1.874	-0.570	0.662	0.477			
	1	0.910	1.364	0.457	1.422	2.219	-0.798	0.613	0.641		0.164	
	2	0.880	1.334	0.426	1.363	2.158	-0.795	0.625	0.642		0.165	
	4	0.795	1.132	0.457	1.304	1.874	-0.570	0.662	0.477		0.000	
	5	1.074	1.599	0.548	2.013	2.281	-0.268	0.543	0.744		0.266	
	6	0.999	1.511	0.487	1.776	2.219	-0.443	0.575	0.724		0.247	
	25	0.910	1.393	0.426	1.481	2.158	-0.677	0.613	0.684		0.206	
	29	0.000	0.000	0.000	0.000	0.000	0.000	1.000	0.000		0.477	
	33	0.895	1.364	0.426	1.422	2.158	-0.736	0.619	0.663		0.186	

BRG. NO. 2 CONFIGURATION F AMBIENT PRESS 7.2PSIA

TEST POINT	NO.	HP	HPU	HPL	HPUL1	HPUL2	HPULD	M	EBL	EBU	DELTA EBL	DELTA EBU
	11	0.838	1.249	0.426	1.481	1.870	-0.389	0.644	0.582			
	7	0.939	1.452	0.426	1.599	2.158	-0.559	0.600	0.726		0.143	
	8	0.939	1.452	0.426	1.599	2.158	-0.559	0.600	0.726		0.143	
	9	0.838	1.249	0.426	1.481	1.870	-0.389	0.644	0.582		0.000	
	10	0.939	1.452	0.426	1.599	2.158	-0.559	0.600	0.726		0.143	
	12	0.969	1.511	0.426	1.717	2.158	-0.441	0.588	0.767		0.185	
	26	0.895	1.393	0.396	1.421	2.158	-0.737	0.619	0.705		0.123	
	34	0.880	1.364	0.396	1.362	2.158	-0.796	0.626	0.684		0.102	

BRG. NO. 1 CONFIGURATION F AMBIENT PRESS 10.5PSIA										DELTA	DELTA
TEST POINT										EBU	EBU
NO.	HP	HPU	HPL	HPUL1	HPUL2	HPULD	M	EBL			
15	1.416	2.146	0.687	2.816	2.850	-0.034	0.373	1.032			
13	1.277	2.022	0.533	2.513	2.596	-0.083	0.435	1.053	0.021		
14	1.247	1.901	0.594	2.456	2.533	-0.077	0.448	0.925	-0.108		
16	1.263	1.901	0.624	2.517	2.533	-0.016	0.441	0.903	-0.129		
17	1.140	1.747	0.533	2.215	2.344	-0.129	0.496	0.859	-0.174		
18	1.169	1.838	0.501	2.334	2.343	-0.008	0.483	0.946	-0.087		
27	1.232	1.901	0.563	2.395	2.533	-0.138	0.455	0.946	-0.086		
31	1.168	1.866	0.470	2.393	2.280	0.113	0.483	0.987	-0.045		
35	1.031	1.593	0.470	2.035	2.091	-0.056	0.544	0.794	-0.238		

BRG. NO. 1 CONFIGURATION F AMBIENT PRESS 7.2PSIA										DELTA	DELTA
TEST POINT										EBU	EBU
NO.	HP	HPU	HPL	HPUL1	HPUL2	HPULD	M	EBL			
23	1.355	2.117	0.594	2.635	2.785	-0.151	0.400	1.077			
19	1.138	1.806	0.470	2.274	2.280	-0.006	0.496	0.945	-0.132		
20	1.200	1.899	0.501	2.394	2.406	-0.012	0.469	0.989	-0.088		
21	1.246	1.992	0.501	2.454	2.532	-0.078	0.448	1.055	-0.022		
22	1.169	1.868	0.470	2.333	2.343	-0.010	0.483	0.988	-0.089		
24	1.200	1.929	0.470	2.393	2.406	-0.013	0.469	1.032	-0.045		
28	1.201	1.931	0.470	2.333	2.469	-0.136	0.469	1.033	-0.044		
32	0.000	0.000	0.000	0.000	0.000	0.000	1.000	0.000	1.077		

BRG. NO. 2 CONFIGURATION F AMBIENT PRESS 10.5PSIA										DELTA	DELTA
TEST POINT										EBU	EBU
NO.	HP	HPU	HPL	HPUL1	HPUL2	HPULD	M	EBL			
15	1.164	1.690	0.638	2.547	2.109	0.438	0.505	0.744			
13	1.395	2.184	0.607	2.959	2.622	0.338	0.406	1.115	0.371		
14	1.324	2.010	0.638	2.842	2.454	0.388	0.437	0.970	0.226		
16	1.207	1.776	0.637	2.607	2.219	0.387	0.487	0.806	0.062		
17	1.308	2.010	0.607	2.842	2.392	0.450	0.443	0.992	0.248		
18	1.308	2.010	0.607	2.842	2.392	0.450	0.443	0.992	0.248		
27	1.279	1.952	0.607	2.783	2.334	0.448	0.456	0.951	0.207		
31	1.395	2.214	0.577	3.017	2.564	0.453	0.406	1.158	0.414		
35	1.323	2.039	0.608	2.782	2.511	0.270	0.437	1.012	0.268		

BRG. NO. 2 CONFIGURATION F AMBIENT PRESS 7.2PSIA										DELTA	DELTA
TEST POINT										EBU	EBU
NO.	HP	HPU	HPL	HPUL1	HPUL2	HPULD	M	EBL			
23	1.204	1.893	0.516	2.545	2.273	0.272	0.488	0.974			
19	1.220	1.893	0.546	2.664	2.215	0.449	0.481	0.953	-0.021		
20	1.234	1.922	0.546	2.664	2.273	0.391	0.475	0.973	-0.000		
21	1.132	1.748	0.516	2.486	2.043	0.443	0.518	0.871	-0.102		
22	1.249	1.981	0.516	2.722	2.273	0.449	0.469	1.036	0.063		
24	1.496	2.476	0.516	3.252	2.733	0.520	0.363	1.386	0.413		
28	1.336	2.155	0.516	2.840	2.503	0.337	0.432	1.159	0.186		
32	0.000	0.000	0.000	0.000	0.000	0.000	1.000	0.000	0.974		

APPENDIX K: REDUCTION OF ROTOR POSITION DATA ACQUIRED DURING ROTOR-BEARING -
ALTERNATOR TESTING

During the course of the rotor-bearing-alternator test program to determine the rotor-bearing response to electromagnetic forces, the data describing the position of the journals in the plane of the bearing pivots was tabulated for each of the 216 test points involved. This data was obtained from the two capacitance probes mounted in each of the bearing supports (see Figures II-23 and II-24). Readout of the distance between these probes and the journals was obtained from the distance meters incorporated in the microdynes.

To determine the eccentricity of the rotor pole faces within the bore of the alternator stator, the experimentally obtained data was adjusted to allow for instrumentation calibration factors, centrifugal growth of the journals and differential thermal expansion between journals, bearing supports and capacitance probes. The eccentricity in the pole face planes was then determined by geometrical relationships.

A computer program was written to reduce the considerable quantity of data accumulated during test. The output from these calculations is shown, for each of the data points taken, in Table K1. Column 1 entitled "RUN" is the test point number, the conditions for which are contained in Tables VII-2 through VII-5. The second column, entitled PLNE, describes the axial plane along the length of the rotor to which the line of data applies. These planes are located as follows:

- Plane 1: In the middle of the large diameter labyrinth positioned upstream of the turbine buckets.
- Plane 2: In the plane of the turbine end journal bearing pivot centerline.
- Plane 3: Half way along the axial length of the pole face adjacent to the turbine end journal bearing.

- Plane 4: Half way along the axial length of the pole face adjacent to the thrust-end journal bearing.
- Plane 5: In the plane of the thrust-end journal bearing pivot centerline.

Columns three and four, entitled H and V, give the calculated distances in mils between the tip of the horizontal and vertical probes and the journals for concentric operation at the speed and temperatures observed at the test point under consideration.

Columns five and six, entitled DH and DV, give the differences between the calculated values of H and V and the measured values, obtained during test, corrected for calibration effects.

Columns seven and eight, entitled E and DE, give the eccentricity in mils of the rotor to the stator in each of the 5 axial planes and the change in eccentricity from a reference point (See Figure K-1). The selected reference point is the zero excitation test point appropriate to the particular configuration, ambient pressure and bearing diametral clearance under test. The evaluated data concerning the zero excitation point appears as the second to the sixth line inclusive on each of the pages of data presented in Table K-1.

Column nine, entitled EREL, gives the distance in mils between the journal center at the zero excitation test point and the journal center at the test point under consideration. Column ten, entitled A, gives the angular position of the rotor center at each of the axial planes relative to the geometric center of the alternator stator.

Column eleven, entitled DA, gives the change in angular position of the journal center between the zero excitation test point and the test point under consideration, relative to the geometric center of the alternator center.

Column twelve, entitled AREL, gives the change in angular position of the journal center between the zero excitation test point and the test point under consideration, relative to the angular position of the journal center at the zero excitation test point.

Column thirteen gives the angle of inclination of the rotor axis to the geometric axis of the turboalternator. Consequently, this angle of inclination is also the amount of misalignment between the thrust runner and thrust stator when the stator has been set up on assembly to be perpendicular to the turboalternator axis and not the rotor axis.

Figure K-1 gives the terminology and sign convention used to describe the position and change in position of the rotor during test.

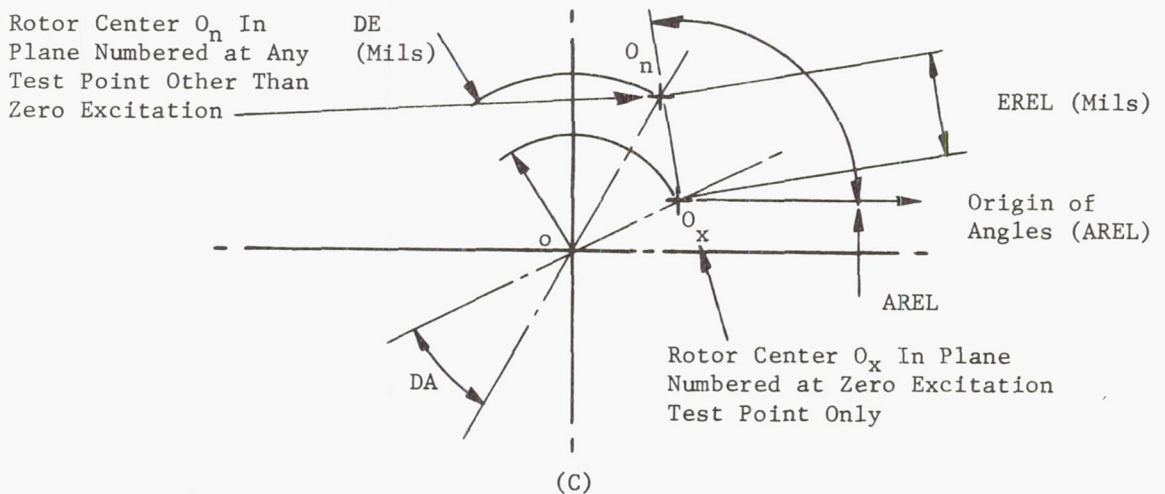
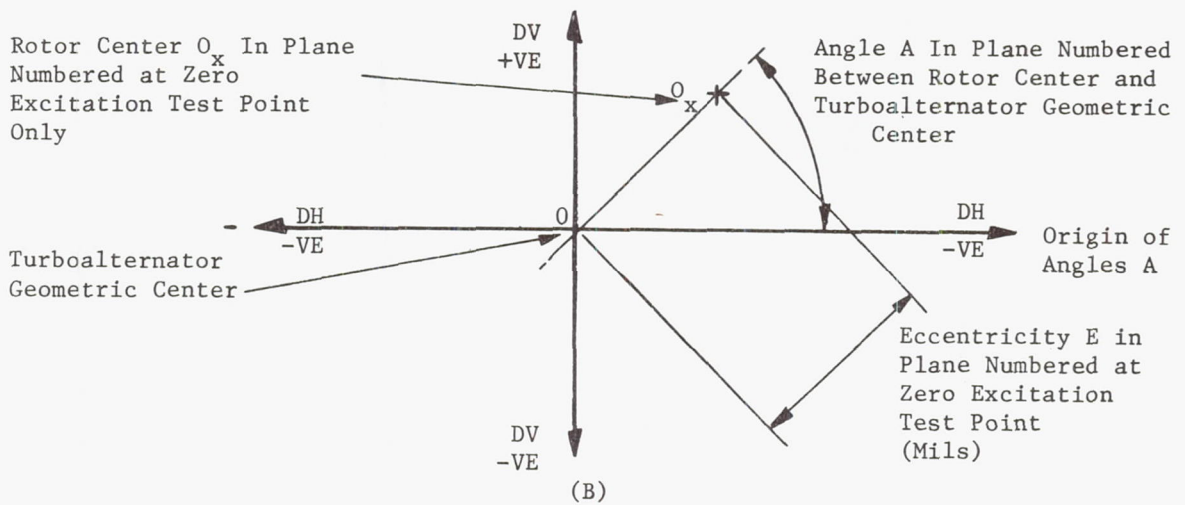
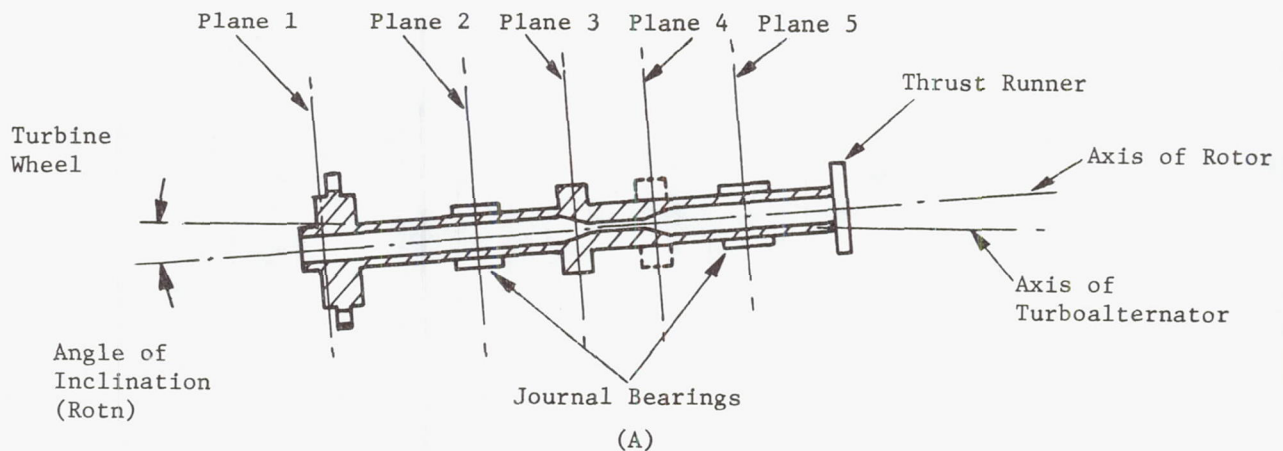


Fig. K-1 Terminology and Sign Convention Used in the Tabulation of Data Describing the Rotor Eccentricity During Test of the Rotor-Bearing-Alternator Simulator

Table K-1

Tabulation of Data Describing the Rotor Eccentricity
During Test of the Rotor-Bearing-
Alternator Simulator

TURBO ALTERNATOR ROTOR POSITION TEST DATA REDUCTION

REDUCTION OF TEST DATA. CONFIGURATION A

CALCULATED DATA

RUN	PLNE	H	V	DH	DV	E	DE	EREL	A	DA	AREL	ROTN
0	0	6.88	7.14	6.01	4.51							
15	1			0.37	0.01	0.37			179.			0.001
15	2	7.23	7.49	0.34	0.09	0.35	0.00	0.00	165.	0.	180.	0.001
15	3			0.30	0.16	0.34			152.			0.001
15	4			0.28	0.22	0.35			142.			0.001
15	5	6.07	4.57	0.25	0.29	0.38	0.00	0.00	131.	0.	180.	0.001
13	1			0.36	-0.01	0.36			181.			0.001
13	2	7.19	7.45	0.32	0.07	0.32	-0.02	0.03	168.	3.	314.	0.001
13	3			0.27	0.13	0.31			154.			0.001
13	4			0.24	0.18	0.30			143.			0.001
13	5	6.12	4.62	0.20	0.25	0.32	-0.06	0.06	130.	-1.	315.	0.001
14	1			0.31	-0.06	0.32			190.			0.001
14	2	7.22	7.48	0.29	0.04	0.29	-0.06	0.07	172.	7.	314.	0.001
14	3			0.27	0.13	0.30			155.			0.001
14	4			0.25	0.19	0.32			143.			0.001
14	5	6.09	4.59	0.23	0.27	0.36	-0.02	0.02	130.	-0.	315.	0.001
16	1			0.25	-0.12	0.28			206.			0.001
16	2	7.23	7.49	0.22	-0.04	0.22	-0.13	0.17	190.	24.	315.	0.001
16	3			0.18	0.04	0.19			167.			0.001
16	4			0.16	0.10	0.19			148.			0.001
16	5	6.05	4.55	0.13	0.18	0.22	-0.16	0.16	127.	-4.	316.	0.001
17	1			0.13	-0.07	0.15			207.			0.001
17	2	7.30	7.56	0.15	0.02	0.15	-0.20	0.21	174.	9.	339.	0.001
17	3			0.16	0.09	0.18			149.			0.001
17	4			0.16	0.15	0.22			138.			0.001
17	5	6.06	4.55	0.17	0.22	0.28	-0.10	0.10	129.	-2.	316.	0.001
18	1			0.05	-0.13	0.14			250.			0.001
18	2	7.35	7.61	0.09	-0.04	0.10	-0.25	0.27	202.	36.	333.	0.001
18	3			0.13	0.05	0.14			158.			0.001
18	4			0.16	0.12	0.20			144.			0.001
18	5	6.03	4.53	0.20	0.20	0.28	-0.10	0.10	135.	4.	298.	0.001
35	1			0.09	-0.20	0.22			245.			0.001
35	2	7.33	7.59	0.11	-0.08	0.14	-0.21	0.28	215.	49.	324.	0.001
35	3			0.13	0.03	0.14			166.			0.001
35	4			0.15	0.11	0.19			143.			0.001
35	5	6.01	4.51	0.17	0.21	0.27	-0.11	0.11	128.	-2.	316.	0.001
27	1			0.17	-0.10	0.20			210.			0.001
27	2	7.34	7.60	0.17	-0.02	0.17	-0.18	0.20	188.	22.	327.	0.001
27	3			0.17	0.05	0.17			164.			0.001
27	4			0.16	0.10	0.19			150.			0.001
27	5	6.16	4.66	0.16	0.16	0.23	-0.15	0.15	135.	5.	303.	0.001
31	1			0.23	-0.14	0.27			211.			0.001
31	2	7.25	7.51	0.20	-0.05	0.21	-0.14	0.19	194.	29.	315.	0.001
31	3			0.17	0.03	0.17			170.			0.001
31	4			0.15	0.09	0.18			149.			0.001
31	5	6.06	4.56	0.12	0.17	0.21	-0.17	0.17	126.	-5.	316.	0.001

TURBO ALTERNATOR ROTOR POSITION TEST DATA REDUCTION

REDUCTION OF TEST DATA. CONFIGURATION A

CALCULATED DATA

RUN	PLNE	H	V	DH	DV	E	DE	EREL	A	DA	AREL	ROTN
0	0	6.88	7.14	6.01	4.51							
23	1			0.33	-0.21	0.39			213.			0.001
23	2	7.34	7.60	0.28	-0.09	0.30	0.00	0.00	197.	0.	180.	0.001
23	3			0.24	0.03	0.24			173.			0.001
23	4			0.21	0.11	0.24			152.			0.001
23	5	6.10	4.60	0.17	0.22	0.28	0.00	0.00	129.	0.	180.	0.001
36	1			-0.05	-0.22	0.22			282.			0.001
36	2	7.31	7.57	0.02	-0.11	0.11	-0.18	0.27	261.	63.	355.	0.001
36	3			0.08	-0.02	0.08			192.			0.001
36	4			0.13	0.05	0.14			158.			0.001
36	5	6.00	4.50	0.18	0.14	0.23	-0.05	0.08	143.	14.	264.	0.001
19	1			0.10	-0.26	0.28			250.			0.001
19	2	7.27	7.53	0.11	-0.14	0.18	-0.12	0.18	230.	33.	343.	0.001
19	3			0.13	-0.02	0.13			190.			0.001
19	4			0.15	0.06	0.16			158.			0.001
19	5	6.02	4.52	0.16	0.16	0.23	-0.05	0.06	135.	6.	283.	0.001
20	1			0.21	-0.23	0.31			227.			0.001
20	2	7.30	7.56	0.20	-0.11	0.23	-0.07	0.08	208.	11.	346.	0.001
20	3			0.20	0.00	0.20			180.			0.001
20	4			0.19	0.08	0.21			157.			0.001
20	5	6.05	4.55	0.18	0.18	0.26	-0.02	0.04	135.	6.	259.	0.001
21	1			0.04	-0.31	0.32			262.			0.001
21	2	7.32	7.58	0.07	-0.19	0.20	-0.10	0.24	251.	53.	335.	0.001
21	3			0.09	-0.07	0.11			219.			0.001
21	4			0.10	0.01	0.10			172.			0.001
21	5	6.06	4.56	0.12	0.12	0.17	-0.11	0.11	135.	6.	299.	0.001
22	1			0.36	-0.27	0.45			216.			0.001
0												
22	2	7.33	7.59	0.30	-0.13	0.33	0.03	0.05	204.	6.	248.	0.001
22	3			0.24	-0.01	0.24			182.			0.001
22	4			0.20	0.08	0.22			158.			0.001
22	5	6.08	4.58	0.15	0.20	0.25	-0.03	0.03	128.	-1.	317.	0.001
24	1			0.44	-0.34	0.55			218.			0.002
24	2	7.38	7.64	0.37	-0.18	0.41	0.12	0.13	207.	9.	228.	0.002
24	3			0.30	-0.04	0.31			188.			0.002
24	4			0.26	0.06	0.27			166.			0.002
24	5	6.17	4.67	0.20	0.19	0.28	-0.00	0.03	135.	7.	225.	0.002
28	1			0.27	-0.34	0.43			231.			0.001
28	2	7.39	7.65	0.23	-0.20	0.31	0.01	0.12	221.	23.	294.	0.001
28	3			0.20	-0.07	0.21			200.			0.001
28	4			0.17	0.02	0.17			173.			0.001
28	5	6.18	4.68	0.14	0.14	0.20	-0.08	0.09	135.	7.	293.	0.001
32	1			0.15	-0.21	0.26			235.			0.001
32	2	7.30	7.56	0.15	-0.11	0.18	-0.12	0.14	216.	19.	352.	0.001
32	3			0.14	-0.01	0.15			185.			0.001
32	4			0.14	0.06	0.16			158.			0.001
32	5	6.04	4.54	0.14	0.15	0.21	-0.07	0.08	135.	6.	292.	0.001

TURBO ALTERNATOR ROTOR POSITION TEST DATA REDUCTION

REDUCTION OF TEST DATA. CONFIGURATION B

CALCULATED DATA

RUN	PLNE	H	V	DH	DV	E	DE	EREL	A	DA	AREL	ROTN
0	0	6.88	7.14	6.01	4.51							
3	1			0.21	0.05	0.22			166.			0.001
3	2	6.70	6.96	0.21	0.15	0.26	0.00	0.00	144.	0.	180.	0.001
3	3			0.21	0.25	0.32			130.			0.001
3	4			0.20	0.32	0.38			123.			0.001
3	5	5.68	4.18	0.20	0.40	0.45	0.00	0.00	117.	0.	180.	0.001
1	1			0.21	-0.01	0.22			183.			0.001
1	2	6.69	6.95	0.21	0.10	0.24	-0.02	0.06	155.	12.	264.	0.001
1	3			0.21	0.20	0.29			137.			0.001
1	4			0.21	0.27	0.35			128.			0.001
1	5	5.67	4.17	0.21	0.37	0.43	-0.03	0.04	120.	3.	254.	0.001
2	1			0.21	-0.01	0.21			183.			0.001
2	2	6.69	6.95	0.21	0.10	0.24	-0.02	0.06	155.	12.	264.	0.001
2	3			0.22	0.20	0.30			137.			0.001
2	4			0.22	0.28	0.35			128.			0.001
2	5	5.66	4.16	0.22	0.37	0.43	-0.02	0.03	120.	4.	241.	0.001
4	1			0.08	-0.08	0.11			226.			0.001
4	2	6.70	6.96	0.09	0.03	0.10	-0.16	0.17	159.	16.	314.	0.001
4	3			0.10	0.14	0.17			125.			0.001
4	4			0.11	0.22	0.25			116.			0.001
4	5	5.67	4.17	0.12	0.32	0.34	-0.11	0.12	110.	-7.	316.	0.001
5	1			0.19	-0.03	0.19			190.			0.001
5	2	6.72	6.98	0.19	0.07	0.20	-0.06	0.08	159.	15.	284.	0.001
5	3			0.18	0.17	0.25			137.			0.001
5	4			0.18	0.24	0.30			127.			0.001
5	5	5.66	4.16	0.18	0.34	0.38	-0.07	0.07	118.	1.	289.	0.001
6	1			0.09	-0.05	0.11			207.			0.001
6	2	6.73	6.99	0.12	0.07	0.14	-0.12	0.12	151.	8.	315.	0.001
6	3			0.15	0.17	0.23			130.			0.001
6	4			0.17	0.25	0.30			124.			0.001
6	5	5.65	4.15	0.19	0.35	0.40	-0.06	0.06	119.	2.	283.	0.001
33	1			0.07	-0.10	0.12			236.			0.001
33	2	6.64	6.90	0.09	0.03	0.09	-0.17	0.17	161.	18.	314.	0.001
33	3			0.11	0.15	0.18			126.			0.001
33	4			0.12	0.23	0.26			117.			0.001
33	5	5.61	4.11	0.14	0.34	0.37	-0.08	0.09	112.	-5.	317.	0.001
25	1			0.34	0.14	0.36			158.			0.001
25	2	6.83	7.09	0.31	0.20	0.37	0.11	0.11	147.	4.	155.	0.001
25	3			0.29	0.26	0.39			138.			0.001
25	4			0.27	0.30	0.41			132.			0.001
25	5	5.77	4.27	0.25	0.36	0.44	-0.02	0.07	125.	8.	224.	0.001
29	1			0.15	-0.12	0.19			218.			0.001
29	2	6.98	7.24	0.16	-0.01	0.16	-0.10	0.17	183.	39.	285.	0.001
29	3			0.18	0.09	0.20			152.			0.001
29	4			0.18	0.17	0.25			138.			0.001
29	5	5.78	4.28	0.20	0.26	0.33	-0.12	0.14	127.	10.	273.	0.001

TURBO ALTERNATOR ROTOR POSITION TEST DATA REDUCTION

REDUCTION OF TEST DATA. CONFIGURATION B

CALCULATED DATA

RUN	PLNE	H	V	DH	DV	E	DE	EREL	A	DA	AREL	ROTN
0	0	6.88	7.14	6.01	4.51							
11	1			0.28	-0.11	0.30			202.			0.001
11	2	6.90	7.16	0.25	0.02	0.25	0.00	0.00	176.	0.	180.	0.001
11	3			0.23	0.14	0.27			148.			0.001
11	4			0.21	0.23	0.31			132.			0.001
11	5	5.74	4.24	0.19	0.34	0.39	0.00	0.00	119.	0.	180.	0.001
34	1			0.04	-0.19	0.20			259.			0.001
34	2	6.65	6.91	0.08	-0.04	0.09	-0.16	0.18	205.	29.	342.	0.001
34	3			0.12	0.11	0.16			138.			0.001
34	4			0.15	0.21	0.26			125.			0.001
34	5	5.56	4.06	0.19	0.35	0.39	0.00	0.00	118.	-0.	94.	0.001
7	1			0.13	-0.18	0.23			234.			0.001
7	2	6.70	6.96	0.15	-0.03	0.15	-0.10	0.11	191.	15.	335.	0.001
7	3			0.16	0.11	0.20			145.			0.001
7	4			0.17	0.22	0.28			129.			0.001
7	5	5.56	4.06	0.19	0.35	0.39	0.00	0.01	118.	-0.	99.	0.001
8	1			0.12	-0.19	0.22			237.			0.001
8	2	6.82	7.08	0.14	-0.03	0.15	-0.10	0.12	192.	16.	335.	0.001
8	3			0.16	0.12	0.20			145.			0.001
8	4			0.18	0.22	0.28			129.			0.001
8	5	5.64	4.14	0.20	0.36	0.41	0.02	0.02	119.	0.	130.	0.001
9	1			0.17	-0.22	0.28			232.			0.001
9	2	6.87	7.13	0.16	-0.08	0.18	-0.07	0.13	206.	30.	314.	0.001
9	3			0.14	0.06	0.16			158.			0.001
9	4			0.14	0.16	0.21			131.			0.001
9	5	5.67	4.17	0.12	0.28	0.31	-0.08	0.09	114.	-5.	317.	0.001
10	1			0.14	-0.19	0.23			233.			0.001
10	2	6.88	7.14	0.14	-0.03	0.15	-0.10	0.12	192.	17.	335.	0.001
10	3			0.14	0.11	0.18			142.			0.001
10	4			0.15	0.22	0.26			124.			0.001
10	5	5.69	4.19	0.15	0.35	0.38	-0.01	0.04	113.	-6.	15.	0.001
12	1			0.26	-0.21	0.34			219.			0.001
12	2	6.92	7.18	0.23	-0.06	0.24	-0.01	0.09	196.	20.	285.	0.001
12	3			0.19	0.07	0.21			160.			0.001
12	4			0.17	0.17	0.24			135.			0.001
12	5	5.79	4.29	0.14	0.30	0.33	-0.06	0.07	115.	-3.	315.	0.001
26	1			0.28	-0.09	0.29			198.			0.001
26	2	6.94	7.20	0.26	0.03	0.26	0.01	0.02	173.	-3.	132.	0.001
26	3			0.24	0.14	0.28			150.			0.001
26	4			0.23	0.22	0.32			136.			0.001
26	5	5.76	4.26	0.22	0.33	0.39	0.00	0.03	124.	5.	205.	0.001
30	1			0.23	-0.21	0.31			222.			0.001
30	2	6.99	7.25	0.21	-0.08	0.23	-0.02	0.10	200.	24.	291.	0.001
30	3			0.20	0.04	0.20			168.			0.001
30	4			0.19	0.13	0.23			145.			0.001
30	5	5.80	4.30	0.18	0.24	0.30	-0.09	0.10	126.	7.	276.	0.001

TURBO ALTERNATOR ROTOR POSITION TEST DATA REDUCTION

REDUCTION OF TEST DATA. CONFIGURATION B

CALCULATED DATA

RUN	PLNE	H	V	DH	DV	E	DE	EREL	A	DA	AREL	ROTN
0	0	6.88	7.14	6.01	4.51							
15	1			0.49	0.16	0.51			162.			0.001
15	2	7.33	7.59	0.41	0.18	0.45	0.00	0.00	157.	0.	180.	0.001
15	3			0.34	0.19	0.39			151.			0.001
15	4			0.29	0.20	0.35			146.			0.001
15	5	6.10	4.60	0.22	0.21	0.31	0.00	0.00	137.	0.	180.	0.001
13	1			0.55	0.12	0.56			168.			0.001
13	2	7.28	7.54	0.45	0.16	0.48	0.03	0.05	161.	4.	203.	0.001
13	3			0.37	0.19	0.41			152.			0.001
13	4			0.30	0.22	0.37			144.			0.001
13	5	6.10	4.60	0.22	0.25	0.33	0.03	0.04	131.	-6.	85.	0.001
14	1			0.50	0.07	0.50			172.			0.001
14	2	7.32	7.58	0.42	0.12	0.43	-0.01	0.06	164.	7.	264.	0.001
14	3			0.34	0.17	0.38			154.			0.001
14	4			0.29	0.21	0.35			145.			0.001
14	5	6.10	4.60	0.22	0.25	0.33	0.03	0.04	131.	-6.	88.	0.001
16	1			0.27	0.00	0.27			179.			0.001
16	2	7.32	7.58	0.24	0.06	0.24	-0.20	0.21	166.	9.	326.	0.001
16	3			0.20	0.11	0.23			152.			0.001
16	4			0.18	0.14	0.23			142.			0.001
16	5	6.07	4.57	0.15	0.19	0.24	-0.06	0.07	129.	-7.	343.	0.001
17	1			0.25	-0.01	0.25			182.			0.001
17	2	7.32	7.58	0.23	0.06	0.24	-0.21	0.21	167.	10.	326.	0.001
17	3			0.22	0.12	0.25			151.			0.001
17	4			0.20	0.16	0.26			141.			0.001
17	5	6.04	4.54	0.19	0.22	0.29	-0.02	0.04	130.	-7.	18.	0.001
18	1			0.25	0.17	0.30			145.			0.000
18	2	7.32	7.58	0.23	0.18	0.30	-0.15	0.18	143.	-14.	1.	0.000
18	3			0.22	0.19	0.29			140.			0.000
18	4			0.22	0.19	0.29			139.			0.000
18	5	6.02	4.52	0.21	0.20	0.29	-0.02	0.02	136.	-0.	321.	0.000
31	1			0.14	0.05	0.15			160.			0.001
31	2	7.33	7.59	0.16	0.11	0.19	-0.25	0.26	147.	-10.	344.	0.001
31	3			0.18	0.16	0.24			139.			0.001
31	4			0.19	0.19	0.27			134.			0.001
31	5	5.98	4.48	0.20	0.24	0.31	0.01	0.04	130.	-6.	57.	0.001
27	1			0.34	0.16	0.38			155.			0.000
27	2	7.21	7.47	0.29	0.17	0.34	-0.11	0.12	149.	-8.	358.	0.000
27	3			0.24	0.18	0.30			143.			0.000
27	4			0.21	0.19	0.28			138.			0.000
27	5	6.16	4.65	0.16	0.20	0.26	-0.05	0.06	130.	-7.	347.	0.000
35	1			0.16	0.09	0.19			151.			0.000
35	2	7.32	7.58	0.18	0.12	0.22	-0.23	0.24	146.	-11.	347.	0.000
35	3			0.19	0.15	0.25			141.			0.000
35	4			0.20	0.18	0.27			139.			0.000
35	5	6.06	4.55	0.22	0.21	0.30	-0.00	0.00	137.	-0.	330.	0.000

TURBO ALTERNATOR ROTOR POSITION TEST DATA REDUCTION

REDUCTION OF TEST DATA. CONFIGURATION B

CALCULATED DATA

RUN	PLNE	H	V	DH	DV	E	DE	EREL	A	DA	AREL	ROTN
0	0	6.88	7.14	6.01	4.51							
23	1			0.51	-0.01	0.51			181.			0.001
23	2	7.44	7.70	0.42	0.06	0.42	0.00	0.00	172.	0.	180.	0.001
23	3			0.33	0.13	0.36			159.			0.001
23	4			0.27	0.17	0.32			148.			0.001
23	5	6.08	4.58	0.20	0.23	0.30	0.00	0.00	131.	0.	180.	0.001
32	1			0.12	0.05	0.13			159.			0.000
32	2	7.36	7.62	0.14	0.08	0.16	-0.26	0.28	149.	-23.	5.	0.000
32	3			0.16	0.12	0.20			143.			0.000
32	4			0.17	0.14	0.22			140.			0.000
32	5	5.96	4.46	0.18	0.17	0.25	-0.05	0.06	136.	6.	287.	0.000
19	1			0.29	-0.05	0.29			189.			0.001
19	2	7.37	7.63	0.25	0.01	0.25	-0.18	0.18	178.	7.	343.	0.001
19	3			0.21	0.06	0.22			165.			0.001
19	4			0.18	0.09	0.20			153.			0.001
19	5	5.99	4.49	0.15	0.14	0.20	-0.10	0.11	137.	6.	299.	0.001
20	1			0.23	-0.10	0.25			204.			0.001
20	2	7.40	7.66	0.21	-0.02	0.22	-0.21	0.22	187.	15.	337.	0.001
20	3			0.20	0.05	0.21			167.			0.001
20	4			0.19	0.10	0.21			152.			0.001
20	5	6.01	4.51	0.18	0.17	0.24	-0.06	0.07	137.	6.	289.	0.001
21	1			0.32	-0.01	0.32			182.			0.001
21	2	7.41	7.67	0.26	0.03	0.26	-0.16	0.16	175.	3.	347.	0.001
21	3			0.21	0.06	0.22			165.			0.001
21	4			0.17	0.08	0.19			154.			0.001
21	5	6.02	4.52	0.12	0.11	0.16	-0.14	0.14	137.	6.	303.	0.001
22	1			0.46	-0.13	0.47			196.			0.001
22	2	7.41	7.67	0.38	-0.04	0.39	-0.04	0.10	185.	14.	290.	0.001
22	3			0.32	0.05	0.32			171.			0.001
22	4			0.27	0.11	0.29			157.			0.001
22	5	6.02	4.52	0.20	0.19	0.28	-0.02	0.04	136.	6.	259.	0.001
24	1			0.37	-0.24	0.44			213.			0.001
24	2	7.24	7.50	0.32	-0.11	0.33	-0.09	0.20	199.	27.	301.	0.001
24	3			0.26	0.01	0.26			178.			0.001
24	4			0.22	0.10	0.24			157.			0.001
24	5	6.14	4.64	0.18	0.21	0.27	-0.03	0.03	130.	-0.	313.	0.001
28	1			0.37	-0.16	0.40			203.			0.001
28	2	7.19	7.45	0.30	-0.06	0.31	-0.11	0.17	191.	19.	313.	0.001
28	3			0.25	0.03	0.25			172.			0.001
28	4			0.21	0.10	0.23			154.			0.001
28	5	6.17	4.67	0.15	0.18	0.24	-0.07	0.07	130.	-1.	314.	0.001
36	1			0.12	0.13	0.17			132.			0.000
36	2	7.36	7.62	0.13	0.14	0.19	-0.23	0.30	134.	-38.	15.	0.000
36	3			0.15	0.15	0.21			135.			0.000
36	4			0.16	0.16	0.22			136.			0.000
36	5	6.05	4.55	0.18	0.17	0.24	-0.06	0.07	137.	6.	288.	0.000

TURBO ALTERNATOR ROTOR POSITION TEST DATA REDUCTION

REDUCTION OF TEST DATA. CONFIGURATION C

CALCULATED DATA

RUN	PLNE	H	V	DH	DV	E	DE	EREL	A	DA	AREL	ROTN
0	0	6.88	7.14	6.01	4.51							
3	1			0.11	-0.34	0.35			253.			0.002
3	2	6.73	6.99	0.20	-0.19	0.27	0.00	0.00	223.	0.	180.	0.002
3	3			0.28	-0.05	0.29			189.			0.002
3	4			0.34	0.05	0.35			171.			0.002
3	5	5.70	4.20	0.42	0.18	0.46	0.00	0.00	157.	0.	180.	0.002
1	1			0.07	-0.34	0.34			258.			0.002
1	2	6.75	7.01	0.18	-0.20	0.27	0.00	0.03	229.	5.	315.	0.002
1	3			0.28	-0.08	0.29			196.			0.002
1	4			0.35	0.01	0.35			179.			0.002
1	5	5.72	4.22	0.45	0.12	0.46	0.01	0.07	165.	8.	245.	0.002
2	1			0.00	-0.34	0.34			269.			0.002
2	2	6.74	7.00	0.12	-0.20	0.24	-0.04	0.08	239.	16.	348.	0.002
2	3			0.23	-0.08	0.24			199.			0.002
2	4			0.31	0.01	0.31			178.			0.002
2	5	5.71	4.21	0.41	0.13	0.43	-0.03	0.06	163.	6.	282.	0.002
4	1			-0.10	-0.31	0.33			288.			0.002
4	2	6.72	6.98	0.03	-0.17	0.18	-0.09	0.17	261.	37.	4.	0.002
4	3			0.15	-0.05	0.16			197.			0.002
4	4			0.24	0.04	0.24			170.			0.002
4	5	5.68	4.18	0.35	0.16	0.39	-0.07	0.07	155.	-1.	343.	0.002
5	1			0.07	-0.46	0.46			261.			0.002
5	2	6.76	7.02	0.16	-0.28	0.32	0.05	0.10	240.	17.	291.	0.002
5	3			0.24	-0.12	0.27			207.			0.002
5	4			0.30	-0.01	0.30			181.			0.002
5	5	5.66	4.15	0.38	0.14	0.40	-0.06	0.06	159.	3.	317.	0.002
6	1			0.06	-0.72	0.73			265.			0.002
6	2	6.83	7.09	0.15	-0.47	0.50	0.22	0.29	252.	29.	279.	0.002
6	3			0.24	-0.24	0.34			225.			0.002
6	4			0.30	-0.07	0.31			193.			0.002
6	5	5.61	4.11	0.38	0.15	0.41	-0.05	0.05	159.	2.	318.	0.002
25	1			-0.06	-0.40	0.41			279.			0.002
25	2	6.74	7.00	0.07	-0.26	0.27	-0.00	0.15	256.	32.	331.	0.002
25	3			0.19	-0.12	0.22			213.			0.002
25	4			0.27	-0.02	0.27			185.			0.002
25	5	5.69	4.19	0.38	0.10	0.40	-0.06	0.09	165.	8.	295.	0.002
29	1			0.01	-0.42	0.42			269.			0.002
29	2	6.69	6.95	0.12	-0.27	0.29	0.02	0.12	247.	23.	315.	0.002
29	3			0.21	-0.13	0.25			211.			0.002
29	4			0.29	-0.03	0.29			186.			0.002
29	5	5.65	4.15	0.38	0.10	0.39	-0.07	0.09	165.	9.	297.	0.002
33	1			-0.17	-0.87	0.89			281.			0.003
33	2	6.83	7.09	-0.03	-0.59	0.59	0.32	0.46	273.	49.	299.	0.003
33	3			0.11	-0.33	0.35			253.			0.003
33	4			0.20	-0.15	0.25			216.			0.003
33	5	5.66	4.16	0.32	0.09	0.34	-0.12	0.13	164.	8.	316.	0.003

TURBO ALTERNATOR ROTOR POSITION TEST DATA REDUCTION

REDUCTION OF TEST DATA. CONFIGURATION C

CALCULATED DATA

RUN	PLNE	H	V	DH	DV	E	DE	EREL	A	DA	AREL	ROTN
0	0	6.88	7.14	6.01	4.51							
11	1			-0.02	-0.74	0.74			271.			0.003
11	2	6.87	7.13	0.12	-0.50	0.52	0.00	0.00	257.	0.	180.	0.003
11	3			0.24	-0.28	0.37			229.			0.003
11	4			0.34	-0.12	0.36			200.			0.003
11	5	5.72	4.22	0.45	0.08	0.46	0.00	0.00	170.	0.	180.	0.003
7	1			-0.02	-0.89	0.89			271.			0.003
7	2	6.82	7.08	0.10	-0.58	0.59	0.07	0.08	260.	3.	283.	0.003
7	3			0.21	-0.30	0.37			235.			0.003
7	4			0.29	-0.10	0.31			198.			0.003
7	5	5.59	4.09	0.40	0.16	0.43	-0.03	0.10	158.	-12.	57.	0.003
8	1			0.09	-0.94	0.95			264.			0.003
8	2	6.87	7.13	0.18	-0.63	0.65	0.13	0.14	254.	-2.	245.	0.003
8	3			0.25	-0.34	0.42			233.			0.003
8	4			0.31	-0.13	0.33			202.			0.003
8	5	5.61	4.11	0.38	0.15	0.41	-0.05	0.10	159.	-11.	41.	0.003
9	1			-0.05	-0.77	0.77			274.			0.003
9	2	6.86	7.12	0.06	-0.50	0.50	-0.01	0.06	263.	6.	4.	0.003
9	3			0.17	-0.25	0.30			237.			0.003
9	4			0.24	-0.08	0.25			197.			0.003
9	5	5.60	4.10	0.34	0.15	0.37	-0.09	0.13	156.	-14.	33.	0.003
10	1			-0.00	-0.85	0.85			270.			0.003
10	2	6.87	7.13	0.11	-0.57	0.58	0.07	0.07	259.	2.	277.	0.003
10	3			0.22	-0.31	0.38			236.			0.003
10	4			0.29	-0.13	0.32			204.			0.003
10	5	5.64	4.14	0.39	0.11	0.40	-0.06	0.07	164.	-6.	24.	0.003
12	1			-1.38	-0.72	1.55			332.			0.005
12	2	6.82	7.08	-0.85	-0.52	1.00	0.48	0.97	329.	72.	359.	0.005
12	3			-0.36	-0.33	0.49			318.			0.005
12	4			-0.01	-0.20	0.20			274.			0.005
12	5	5.78	4.28	0.44	-0.03	0.44	-0.02	0.11	183.	13.	279.	0.005
26	1			-0.07	-0.55	0.55			278.			0.002
26	2	6.75	7.01	0.06	-0.38	0.39	-0.13	0.13	261.	4.	64.	0.002
26	3			0.18	-0.23	0.30			232.			0.002
26	4			0.27	-0.13	0.30			205.			0.002
26	5	5.74	4.24	0.38	0.01	0.38	-0.08	0.10	178.	8.	316.	0.002
30	1			0.05	-0.63	0.64			266.			0.002
30	2	6.67	6.93	0.14	-0.43	0.45	-0.07	0.08	252.	-4.	103.	0.002
30	3			0.22	-0.24	0.32			228.			0.002
30	4			0.28	-0.10	0.29			200.			0.002
30	5	5.59	4.09	0.35	0.08	0.36	-0.10	0.10	168.	-2.	357.	0.002
34	1			-0.17	-0.94	0.95			280.			0.003
34	2	6.77	7.03	-0.03	-0.65	0.65	0.14	0.21	273.	16.	315.	0.003
34	3			0.10	-0.39	0.40			255.			0.003
34	4			0.20	-0.20	0.28			226.			0.003
34	5	5.58	4.08	0.32	0.04	0.32	-0.14	0.14	172.	3.	344.	0.003

TURBO-ALTERNATOR ROTOR POSITION TEST DATA REDUCTION

REDUCTION OF TEST DATA. CONFIGURATION C

CALCULATED DATA

RUN	PLNE	H	V	DH	DV	E	DE	EREL	A	DA	AREL	ROTN
0	0	6.88	7.14	6.01	4.51							
15	1			0.06	-1.34	1.34			268.			0.003
15	2	7.18	7.44	0.18	-1.00	1.01	0.00	0.00	260.	0.	180.	0.003
15	3			0.30	-0.68	0.74			246.			0.003
15	4			0.39	-0.45	0.59			229.			0.003
15	5	5.92	4.42	0.50	-0.15	0.52	0.00	0.00	197.	0.	180.	0.003
13	1			0.11	-1.50	1.50			266.			0.003
13	2	7.15	7.41	0.21	-1.14	1.16	0.15	0.15	259.	-0.	259.	0.003
13	3			0.31	-0.81	0.87			249.			0.003
13	4			0.38	-0.58	0.69			237.			0.003
13	5	5.95	4.45	0.46	-0.27	0.54	0.02	0.12	211.	13.	285.	0.003
14	1			0.08	-1.40	1.40			267.			0.003
14	2	7.17	7.43	0.19	-1.05	1.06	0.05	0.05	259.	-0.	259.	0.003
14	3			0.30	-0.72	0.78			248.			0.003
14	4			0.37	-0.49	0.61			233.			0.003
14	5	5.91	4.41	0.46	-0.18	0.50	-0.02	0.04	202.	4.	317.	0.003
16	1			-0.06	-1.33	1.33			273.			0.003
16	2	7.18	7.44	0.07	-0.99	0.99	-0.02	0.11	266.	6.	4.	0.003
16	3			0.20	-0.67	0.70			254.			0.003
16	4			0.29	-0.44	0.53			237.			0.003
16	5	5.92	4.42	0.41	-0.15	0.43	-0.09	0.09	201.	3.	1.	0.003
17	1			0.09	-1.53	1.54			266.			0.004
17	2	7.17	7.43	0.20	-1.16	1.18	0.16	0.16	260.	1.	265.	0.004
17	3			0.30	-0.81	0.86			250.			0.004
17	4			0.37	-0.56	0.67			237.			0.004
17	5	5.92	4.41	0.46	-0.23	0.51	-0.00	0.09	207.	10.	295.	0.004
18	1			0.07	-1.49	1.49			267.			0.003
18	2	7.14	7.40	0.17	-1.13	1.14	0.13	0.13	262.	2.	277.	0.003
18	3			0.26	-0.79	0.83			252.			0.003
18	4			0.32	-0.55	0.64			239.			0.003
18	5	5.87	4.37	0.41	-0.24	0.47	-0.05	0.12	210.	13.	317.	0.003
31	1			-0.04	-1.45	1.45			271.			0.004
31	2	7.09	7.36	0.09	-1.09	1.09	0.08	0.13	265.	6.	316.	0.004
31	3			0.21	-0.75	0.78			254.			0.004
31	4			0.30	-0.50	0.58			239.			0.004
31	5	5.82	4.32	0.41	-0.19	0.45	-0.07	0.09	205.	7.	339.	0.004
27	1			0.05	-1.83	1.83			268.			0.004
27	2	7.28	7.54	0.15	-1.39	1.40	0.38	0.40	264.	4.	276.	0.004
27	3			0.24	-0.98	1.01			256.			0.004
27	4			0.30	-0.68	0.75			246.			0.004
27	5	5.94	4.44	0.39	-0.30	0.49	-0.03	0.19	218.	21.	306.	0.004
35	1			0.08	-1.65	1.65			267.			0.004
35	2	7.12	7.38	0.19	-1.23	1.24	0.23	0.23	261.	2.	269.	0.004
35	3			0.29	-0.83	0.88			251.			0.004
35	4			0.36	-0.55	0.66			237.			0.004
35	5	5.83	4.33	0.45	-0.19	0.49	-0.03	0.05	203.	5.	319.	0.004

TURBO ALTERNATOR ROTOR POSITION TEST DATA REDUCTION

REDUCTION OF TEST DATA. CONFIGURATION C

CALCULATED DATA

RUN	PLNE	H	V	DH	DV	E	DE	EREL	A	DA	AREL	ROTN
0	0	6.88	7.14	6.01	4.51							
23	1			-0.02	-1.68	1.68			271.			0.004
23	2	7.18	7.44	0.13	-1.29	1.30	0.00	0.00	264.	0.	180.	0.004
23	3			0.27	-0.93	0.96			254.			0.004
23	4			0.36	-0.67	0.76			241.			0.004
23	5	5.93	4.43	0.49	-0.33	0.59	0.00	0.00	214.	0.	180.	0.004
32	1			0.04	-1.67	1.67			269.			0.004
32	2	7.05	7.31	0.14	-1.27	1.28	-0.01	0.02	264.	-1.	132.	0.004
32	3			0.23	-0.90	0.93			255.			0.004
32	4			0.30	-0.64	0.71			245.			0.004
32	5	5.80	4.30	0.39	-0.30	0.49	-0.11	0.11	217.	3.	20.	0.004
19	1			0.06	-1.74	1.74			268.			0.004
19	2	7.08	7.34	0.17	-1.31	1.32	0.02	0.04	263.	-2.	208.	0.004
19	3			0.27	-0.91	0.95			254.			0.004
19	4			0.34	-0.62	0.71			241.			0.004
19	5	5.80	4.30	0.44	-0.25	0.50	-0.09	0.10	210.	-4.	57.	0.004
20	1			0.03	-1.82	1.82			269.			0.004
20	2	7.15	7.41	0.16	-1.37	1.38	0.09	0.09	263.	-1.	249.	0.004
20	3			0.28	-0.96	1.01			254.			0.004
20	4			0.37	-0.67	0.77			241.			0.004
20	5	5.84	4.34	0.49	-0.29	0.57	-0.03	0.04	211.	-4.	86.	0.004
21	1			-0.07	-1.62	1.62			273.			0.004
21	2	7.13	7.39	0.06	-1.24	1.24	-0.05	0.09	267.	3.	34.	0.004
21	3			0.17	-0.89	0.91			259.			0.004
21	4			0.26	-0.64	0.69			248.			0.004
21	5	5.87	4.37	0.37	-0.32	0.49	-0.11	0.12	221.	7.	8.	0.004
22	1			0.04	-1.72	1.72			269.			0.004
22	2	7.15	7.41	0.16	-1.32	1.33	0.03	0.04	263.	-1.	225.	0.004
22	3			0.26	-0.95	0.98			254.			0.004
22	4			0.34	-0.68	0.76			243.			0.004
22	5	5.89	4.39	0.44	-0.34	0.55	-0.04	0.05	218.	3.	355.	0.004
24	1			0.09	-1.86	1.87			267.			0.004
24	2	7.22	7.48	0.21	-1.44	1.46	0.16	0.18	262.	-3.	242.	0.004
24	3			0.32	-1.05	1.10			253.			0.004
24	4			0.40	-0.77	0.87			243.			0.004
24	5	5.96	4.46	0.50	-0.41	0.65	0.06	0.08	219.	5.	262.	0.004
28	1			0.05	-1.93	1.93			269.			0.004
28	2	7.27	7.53	0.16	-1.49	1.50	0.21	0.21	264.	-1.	261.	0.004
28	3			0.27	-1.09	1.12			256.			0.004
28	4			0.34	-0.80	0.87			247.			0.004
28	5	5.98	4.47	0.44	-0.43	0.62	0.02	0.10	224.	10.	298.	0.004
36	1			0.04	-1.98	1.98			269.			0.005
36	2	7.15	7.41	0.15	-1.50	1.51	0.21	0.21	264.	-0.	263.	0.005
36	3			0.26	-1.05	1.08			256.			0.005
36	4			0.33	-0.72	0.79			246.			0.005
36	5	5.81	4.31	0.42	-0.31	0.52	-0.07	0.07	216.	2.	22.	0.005

TURBO ALTERNATOR ROTOR POSITION TEST DATA REDUCTION

REDUCTION OF TEST DATA. CONFIGURATION D

CALCULATED DATA

RUN	PLNE	H	V	DH	DV	E	DE	EREL	A	DA	AREL	ROTN
0	0	6.88	7.14	6.01	4.51							
3	1			0.35	-3.45	3.47			264.			0.005
3	2	6.89	7.15	0.25	-2.96	2.97	0.00	0.00	265.	0.	180.	0.005
3	3			0.16	-2.50	2.51			266.			0.005
3	4			0.09	-2.18	2.18			268.			0.005
3	5	5.95	4.45	0.00	-1.75	1.75	0.00	0.00	270.	0.	180.	0.005
1	1			0.46	-4.18	4.21			264.			0.006
1	2	6.88	7.14	0.32	-3.51	3.53	0.56	0.56	265.	-0.	263.	0.006
1	3			0.19	-2.89	2.90			266.			0.006
1	4			0.10	-2.44	2.44			268.			0.006
1	5	5.93	4.43	-0.03	-1.87	1.87	0.11	0.12	271.	1.	284.	0.006
2	1			0.47	-3.78	3.81			263.			0.005
2	2	6.87	7.13	0.33	-3.23	3.24	0.27	0.28	264.	-1.	254.	0.005
2	3			0.20	-2.71	2.72			266.			0.005
2	4			0.10	-2.34	2.34			268.			0.005
2	5	5.93	4.43	-0.02	-1.86	1.86	0.11	0.11	271.	1.	283.	0.005
4	1			0.36	-3.66	3.67			264.			0.005
4	2	6.79	7.05	0.23	-3.14	3.15	0.18	0.18	266.	1.	276.	0.005
4	3			0.11	-2.67	2.67			268.			0.005
4	4			0.02	-2.32	2.32			269.			0.005
4	5	5.90	4.40	-0.09	-1.88	1.88	0.13	0.15	273.	3.	305.	0.005
5	1			0.34	-3.75	3.76			265.			0.005
5	2	6.86	7.12	0.22	-3.22	3.22	0.25	0.26	266.	1.	277.	0.005
5	3			0.11	-2.72	2.72			268.			0.005
5	4			0.03	-2.36	2.36			269.			0.005
5	5	5.89	4.39	-0.07	-1.91	1.91	0.15	0.17	272.	2.	295.	0.005
6	1			0.39	-3.92	3.94			264.			0.005
6	2	6.82	7.08	0.26	-3.34	3.35	0.38	0.38	265.	0.	268.	0.005
6	3			0.15	-2.80	2.81			267.			0.005
6	4			0.06	-2.42	2.42			268.			0.005
6	5	5.86	4.36	-0.04	-1.92	1.92	0.17	0.18	271.	1.	285.	0.005
25	1			0.43	-3.41	3.44			263.			0.004
25	2	6.91	7.17	0.29	-2.98	2.99	0.02	0.05	264.	-1.	205.	0.004
25	3			0.17	-2.58	2.58			266.			0.004
25	4			0.08	-2.29	2.29			268.			0.004
25	5	5.95	4.45	-0.04	-1.92	1.92	0.17	0.17	271.	1.	283.	0.004
29	1			0.37	-4.10	4.11			265.			0.006
29	2	6.83	7.09	0.25	-3.47	3.48	0.51	0.51	266.	1.	270.	0.006
29	3			0.14	-2.88	2.89			267.			0.006
29	4			0.06	-2.46	2.46			269.			0.006
29	5	5.90	4.40	-0.04	-1.92	1.92	0.17	0.17	271.	1.	284.	0.006
33	1			0.39	-4.13	4.15			265.			0.006
33	2	6.78	7.04	0.24	-3.53	3.54	0.57	0.57	266.	1.	271.	0.006
33	3			0.11	-2.96	2.97			268.			0.006
33	4			0.01	-2.56	2.56			270.			0.006
33	5	5.89	4.39	-0.12	-2.04	2.04	0.29	0.31	273.	3.	293.	0.006

TURBO ALTERNATOR ROTOR POSITION TEST DATA REDUCTION

REDUCTION OF TEST DATA. CONFIGURATION D

CALCULATED DATA

RUN	PLNE	H	V	DH	DV	E	DE	EREL	A	DA	AREL	ROTN
0	0	6.88	7.14	6.01	4.51							
11	1			0.24	-3.59	3.60			266.			0.005
11	2	6.80	7.06	0.16	-3.10	3.10	0.00	0.00	267.	0.	180.	0.005
11	3			0.09	-2.63	2.64			268.			0.005
11	4			0.04	-2.30	2.30			269.			0.005
11	5	5.94	4.44	-0.03	-1.87	1.87	0.00	0.00	271.	0.	180.	0.005
7	1			0.40	-4.07	4.09			264.			0.006
7	2	6.81	7.07	0.27	-3.45	3.46	0.36	0.37	266.	-1.	254.	0.006
7	3			0.15	-2.88	2.88			267.			0.006
7	4			0.06	-2.46	2.46			269.			0.006
7	5	5.87	4.37	-0.05	-1.93	1.93	0.06	0.06	272.	1.	290.	0.006
8	1			0.38	-4.01	4.02			265.			0.006
8	2	6.84	7.10	0.24	-3.42	3.42	0.32	0.33	266.	-1.	255.	0.006
8	3			0.12	-2.87	2.87			268.			0.006
8	4			0.03	-2.47	2.47			269.			0.006
8	5	5.90	4.40	-0.09	-1.97	1.97	0.10	0.11	273.	2.	300.	0.006
9	1			0.20	-3.85	3.86			267.			0.005
9	2	6.79	7.05	0.11	-3.31	3.31	0.21	0.22	268.	1.	283.	0.005
9	3			0.03	-2.81	2.81			269.			0.005
9	4			-0.03	-2.45	2.45			271.			0.005
9	5	5.87	4.37	-0.10	-1.98	1.98	0.11	0.13	273.	2.	304.	0.005
10	1			0.35	-3.95	3.96			265.			0.005
10	2	6.79	7.06	0.23	-3.38	3.38	0.28	0.29	266.	-1.	257.	0.005
10	3			0.11	-2.84	2.84			268.			0.005
10	4			0.02	-2.46	2.46			269.			0.005
10	5	5.90	4.40	-0.09	-1.97	1.97	0.10	0.11	273.	2.	300.	0.005
12	1			0.44	-3.71	3.74			263.			0.005
12	2	6.85	7.11	0.29	-3.20	3.22	0.11	0.17	265.	-2.	219.	0.005
12	3			0.16	-2.73	2.73			267.			0.005
12	4			0.06	-2.38	2.39			269.			0.005
12	5	5.97	4.47	-0.06	-1.95	1.95	0.07	0.08	272.	1.	292.	0.005
26	1			0.44	-3.72	3.74			263.			0.005
26	2	6.90	7.16	0.30	-3.20	3.22	0.12	0.17	265.	-2.	219.	0.005
26	3			0.16	-2.72	2.73			267.			0.005
26	4			0.07	-2.38	2.38			268.			0.005
26	5	5.96	4.46	-0.05	-1.93	1.93	0.06	0.06	271.	0.	286.	0.005
30	1			0.39	-4.30	4.32			265.			0.006
30	2	6.82	7.08	0.26	-3.63	3.64	0.54	0.54	266.	-1.	260.	0.006
30	3			0.14	-3.01	3.01			267.			0.006
30	4			0.05	-2.56	2.56			269.			0.006
30	5	5.88	4.38	-0.06	-1.99	1.99	0.11	0.12	272.	1.	285.	0.006
34	1			0.35	-4.26	4.27			265.			0.006
34	2	6.86	7.12	0.22	-3.61	3.61	0.51	0.51	266.	-1.	263.	0.006
34	3			0.11	-3.00	3.00			268.			0.006
34	4			0.02	-2.57	2.57			270.			0.006
34	5	5.86	4.36	-0.09	-2.01	2.01	0.14	0.15	272.	2.	292.	0.006

TURBO ALTERNATOR ROTOR POSITION TEST DATA REDUCTION

REDUCTION OF TEST DATA. CONFIGURATION D

CALCULATED DATA

RUN	PLNE	H	V	DH	DV	E	DE	EREL	A	DA	AREL	ROTN
0	0	6.88	7.14	6.01	4.51							
15	1			0.52	-3.70	3.73			262.			0.005
15	2	7.29	7.55	0.32	-3.18	3.20	0.00	0.00	264.	0.	180.	0.005
15	3			0.15	-2.70	2.71			267.			0.005
15	4			0.02	-2.36	2.36			270.			0.005
15	5	6.21	4.71	-0.14	-1.92	1.92	0.00	0.00	274.	0.	180.	0.005
13	1			0.71	-4.66	4.72			261.			0.007
13	2	7.32	7.58	0.47	-3.88	3.91	0.72	0.72	263.	-1.	258.	0.007
13	3			0.25	-3.16	3.17			265.			0.007
13	4			0.10	-2.64	2.64			268.			0.007
13	5	6.22	4.72	-0.11	-1.97	1.97	0.05	0.06	273.	-1.	234.	0.007
14	1			0.86	-4.47	4.56			259.			0.007
14	2	7.28	7.54	0.57	-3.74	3.78	0.58	0.61	261.	-3.	246.	0.007
14	3			0.30	-3.05	3.07			264.			0.007
14	4			0.10	-2.56	2.56			268.			0.007
14	5	6.22	4.72	-0.15	-1.93	1.93	0.01	0.01	275.	0.	315.	0.007
16	1			0.54	-4.11	4.14			262.			0.006
16	2	7.26	7.52	0.35	-3.50	3.51	0.31	0.31	264.	0.	266.	0.006
16	3			0.16	-2.93	2.93			267.			0.006
16	4			0.03	-2.52	2.52			269.			0.006
16	5	6.15	4.65	-0.14	-1.99	2.00	0.08	0.08	274.	-0.	263.	0.006
17	1			0.72	-4.56	4.61			261.			0.007
17	2	7.25	7.51	0.48	-3.82	3.85	0.65	0.66	263.	-1.	257.	0.007
17	3			0.26	-3.14	3.15			265.			0.007
17	4			0.10	-2.64	2.65			268.			0.007
17	5	6.13	4.63	-0.11	-2.01	2.02	0.09	0.10	273.	-1.	250.	0.007
18	1			0.64	-4.62	4.66			262.			0.007
18	2	7.19	7.45	0.42	-3.87	3.90	0.70	0.70	264.	-0.	262.	0.007
18	3			0.21	-3.18	3.18			266.			0.007
18	4			0.06	-2.68	2.68			269.			0.007
18	5	6.11	4.61	-0.14	-2.03	2.04	0.12	0.12	274.	-1.	265.	0.007
27	1			0.63	-4.49	4.53			262.			0.007
27	2	7.32	7.58	0.41	-3.78	3.80	0.60	0.60	264.	-0.	262.	0.007
27	3			0.21	-3.11	3.12			266.			0.007
27	4			0.07	-2.64	2.64			269.			0.007
27	5	6.14	4.64	-0.12	-2.02	2.03	0.10	0.11	273.	-1.	257.	0.007
31	1			0.70	-4.82	4.87			262.			0.008
31	2	7.26	7.52	0.41	-4.05	4.07	0.87	0.87	264.	-0.	264.	0.008
31	3			0.14	-3.33	3.33			268.			0.008
31	4			-0.05	-2.81	2.81			271.			0.008
31	5	6.23	4.72	-0.30	-2.15	2.17	0.25	0.28	278.	4.	303.	0.008
35	1			0.69	-4.75	4.80			262.			0.008
35	2	7.17	7.43	0.44	-3.96	3.99	0.79	0.79	264.	-0.	262.	0.008
35	3			0.20	-3.24	3.24			266.			0.008
35	4			0.03	-2.71	2.71			269.			0.008
35	5	6.07	4.57	-0.19	-2.04	2.05	0.12	0.13	275.	1.	289.	0.008

TURBO ALTERNATOR ROTOR POSITION TEST DATA REDUCTION

REDUCTION OF TEST DATA. CONFIGURATION D

CALCULATED DATA

RUN	PLNE	H	V	DH	DV	E	DE	EREL	A	DA	AREL	ROTN
0	0	6.88	7.14	6.01	4.51							
23	1			0.46	-3.93	3.95			263.			0.006
23	2	7.34	7.60	0.27	-3.35	3.36	0.00	0.00	265.	0.	180.	0.006
23	3			0.10	-2.81	2.81			268.			0.006
23	4			-0.03	-2.42	2.42			271.			0.006
23	5	6.30	4.80	-0.19	-1.92	1.93	0.00	0.00	276.	0.	180.	0.006
19	1			0.63	-4.71	4.75			262.			0.007
19	2	7.21	7.47	0.40	-3.94	3.96	0.61	0.61	264.	-1.	258.	0.007
19	3			0.19	-3.23	3.23			267.			0.007
19	4			0.04	-2.71	2.71			269.			0.007
19	5	6.13	4.63	-0.15	-2.05	2.06	0.13	0.14	274.	-1.	256.	0.007
20	1			0.58	-4.68	4.71			263.			0.007
20	2	7.24	7.50	0.37	-3.92	3.94	0.58	0.58	265.	-1.	260.	0.007
20	3			0.17	-3.21	3.22			267.			0.007
20	4			0.03	-2.70	2.70			269.			0.007
20	5	6.17	4.67	-0.15	-2.05	2.06	0.13	0.14	274.	-1.	255.	0.007
21	1			0.46	-4.33	4.36			264.			0.006
21	2	7.23	7.49	0.26	-3.68	3.69	0.34	0.34	266.	1.	272.	0.006
21	3			0.08	-3.08	3.08			269.			0.006
21	4			-0.06	-2.64	2.65			271.			0.006
21	5	6.16	4.66	-0.23	-2.09	2.10	0.17	0.17	276.	1.	285.	0.006
22	1			0.63	-4.58	4.62			262.			0.007
22	2	7.27	7.53	0.40	-3.84	3.86	0.51	0.51	264.	-1.	256.	0.007
22	3			0.18	-3.16	3.16			267.			0.007
22	4			0.02	-2.67	2.67			269.			0.007
22	5	6.24	4.74	-0.18	-2.04	2.04	0.12	0.12	275.	-1.	265.	0.007
24	1			0.78	-4.82	4.88			261.			0.008
24	2	7.35	7.61	0.51	-4.03	4.06	0.70	0.72	263.	-2.	251.	0.008
24	3			0.25	-3.29	3.30			266.			0.008
24	4			0.06	-2.76	2.76			269.			0.008
24	5	6.28	4.78	-0.17	-2.08	2.09	0.16	0.16	275.	-1.	265.	0.008
28	1			0.61	-4.67	4.70			263.			0.007
28	2	7.35	7.61	0.38	-3.92	3.94	0.58	0.58	264.	-1.	260.	0.007
28	3			0.17	-3.23	3.23			267.			0.007
28	4			0.01	-2.73	2.73			270.			0.007
28	5	6.20	4.70	-0.18	-2.08	2.09	0.17	0.17	275.	-1.	269.	0.007
32	1			0.62	-5.08	5.12			263.			0.008
32	2	7.22	7.48	0.39	-4.23	4.25	0.89	0.90	265.	-1.	262.	0.008
32	3			0.18	-3.44	3.45			267.			0.008
32	4			0.03	-2.87	2.87			269.			0.008
32	5	6.09	4.59	-0.16	-2.14	2.15	0.22	0.23	274.	-1.	263.	0.008
36	1			0.63	-5.10	5.14			263.			0.008
36	2	7.21	7.47	0.40	-4.23	4.25	0.89	0.89	265.	-1.	262.	0.008
36	3			0.18	-3.42	3.42			267.			0.008
36	4			0.02	-2.83	2.83			270.			0.008
36	5	6.02	4.52	-0.18	-2.08	2.09	0.16	0.16	275.	-1.	269.	0.008

TURBO ALTERNATOR ROTOR POSITION TEST DATA REDUCTION

REDUCTION OF TEST DATA. CONFIGURATION E

CALCULATED DATA

RUN	PLNE	H	V	DH	DV	E	DE	EREL	A	DA	AREL	ROTN
0	0	6.88	7.14	6.01	4.51							
3	1			0.20	-3.27	3.27			266.			0.004
3	2	6.78	7.04	0.12	-2.85	2.85	0.00	0.00	268.	0.	180.	0.004
3	3			0.05	-2.46	2.46			269.			0.004
3	4			-0.01	-2.17	2.17			270.			0.004
3	5	5.85	4.35	-0.08	-1.81	1.81	0.00	0.00	272.	0.	180.	0.004
1	1			0.28	-3.56	3.57			266.			0.005
1	2	6.77	7.04	0.19	-3.07	3.08	0.23	0.23	267.	-1.	254.	0.005
1	3			0.10	-2.61	2.61			268.			0.005
1	4			0.04	-2.28	2.28			269.			0.005
1	5	5.86	4.36	-0.03	-1.86	1.86	0.05	0.06	271.	-1.	230.	0.005
2	1			0.29	-3.55	3.56			265.			0.004
2	2	6.78	7.04	0.18	-3.08	3.08	0.23	0.24	267.	-1.	257.	0.004
2	3			0.08	-2.64	2.64			268.			0.004
2	4			0.00	-2.32	2.32			270.			0.004
2	5	5.87	4.37	-0.09	-1.92	1.92	0.10	0.10	273.	0.	279.	0.004
4	1			0.17	-3.52	3.52			267.			0.004
4	2	6.75	7.01	0.09	-3.04	3.04	0.19	0.20	268.	1.	278.	0.004
4	3			0.02	-2.60	2.60			269.			0.004
4	4			-0.03	-2.28	2.28			271.			0.004
4	5	5.82	4.32	-0.09	-1.87	1.87	0.06	0.06	273.	0.	285.	0.004
5	1			0.29	-3.87	3.88			266.			0.005
5	2	6.83	7.09	0.20	-3.29	3.30	0.45	0.45	267.	-1.	261.	0.005
5	3			0.11	-2.75	2.75			268.			0.005
5	4			0.05	-2.36	2.36			269.			0.005
5	5	5.90	4.40	-0.03	-1.86	1.86	0.05	0.06	271.	-1.	228.	0.005
6	1			0.09	-3.98	3.99			269.			0.006
6	2	6.84	7.10	0.07	-3.36	3.36	0.51	0.51	269.	1.	276.	0.006
6	3			0.05	-2.77	2.77			269.			0.006
6	4			0.03	-2.35	2.35			269.			0.006
6	5	5.81	4.31	0.02	-1.81	1.81	-0.01	0.09	269.	-3.	177.	0.006
25	1			0.32	-3.76	3.78			265.			0.005
25	2	6.91	7.17	0.23	-3.20	3.21	0.36	0.37	266.	-2.	252.	0.005
25	3			0.15	-2.67	2.68			267.			0.005
25	4			0.09	-2.30	2.30			268.			0.005
25	5	5.81	4.31	0.02	-1.81	1.81	-0.00	0.09	270.	-3.	179.	0.005
29	1			0.26	-3.98	3.99			266.			0.006
29	2	6.85	7.11	0.17	-3.37	3.37	0.52	0.52	267.	-0.	264.	0.006
29	3			0.09	-2.80	2.80			268.			0.006
29	4			0.04	-2.39	2.39			269.			0.006
29	5	5.77	4.27	-0.04	-1.86	1.86	0.04	0.06	271.	-1.	230.	0.006
33	1			0.22	-4.02	4.02			267.			0.006
33	2	6.78	7.04	0.12	-3.42	3.42	0.57	0.57	268.	0.	270.	0.006
33	3			0.03	-2.86	2.86			269.			0.006
33	4			-0.03	-2.45	2.46			271.			0.006
33	5	5.85	4.35	-0.12	-1.94	1.94	0.13	0.13	273.	1.	289.	0.006

TURBO ALTERNATOR ROTOR POSITION TEST DATA REDUCTION

REDUCTION OF TEST DATA. CONFIGURATION E

CALCULATED DATA

RUN	PLNE	H	V	DH	DV	E	DE	EREL	A	DA	AREL	ROTN
0	0	6.88	7.14	6.01	4.51							
11	1			0.23	-3.56	3.57			266.			0.005
11	2	6.85	7.11	0.17	-3.03	3.04	0.00	0.00	267.	0.	180.	0.005
11	3			0.11	-2.54	2.55			268.			0.005
11	4			0.06	-2.19	2.19			268.			0.005
11	5	5.91	4.41	0.00	-1.74	1.74	0.00	0.00	270.	0.	180.	0.005
7	1			0.27	-4.03	4.04			266.			0.006
7	2	6.77	7.03	0.19	-3.41	3.41	0.37	0.37	267.	-0.	267.	0.006
7	3			0.12	-2.83	2.83			268.			0.006
7	4			0.06	-2.41	2.41			269.			0.006
7	5	5.88	4.37	-0.01	-1.88	1.88	0.14	0.14	270.	0.	275.	0.006
8	1			0.40	-4.08	4.10			264.			0.006
8	2	6.85	7.11	0.29	-3.43	3.44	0.40	0.41	265.	-2.	253.	0.006
8	3			0.19	-2.82	2.82			266.			0.006
8	4			0.11	-2.38	2.38			267.			0.006
8	5	5.90	4.40	0.01	-1.82	1.82	0.08	0.08	270.	-0.	265.	0.006
9	1			0.22	-3.93	3.94			267.			0.005
9	2	6.83	7.09	0.13	-3.35	3.35	0.32	0.32	268.	1.	277.	0.005
9	3			0.04	-2.81	2.81			269.			0.005
9	4			-0.02	-2.42	2.42			270.			0.005
9	5	5.88	4.38	-0.10	-1.93	1.93	0.19	0.21	273.	3.	300.	0.005
10	1			0.28	-3.96	3.97			266.			0.006
10	2	6.83	7.09	0.19	-3.35	3.36	0.32	0.32	267.	-0.	266.	0.006
10	3			0.10	-2.79	2.79			268.			0.006
10	4			0.04	-2.39	2.39			269.			0.006
10	5	5.86	4.36	-0.04	-1.87	1.87	0.13	0.13	271.	1.	289.	0.006
12	1			0.38	-4.02	4.04			265.			0.006
12	2	6.87	7.13	0.27	-3.39	3.40	0.36	0.37	265.	-1.	254.	0.006
12	3			0.16	-2.81	2.81			267.			0.006
12	4			0.08	-2.39	2.39			268.			0.006
12	5	5.94	4.43	-0.02	-1.85	1.85	0.11	0.11	271.	1.	283.	0.006
26	1			0.29	-4.11	4.12			266.			0.006
26	2	6.93	7.19	0.21	-3.45	3.46	0.42	0.42	267.	-0.	264.	0.006
26	3			0.13	-2.84	2.84			267.			0.006
26	4			0.07	-2.40	2.40			268.			0.006
26	5	5.83	4.33	-0.00	-1.83	1.83	0.09	0.09	270.	0.	276.	0.006
30	1			0.27	-4.23	4.24			266.			0.006
30	2	6.84	7.10	0.18	-3.59	3.59	0.55	0.55	267.	0.	269.	0.006
30	3			0.09	-2.99	2.99			268.			0.006
30	4			0.03	-2.56	2.56			269.			0.006
30	5	5.79	4.28	-0.05	-2.00	2.00	0.26	0.27	272.	2.	282.	0.006
34	1			0.19	-4.17	4.17			267.			0.006
34	2	6.79	7.05	0.11	-3.54	3.54	0.50	0.51	268.	1.	276.	0.006
34	3			0.04	-2.95	2.95			269.			0.006
34	4			-0.02	-2.53	2.53			270.			0.006
34	5	5.82	4.32	-0.09	-1.99	1.99	0.25	0.27	272.	3.	290.	0.006

TURBO ALTERNATOR ROTOR POSITION TEST DATA REDUCTION

REDUCTION OF TEST DATA. CONFIGURATION E

CALCULATED DATA

RUN	PLNE	H	V	DH	DV	E	DE	EREL	A	DA	AREL	ROTN
0	0	6.88	7.14	6.01	4.51							
15	1			0.57	-3.59	3.64			261.			0.005
15	2	7.24	7.50	0.37	-3.09	3.11	0.00	0.00	263.	0.	180.	0.005
15	3			0.20	-2.63	2.63			266.			0.005
15	4			0.07	-2.29	2.29			268.			0.005
15	5	6.24	4.74	-0.10	-1.86	1.86	0.00	0.00	273.	0.	180.	0.005
13	1			0.85	-4.32	4.40			259.			0.007
13	2	7.17	7.43	0.57	-3.64	3.68	0.57	0.58	261.	-2.	250.	0.007
13	3			0.31	-3.01	3.02			264.			0.007
13	4			0.13	-2.55	2.55			267.			0.007
13	5	6.26	4.76	-0.11	-1.97	1.97	0.10	0.10	273.	0.	279.	0.007
14	1			0.81	-4.19	4.27			259.			0.006
14	2	7.19	7.45	0.55	-3.55	3.59	0.47	0.49	261.	-2.	249.	0.006
14	3			0.30	-2.94	2.96			264.			0.006
14	4			0.12	-2.51	2.51			267.			0.006
14	5	6.25	4.75	-0.10	-1.96	1.96	0.09	0.09	273.	0.	274.	0.006
16	1			0.39	-3.56	3.58			264.			0.004
16	2	7.20	7.46	0.24	-3.11	3.11	-0.00	0.14	266.	3.	354.	0.004
16	3			0.10	-2.68	2.68			268.			0.004
16	4			-0.00	-2.37	2.37			270.			0.004
16	5	6.19	4.68	-0.13	-1.98	1.99	0.12	0.13	274.	1.	287.	0.004
17	1			0.64	-4.42	4.47			262.			0.007
17	2	7.19	7.45	0.42	-3.72	3.75	0.63	0.63	264.	0.	266.	0.007
17	3			0.22	-3.07	3.08			266.			0.007
17	4			0.08	-2.60	2.60			268.			0.007
17	5	6.16	4.66	-0.11	-2.00	2.00	0.14	0.14	273.	0.	275.	0.007
18	1			0.50	-4.55	4.58			264.			0.007
18	2	7.18	7.44	0.32	-3.82	3.83	0.72	0.73	265.	2.	274.	0.007
18	3			0.15	-3.14	3.14			267.			0.007
18	4			0.03	-2.65	2.65			269.			0.007
18	5	6.14	4.63	-0.13	-2.02	2.02	0.16	0.16	274.	1.	282.	0.007
27	1			0.53	-2.55	2.61			258.			0.002
27	2	7.17	7.43	0.32	-2.40	2.42	-0.69	0.69	262.	-1.	86.	0.002
27	3			0.13	-2.26	2.26			267.			0.002
27	4			-0.01	-2.16	2.16			270.			0.002
27	5	6.24	4.73	-0.18	-2.03	2.04	0.17	0.19	275.	2.	297.	0.002
31	1			0.61	-4.58	4.62			262.			0.007
31	2	7.09	7.35	0.41	-3.84	3.86	0.75	0.75	264.	1.	267.	0.007
31	3			0.23	-3.15	3.16			266.			0.007
31	4			0.09	-2.65	2.65			268.			0.007
31	5	6.13	4.63	-0.07	-2.01	2.01	0.15	0.15	272.	-1.	261.	0.007
35	1			0.44	-4.41	4.43			264.			0.006
35	2	7.09	7.35	0.28	-3.73	3.74	0.63	0.65	266.	3.	278.	0.006
35	3			0.14	-3.10	3.11			267.			0.006
35	4			0.04	-2.65	2.65			269.			0.006
35	5	6.14	4.64	-0.09	-2.07	2.07	0.21	0.21	273.	-0.	269.	0.006

TURBO ALTERNATOR ROTOR POSITION TEST DATA REDUCTION

REDUCTION OF TEST DATA. CONFIGURATION E

CALCULATED DATA

RUN	PLNE	H	V	DH	DV	E	DE	EREL	A	DA	AREL	ROTN
0	0	6.88	7.14	6.01	4.51							
23	1			0.37	-3.85	3.87			264.			0.005
23	2	7.20	7.46	0.24	-3.27	3.28	0.00	0.00	266.	0.	180.	0.005
23	3			0.11	-2.74	2.74			268.			0.005
23	4			0.02	-2.35	2.35			269.			0.005
23	5	6.24	4.73	-0.09	-1.86	1.86	0.00	0.00	273.	0.	180.	0.005
19	1			0.52	-4.59	4.62			263.			0.007
19	2	7.15	7.41	0.35	-3.84	3.86	0.58	0.58	265.	-1.	259.	0.007
19	3			0.19	-3.15	3.16			267.			0.007
19	4			0.07	-2.66	2.66			269.			0.007
19	5	6.14	4.63	-0.08	-2.02	2.02	0.16	0.16	272.	-0.	267.	0.007
20	1			0.52	-4.55	4.58			264.			0.007
20	2	7.17	7.43	0.33	-3.81	3.82	0.54	0.54	265.	-1.	260.	0.007
20	3			0.15	-3.12	3.12			267.			0.007
20	4			0.03	-2.62	2.62			269.			0.007
20	5	6.18	4.68	-0.13	-1.98	1.98	0.12	0.13	274.	1.	288.	0.007
21	1			0.40	-4.18	4.20			265.			0.006
21	2	7.15	7.41	0.22	-3.57	3.57	0.29	0.29	266.	1.	273.	0.006
21	3			0.06	-2.99	2.99			269.			0.006
21	4			-0.05	-2.58	2.58			271.			0.006
21	5	6.16	4.66	-0.20	-2.04	2.05	0.19	0.22	276.	3.	300.	0.006
22	1			0.41	-4.41	4.43			265.			0.007
22	2	7.18	7.44	0.25	-3.71	3.72	0.44	0.44	266.	0.	268.	0.007
22	3			0.11	-3.06	3.06			268.			0.007
22	4			-0.00	-2.59	2.59			270.			0.007
22	5	6.19	4.69	-0.14	-1.98	1.99	0.13	0.14	274.	1.	289.	0.007
24	1			0.59	-4.45	4.49			262.			0.007
24	2	7.23	7.49	0.39	-3.76	3.78	0.50	0.51	264.	-2.	253.	0.007
24	3			0.19	-3.12	3.12			266.			0.007
24	4			0.06	-2.65	2.65			269.			0.007
24	5	6.27	4.76	-0.12	-2.06	2.06	0.20	0.21	273.	1.	278.	0.007
28	1			0.42	-4.45	4.47			265.			0.007
28	2	7.23	7.49	0.27	-3.76	3.77	0.48	0.48	266.	0.	266.	0.007
28	3			0.13	-3.11	3.11			268.			0.007
28	4			0.03	-2.64	2.64			269.			0.007
28	5	6.25	4.74	-0.10	-2.04	2.04	0.18	0.18	273.	0.	273.	0.007
32	1			0.56	-4.71	4.74			263.			0.007
32	2	7.09	7.35	0.35	-3.96	3.97	0.69	0.69	265.	-1.	261.	0.007
32	3			0.15	-3.25	3.26			267.			0.007
32	4			0.01	-2.75	2.75			270.			0.007
32	5	6.13	4.63	-0.17	-2.10	2.11	0.25	0.26	275.	2.	288.	0.007
36	1			0.48	-4.68	4.70			264.			0.007
36	2	7.14	7.40	0.30	-3.95	3.96	0.68	0.68	266.	-0.	265.	0.007
36	3			0.13	-3.27	3.28			268.			0.007
36	4			0.01	-2.79	2.79			270.			0.007
36	5	6.10	4.60	-0.14	-2.16	2.17	0.31	0.31	274.	1.	280.	0.007

TURBO ALTERNATOR ROTOR POSITION TEST DATA REDUCTION

REDUCTION OF TEST DATA. CONFIGURATION F

CALCULATED DATA

RUN	PLNE	H	V	DH	DV	E	DE	EREL	A	DA	AREL	ROTN
0	0	6.88	7.14	6.01	4.51							
3	1			0.29	-4.82	4.83			267.			0.006
3	2	6.77	7.03	0.17	-4.18	4.19	0.00	0.00	268.	0.	180.	0.006
3	3			0.07	-3.59	3.59			269.			0.006
3	4			-0.01	-3.17	3.17			270.			0.006
3	5	5.82	4.32	-0.10	-2.62	2.62	0.00	0.00	272.	0.	180.	0.006
1	1			0.43	-5.09	5.11			265.			0.006
1	2	6.79	7.05	0.28	-4.41	4.42	0.24	0.25	266.	-1.	246.	0.006
1	3			0.14	-3.78	3.78			268.			0.006
1	4			0.04	-3.32	3.32			269.			0.006
1	5	5.86	4.35	-0.09	-2.74	2.74	0.12	0.12	272.	-0.	264.	0.006
2	1			0.38	-5.08	5.09			266.			0.006
2	2	6.77	7.03	0.24	-4.39	4.40	0.21	0.22	267.	-1.	252.	0.006
2	3			0.11	-3.75	3.75			268.			0.006
2	4			0.02	-3.29	3.29			270.			0.006
2	5	5.82	4.32	-0.10	-2.70	2.70	0.08	0.08	272.	-0.	269.	0.006
4	1			0.33	-4.95	4.96			266.			0.006
4	2	6.76	7.02	0.19	-4.28	4.28	0.10	0.10	267.	-0.	262.	0.006
4	3			0.06	-3.65	3.65			269.			0.006
4	4			-0.04	-3.20	3.20			271.			0.006
4	5	5.78	4.28	-0.15	-2.62	2.63	0.01	0.05	273.	1.	355.	0.006
5	1			0.62	-5.45	5.48			263.			0.007
5	2	6.91	7.17	0.40	-4.69	4.71	0.52	0.56	265.	-3.	246.	0.007
5	3			0.20	-3.99	3.99			267.			0.007
5	4			0.05	-3.48	3.48			269.			0.007
5	5	5.95	4.45	-0.14	-2.83	2.84	0.21	0.22	273.	1.	280.	0.007
6	1			0.55	-5.35	5.38			264.			0.007
6	2	6.83	7.09	0.36	-4.62	4.63	0.44	0.47	266.	-2.	247.	0.007
6	3			0.18	-3.93	3.94			267.			0.007
6	4			0.05	-3.44	3.44			269.			0.007
6	5	5.84	4.34	-0.12	-2.80	2.81	0.19	0.19	272.	0.	275.	0.007
25	1			0.61	-5.37	5.41			263.			0.007
25	2	6.91	7.17	0.40	-4.59	4.61	0.42	0.46	265.	-3.	241.	0.007
25	3			0.20	-3.86	3.86			267.			0.007
25	4			0.05	-3.33	3.33			269.			0.007
25	5	5.86	4.36	-0.14	-2.65	2.66	0.04	0.05	273.	1.	315.	0.007
33	1			0.43	-5.61	5.62			266.			0.008
33	2	6.82	7.08	0.25	-4.76	4.77	0.59	0.59	267.	-1.	263.	0.008
33	3			0.09	-3.98	3.98			269.			0.008
33	4			-0.03	-3.42	3.42			271.			0.008
33	5	5.77	4.27	-0.18	-2.69	2.70	0.08	0.11	274.	2.	318.	0.008

TURBO ALTERNATOR ROTOR POSITION TEST DATA REDUCTION

REDUCTION OF TEST DATA. CONFIGURATION F

CALCULATED DATA

RUN	PLNE	H	V	DH	DV	E	DE	EREL	A	DA	AREL	ROTN
0	0	6.88	7.14	6.01	4.51							
11	1			0.40	-5.07	5.08			265.			0.006
11	2	6.83	7.09	0.24	-4.40	4.41	0.00	0.00	267.	0.	180.	0.006
11	3			0.08	-3.78	3.79			269.			0.006
11	4			-0.03	-3.34	3.34			270.			0.006
11	5	5.89	4.39	-0.17	-2.77	2.77	0.00	0.00	273.	0.	180.	0.006
7	1			0.37	-5.48	5.49			266.			0.007
7	2	6.87	7.13	0.20	-4.71	4.71	0.30	0.31	268.	1.	277.	0.007
7	3			0.04	-3.99	3.99			269.			0.007
7	4			-0.07	-3.47	3.47			271.			0.007
7	5	5.84	4.34	-0.21	-2.81	2.82	0.04	0.06	274.	1.	319.	0.007
8	1			0.54	-5.45	5.48			264.			0.007
8	2	6.85	7.11	0.34	-4.69	4.70	0.29	0.31	266.	-1.	251.	0.007
8	3			0.14	-3.98	3.98			268.			0.007
8	4			0.01	-3.47	3.47			270.			0.007
8	5	5.85	4.35	-0.17	-2.81	2.82	0.04	0.04	273.	0.	276.	0.007
9	1			0.36	-5.17	5.18			266.			0.006
9	2	6.76	7.02	0.19	-4.49	4.50	0.09	0.11	268.	1.	299.	0.006
9	3			0.02	-3.87	3.87			270.			0.006
9	4			-0.10	-3.42	3.42			272.			0.006
9	5	5.88	4.37	-0.25	-2.84	2.85	0.08	0.11	275.	1.	317.	0.006
10	1			0.46	-5.29	5.31			265.			0.007
10	2	6.79	7.05	0.28	-4.57	4.58	0.17	0.18	266.	-0.	255.	0.007
10	3			0.11	-3.90	3.91			268.			0.007
10	4			-0.01	-3.42	3.42			270.			0.007
10	5	5.84	4.34	-0.16	-2.81	2.81	0.04	0.04	273.	-0.	266.	0.007
12	1			0.52	-5.51	5.54			265.			0.007
12	2	6.86	7.12	0.33	-4.75	4.76	0.35	0.36	266.	-1.	255.	0.007
12	3			0.15	-4.04	4.05			268.			0.007
12	4			0.02	-3.54	3.54			270.			0.007
12	5	5.92	4.42	-0.15	-2.88	2.89	0.11	0.12	273.	-0.	262.	0.007
26	1			0.53	-5.71	5.74			265.			0.008
26	2	6.95	7.21	0.35	-4.85	4.86	0.45	0.46	266.	-1.	255.	0.008
26	3			0.19	-4.04	4.05			267.			0.008
26	4			0.08	-3.46	3.46			269.			0.008
26	5	5.79	4.29	-0.07	-2.72	2.72	-0.06	0.11	272.	-2.	151.	0.008
34	1			0.42	-5.69	5.70			266.			0.008
34	2	6.82	7.08	0.25	-4.82	4.82	0.42	0.42	267.	0.	268.	0.008
34	3			0.09	-4.01	4.01			269.			0.008
34	4			-0.03	-3.43	3.43			270.			0.008
34	5	5.71	4.21	-0.17	-2.68	2.69	-0.09	0.09	274.	0.	85.	0.008

TURBO ALTERNATOR ROTOR POSITION TEST DATA REDUCTION

REDUCTION OF TEST DATA. CONFIGURATION F

CALCULATED DATA

RUN	PLNE	H	V	DH	DV	E	DE	EREL	A	DA	AREL	ROTN
0	0	6.88	7.14	6.01	4.51							
15	1			0.15	-3.33	3.33			267.			0.004
15	2	7.07	7.33	0.08	-2.93	2.93	0.00	0.00	268.	0.	180.	0.004
15	3			0.01	-2.55	2.55			270.			0.004
15	4			-0.04	-2.28	2.28			271.			0.004
15	5	5.98	4.48	-0.10	-1.94	1.94	0.00	0.00	273.	0.	180.	0.004
13	1			0.16	-3.43	3.43			267.			0.004
13	2	7.11	7.37	0.10	-3.02	3.03	0.10	0.10	268.	-0.	260.	0.004
13	3			0.04	-2.65	2.65			269.			0.004
13	4			-0.00	-2.38	2.38			270.			0.004
13	5	5.99	4.49	-0.06	-2.03	2.03	0.09	0.10	272.	-1.	244.	0.004
14	1			0.14	-3.62	3.62			268.			0.004
14	2	7.08	7.34	0.07	-3.16	3.16	0.23	0.23	269.	0.	272.	0.004
14	3			0.00	-2.73	2.73			270.			0.004
14	4			-0.04	-2.43	2.43			271.			0.004
14	5	5.99	4.49	-0.11	-2.03	2.03	0.09	0.09	273.	-0.	273.	0.004
16	1			-0.03	-3.37	3.37			271.			0.004
16	2	7.05	7.31	-0.09	-2.96	2.97	0.04	0.17	272.	3.	347.	0.004
16	3			-0.14	-2.59	2.59			273.			0.004
16	4			-0.17	-2.31	2.32			274.			0.004
16	5	5.97	4.47	-0.22	-1.97	1.98	0.04	0.12	276.	3.	348.	0.004
17	1			0.34	-3.61	3.63			265.			0.004
17	2	6.95	7.21	0.20	-3.14	3.15	0.22	0.25	266.	-2.	241.	0.004
17	3			0.06	-2.71	2.71			269.			0.004
17	4			-0.03	-2.39	2.39			271.			0.004
17	5	5.90	4.40	-0.16	-1.99	1.99	0.05	0.07	275.	2.	319.	0.004
18	1			0.38	-4.45	4.46			265.			0.007
18	2	7.10	7.36	0.23	-3.74	3.75	0.82	0.83	266.	-2.	259.	0.007
18	3			0.09	-3.09	3.09			268.			0.007
18	4			-0.01	-2.62	2.62			270.			0.007
18	5	5.88	4.38	-0.14	-2.01	2.01	0.07	0.08	274.	1.	296.	0.007
27	1			0.17	-4.09	4.09			268.			0.006
27	2	7.13	7.39	0.08	-3.49	3.49	0.57	0.57	269.	0.	270.	0.006
27	3			-0.01	-2.94	2.94			270.			0.006
27	4			-0.07	-2.54	2.54			272.			0.006
27	5	5.94	4.44	-0.15	-2.03	2.04	0.09	0.10	274.	1.	300.	0.006
31	1			0.17	-4.47	4.47			268.			0.006
31	2	7.14	7.40	0.06	-3.79	3.79	0.86	0.86	269.	1.	271.	0.006
31	3			-0.03	-3.15	3.15			271.			0.006
31	4			-0.10	-2.70	2.70			272.			0.006
31	5	5.94	4.44	-0.19	-2.11	2.12	0.18	0.19	275.	2.	298.	0.006
35	1			0.15	-4.18	4.18			268.			0.006
35	2	7.02	7.28	0.06	-3.56	3.56	0.63	0.63	269.	1.	271.	0.006
35	3			-0.02	-2.98	2.98			270.			0.006
35	4			-0.08	-2.57	2.57			272.			0.006
35	5	5.91	4.40	-0.16	-2.03	2.04	0.10	0.11	274.	1.	302.	0.006

TURBO ALTERNATOR ROTOR POSITION TEST DATA REDUCTION

REDUCTION OF TEST DATA. CONFIGURATION F

CALCULATED DATA

RUN	PLNE	H	V	DH	DV	E	DE	EREL	A	DA	AREL	ROTN
0	0	6.88	7.14	6.01	4.51							
23	1			-0.08	-3.95	3.95			271.			0.005
23	2	7.10	7.36	-0.08	-3.41	3.41	0.00	0.00	271.	0.	180.	0.005
23	3			-0.08	-2.91	2.91			272.			0.005
23	4			-0.08	-2.55	2.56			272.			0.005
23	5	5.97	4.46	-0.08	-2.09	2.10	0.00	0.00	272.	0.	180.	0.005
19	1			0.18	-4.31	4.32			268.			0.006
19	2	7.06	7.32	0.08	-3.65	3.66	0.24	0.29	269.	-3.	236.	0.006
19	3			-0.01	-3.04	3.04			270.			0.006
19	4			-0.07	-2.60	2.60			272.			0.006
19	5	5.86	4.36	-0.16	-2.03	2.04	-0.06	0.10	274.	2.	40.	0.006
20	1			0.21	-4.37	4.37			267.			0.006
20	2	7.10	7.36	0.11	-3.69	3.69	0.28	0.33	268.	-3.	236.	0.006
20	3			0.02	-3.05	3.05			270.			0.006
20	4			-0.05	-2.60	2.60			271.			0.006
20	5	5.88	4.38	-0.14	-2.01	2.01	-0.08	0.10	274.	2.	59.	0.006
21	1			-0.12	-4.14	4.14			272.			0.006
21	2	7.11	7.37	-0.15	-3.53	3.54	0.12	0.14	272.	1.	299.	0.006
21	3			-0.17	-2.97	2.97			273.			0.006
21	4			-0.19	-2.56	2.57			274.			0.006
21	5	5.87	4.37	-0.21	-2.04	2.05	-0.04	0.14	276.	4.	22.	0.006
22	1			0.04	-4.21	4.21			269.			0.006
22	2	7.08	7.34	0.01	-3.61	3.61	0.20	0.22	270.	-1.	246.	0.006
22	3			-0.02	-3.05	3.05			270.			0.006
22	4			-0.04	-2.64	2.64			271.			0.006
22	5	5.91	4.41	-0.07	-2.12	2.12	0.03	0.03	272.	-0.	249.	0.006
24	1			0.12	-4.23	4.23			268.			0.005
24	2	7.13	7.39	0.07	-3.67	3.67	0.25	0.30	269.	-2.	239.	0.005
24	3			0.03	-3.14	3.14			269.			0.005
24	4			-0.00	-2.76	2.76			270.			0.005
24	5	6.02	4.52	-0.05	-2.28	2.28	0.18	0.19	271.	-1.	259.	0.005
28	1			0.07	-4.41	4.41			269.			0.006
28	2	7.13	7.39	0.02	-3.78	3.78	0.36	0.38	270.	-2.	255.	0.006
28	3			-0.03	-3.19	3.19			271.			0.006
28	4			-0.07	-2.76	2.76			271.			0.006
28	5	6.00	4.50	-0.12	-2.21	2.22	0.12	0.13	273.	1.	286.	0.006